NASA

AN ALL SKY STUDY OF FAST X-RAY TRANSIENTS

ALANNA CONNORS

LABORATORY FOR HIGH ENERGY ASTROPHYSICS

National Aeronautics And Space Administration

Goddard Space Flight Center

Greenbelt, Maryland 20771

AN ALL SKY STUDY OF FAST X-RAY TRANSIENTS[*]

Alanna Connors

Laboratory for High Energy Astrophysics
NASA/Goddard Space Flight Center
Greenbelt, Maryland 20771 USA

April 1988

ABSTRACT

Title of Dissertation: "An All Sky Study of Fast X-Ray Transients"

Alanna Connors, Doctor of Philosophy, 1988

Dissertation directed by: Dr. Elihu Boldt, Adjunct Professor,

Department of Physics and Astronomy

In the HEAO 1 A-2 survey of fast X-ray transients, we searched 2-20 keV scanning data for brief increases in flux, >4 millicrabs, on timescales ~1-10^4 s above a 12 hour average. We divided the search into two regions, an "all-sky" survey of the Galaxy, and a survey of the Magellanic Clouds. In the Magellanic Clouds survey, we found 37 events, and identified all with 4 of the 5 brightest sources in the LMC, plus 2 as flares from a foreground star. We found no X-ray bursts, no γ-ray bursts, and no events from the SMC. In the "all-sky" survey, after excluding well-known variable sources, out of the equivalent of ~104 days of data, we found 15 events, falling into two broad categories: flares from coronal sources, roughly isotropically distributed, with optically thin thermal spectra; and harder fast transients apparently distributed near the Galactic plane. We identified the first as flares from ubiquitous active cool dwarf stars. We hypothesized that the second may have been from distant Be-neutron star binaries. However, at least two of the harder, more luminous events remain unidentified. Intriguing questions for future research include the nature of these rare events, and how they may fit into a hierarchy of hard fast transients from γ-ray bursts to outbursts from pulsar systems; testing the "Be-neutron star" hypothesis; and more detailed understanding of the role of flaring activity in the atmospheres of main sequence stars.

AN ALL SKY STUDY OF FAST X-RAY TRANSIENTS

by

Alanna Connors

Dissertation submitted to the Faculty of the Graduate School

of the University of Maryland in partial fulfillment

of the requirements for the degree of

Doctor of Philosophy

1988

Advisory Committee:

    Adjunct Professor <u>Elihu Boldt</u>

    Professor <u>George Gloeckler</u>

    Dr. <u>Peter Serlemitsos</u>

    Associate Professor <u>Jordan Goodman</u>

    Professor <u>David Zipoy</u>

For those who may come after

ACKNOWLEDGMENTS

I find I have not enough time or space to sufficiently thank everyone who has helped during the long creation of this project. I hope to thank in person those who are not specifically mentioned here. This work would not have been possible without the support and facilities of the Laboratory for High Energy Astrophysics of NASA/GSFC, made available to me through the ever benign influences of G. Gloeckler, F. McDonald, and S. Holt. It is a pleasure to thank my academic and technical advisors in the X-Ray group, E. A. Boldt, P. J. Serlemitsos, and J. H. Swank, who I think may have spent more time and energy then they had on this project, and often did so on very short notice. On a personal level over the years I have also appreciated their examples as scientists and individuals. I recall the careful and thoughtful emphasis of E. Boldt on understanding the connections to "the big picture", and his quiet and complete attention when some aspect suggested an interesting line of investigation. I recall the insistence of J. H. Swank that a work aspiring to be a work of science should follow 'a thread of truth' through every detail of analysis and interpretation. She also frequently took pains to make the life of graduate students a little more hospitable, even when she herself was probably working longer hours. P. J. Serlemitsos, who initiated this project, pored over reams of computer output as the project got under way, and encouraged me to be down to earth and practical throughout.

Thanks are due to my Dissertation Examination Committee (E. A. Boldt, P. J. Serlemitsos, J. H. Swank, G. Gloeckler, J. Goodman, and D. Zipoy), who waded through 3 lbs 10 oz of text and figures without a Table of Contents. Thanks, too, to the "Ad Hoc Local Thesis

spouse A. Couch) has challenged me with examples of scholarly and fundamentally original visions for nearly fourteen years. I also acknowledge the indirect influence of D. Heath, as she led me to consider ways of presenting an overview of the X-ray sky; and from my early days of teaching at Maryland, I acknowledge the emphasis and example (of D. Falk, E. Redish, and J. Layman, among others) on providing both some historical, social, and philosophical overview, and on appealing to as many senses as possible, to allow people who learn in very different ways to assimilate the information. I had hoped this introduction would enable someone completely unfamiliar with the basic framework, issues, vocabulary, and standard procedures of X-ray astronomy, to comprehend enough of the field to grasp any cogent ideas much more quickly and completely than I think I did, as a newcomer. It remains to be seen whether this kind of introduction will work as I had planned. In Chapter 2, I am indebted to the work of J. Esposito and K. Jahoda for the histogram plots and sky maps, respectively; and also to F. Marshall, J. Swank, P. Serlemitsos, A. Tennant, and R. Shafer for discussions of spurious signals. Chapters 3 and 4 owe much to discussions with J. Swank, R. Kelley, and A. Szymkowiak; and the overviews to the comments of E. Boldt, although they are still not as clear as one could wish. In Chapter 5, I relied heavily on earlier work done by L. Kaluzienski (and also R. Griffiths) using HEAO 1; on later work done with K. Jensen using HEAO 2 and EXOSAT; and on earlier analysis of the OSO-8 event by A. Bunner, P. Serlemitsos, and J. Swank. Discussions with R. Mushotzky, R. Petre, K. Jahoda, and G. Madejski, on the properties of future missions in the U.S. and abroad, formed the basis for the discussions of future

vi

TABLE OF CONTENTS

LIST OF TABLES

LIST OF FIGURES

Chapter 1

Introduction

A. First Light

"Le mythe est né de la science; la science seule l'expliquera."

(Depuis, op. cit. de Santillana and von Dechend 1969)

In a preface to their classic essay on origins of the myth, as a vehicle for the preservation and transmission of human knowledge in the ages before writing, Santillana writes:

"Many, many years before, I had questioned myself, in a note, about the meaning of fact in the crude empirical sense, as applied to the ancients. It represents, I thought, not the intellectual surprise, not the direct wonder and astonishment, but first of all an immense, steady, minute attention to the seasons. What is a solstice or an equinox? It stands for the capacity of coherence, deduction, imaginative intention and reconstruction with which we could hardly credit our forefathers. And yet there it was. I saw.

"Mathematics was moving up to me from the depth of centuries; not after myth, but before it. Not armed with Greek rigor, but with the imagination of astrological power, with the understanding of astronomy. Number gave the key. Way back in time, before writing was invented, it was measures and counting that provided the armature, the frame on which the rich texture of myth was to grow.

"...The earliest social scientist, Democritus of Abdera, put it in one striking sentence: men's progress was the work not of the mind

1

but of the _hand_. His late successors have taken him too literally, and concentrated on artifacts. They have been unaware of the enormous intellectual effort involved, from metallurgy to the arts, but especially in astronomy. The effort of sorting out and identifying the only presences which totally eluded the action of our hands led to those pure objects of contemplation, the stars in their courses." (de Santillana and von Dechend 1969, p. ix; the emphasis is their own.)

Kuhn (1970) has documented the extreme difficulty, in astronomy as in any other science, of first correctly recognizing a useful underlying pattern from the details of observations; and second, of working out how those details come to be ordered by the newly perceived pattern (or 'paradigm'). Once such a pattern has been completely incorporated, it seems obvious. One relies on it, without thinking, to sort and comprehend a hierarchy of observational data; but the initial understanding required a great struggle of vision.

Imagine that one glances idly out an office window to watch an open meadow, an autumn field of grain or seeded grasses, that stretches into the distance. One is well aware, having interacted directly with grass and breezes for years, that the alternating waves of denser brightness and darker color drifting across the brown meadow grass indicate the action of the wind; a force which is not directly visible to the observer, but whose results one can see. (Further, one may have studied the motions of air masses of different temperature and so may be aware that the heat of the sun is what powers the wind, and so forth.)

Consider the number of intellectual steps that allow an observer to reach just the first conclusion. First, from tramping through

2

meadows (that is, direct interaction) one has gained detailed knowledge of the physical properties of grass and wind; second, one has observed, many times, that the individual stalks of grass one views at a distance have properties similar to those one has observed close at hand. It then takes no great feat of imagination, when seeing a wave of changing brightness ripple across a distant meadow, to envision in detail the interactions of individual stalks of grass under the combined forces of wind pressure, the resilience or stiffness of each stalk, and perhaps the weight of seeds at its head.

Compare this to the long effort to understand an analogous phenomenon among the stars, the density waves forming the spiral structure of the Milky Way. Originally, this track burned by the impetuous Phaeton across the sky served as something like a benchmark for the precession of the equinoxes. Two subtle assumptions provided a framework for a deeper understanding: one was that the natural laws operating at great distances were essentially the same as those one could observed more closely; the second was the idea of being able to map the world one observes at all. About the intellectual effort that led to the latter, de Santillana and von Dechend (1969) wrote that in classical antiquity, archaic time defined the universe, and space was synonymous with absence or emptiness, in contrast to the modern notion of three Cartesian dimensions (or four relativistic ones), with space delineated in the mind's eye by 'chalky axes' (Minkowski 1908). They suggest the first signs of this more modern description of space "coincided with the invention of perspective in the 15th century" (ibid p. 324). These twin ideas were not applied to astronomy until later (perhaps a reflection of the extreme difficulty of investigating

a domain where no direct experimentation was possible). In the late 1500s, Copernicus made a step towards extending this new idea of space to the cosmos when, to simplify the ever more complicated calculations of the Ptolmeic system, he took the Earth out of the center of the frame and allowed it to orbit about the Sun (Kuhn 1970). The idea that the objects in the heavens were essentially the same in nature as what one observes on Earth may have crystallized in 1611 with Galileo's observations (through his telescope, a new 'work of the hand') of Earth-like features on celestial objects such as the moon; and his calculations of the height of lunar mountains from their changing shadows may have extended the idea of mapping, common on the surface of the earth, to the heavens (Morrison and Morrison 1987; Drake 1978; E. Cavicchi private communication).

Once these two paradigms had gained general acceptance, their practical application to the mapping of even the Milky Way was not straightforward. There is still some controversy over the proper calibration and interpretation of the stars used as distance markers (Sandage and Tammann 1985; Wesdelink 1985). The tedious effort of making a three-dimensional map of the Milky Way was requisite for understanding its structure; Lin and Lau (1979) point out that observations and cataloguing of the shapes of distant galaxies also provided impetus for perceiving an overall "Grand Design". Once this "Grand Design" had been hypothesized, there was still the difficult effort of showing that this was a useful description, and deriving some new understanding from it. Early efforts by Lindblad (op. cit. Lin, Yuan, and Shu 1969) involving calculations of the orbits of individual stars were not convincing because of their incomplete

4

accounting; later calculations used a fluid approximation to develop

the current understanding of the spiral structure as standing gravity

waves, delineated by bright stars on the 'crest' (in denser star

formation regions), much as brighter bands of grain delineated the

invisible force of the wind in the earlier analogy (Lin and Lau 1979

and references therein).

De Santillana and von Dechend (1969) suggested that, in human

history, understanding and communication through numbers was more

basic than and preceded communication through common languages; we

turn this on its side to point out that where the common sense of

direct experience fails, astronomers have used counting and measure as

a guide.

B. Overview of the Problem

This is a 'counting' thesis, a work based on gathering and

sorting, in the earliest traditions of astronomy. Instead of human

vision, we have observed the heavens with satellites carrying X-ray

detecting collimated proportional counters (OSO-8 and HEAO 1), and

X-ray telescopes with proportional counters, channel multiplier arrays

at the focus (HEAO 2 and EXOSAT). Unlike the human eye, for these

modern 'works of the hand', there was a tradeoff between larger field

of view and finer spatial resolution, and between the ability to

record both variability and color (energy). For gathering and sorting

the data, we have used, not human memory (aided in long term storage

and transmission by the mnemonic of myth), not written records of the

hand and eye, but the electronic memory and sorting capacities of an

IBM mainframe, a VAX mainframe, and several smaller VAX and PDP

5

machines.

In contrast to works which examine one outstanding object or one class of similar objects, this thesis is based on a statistical study of a specific phenomena, variability in ~2-20 keV X-rays on time-scales of seconds to hours, which can arise from very disparate physical situations and correspondingly disparate classes of objects. The bulk of this work concerns a complete survey of variations in flux greater than about 10^{-10} ergs-cm^{-2}-s^{-1} for times of ~1 s to several hours, over the whole sky, using X-ray data from the A-2 experiment of the HEAO 1 satellite. In a compromise between broad sky coverage and good spatial resolution, the A-2 detectors viewed the sky through collimators limiting the field of view to ~3°x3° that were moved systematically across the whole sky. We have assumed throughout that the glimpses of the variable sky sampled in this manner are represenative of the whole.

In this thesis, we were interested in investigating types of short, transient, events not addressed in detail by other observers, which in practice meant considering variable sources with average (over a week) luminosities of something less than ~3x10^{-11} ergs-cm^{-2}-s^{-1} (2-20 keV). Some types of events which met this criteria included faint Type I or Type II X-ray bursts from distant or obscured sources; faint X-ray counterparts to gamma-ray bursts; flares from active cool dwarf stars or active cool subgiants; pulsations and outbursts from Be-neutron star systems; and outbursts from cataclysmic variables. We compared characteristics such as spectra, brightness, and short term variability to sort these events into natural classes, and measured their rates of occurence. When

considered in the larger context of X-ray variability over the whole sky, this work helps illuminate the details of the grand flow of energy through the Galaxy.

We reiterate that the sample studied here is quite small. The HEAO 1 A-2 experiment viewed less than 1/1000 of the sky at a time, and its total 'on' time (for the purposes of this search) was just over 104 days. Because of the low signal to noise ratio inherent in the faint, short events studied here, and because of the limited amount of previous X-ray data (when compared to archival optical data), the classifications we give for our events may not always be correct. Therefore the outcome of this project is primarily to suggest or confirm trends. If one wants more than a partial understanding, it will be necessary to both observe members of the various classes of X-ray varying objects across a broader spectrum (note that in most X-ray papers "identification" is still synonymous with "optical identification"), and to do more complete X-ray studies to fill the gaps in the sparse archival X-ray data.

C. Brief Overview of the Variable X-ray Sky

In a recent popular article, Alfven (1986) noted that in the days of optical observing, astronomers could observe 'only the surfaces of stars'; that is, mainly the photospheres of main-sequence stars. There were many states of matter unobservable at optical wavelengths, matter that was too cool or too hot, for example, to radiate primarily between 3000-7000 Å. New technologies and instrumentation, developed primarily after WW II, enabled astronomers to observe in the radio, infrared, ultraviolet, X-ray, and gamma-ray regimes (Longair 1981).

Radio telescopes mapped out cool clouds of hydrogen and more complex molecules, as well as radiation from extremely energetic particles in environments as diverse as quasars and the Sun. Longair (1981) remarks that no astronomer would have believed the enormous amount of energy radiated in these hitherto invisible wavelengths.

Boldt (1987) has noted that data from the earliest rocket observations already contained evidence for two of the hallmarks of the (extra-solar) X-ray sky: intense, variable emission from point sources, and a diffuse overall background 'glow'. These rocket observations had the drawback of only being able to observe for a few minutes per launch. Mapping of the X-ray sky had to wait for the launch of the first X-ray Explorer Satellite, named Uhuru after its December 12, 1970 launch from the coast of Kenya. It was followed by more than a dozen U.S., European, and Japanese X-ray satellites. Only two of these, Ariel 5 and HEAO 1, were specifically sky survey missions. (The Vela satellites also surveyed the X-ray sky over a number of years, although it was not their primary mission.)

Data sent back from the first sky survey instruments revealed bright, variable X-ray sources superposed on a glowing background that covered the whole celestial sphere, like very nearby individual seeds or more distant colorful berries that stand out, in one's vision, against a meadow landscape as it recedes into an unresolved haze in the distance. This roughly isotropic, unresolved X-ray bright haze, covering the whole celestial sphere, was termed the cosmic X-ray background. Contrast this with a view of the night sky at optical wavelengths, which appears mostly dark; sprinkled with the numerous 'constant' stars, that recede in the distance into a standing wave of

starlight, as one looks towards the denser star formation regions delineating the Galactic plane. In the X-ray sky (as observed by UHURU, for instance), perhaps one to two dozen variable luminous sources lined the Galactic plane; another two to three dozen spread out in a broad halo about the Galactic center; and these were superposed on perhaps two dozen extra-Galactic sources, including active galactic nuclei and hot X-ray glowing gases from clusters and supercluster of galaxies distributed isotropically about the sky. Since this work focuses on variability, we concentrate here on X-ray sources found in the galaxy.

Non-degenerate stars (main sequence stars, subgiants, bright giants and super giants), which dominate the night sky at optical wavelengths, were among the least prominent in X-rays. For most (save stars with active coronae) an average ratio of X-ray luminosity to bolometric luminosity of about 10^{-6} (with a wide spread) was found to be a reasonable approximation (Bradt and McClintock 1983; Helfand and Caillault 1982; Pallavicini et al. 1981). From densities and optical luminosities in Allen (1973), we estimate the total power released in X-rays in our galaxy by these non-degenerate, magnetically inactive stars to be on the order of 10^{37} ergs-s^{-1}.

Stars with active coronae exhibited a much higher ratio of X-ray to optical luminosity. There are two classes of stars which exhibit such stellar activity: magnetic (or "active", or "spotted") cool dwarf stars; and active cool giants-subgiants. The latter occur most often in nearly synchronous binaries with a faint, smaller mass companion, called RS CVn-type binaries. (The current understanding is that the smaller companion affects the X-ray activity of the sub-giant

9

primarily by keeping its rotation rate high; Pallavicini et al.
1981). The quiescent X-ray luminosities of these sources is apt to be
on the order of 10^{29} ergs-s^{-1}. These spotted stars are more X-ray
luminous when they flare, with peak luminosities on the order of 10^{32}
ergs-s^{-1}, and the total energy released in a typical flare on the
order of 10^{36} ergs-s^{-1}. However, the space density of these spotted
subgiants, though not well measured, is probably at least an order of
magnitude less than that of the magnetically active cool dwarf stars.

Active cool dwarf stars (flare stars; dMe-dKe) exhibit lower
quiescent luminosities (10^{26-29} ergs-s^{-1}), but have a space density of
~0.04 per cubic parsec (see Appendix C). So far no correlation has
been found between the activity of a flare star and whether or not it
has a companion; instead, correlations with rotation rate and/or
quiescent (U-band) luminosity have been measured. From Lacy, Moffet,
and Evans (1976) we find the average power radiated in the U-band
during stellar flares, $<L_U^*>$, roughly follows the relation
$<L_U^*> \sim 10^5 (q_U)^{0.77}$, where q_U is the quiescent U-band luminosity of
the star. From Chapters 3 and 5, and Appendix C of this work, we find
the total expected energy radiated in X-rays during stellar flares is
roughly one-tenth that radiated in the U-band (with a wide scatter).
Using estimates of the percentages of active stars, and their
luminosities, from Joy and Abt (1974), number densities from Allen
(1973), and assuming a uniform disk distribution of scale height
~300 pc, we estimate the total mean power radiated in X-ray flares
over the whole galaxy from stars with active coronae to be
~5×10^{36} ergs-s^{-1} (2-20 keV). For comparison, the X-ray emission from
the Galactic ridge is estimated to be ~10^{38} ergs-s^{-1} (Worral et al.

1982; Warwick et al. 1985; Caillaut et al. 1986). (We point out that the peak X-ray luminosities of these events are actually quite low, less than 10^{32} ergs-s^{-1}, and so would have been indistinguishable from an unresolved background glow when Uhuru viewed the sky. It is only the high space densities of these cool dwarf stars that allows them to contribute a measurable fraction of the overall X-ray luminosity of the Milky Way.)

At the other extreme, one finds luminous X-ray binaries: stars with compact companions (accreting neutron stars or black holes) that are among the most prominent sources in the X-ray sky, with L_X/L_{OPT} as high as 10^4 (Bradt and McClintock 1983). These dramatically variable systems dominate any (~2-20 keV) X-ray map of the sky. (The X-ray brightness of these systems containing compact objects is responsible for the contention that while one observes the middle age of a star with optical radiation, in X-rays one can view the end of a star's life.) Following Bradt and McClintock (1983) we divide these, according to their optical counterparts, into systems with low-mass and high-mass main sequence companions (although there is some overlap at masses of several M_0). They point out that the positions of the high mass X-ray binaries map out the spiral arms (and star formation regions) near the Galactic plane, while the positions of the (on average older; Cowley et al. 1987) low mass systems spread out in a halo around the Galactic center. (See also van Paradijs 1983.) Another indication of relative age can be found in the differing magnetic field strengths of the neutron stars in the two types of systems, as high mass systems more often are pulsars (showing they have compact companions with magnetic fields $>10^{11}$ gauss).

Van den Heuvel and Rappaport (1986) divide the high mass binaries into three categories, based roughly on their accretion rates. In two of their categories, "massive wind driven systems" and "disk driven systems", the systems continuously emit X-rays, with $L_X \geq 10^{37}$ ergs-s^{-1}. However, others lump these two consistently luminous groups together (Stella, White, and Rosner 1986). There are about ten such highly luminous high mass systems documented. Cowley et al. (1984) has suggested that roughly an equal number of all classes of bright X-ray sources may be hidden from identification on the far side of the Galactic plane by distance and high column density. Overall we estimate that ~20 of these massive supergiant and bright giant binaries contribute ~5x10^{38} ergs-s^{-1} to the total galactic luminosity in X-rays.

The less luminous, less massive, sub-category of high mass X-ray binaries contains transient X-ray sources such as Be-plus-neutron star binaries in wide/eccentric orbits. Since from Allen (1973) there are roughly two orders of magnitude more early-type subgiants and main-sequence stars than more massive systems, if one (naively) assumed an equal incidence of binaries containing compact objects in each, one might expect ~2x10^3 neutron star binaries with such early-type stars as optical counterparts. One would also expect the majority to have strong magnetic fields, ~10^{12} gauss. However, systems that are only transient X-ray sources (such as Be-plus-neutron star binaries, which apparently only turn 'on' during periods of optical activity, and even then have outbursts that occur mainly at periastron) are apt to be difficult to count. We can make a crude estimate based on the investigations of small segments of the Galactic plane described in

Chapter 3. We assume our rough measurement of a time-averaged flux of $\sim 3 \times 10^{-11}$ ergs-cm^{-2}-s^{-1} from several apparently hard, variable, sources in a 3°x3° field at Galactic coordinates (255°,9°) to be represenative of the the whole plane. If one assumes these sources are distributed isotropically throughout a disk of scale height ~100 pc, and that some fraction of this emission is due to Be-plus-neutron star binaries, one estimates an upper limit to the total X-ray contribution of these hard, transient, predominantly pulsar, systems of several times 10^{36} ergs-s^{-1} (2-20 keV) over the whole Galaxy. (For comparison, for cosmic rays, one estimates, for a "leakout" time of $\sim 10^7$ years, and a total Galactic energy of $\sim 10^{54-55}$ ergs (Allen 1973), an average power input of $\sim 10^{40}$ ergs-s^{-1}.)

Similarly, we can roughly categorize the low mass X-ray binaries by their average X-ray luminosities. From the 43 low-mass and globular cluster systems listed in Bradt and McClintock (1983) we delineate roughly three classes of sources. The brightest persistent sources, with $L_X \sim 3 \times 10^{37-38}$ ergs-s^{-1}, constitute ~30% of the (identified) low-mass X-ray binaries. Following the suggestion of Cowley et al. (1984; 1987), we estimate there are ~28 such luminous systems, and infer they contribute $\sim 3 \times 10^{39}$ ergs-s^{-1} to the overall X-ray luminosity of the Galaxy. Roughly another 30% (of low mass systems with distance determinations) have average luminosities $\sim 10^{37}$ ergs-s^{-1}. These 'moderate' luminosity, moderate accretion rate sources exhibit the highest rate of X-ray bursts, ~1 per hour when bursting (Bradt and McClintock 1983). We estimate overall that these moderate luminosity low mass X-ray binaries add $\sim 3 \times 10^{38}$ ergs-s^{-1} to the X-ray luminosity of the Galaxy, and that X-ray bursts account for

something like 3% of this total. The remaining 40% of the low mass binaries were either soft transient sources (albeit some with peak luminosities as high as ~10^{38} ergs-s^{-1}), or have luminosities less than 10^{36} ergs-s^{-1}, and so we estimate they contribute something less than ~10^{38} ergs-s^{-1} to the time averaged X-ray luminosity of the Galaxy.

We have not yet discussed systems containing white dwarfs (except indirectly, as a few RS CVn-types have white dwarf companions; we treated them as active-coronae stars). Those that produce the most X-ray emission are close binaries in which a low mass star transfers matter (through an accretion disk) to its white dwarf companion, and are named cataclysmic variables (Patterson 1984). These systems have relatively low X-ray luminosities, 10^{29-34} ergs-s^{-1}, and their space density is not well measured. Using estimates of number densities from Patterson (1984), and luminosities from Bradt and McClintock (1983), we estimate a rough combined X-ray luminosity of several times 10^{37} ergs-s^{-1} (considerably less than from binaries containing neutron stars or black holes).

Since this work is mainly concerned with 1-10^4 s variability, we have not mentioned supernovae remnants, even though a few (such as the Crab and Vela) contain lone pulsars (with periods of ~33 and 69 ms, respectively). Luminosities of the closest supernova remnants are something like ~10^{36} ergs-s^{-1} (2-20 keV); estimates of their total contribution to the X-ray luminosity of the Galaxy range from enough to account for most of the luminosity of the Galactic ridge (~ 10^{38} ergs-s^{-1}), to nearly an order of magnitude less (Koyama, Ikeuchi, and Tomasaka 1987).

From this sketchy overview, one sees that the variable part of
the signal from the X-ray sky carries, in some cases, only a small
fraction of the total energy (as in Type I or II X-ray bursts). Yet
it can carry with it clues to the underlying physical properties of a
system. One can think of X-ray variability as falling into two rough
categories. The first category encompasses all cases where the
reception of the radiation is somehow interrupted: that is, where
radiation from a region is continuously emitted, but no longer reaches
a detector stationed at Earth because of purely 'geometrical'
considerations. For example, an object, such as the optical
companion, moves into the line of sight, as in an X-ray eclipse; or
the emitting region rotates out of the observer's line of sight (as
does the pole of a magnetic neutron star, on a pulsar; or an active
region, on a flare star). Many of these events are strongly
periodic. They have allowed observers to constrain the sizes and
masses of binaries, to set constraints on models of magnetic field
generation in main sequence stars, and in a handful of cases to
determine the size and mass of both members of an X-ray binary to
obtain the first measurements of the mass of a neutron star (Shapiro
and Teukolsky 1983 and references therein).

The second category involves the transient release of stored
energy through a variety of mechanisms. These events are not
necessarily periodic (although some are quasi-periodic). Many exhibit
a roughly exponential rise and decay which is often accompanied by
cooling on roughly the time-scales of the intensity decay (Serlemitsos
private communication). These time-scales, together with observations
of the spectra, and of the total energy released, give clues to the

underlying physical phenomena in very different ways. For example, stellar flares, in an electromagnetic release of energy, indicate the geometry of portions of the stellar coronae. One indirectly observes the dimensions of these hot plasma-filled loops by measuring the rise times of stellar flares (Batchelor 1984; also see Chapter 5). Type I X-ray bursts, when modeled as black-body radiation released in a thermonuclear flash, provided the evidence that low mass X-ray binaries which were not pulsars also contained neutron stars (Swank et al. 1977; also see Shapiro and Teukolsky 1986 and references therein). X-ray bursts emit only a small fraction of the time-averaged power released in X-rays by these systems, but indicate dimension, temperature, and may (with better data in the future) indicate chemical composition and depth of accreting matter (Ebisuzaki 1987). The high luminosity and rapid variability of the most luminous X-ray binaries provided evidence for both the efficient conversion of gravitational potential energy into radiation, and for a compact emitting region; the high luminosities of the 'classic' X-ray transients were considered evidence of deep gravitational wells, while the transient nature of the outbursts delineated binary orbits wider and/or more eccentric than those of the more persistent X-ray sources. In this study of the X-ray sky, we found examples of each category.

D. Overview of the Thesis

In Chapter 2, we briefly describe the HEAO 1 A-2 experiment, and discuss the mechanics of the HEAO 1 A-2 Fast Transient Search, an all sky survey of the (~2-20 keV) A-2 data for increases in flux above the

mean of greater than ~6σ significances (corresponding to ≥ 10^{-10} ergs-cm^{-2}-s^{-1}) with durations ~1 s to ~hours. This survey provided the foundation for this thesis. We divided the sky into three regions, the "source-free" sky, comprising roughly 50% of the data; the "source" regions, covering an additional ~40% (we still excluded regions around bright variable sources such as Cyg X-1); and a survey of the Magellanic Cloud region, covering about 3% of the total database.

Chapter 3 contains the results of the "source-free" and "source" regions, which we have combined to call the "all-sky" fast transient survey. We published initial results of the "source-free" portion in Connors, Serlemitsos, and Swank (1986). In that paper, we found six out of the eight fast transient events we reported to be consistent with a class of highly luminous hard flares from cool dwarf stars. However, two of the eight fast transients clearly did not originate in nearby stellar coronae, as their spectra showed indications of quite high intrinsic absorption ($N_H \geq 10^{22}$ cm^{-2}). At that time, we found their characteristics did not match those of any type of identified X-ray transient.

To check our original conclusions, we extended our survey closer to regions containing sources brighter than ~3x10^{-11} ergs-cm^{-2}-s^{-1}, including the Galactic plane. If our identification of the majority of the events as hard flares from dMe-dKe stars were correct, we would expect to find an equal rate (~60% more) in the unexplored "source" portions of the data. However, if a significant fraction were from a class of events with intrinsic luminosities higher than about 10^{36} ergs-s^{-1}, we expected to find a greater proportion of new events as we

17

extended the HEAO 1 A-2 fast transient search to "source" regions such as the Galactic plane.

We discuss the results of this second phase of the survey in the latter half of Chapter 3. We did indeed find three more events with properties consistent with those of stellar coronal flares; but we also detected four events (three apparently from the same source), with hard spectra, along the Galactic plane. We noted also that a careful mapping of a small swath of the Vela region indicated the existence of a class of hard, variable (~seconds to minutes) sources in that region along the plane, with fluxes on the order of 10^{-9-10} ergs-cm^{-2}-s^{-1}, but that lasted for only ~3-12 hours. We therefore suggested a likely identification for this class of hard varying sources to be outbursts from distant Be plus neutron star systems (although we did not rule out classes of cataclysmic variables proposed by Hertz and Grindlay 1984). These tentative identifications appear to be supported by the results of a more extensive map of the Galactic plane with the Japanese satellite GINGA. Koyama et al 1988) reported detecting hard, variable, sources on the plane, which they suggest may be Be plus neutron star systems. In the light of these more recent findings, we suggest in Chapter 3 that at least one of the original unidentified events may be associated with such a system. We suggested that if the short term variability (detected most prominently from the source that triggered three times) can be shown to be pulsations, as is consistent with what has been observed from identified Be-neutron star systems (van den Heuvel and Rappaport 1986; Stella, White, and Rosner 1986), we would consider it strong evidence for the proposed Be-neutron star binary identification. (We

note, however, that we cannot rule out an association of these hard transients with the sources of gamma-ray bursts, although it is not the interpretation we prefer, as the one classic gamma-ray burst observed through the front of the A-2 detectors coincided in space and time with emission from one of these hard transient sources.)

From this HEAO 1 A-2 all sky survey, we set an upper limit on the gamma-ray burst rate. If the gamma-ray burst observed by HEAO 1 A-2 and A-4 (but not in data meeting our search criteria) is represenative, we measure a 90% upper limit on the gamma-ray burst rate of < 1300 per year over the whole sky above gamma-ray burst fluence limits of 10^{-9}-10^{-8} ergs-cm^{-2}. Although comparisons with differing detectors is fraught with systematic difficulties, we point out at the end of Chapter 3 that the shape of the combined HEAO 1 A-2/A-4 gamma-ray burst Log-Number versus Log Fluence function is consistent with a flattening around fluences of 10^{-7} ergs-cm^{-2}, such as one might expect if gamma-ray bursts are on average no more energetic than an unusually long or bright stellar coronal flare (although in gamma-ray bursts the energy is released in a dramatically shorter time), with E ~ 10^{35-36} ergs.

In Chapter 4, we describe the results of the last section of the HEAO 1 A-2 fast transient search, the survey of the Magellanic Cloud region. We identified all but two thirty-seven fast transient events with four of the five brightest X-ray sources observed in the LMC, including two with the low mass binary LMC X-2, five with the high mass binary (and black hole candidate) LMC X-1, eight with outbursts from the eccentric high mass binary A0538-66 (the LMC Transient), and the remaining twenty with bright flares (plus one eclipse) from the

high mass pulsar system LMC X-4. (Two we identified as flares from a foreground RS CVn-type system.) We remark that if the distance to the LMC is 55 kpc, several of the events we identified with LMC X-4 (and one outburst from the LMC Transient) reached luminosities of up to 5×10^{39} ergs-s^{-1}, about a factor of twenty over the (hydrogen) Eddington luminosity limit. Ebisuzaki (1987) has proposed using the luminosities of X-ray bursts as "standard candles" for re-measuring the distance to the LMC. However, this survey found no X-ray bursts from the LMC (or SMC). In Chapter 4 we find a 90% upper limit on the average rate of X-ray bursts per year from the LMC of less than 0.43.

In Chapter 5 we left the analysis of the fast transient search, and consider two bright events in detail. The first is the dMe pair LDS 131 (with the X-ray name H0449-55), source of a flare which we used (in Chapter 3) as a "prototype" of a class of hard, luminous, flares from cool dwarf stars. We discuss the spectra and light curve of the bright HEAO 1 event, and infer the geometry of the flaring loop system. From follow-up optical, ultraviolet, and X-ray observations of the cool dwarf pair, we tentatively suggest that that the hard, luminous, flare which triggered the HEAO 1 search was a rare member of the tail of the flare size - flare rate distribution of normal stellar flares, rather than a member of a separate class of energetic events.

In the second portion of Chapter 5, we consider a bright (at peak ~50% brighter than the Crab Nebula + pulsar), unidentified, ~12 minute event observed with the OSO-8 satellite. We note that the highly absorbed spectrum probably indicated a distance of 2 kpc or greater, suggesting a high luminosity indicative of an origin on a compact object. We consider possible identifications for this event, but find

20

the ~10 s spikes characterizing the light curve atypical for Be plus neutron star systems, and the spectrum too hard to be black-body radiation from a Type I X-ray burst, and not sufficiently variable for identification with a classic gamma-ray burst.

In the concluding chapter, we summarize our results, and explore what possible underlying patterns fast transient events presumably from compact objects could be delineating (X-ray bursts; "classic" gamma-ray bursts; soft gamma-ray repeating bursts; the hard transient events described here; and other unidentified fast transients observed by other researchers). Unfortunately, events such as the OSO-8 event described in Chapter 5 still defy classification, demonstrating that our understanding of these events is still incomplete. We conclude with a discussion of the prospects for future investigations in each of these areas.

The Mechanics of the HEAO 1 A-2 Fast Burst Search

A. Introduction

In August 1977, the first High Energy Astrophysical Observatory, HEAO 1, was launched into a low Earth (93 minute) orbit, carrying four different experiments (A-1 through A-4) to map the sky in X-rays from ~0.1-1000 keV. The HEAO 1 satellite spun with a period of 32-35 minutes, so that the four experiments swept over a circular strip of sky 21-23 times in 12 hours. The satellite spin axis was stepped by ~0.5° per 12 hrs, so that as the Earth moved about the Sun, the HEAO 1 spin axis was constrained to point toward the Sun. In this manner, the instruments on HEAO 1 viewed the whole sky $2\frac{1}{2}$-3 times, one thin band at a time, before the demise of the satellite in January 1979. (After about February 1978 the satellite also operated in a "pointed" mode, during which one or another of the experiments was pointed steadily at a source for ~10^4 s.) As we noted in the introduction, data sent back from earlier sky survey satellites had revealed fields of discrete X-ray sources on an unresolved isotropic bright X-ray haze, the cosmic X-ray background.

The A-2 experiment, a collaborative effort led by E. Boldt of GSFC and G. Garmire of Pennsylvania State University, and with collaborators at GSFC, JPL, and the University of California, Berkely, was designed to study the properties of this unresolved bright haze. To this end, it incorporated features to discriminate signals due to X-rays from those due to charged particles or other background events,

and novel geometries to monitor both the internal detector background and the diffuse glow from the X-ray sky. We briefly describe the attributes of the HEAO 1 A-2 experiment in §B. In the fast burst search described here, we exploited the stability and predictability of the A-2 detectors for quite a different project: to search for sudden "flashes" of X-ray flux ($\geq 10^{-10}$erg-cm^{-2}-s^{-1} for 1-10^{4}s) among the discrete sources and diffuse sky glow.

We performed this search in three phases. The first two (the "source-free" and "source-full" searches) comprised the "all sky" survey of the Galaxy, and the third a survey of the Magellanic Clouds region. In the all-sky survey, we were primarily interested in uncovering new fast transients, and so did not examine events from data when known variable sources, such as Cyg X-1, KZ Tra (X1627-673), or the Rapid Burster (X1730-333), were in the instrument fields of view. In the survey of the Magellanic Clouds region, we used the same search algorithms, but kept and scrutinized each of the events, whether or not an X-ray source identified as variable was in the instrument fields of view at the time.

For the all-sky survey of fast transients, we divided the sky into two (roughly equal) portions. In the first phase of our fast burst search, we looked only at regions of sky free of known X-ray sources brighter than ~1 milliCrab, where 1 millicrab is ~3.4x10^{-11} ergs-cm^{-2}-s^{-1} (2-20 keV), assuming a Crab-like spectrum. In this "source-free sky" phase, we compared the observed X-ray flux, every 1 and 5s, with averages of the diffuse-sky plus detector backgrounds. The second phase of the fast burst search covered the whole sky, including regions containing known sources. For the "source-full"

phase, we compared the count rate each ~5, 15, and 60s with a 12 hr average for that swath of sky, taken from the ARK5 database compiled by R. Shafer (1983). Any event more than ~6σ above the expected count-rate triggered the search. In Sections 2.C and 2.D we discuss the mechanics of the "source-free" and "source-full" searches, respectively, in more detail.

In Chapter 3, we discuss the results from both phases of the "all-sky" fast transient survey, and propose identifications. We discuss the events from the direction of the Magellanic Clouds in Chapter 4.

B. Description of the Instruments

In a phenomenological survey such as this one, which was designed to approach the faintest detectable limits, it was important to understand sources of spurious, time variable signals. In fact, we found these systematic effects much more important than the statistical uncertainties. Therefore we devote this section to a brief description of the A-2 instruments, with an eye toward understanding ways of discerning cosmic X-rays from other sources of signals. A more complete description is given in Rothschild et al. (1979).

HEAO 1 A-2, called the Cosmic X-ray Experiment, viewed the X-ray sky through six multi-wire, multi-layer gas proportional counters that were mechanically collimated. That is, metal slats (Al for the argon detector, detector 5; and Cu for the xenon detectors, detectors 3, 4, and 6), crossed in a rectangular, egg-crate, construction, mechanically limited the amount of sky that could be seen to 3°x6°, 3°x3°, and 3°x1.5°. The six detectors covered four energy ranges.
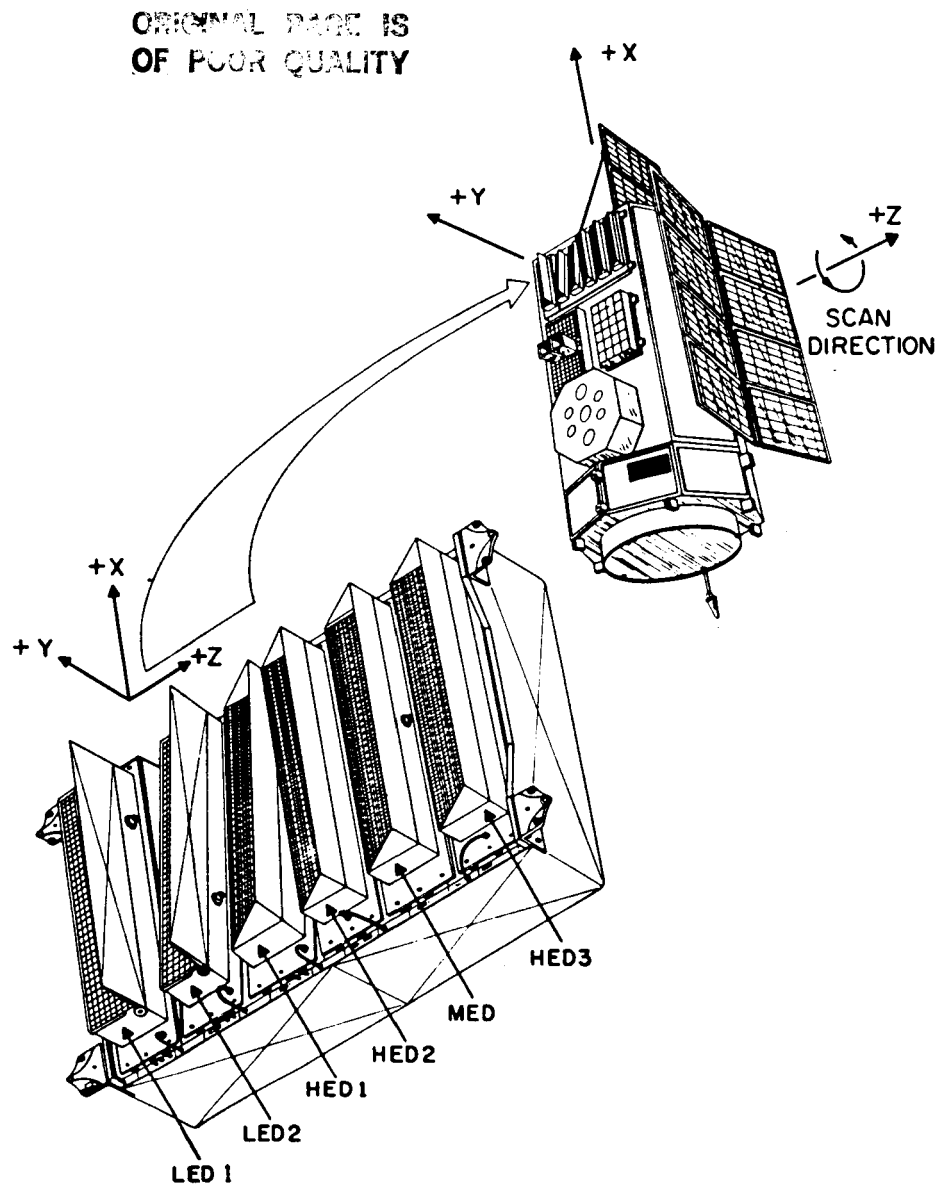
Figure 2.1 Overview of the HEAO 1 A-2 detectors, and of their placement in the HEAO 1 spacecraft. This figure was reproduced from from Rothschild et al. (1979).

Detectors 1 and 2, named the Low Energy Detectors (LEDs), were thin polypropylene window, propane-filled flow counters, sensitive to X-rays with energies between 0.15-3 keV (~4-80 Å). This search did not use them except in a few cases to constrain event spectra at low energies.

Detector 5, the Medium Energy Detector (MED), was argon-filled, with a front window of thin Beryllium, giving it a spectral window of 1.6-30 keV (~0.6-8 Å). Detectors 3, 4, and 6, the High Energy Detectors (HEDs 1, 2, and 3), used xenon as the active gas, giving them more quantum efficiency at higher energies. Detectors 3 and 6 (HEDs 1 and 3) incorporated a front layer of propane sandwiched between sheets of aluminized mylar. (Propane responds only weakly to X-rays, but strongly to the passage of charged particles, so these layers could be used to monitor the flux charged particles incident through the front of the detector.) HED 1 and 3 were sensitive to X-rays with energies ~3-60 keV (~0.2-6 Å). Detector 4 (HED 2) was almost identical save that it did not have this front propane layer. It therefore had slightly higher response at low energies. The fast burst search operated on data from these four detectors.

Figure 2.1 (reproduced from Rothschild et al. 1979), illustrates the placement of the detectors on the HEAO 1 satellite. If we define +Y to be the look-direction of HED2, MED, and HED3 (also LED1), and +Z to be the satellite spin-axis, that points toward the sun, then HED 1 (also LED2) is offset from +Y by a rotation of -6° (6° clockwise) about the +Z axis. This gave us two nearly identical but independent views of the sky. Two of the other three HEAO 1 experiments are also visible in Figure 2.1. HEAO 1 A-1, named the Large Area Sky Survey

(LASS, 0.5-20 keV, (Wood et al. 1984), had one proportional counter facing the +Y direction, but six pointing 180° degrees away in the -Y direction. When available, we used information from A-1 to constrain the time history of events found by our search. The scintillation counters comprising HEAO 1 A-4 (15-1500 keV; Matteson 1978) are visible below the A-1 and A-3 detectors also facing the +Y direction. We occasionally used both A-4 light-curves and A-4 spectral information to help identify some of the burst-search triggers. We have not used information from the Modulation Collimator, HEAO 1 A-3, although in the future we may be able to use it to constrain some of the event source positions.

Robinson-Saba (1982) has written an excellent description of the physics, design, and calibration of gas proportional counters for X-ray astrophysics. Here we summarize just those aspects of proportional counter design that we shall need to refer to in our discussions of sources of spurious temporal variability. Figure 2.2 shows a schematic diagram of a simple proportional counter. It represents the cross-section of a gas-filled cylinder, with a wire anode running down the center. A positive voltage is applied between the wire and the cylinder wall, so that negatively charged electrons will drift toward the anode, in the center, and positively charged ions to the grounded outer wall. (Typical dimensions of such an instrument are ≤ cm in diameter, and tens of cm in length.) If an incoming photon has the right energy, it can be absorbed by the active gas via the photo-electric effect, knocking an electron out and ionizing the atom. (The absorption cross section is largest for incoming photon energies just above the absorption edges of the
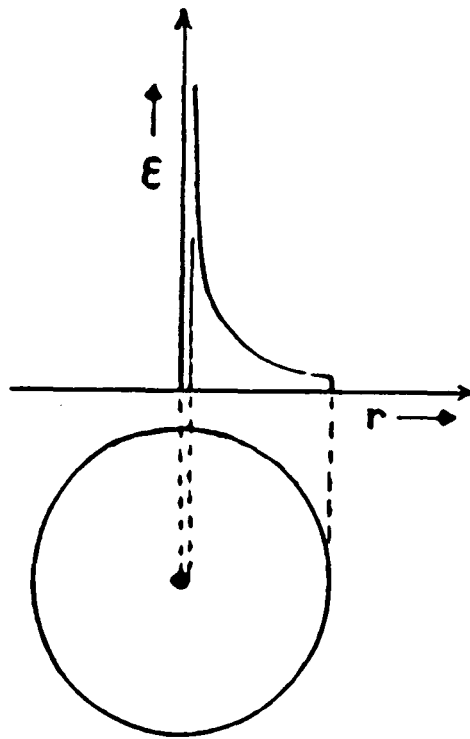
Figure 2.2 Schematic diagram of a simple (cylindrical) proportional counter, with a wire anode in the center, and the grounded outer wall serving as the cathode, from Rossi (1952), showing the electric field is a steep function of the radius.

innermost shells, eventually falling as roughly the energy to the inverse third power as the photon energy increases. For argon, the K absorption edge is at ~3.2 keV; for xenon, at ~35 keV; and three xenon L edges are at ~4.8 keV, 5.1 keV, and 5.5 keV. See Bethe and Salpeter 1977; Weast et al. 1974; Henke et al. 1982). The freed electron then retains sufficient kinetic energy to collisionally ionize ~N-1 more atoms, where N is roughly proportional to the energy E of the incoming photon, divided by the gas ionization potential ϵ. In a proportional counter, the electric field near the anode wire is adjusted to be strong enough to accelerate each of the N initial electrons into more ionizing collisions. Through a cascade of collisional ionization, electron reabsorption, photon emission, and photo-electric ionization, the total signal will be MxN, or ~MxE/ϵ. For the A-2 detectors, the multiplication factor M was about 2-4x10^3 for cylinders of dimension ~0.5" with anode wire diameters of 2 mil, and voltages of ~2000V (Robinson-Saba 1983).

Note that the detector described above will react to any sort of ionizing radiation, including charged particles such as cosmic rays. However, X-ray photons, which interact mainly through the photo-electric effect, deposit all their energy in a short distance. Charged particles (such as those trapped in the Earth's radiation belts) ionize through collisions, and so leave a wake of ion pairs (the length of which depends on the speed of the charged particle). Two methods of distinguishing among photon and charged particle events have been used in astrophysical detectors. One is based on the pulse shape; The A-2 detectors relied on "anticoincidence" (Rossi 1952; Evans 1967).

Figure 2.3.a shows a cut-away view of the multi-wire, multi-layer HEAO 1 A-2 proportional counters. Below the rectangular counters, one sees that the sensitive volume of the detector has been partitioned into an array of 0.48"x0.48"x21.5" rectangular proportional counter cells. The grounded outer cylinder of Figure 2.2 has been replaced, in each cell, by thin grounded wires, spaced ~0.04" apart. A charged particle, laying down its distinctive track of ion pairs, can travel freely from one cell into the next. Events that trigger in two or more cells simultaneously can then be rejected ("anticoincidence").

In Figure 2.3.b we diagram the A-2 detector grid connections. One layer of cells on the sides and bottom of each detector was used to reject signals from ionizing radiation that entered through the detector walls. In MED and HED2, the signals from the anodes along both side walls formed the first veto rate, V1, while those from the bottom layer of anodes comprised V2. In HED1 and HED3, counts from the front layer of propane formed the second veto rate, V2, while those from both sides and bottom were connected to form V1. Within the volume used to detect X-rays, every other anode in each of 2 layers was wired together to form the detector "left" (L1, L2), and "right" (R1, R2) rates. Active on-board electronics rejected any event that triggered the veto rates, either both left and right sides, or both first and second layers, in each detector. This eliminated over 99% of the counts from the continual rain of cosmic rays that bathed the satellite (Tennant 1983; see Chapter 4).

What remained, an internal detector background from the residual cosmic ray events, was monitored through differing size collimators on the "left" and "right" sides of the detectors. All were 3° wide FWHM

CUTAWAY VIEW OF PROPORTIONAL COUNTER

ANODE

GND PLANE

.460

COLLIMATOR

LI

VI

L2

LAYER NOT PRESENT I HED II

RI

VI

R2

V2

LED, MED, HED II

COLLIMATOR

LI

L2

V2

RI

VI

R2

ALPHA

HED I/III
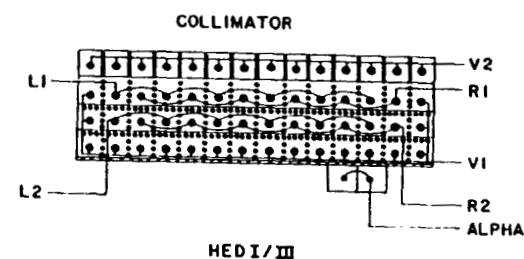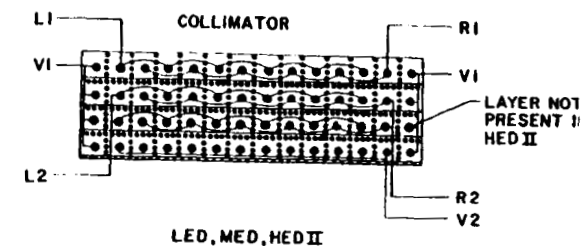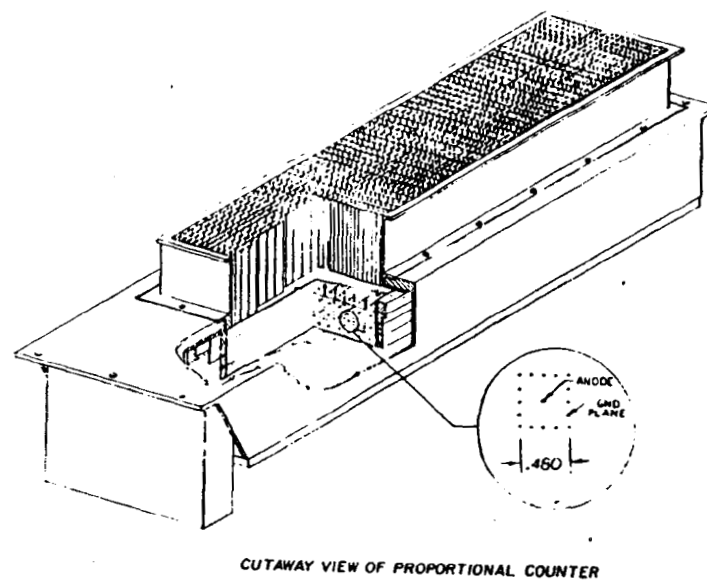
DETECTOR GRID CONNECTIONS

Figure 2.3.a Cut-away view of a HEAO 1 A-2 proportional counter, also from Rothschild et al. (1979).

Figure 2.3.b Diagram of the detector grid connections (ibid).

perpendicular to the scan direction. The "left" side of each was also 3° FWHM in the scan direction; while the "right" sides of HED1 and HED2 were 6° FWHM, and those of MED and HED3 were 1.5° FWHM in the scan direction. From the wiring diagrams in Figure 2.3.b, one sees that each side contained background counts from essentially the same active volume of each detector, but differing fractions of the diffuse X-ray sky glow. In regions that did not contain bright sources, this could be used to measure the contributions of each to the total count rate. (See Shafer 1983 for a thorough, quantitative, discussion.) However, several times a day the satellite was showered with an increased flux of charged particles, and thus an increase in detector background count-rate. The detector "anticoincidence" and "veto" rates were accumulated every 40.96s, as part of the housekeeping rates available for software tests of data quality.

In this search, we used three tests for times of increased particle contamination. One was simply a limit on the total anticoincidence rate for each detector. One due to F. Marshall (unpublished) checks for soft electrons (that might be too slow to trigger the anticoincidence) by setting limits on the HED3 propane layer veto rate, minus a fraction due to the few counts from X-rays. The third is the standard electron contamination flag determined by A. Rose (see Tennant 1983). It sets limits on a linear combination of the anticoincidence and veto rates from each detector. We also considered the geometry of the orbit. We excluded times when the spacecraft passed through the South Atlantic and the North Pacific Anomalies, regions of particularly high particle flux. For the "source-free" search, we also considered the position of the

32

spacecraft with respect to the Earth's magnetic field, as parametrized by McIlwain's 'L' parameter (Tennant 1983 and McIlwain 1961; see also Section 2.C).

The tests for cosmic ray contamination were not the only data quality tests. Since HEAO 1 was in a low-Earth orbit, the X-ray sky was occulted by the Earth's disk nearly half the time. Also, as the detector fields of view swept over the Earth's upper atmosphere, they would occasionally register an increase in count-rate from soft X-rays from the Sun reflecting off the upper layers of the atmosphere. We therefore excluded times from our search when the detectors were pointing within 200 km of the Earth's rim. This reduced the "on" time of each instrument by about 1/2.

We also required the instruments to pass the standard detector status tests, including voltage stability, proper data format, and no bit errors. For the "all-sky" portion of our search, we also found it necessary to check both the magnitude of the position errors, and the type of scanning motion the satellite was performing at each time. When the detectors were not moving as expected, our calculation of the 12 hr average for that position was not correct.

When a detector passed all these tests, which were calculated every 40.96s, it was designated "on" for the purposes of the fast burst search. Typically, each detectors was "on" only 1/4-1/3 of the time. That is, though the instruments spun past each strip of sky 21-23 times in 12 hours, they were apt to be on for only 6-8 passes over a source during that time. Of the four instruments, HED 1 and HED 3 (which both had a propane veto layer in front) were the most reliable; while HED 2 most frequently had contaminated rates.

C. Phase 1: Gleaning Good Events From "Source-Free" Data

In the early stage of our fast burst search (published in Connors, Serlemitsos, and Swank 1986) we considered only the simpler problem of finding these flashes of X-rays among regions free of sources brighter than ~1 millicrab. Our search ran on the XRATES database described by R. Shafer (1983), and references therein. This contained X-ray rates from all the instruments over the whole lifetime of the satellite, ordered by time, and including data quality and detector status flags. Among these was a source-in-field-of-view flag, which was based on a catalog of X-ray sources known prior to 1981. All flags were updated every major frame of the spacecraft telemetry, or every 40.96 s. Regions of sky as far as $14°$ from a source could therefore have been labeled "source" data. For this first phase of our search, along with the data quality tests described in the previous section, if this flag indicated a source was in a detector's field of view, we designated that detector "off". This last requirement reduced our "on" time by about 1/2. The HED1 and HED3 instruments together were on for the equivalent of 64 continuous days (about 55 days each), the MED for 54, and the HED2 for 49.

As described in the previous section, each instrument measured four rates, two from each "side" of its two layers (L1, R1, L2, and R2). For better signal to noise ratio, we used the top layer of each of the xenon proportional counters, but both layers of the argon proportional counter. Overall, our greatest response was in the energy range 2-20 keV. (We could have preferentially selected against extremely hard events, by choosing only the top layer. However, the

34

softer rates were less susceptible to charged particle

contamination.) We used all three available fields of view, adding

together both sides of the three co-aligned detectors ($3°x3°$ and

$3°x1.5°$ for MED(L1+R1+L2+R2) and HED3(L1+R1), or $3°x3°$ and $3°x6°$ for

HED2(L1+R1)), but keeping separate the left and right sides of the one

offset detector ($3°x3°$ for HED1(L1) and $3°x6°$ for HED1(R1)).

In this early stage of our work, we concentrated on the shortest

feasible integration times, which were 5.12 and 1.28 s for this form

of "rates" data. We chose the burst search thresholds so that one

would expect a trigger on purely Poisson statistical fluctuations to

occur about once a decade for the 5.12s data, or roughly once in three

years for the 1.28 s data. (Barring non-Poisson effects, this was

equivalent to ~6σ. At this high confidence level, we found

systematic effects - signals from sources other than cosmic X-rays

that had not been excluded out by the automatic checks described

earlier - rather than statistical fluctuations, were the major source

of spurious events.) We also required coincidence when more than one

of the three co-aligned instruments (HED2, MED, and HED3) was on.

That is, rather than summing the rates from the co-aligned detectors,

we required them to be above their respective thresholds

simultaneously to trigger the burst search:

2.C.1 COUNTS(HED2)>THRESHOLD(HED2) <u>and</u> COUNTS(MED)>THRESHOLD(MED) <u>and</u>

COUNTS(HED3)>THRESHOLD(HED3); <u>or</u> COUNTS(HED1)>THRESHOLD(HED1).

Our threshold varied in accordance with how many of the three co-

aligned detectors was on (to keep the probability of triggering on

statistical fluctuations at ~6σ). If BACK(DET) was the expected

count-rate from instrument plus diffuse sky glow, we required

2.C.2   THRESHOLD(DET,# on) = BACK(DET) + n(# on)·√BACK(DET).

We set $n(3)$, $n(2)$, and $n(1)$ at ~3, 4 and 6, respectively. The
background rate was usually 57 counts per 5.12 s for HED3(L1+R1) and
MED(L1+R1+L2+R2), and 136 counts per 5.12 s for HED2(L1+R1). These
rates rose with cosmic ray flux. Studies of HEAO 1 A-2 background
rates (Tennant 1983 and references therein) showed a correlation with
the McIlwain (1961) parameter L, where L labels a line of the Earth's
magnetic field by its height at the magnetic equator, measured in
Earth radii, and determines the energy of cosmic rays screened by the
Earth's field. For the HEAO 1 orbit, L ranged between 1 and 2. For
L≤1.2, when all three of the co-aligned detectors were on, we set the
computer search threshold at 80 counts per 5.12 s for HED3 and MED,
and 171 counts per 5.12 s for HED2. This corresponds to a flux level
of roughly 4 millicrabs, or about 10^{-10} ergs-cm^{-2}-s^{-1} in the 2-20 keV
range. If only two of the co-aligned detectors were on (usually HED3
and MED), for L≤1.2 the search threshold was raised to 87 counts per
5.12 s for each, or about 5 millicrabs. If only one of the three was
on, and L≤1.2, we required the rates to be above 102 counts per 5.12 s
for HED3 and MED, and 206 counts per 5.12 s for HED2. This was about
8 millicrabs. The computer search threshold for the (independent)
offset detector, the HED1, was never set less than this highest level.

When the McIlwain L parameter was greater than 1.2, the typical
background rate rose at a rate of about 1 count per second per layer
times (L-1.2) (Tennant 1983). For periods of high McIlwain L, we
raised our thresholds accordingly.

For this source-free search, we processed the data twice: once
with an integration time of 5.12 s, then with an integration time of

1.28 s. Since the expected number of background counts in each time bin was reduced by 1/4 during this second pass through the data, we reduced our effective threshold for events with durations less than 1.28 s by ~1/2.

Once we had completely processed the data with this burst-search algorithm, we sifted through the list of triggers to discard those not from cosmic X-rays. We eliminated those that did not come from a point source by rejecting times when the rates in each detector were high for longer than the ~30-60 s it took for an instrument to scan past a point source. The majority of these were from the rising or falling edge of an electron storm. Since the data quality flags were calculated every 40.96 (every major frame), we occasionally found the last (or first) few 5.12 s rates to be high just before (or after) a major frame registered quite high electron contamination rates. We also saw the types of events described by Tennant (1983) in his Appendix C, including: occasional reflections of soft solar X-rays from the Earth's upper atmosphere; gamma-rays from a massive solar flare on July 11, 1978 (D.O.Y. 557); electrons apparently triggering a Cu fluorescence line in the MED collimators; and what Tennant describes as Auroral X-rays. (Also see the description of "trash times" in Shafer 1983.) Another indication of the quality of the data was the form of the spectrum from each event, when it was available. If an event was near a major frame with high electron rates, but the spectrum seen in all available detectors was consistent with that from X-rays rather than cosmic rays, we did not reject that event.

For this source-free search, we also eliminated a few triggers that were near UHURU or ARIEL V X-ray sources that had not been

signaled by the automatic source-in-field-of-view flag. We also considered the effect of the intrinsic fluctuations in the diffuse cosmic X-ray background studied by Shafer (1983), but found them to be at most 10% of the statistical fluctuations at these integration times. We therefore did not take them into account.

With the procedures described here, one could distinguish four classes of short transients:

1. Events that lasted for at most one integration interval. For the shortest integration time used, this would imply that the event had a lifetime of ~1 s or less.

2. Events that lasted more than one integration interval, but less than the entire 90 s that a single point source could have been in the field of view of both the co-aligned and offset detectors. This would imply a lifetime between 1 and 90 s.

3. Events that lasted at least as long as it took the instruments to scan across a point source once, with all four detectors, but less than two complete scans. Since the rotation period was ~32-35 minutes, this would imply an event duration between 90 and 4×10^3 s.

4. Events that lasted for more than one complete scan. These would have had lifetimes comparable to those seen with the ARIEL V fast transient sky survey (Pye and McHardy 1983) with durations greater than 4×10^3 s.

Our 5.12 s fast burst search algorithm found only six events, five of them new, all of type 3, with lifetimes greater than 90 s but less than 4×10^3 s. We found no new events when we repeated the search
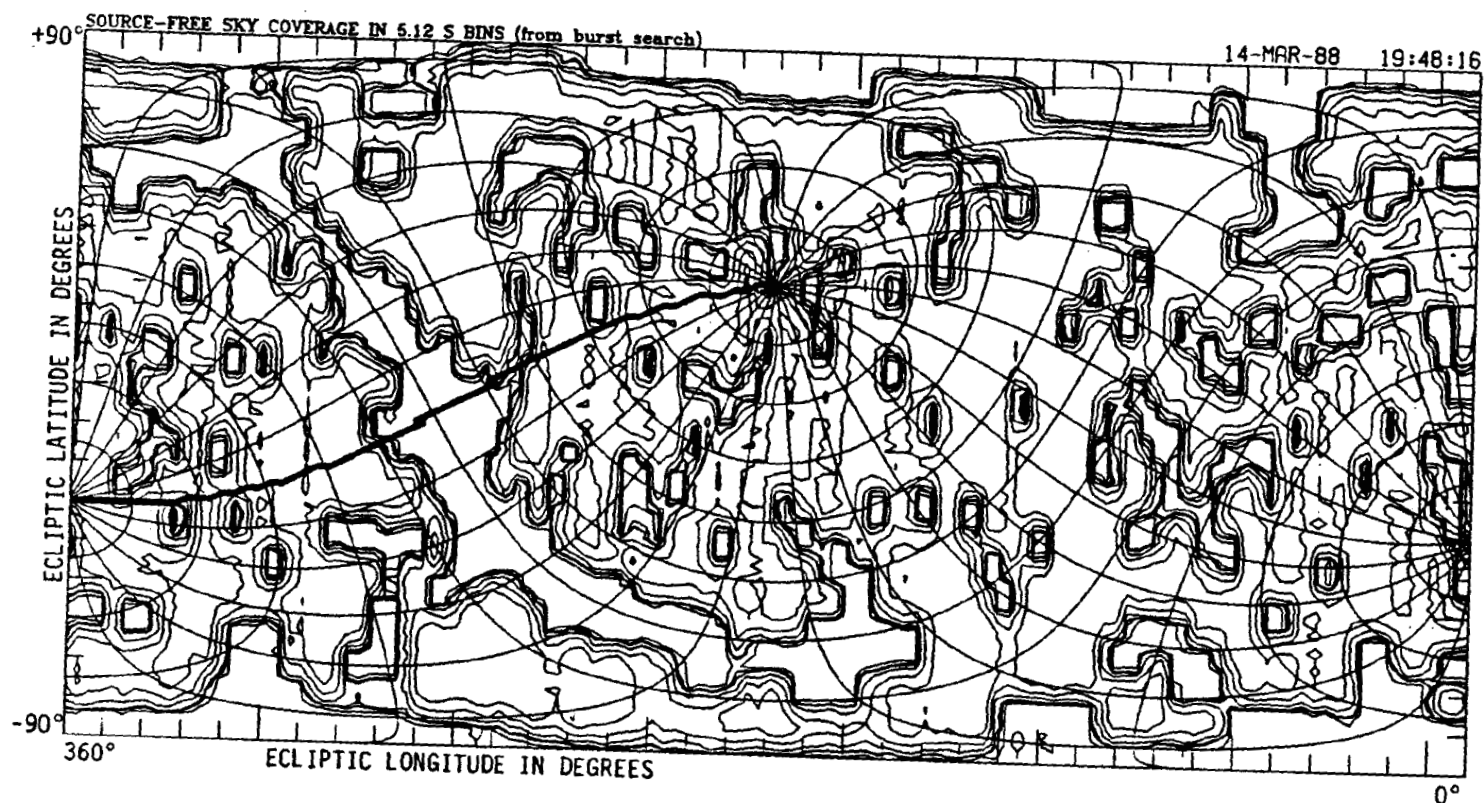
Figure 2.4 Three-dimensional map representing the source-free sky coverage. The the map is divided into 3°x1.5° rectangular bins, with no correction for unequal areas, so that the Ecliptic poles each stretch along an entire side of the map. The Z axis (height) represents the total number of good 5.12 s intervals, in each 3°x1.5° bin, in the "source-free" sky survey.

with an integration time of 1.28 s. We discuss these events in more detail in Chapter 3.

D. <u>Phase 2: Gleaning Good Events From the Whole Sky</u>

We display a map of the regions of sky (in Ecliptic coordinates) covered by the source-free search in Figure 2.4. The contours in the coverage map represent the total number of 5.12 s integration bins, per 3°x3°, during which the HED3 detector axis pointed towards that region. We presented this map in rectangular Ecliptic coordinates, with no corrections for the unequal areas in each 3°x1.5° bin, to better represent the experiment's view of the sky. Since, while in scanning mode, the look-direction of the detectors swept out great circles on the sky which passed over the Ecliptic poles, a source ~1.5° from an Ecliptic pole was viewed over 30 times more often than one near the Ecliptic equator. Also, there appears to be a slight bias against the Galactic plane, due to the exclusion of regions containing sources. This made it difficult to conclude anything about the distribution of the events from the "source-free" sky search; were they isotropic, or did they tend toward the Galactic plane?

To attack this problem, we undertook, in this second phase of our fast burst search, to look for short X-ray transients over the whole sky, including the Galactic plane and Magellanic Clouds. We also expected to gain about a factor of two in detector "on" time by relaxing the "no source in field of view" restriction. We found we could not completely ignore the presence of known X-ray sources without being swamped with literally hundreds of triggers from objects such as Cygnus X-1 or Vela X-1. We therefore made a table of 17

bright variable sources, to exclude data from times when they were in the fields of view. We list these sources and their distinguishing characteristics in Table 3.1. Since the satellite moved (most of the time) in Ecliptic coordinates, scanning in Ecliptic latitude and precessing in Ecliptic longitude, we found it convenient to list these sources by their Ecliptic coordinates, with $\pm 3°$ limits on each coordinate. Whenever a detector axis pointed within one of these $6° \times 6°$ boxes, it was designated "off" for the purposes of this all-sky search.

Aside from this table of bright varying sources, the all-sky fast burst search program referenced a catalog of X-ray sources (of almost all reported X-ray sources brighter than ~1 millicrab at 2-20 keV), also in Ecliptic coordinates, and also listing $\pm 3°$ limits. Whenever the program triggered on an event, it used a look-up table to find what catalog sources were in the field of view of all the triggering detectors at that time. If more than one source satisfied these criteria, it chose the one designated in the catalog as more variable, or brighter, in that order. If one particular source in the catalog was identified by the burst search as the source of more than six triggers, it automatically moved that source to the table of bright varying sources. Henceforth it would find any time containing that source to be "off". Sources such as KZ TrA (X1627-673) and the Rapid Burster (X1730-333) fell into this category.

We used the same detector rates (HED1 L1, HED1 R1, HED2 L1+R1, MED L1+R1+L2+R2, and HED3 L1+R1) as in the earlier form of the search, and again required coincidence among co-aligned detectors. We also employed the same form for the search trigger threshold:

41

2.0.1   THRESHOLD(DET) = BACK(DET) + n·√BACK(DET).

However, since none of our original events had durations less than
~80 s, we attempted to lower our effective threshold for these longer
events by considering 15.36 and 61.44 s intervals, as well as the
original 5.12 s.

Consider the response of the detectors to a point source, as they
scanned across it (Shafer 1983; Rothschild et al. 1979). If we
designate time bin "i" as the one which contains the peak flux, and
assume triangular response, then one can show that on average, the
total flux in time bin "i+1" summed with that from bin "i-1" is
approximately half that from bin "i". We calculate this factor more
explicitly, for the actual detector geometries involved, in the first
part of Appendix A. So we required, for each 5.12 s interval, that
either the rates in all co-aligned detectors are above our original
threshold formula, with n(3), n(2), and n(1) ~ 3, 4, and 6, as before;
or that the peak flux in time bin "i" (in all co-aligned detectors) is
above a slightly lower threshold, and that the sum of the flux in time
bins "i-1" and "i+1" is greater than about 1/2 that same lower
threshold. We list the values of n(# on) we used for this search in
Table 2.1, for 1, 2, and 3 detectors "on"; and for 5.12 s, 15.36 s,
and 61.44 s time intervals. For the last case, we required that not
only did the co-aligned instruments satisfy our 15.36 s search
criteria, but 6° (or ~6 5.12 s time bins) later, the offset detectors
did as well. The Poisson probabilities associated with each type of
trigger are also discussed in Appendix A.

42

Table 2.1 All-Sky Search Threshold Values

Time Interval For Trigger	Value Of 'n' For: 1 Detector On	2 Detectors On	3 Detectors On
5.12 s	6.00	3.89	2.98
15.36 s	4.23	2.68	1.96
61.44 s	2.68	1.96	1.51

Obviously we could not use the same calculation for background as in the source-free search. Instead, we turned to the ARK5 database of R. Shafer (1983). This is a particularly clean, carefully constructed database of 12 hour sums of all the 1.28 s rates of all the A-2 instruments. It is in the form of great circles on the sky, each divided into 1800 0.2° bins. Since the satellite's spin axis was stepped ~0.5° every 12 hours, each great circle corresponded to about 12 hours of scans. Shafer (1983) gives a complete description. To calculate the expected count rate, the all-sky fast burst search first determined which great circle corresponded to that time, and then added together all the 0.2° bins corresponding to that position. For a 5.12 s integration time, during which a detector look direction swept through ~0.9°, the procedure which calculated the expected count rate would typically add together four 0.2° bins, plus a fraction of a fifth.

Calculating the background from the ARK5 database in this manner introduced several problems not associated with our earlier search. First, it was possible for the 1.28 s rates to overflow, for sources brighter than 200 cts/s (Rothschild et al. 1979; Shafer 1983). The 5.12 s rates did not have this problem. Second, it was occasionally possible for one of the 0.2° bins used to calculate the expected count rate to be empty of data. If either of these was the case, the affected detector was designated "off" during that 5.12 s interval. A third problem arose from a changing mean in the vicinity of bright sources (> 500 counts per 5.12 s). Not only did the mean HEAO 1 satellite spin axis move about 0.5° per 12 hrs, but it performed apparently random walk motion, "jittering" in position, by at most ±1°
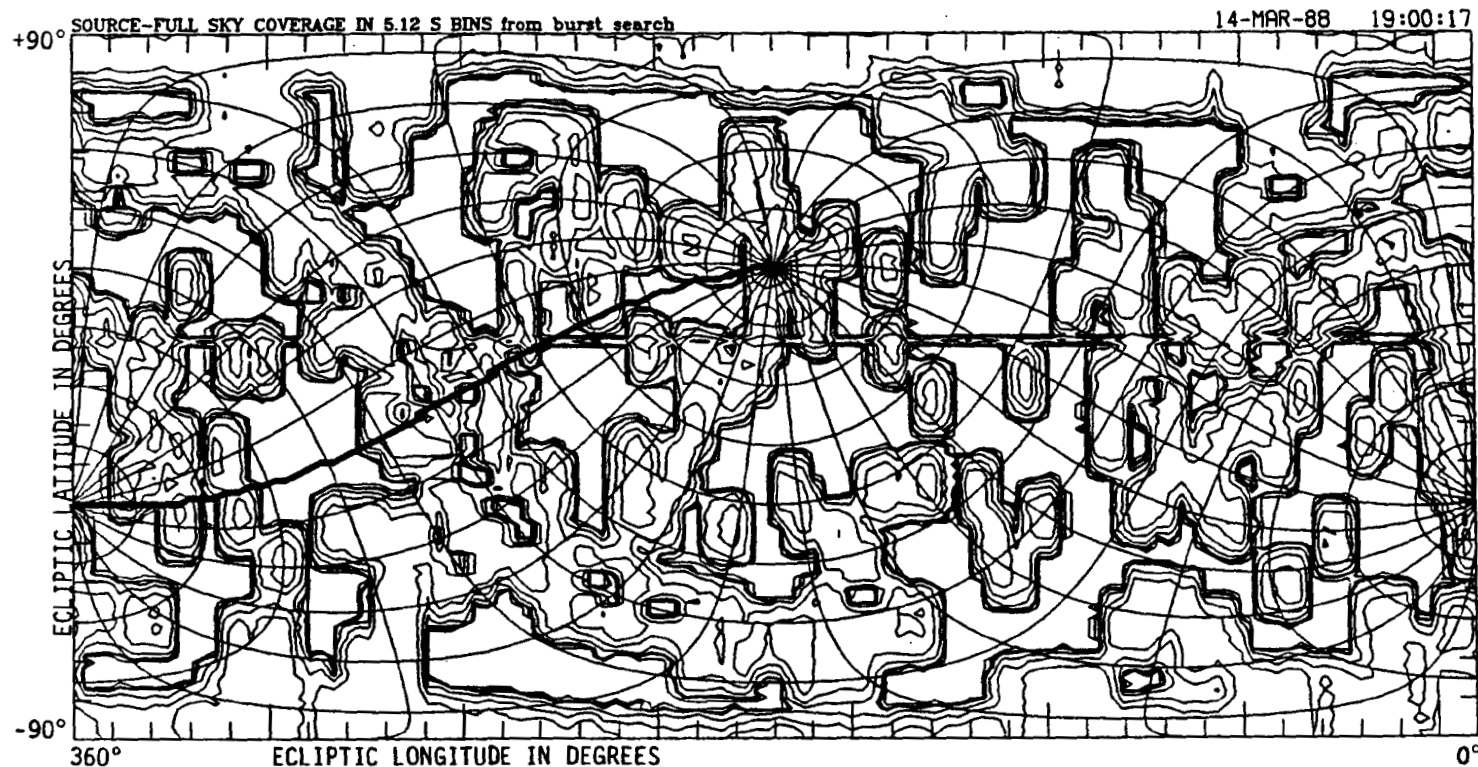
Figure 2.5 Three dimensional map representing the "source-full" sky coverage (i.e. the "all-sky" coverage minus the "source-free" sky coverage). The the map is divided into 3°x1.5° rectangular bins, with no correction for unequal areas, so that the Ecliptic poles each stretch along an entire side of the map. The Z axis (height) represents the total number of good 5.12 s intervals, in each 3°x1.5° bin, in the all-sky survey, that were not designated "source-free".

about the mean spin axis position, on time-scales of several major frames. It was therefore possible for a nearby bright source to wobble into the edge of the instrument fields of view from the off-scan direction. The 12 hour mean might still be quite low, but if the source were bright enough, even if it did not intrinsically vary, it was possible for the all-sky search algorithm to trigger on it during the scans when the source moved more prominently into the field of view (due to this movement in the off-scan direction). Steady sources that triggered in this manner included CAS A, the Tycho SNR and the Crab SNR. We therefore eliminated, after the fact, any triggers for which a changing mean was a possible explanation.

Fourth, this method of comparing 5.12 s rates to the ARK5 12 hour average was very sensitive to errors in position. Any deviations from normal scanning motion, such as the satellite maneuvers for "pointed" observations, could cause spurious triggers of this type. We therefore designated all detectors "off" whenever the scan rate was too slow, too fast, or in the wrong direction; or when the estimated Y-axis or Z-axis position uncertainties were greater than $0.05°$ per 5.12 s.

In Figures 2.5, 2.6 and 2.7 we displayed three contour maps of the sky covered by this all sky fast burst search. In the first two we presented the density of satellite coverage, in the same units used for Figure 2.4, of the additional coverage added by the all-sky search, and of the total coverage of the all-sky search, respectively. (One might think of Figure 2.5, which was made by subtracting the "source-free" sky coverage from that of the "all-sky" search, as representing the coverage of the "source-full" sky.)

46
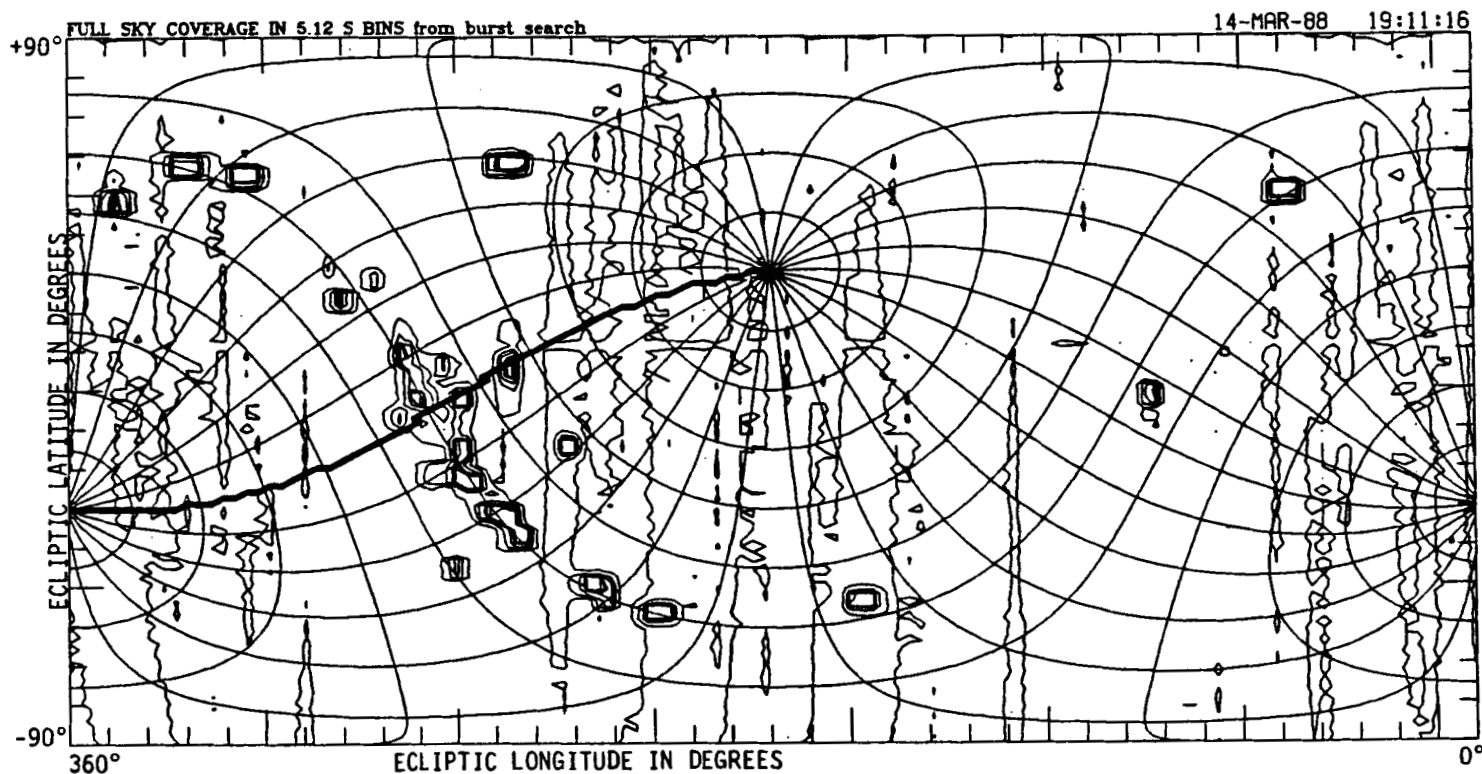
Figure 2.6 Three dimensional map representing the "all-sky" coverage (i.e. the "source-full" coverage plus the "source-free" sky coverage). The the map is divided into 3°x1.5° rectangular bins, with no correction for unequal areas, so that the Ecliptic poles each stretch along an entire side of the map. The Z axis (height) represents the total number of good 5.12 s intervals, in each 3°x1.5° bin, in the all-sky survey.

In the fourth contour map, Figure 2.7, we illustrated the differences in average X-ray flux over the whole sky by displaying the mean HED3 5.12 s background-subtracted count-rate in each rectangular 3°x1.5° bin. (We reiterate that these are not bins of equal area). We chose to display the HED3 count rate because it was the detector that was on the most often. For Figure 2.7, we chose to display the sum of the 1.5° and 3° fields of view in the first layer of HED3 since this was the quantity used by the fast transient search programs. This map therefore could be considered as the X-ray sky as viewed by the HEAO 1 A-2 fast transient search. Since the all-sky search threshold was a monotonic function of the expected count rate in each time bin, this figure illustrates the changing search thresholds across the sky. We point out that the "source-full" sky did not contain a greater fraction of the Galactic plane than did the "source-free" search, contrary to our original expectations, due to the exclusion of ±3°x3° regions around bright variable sources. However, the source-full sky did contain more regions with higher average count rates, and more closer to the Galactic center.

We illustrate the differences in "all-sky" and "source-free" sky coverage with five histograms of the number of good 5.12 s intervals at various levels of mean HED3 flux, in Figure 2.8, at the end of this chapter. In the first histogram we presented the "source free" sky coverage (corresponding to Figures 2.4 and 2.7); in the second we displayed just the additional coverage added by the all-sky search (corresponding to Figures 2.5 and 2.7); while in the third we presented the total coverage (from Figures 2.6 and 2.7) for the all-sky fast transient search. Although for all cases the most probable
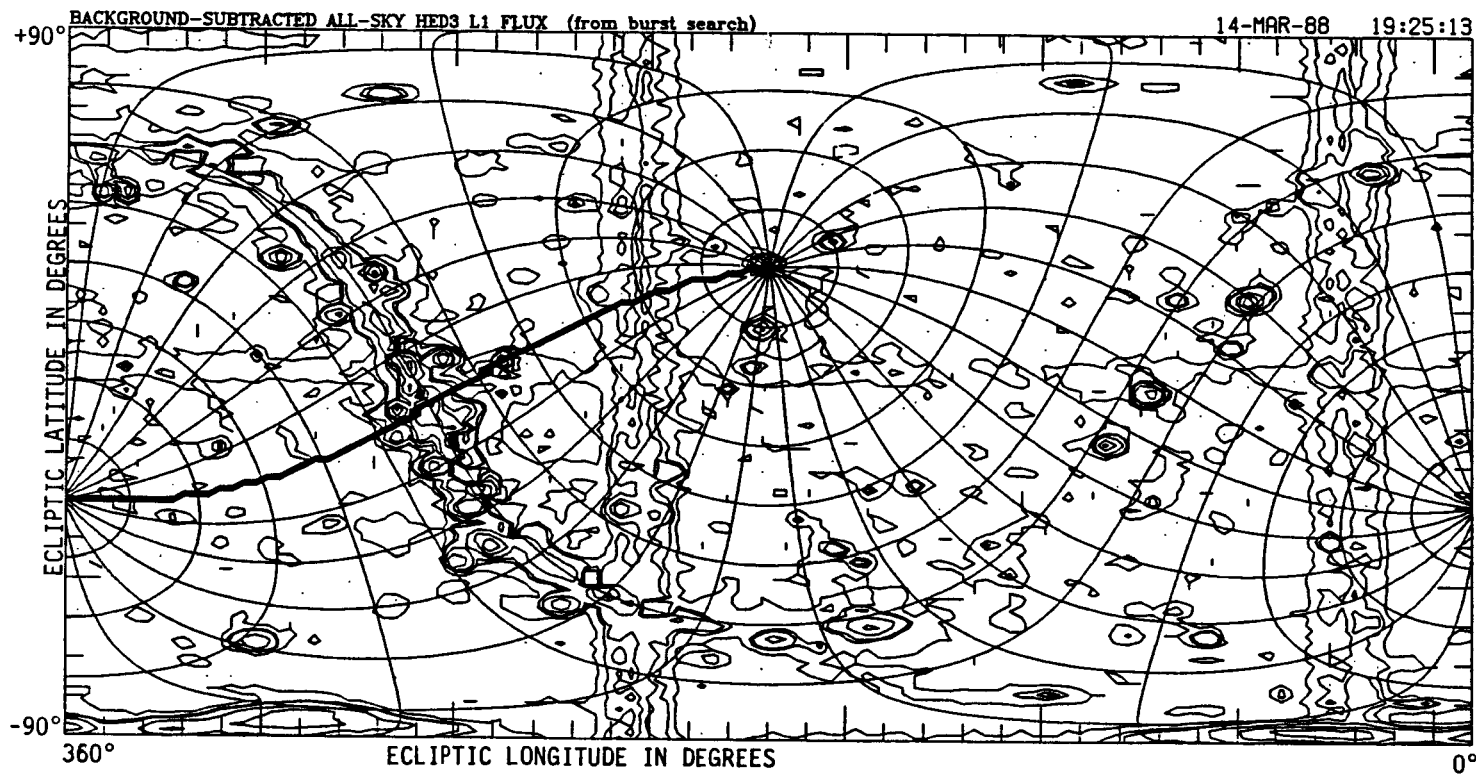
Figure 2.7 A three dimensional map representing the average X-ray flux over the whole sky, in 3°x1.5° rectangular bins (not of equal area). The map is divided into 3°x1.5° rectangular bins, with no correction for unequal areas, so that the Ecliptic poles each stretch along an entire side of the map. The Z axis (height) gives the mean background-subtracted HED3 layer 1 5.12 s count rate, averaged over each 3°x1.5° bin.

count-rate was zero (effectively blank sky), the addition of "source-full" sky changed the mean count-rate from ~0.8 HED3 cts per 5.12 s, for the source-free portion of the search, to ~2.9 HED3 cts per 5.12 s, for the all sky phase of the search, with the addition of a long tail in the high mean flux direction. In the last two plots we present similar histograms of the source-free and source-full sky coverage, but limited to ±15° on either side of the Galactic plane, to demonstrate that the "source-full" sky did not contain a greater percentage of Galactic plane data than the "source-free" sky.

For the "all-sky" fast transient search, considering just good 5.12 s intervals, one finds the HED1 and HED3 instruments were on for the equivalent of 104.45 continuous days each (about 86.7 days of that overlapping); the MED for 79.6; and HED2 for 47.6. This was about a factor of two increase over the first phase, the "source-free" sky fast transient search. Recall that the all-sky search algorithm also looked at 15.36 s and 61.44 s intervals, to lower the search threshold for events longer than ~1 minute. We found that three adjacent 5.12 s intervals were good (allowing the use of the lower 15.36 s threshold) for 100.7 d of the data; and the corresponding three 5.12 s intervals in HED1 data, 30 s later, were good (allowing the use of the lower 61.44 s threshold) for the equivalent of 86.72 days.

We treated the region around the Magellanic Clouds as a special case of the all sky search, since the region was too crowded to require eliminating all triggers within ±3° of known LMC/SMC X-ray sources. Instead, we generated 99% confidence position limits (in the manner described in Chapter 4 and Appendix B) for each event in the Magellanic Clouds region. We then scrutinized the spectra, and long

and short term (<100 s) light curves of the individual events. One can see, from Figure 2.5, that since the Magellanic Clouds lie so close to the South Ecliptic Pole, there was a wealth of coverage of that region.

We discuss both the triggers from the Magellanic Clouds region, and those from the rest of the sky, in detail in the following two chapters.

Figure 2.8 Five histograms of coverage per mean HED3 flux. The ordinate in each is the number of good 5.12 s intervals that has a background-subtracted mean HED3 layer 1 count rate (calculated for the 3°x1.5° rectangular bins illustrated in Figures 2.4 and 2.5) falling within that bin. The abcissa is the background-subtracted mean HED3 layer 1 5.12 s count rate, in 100 bins of width 1 ct per 5.12 s.
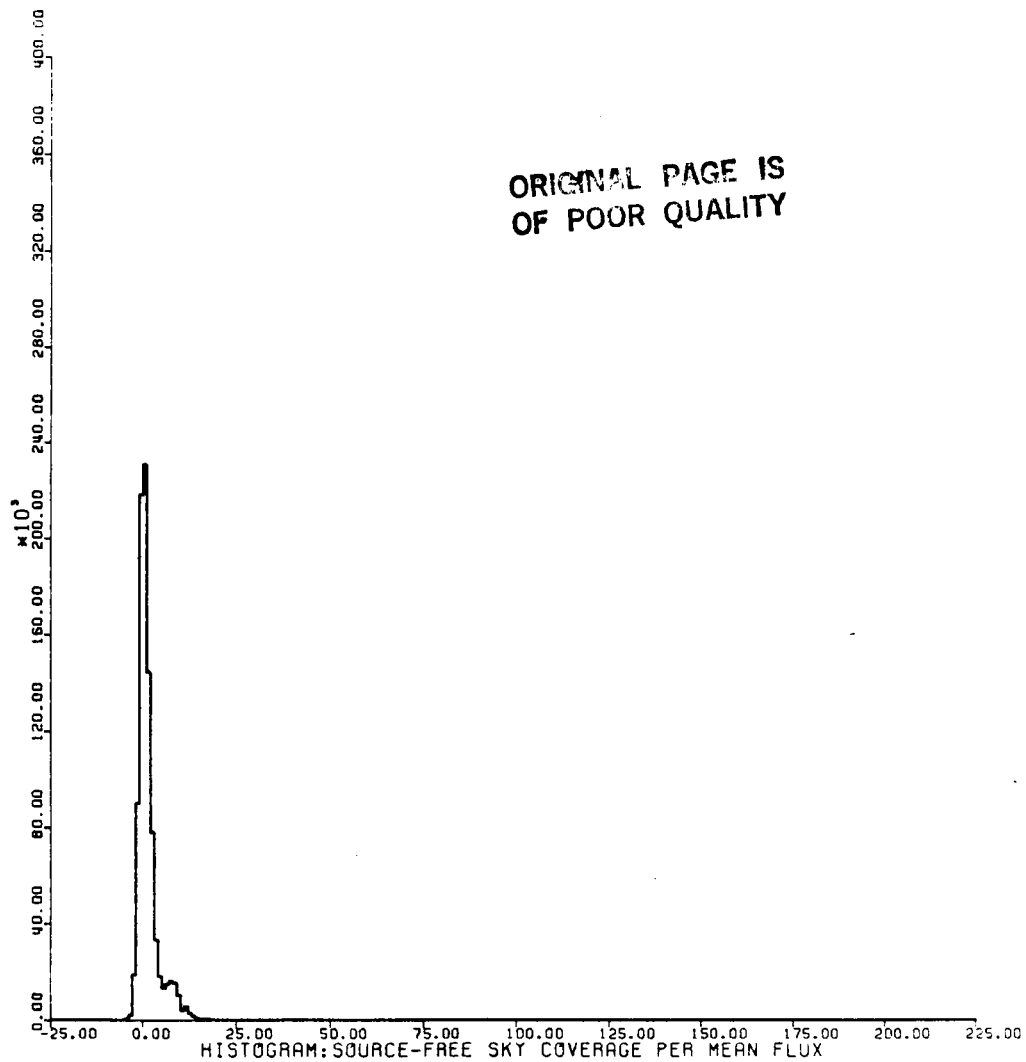
Figure 2.8.a Histogram of the "source-free" sky coverage per mean

HED3 flux, for the whole sky.

ORIGINAL PAGE IS
OF POOR QUALITY

HSTGRM:SOURCE FULL SKY COVERAGE PER MEAN H3 FLUX
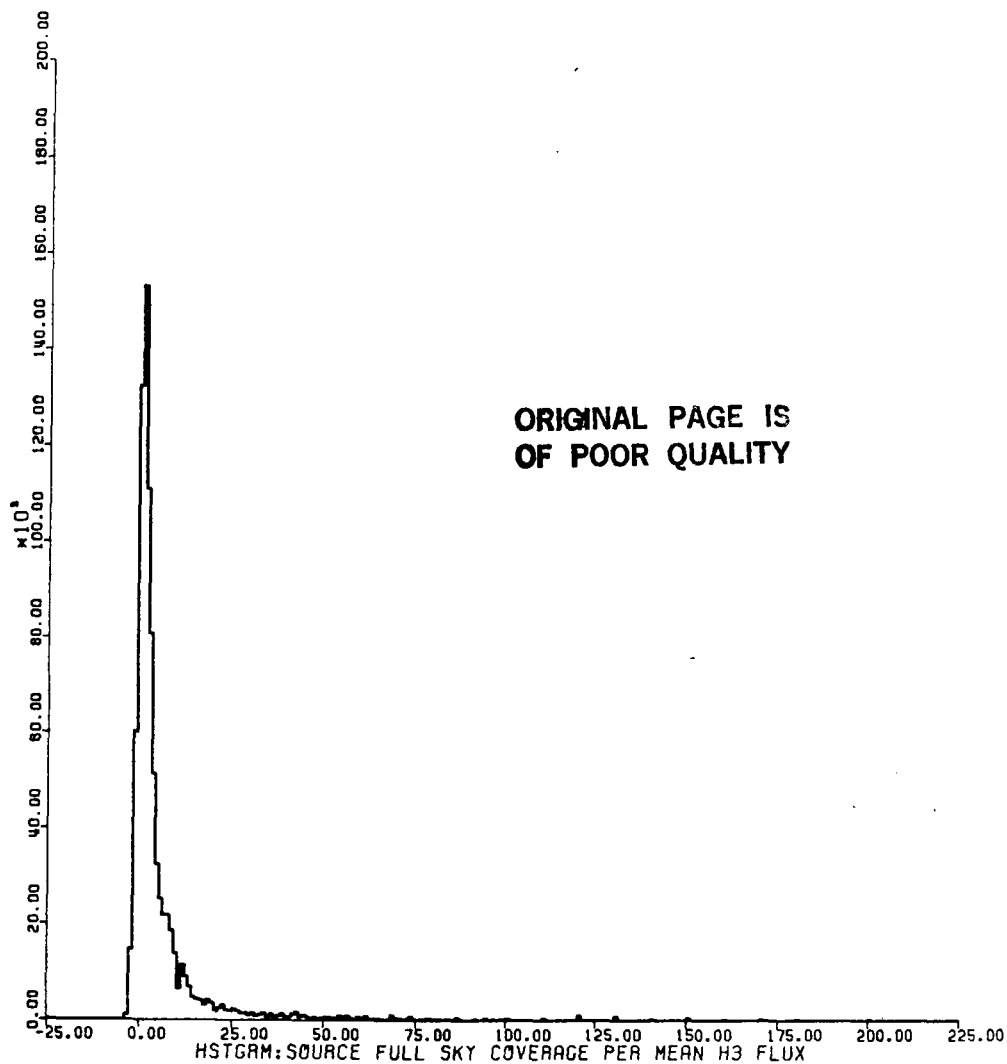
Figure 2.8.b Histogram of the "source-full" sky coverage ("all-sky"
coverage minus that for the "source-free" search) per mean HED3
flux, for the whole sky.
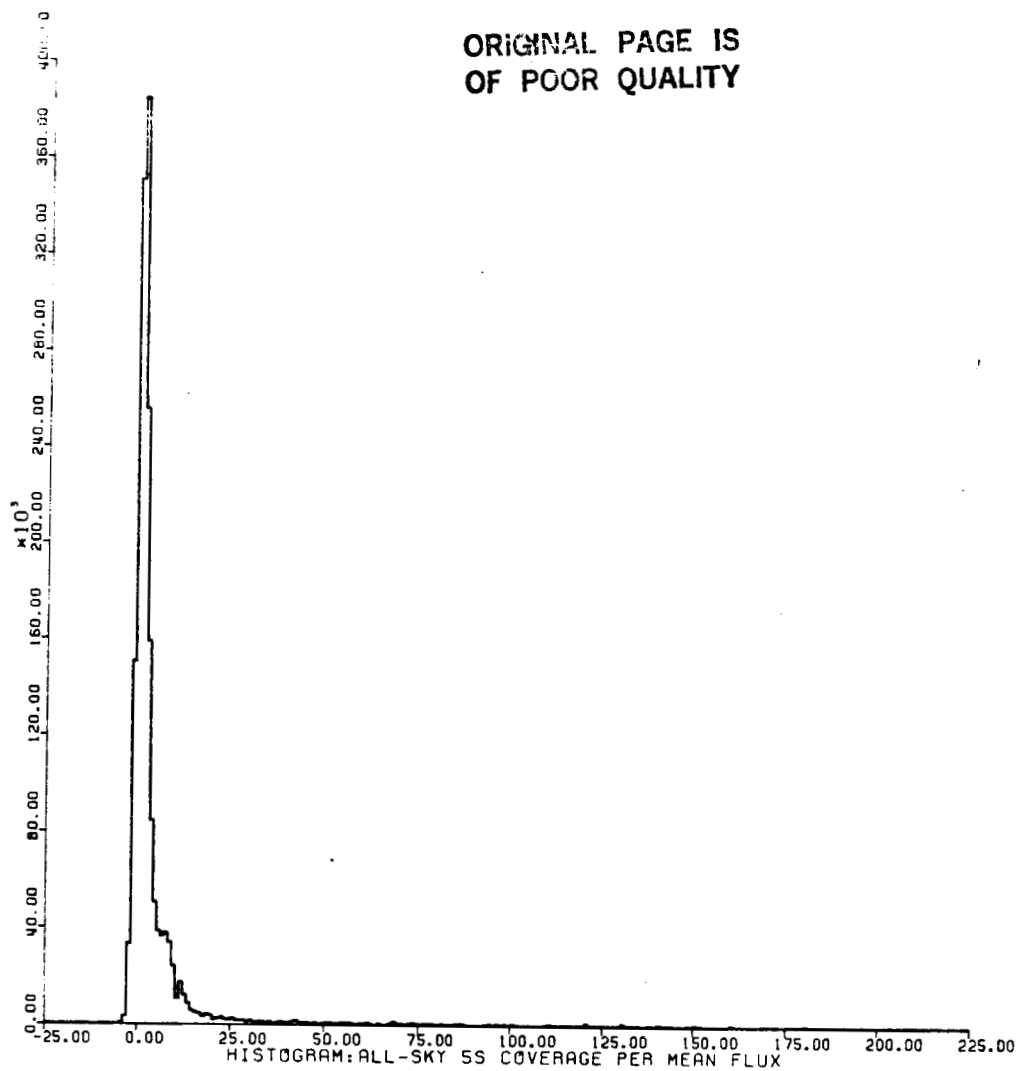
Figure 2.8.c Histogram of the "all-sky" coverage ("source-free" plus "source-full") per mean HED3 flux, for the whole sky.

55

×10²

800.00 720.00 640.00 560.00 480.00 400.00 320.00 240.00 160.00 80.00 0.00

-25.00   0.00   25.00   50.00   75.00   100.00   125.00   150.00   175.00   200.00   225.00

HSTGRM.GPLONE SOURCEFREE CVRGE PER MEAN H3 FLUX
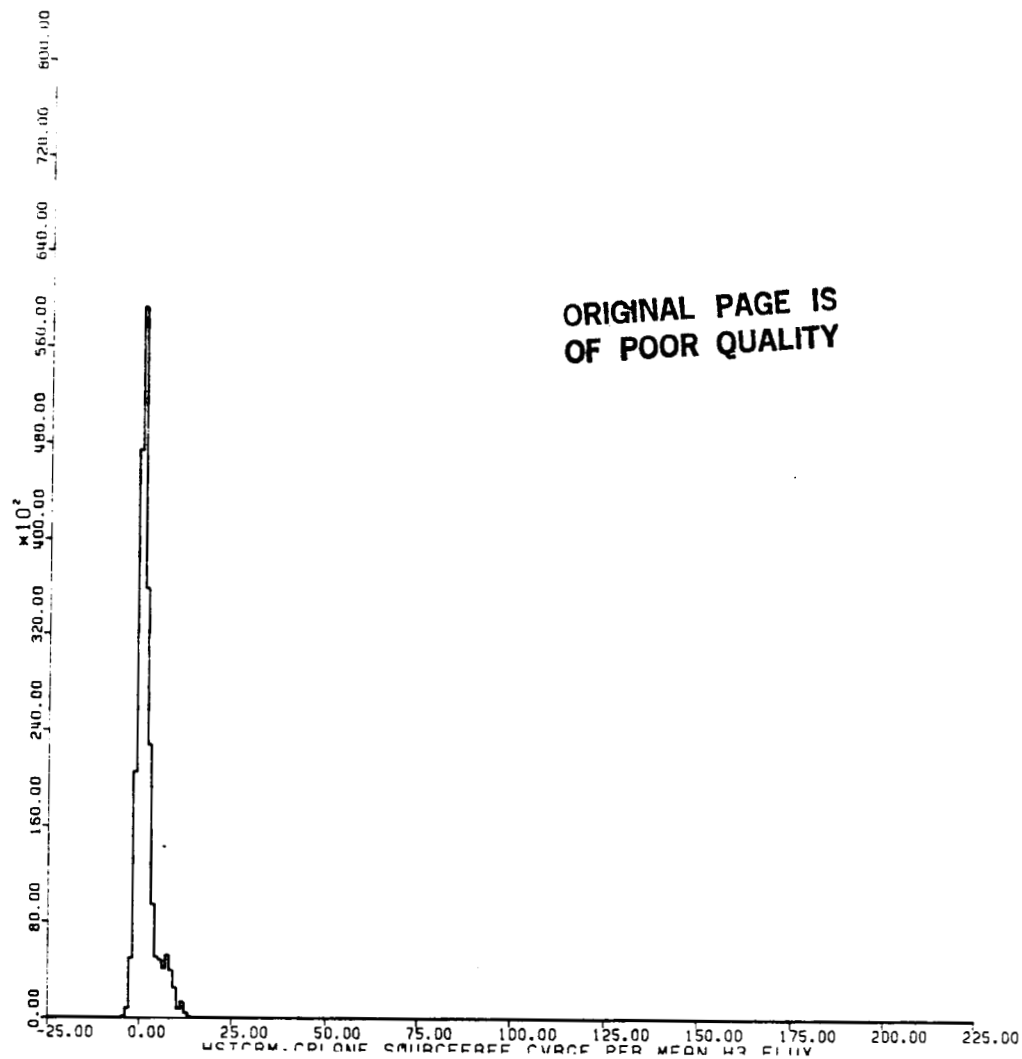
Figure 2.8.d Histogram of the "source-free" sky coverage per mean
HED3 flux, but limited to data ±15° on either side of the Galactic
plane.

HSTGRM:GPLANE SOURCEFULL CVRGE PER MEAN H3 FLUX
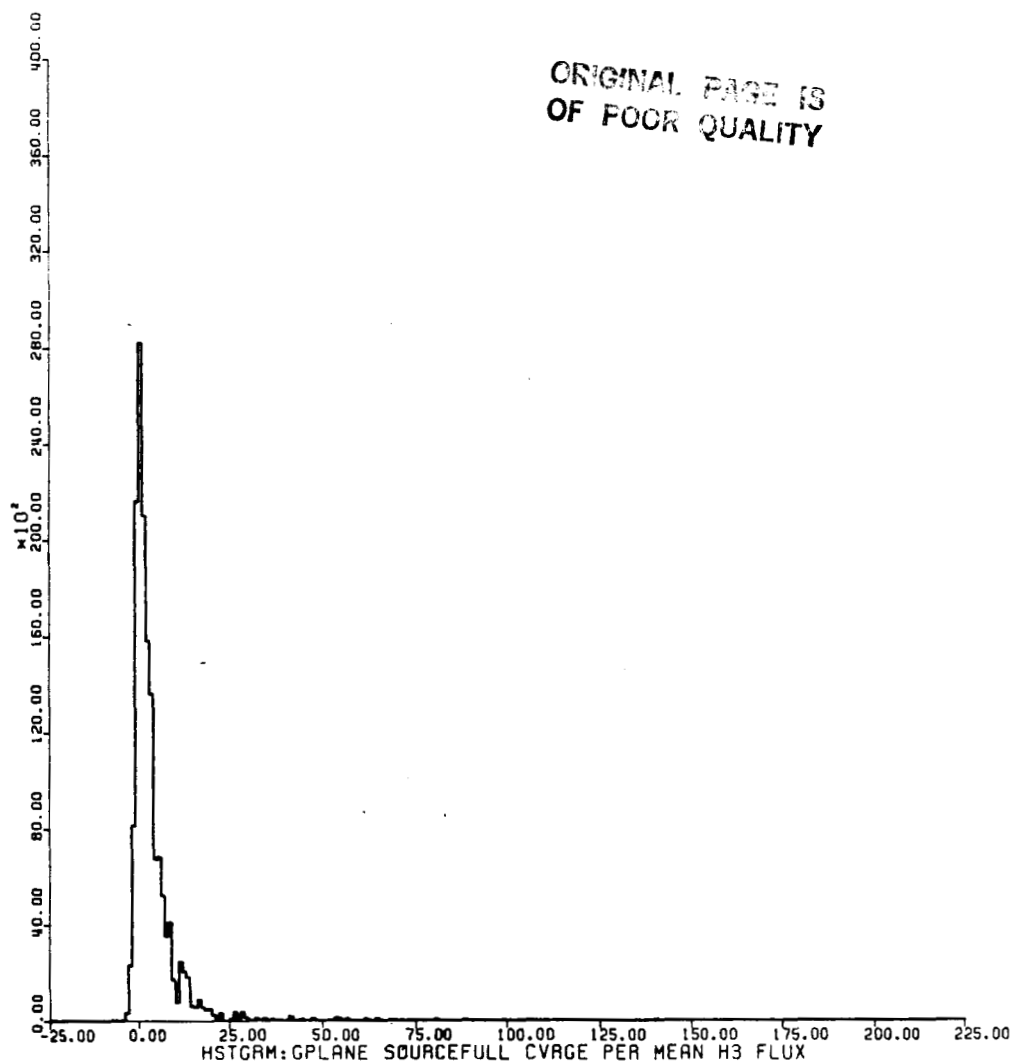
Figure 2.8.e Histogram of the "source-full" sky coverage ("all-sky"
coverage minus that for the "source-free" search) per mean HED3
flux, but limited to data ±15° on either side of the Galactic
plane.

Chapter 3

Results from the HEAO 1 A-2 All Sky Survey

A. Introduction

In this chapter, we consider the results of the HEAO 1 A-2 all
sky survey. As described in the preceding chapter, we divided the
HEAO 1 A-2 fast transient search into three phases, dictated by the
type of analysis necessary for each: the "source free" survey, the
"source" survey, and a survey of the Magellanic Clouds. We expected
the first two phases to uncover the same types of sources, although we
used slightly different search algorithms for each. We combined the
"source-free" and "source" phases of our work into an all-sky survey,
which we describe in this chapter. This all-sky survey was designed
to look for 'new' fast transients, and so discarded events from
variable sources that had been studied previously. In consequence, in
this survey, we studied stars that were predominantly "X-ray faint" -
that is, systems with average quiescent fluxes of something less than
a millicrab, that were only detectable by HEAO 1 A-2 during brief
episodes of outburst or flare activity. (The third phase, a survey of
all data when the detectors pointed towards the Magellanic Clouds, was
qualitatively different, as we scrutinized events from highly luminous
X-ray binaries. We tell of our survey of the Magellanic Clouds in
Chapter 4).

In this all-sky survey, out of the equivalent of ~123 days of
data (~2x10^6 5 s intervals, during which at least one out of four
detectors was on), we found fifteen events. Although these divisions
became indistinct (particularly for the fainter events) in our 2-
20 keV energy range, we argued that we observed primarily two

58

categories of fast transient events. The first, from isotropically distributed sources, with negligible persistent emission, was comprised of events with optically thin thermal spectra, that we characterized as 'coronal flares'. The second category contained 'hard fast transients', presumably from systems containing compact objects, which tended to be highly absorbed ($N_H \sim 10^{23}$ cm^{-2}) and/or to have hard power law spectra (photon index $\sim$ 1), to show indications of ~1 minute variability, and to be distributed near the Galactic plane.

We began with a brief digression on the kinds of sources we excluded from this survey. Partly for completeness, and partly to set the stage for the fast transient survey results, we presented in §3.B a summary of the hundreds of events we discarded. This gave us an overview of $1-10^4$ s variability throughout our Galaxy, as observed through the ~3°x3° collimators of the 2-20 keV HEAO 1 A-2 detectors. We found the variable X-ray sky to be dominated by highly luminous X-ray binaries, followed by systems (from classical X-ray transients to X-ray bursters) that were not always bright, but had outbursts with luminosities near the Eddington limit. We also noted a few fainter events, such as flares from an RS CVn type system, less luminous outbursts from Be-neutron star systems, and variability from a Cataclysmic Variable. These last were somewhat similar to the events of the HEAO 1 A-2 all-sky fast transient survey, in that the quiescent flux from these systems was faint, although still detectable by HEAO 1. The new events from this all-sky survey came from sources that were predominantly X-ray dark, and were only rendered visible by the sudden illumination of one of these fast transient outbursts.

In §3.C, we moved to a discussion of the first phase of the all-

sky fast transient survey, in which we examined only those regions of sky designated "source-free" (see Chapter 2). We published the results of this initial phase in Connors, Serlemitsos, and Swank (1986). Out of the equivalent of ~64 days of scanning data (during which at least 1 detector was on), we found five new events, and two that had been previously identified as coronal flares from active cool dwarf stars. (Although not in data satisfying our search criteria, we also included an ~80 s transient found in a HEAO 1 A-2 blank sky point; Tennant and Swank 1983). As we show in Table 3.3, all but two of these eight events exhibited spectra consistent with the 'coronal transients' defined above. The remaining two exhibited strong evidence of high intrinsic absorption. We found a natural explanation of these six unabsorbed events to be stellar flares from the coronae of active cool dwarf (dMe-dKe) stars. Two of these fast transient events had already been identified as such, and we found the spectra and light curves of the other four unabsorbed events to be similar. We then asked if the rates of these events over the whole sky matched what one predicts from such stellar flares, but found this rate had not been measured in 2-20 keV X-rays before. Further, while optical identifications of dMe-dKe stars were only ~2/3 complete even as close as 5 pc, we estimated the events detected in this fast transient search could have come from cool dwarf stars as distant as ~60-70 pc. We therefore approached statistical extrapolations of flare rates to 2-20 keV X-rays from three different perspectives. First, we considered rates of stellar flaring measured in the U-band, and extrapolated these rates in a reasonable manner to 2-20 keV X-rays. To test this argument, we also predicted the rate of X-ray

flares seen in Einstein observations of dMe-dKe stars, and then extrapolated the Einstein rates to what we observed with HEAO 1 A-2. As our third method, we calculated how many flares we predicted should have been found by a fast transient search such as this, but only from those stars already identified by serendipity and optical survey work as flare stars. To increase the small number of events in this category, we added to this A-2 survey the results of a similar survey performed on A-1 data by Ambruster and Wood (1986). In all cases, we found our prediction of event rates matched our results, to within the large uncertainties of our measurements.

After this lengthy statistical argument, at the end of §3.C, we returned to the two events from the source-free transient search that showed indications of high absorption. They could not have been flares from any kind of main sequence coronal source, because of this dearth of low energy photons. We noted that their characteristics did not match those of any identified X-ray transient, and so left them unidentified.

We then considered the rest of the sky (the "source-full" sky), in the second phase of this all-sky survey, and discussed our findings in §3.D. We expected, that by almost doubling the amount of data surveyed, we would nearly double the number of stellar flares found, and that they would be distributed roughly isotropically. If the events were more intrinsically luminous (perhaps originating on compact objects rather than coronae of main sequence stars), they should be evident as a handful of new events along the Galactic plane. To penetrate the "source" regions, even when using the algorithm which compared rates every 5, 15, and 60 s with a 12 hour

average for that position on the sky, we still needed to exclude ±3°
regions around the most luminous variable sources (or be swamped with
hundreds of triggers to investigate). As we noted in Chapter 2, this
excluded a considerable fraction (~20%) of the Galactic plane, so that
even this "source-full" phase of the fast transient survey was
slightly biased against a disk distribution of events.

Out of the equivalent of ~59 additional days of scanning data
(during which at least one out of four detectors was on) from the
"source-full" sky, we found eight more fast transient events, seven of
them new. One had been identified by Hueter (1987) as an energetic
gamma-ray burst that penetrated the A-2 detectors through the sides.
Three of the new events we identified as coronal flares from active
cool dwarf stars. This number was consistent with what we predicted
based on our "source-free" survey. The remaining four events were
more puzzling. Three occurred within $3\frac{1}{2}$ days of each other, and from
approximately the same direction. One was spatially coincident with a
Cygnus OB association, and had 58 early-type emission-line objects in
its error box. All four exhibited hard (power law photon index ~0.8-
1.6); all occurred within 10° of the plane of the Galaxy; and two
(of the repeating events) showed evidence for <100 s variability. We
considered but rejected identifications with distant gamma-ray
bursters, X-ray bursters, "dippers", or luminous flares from
consistently bright X-ray binaries (such as KZ Tra or LMC X-4).

To the consideration of these events, we added recent preliminary
findings from investigations of a small swath of the Galactic plane.
We originally mapped out the region around Galactic l^{II}, b^{II} ~
260°,-10° in order to understand the low level persistent emission

around the time of a gamma-ray burst observed with HEAO 1 A-2 and A-4 (Connors, Hueter, and Serlemitsos 1988). Our data indicated there were probably three hard, ~few hour, few millicrab transients near this section of the Galactic plane. (One has tentatively been identified as a Be-neutron star transient by Buckley et al. 1988.)

We hypothesize these hard variable sources near the Galactic plane, plus the hard transients of the HEAO 1 A-2 survey of the "source-full" sky, may be evidence of a class of hard, ~few hour transients lining the Galactic plane. The most plausible source population would be outbursts from ~100-1000 Be-neutron star systems (>50% of which are expected to be pulsars). Observations by the Japanese satellite Ginga have provided strong independent evidence for the existence of such a class (Koyama et al. 1988). In light of this hypothesis, we re-examined the two unidentified and highly absorbed events from the "source-free" survey, and found it possible that one, near the Galactic plane, could belong to this class of hard Galactic plane transients, but the other, at high Galactic latitude, and with more stringent constraints on quiescent flux, probably did not. This last event remains a puzzle.

In the final section of Chapter 3, §3.E, we consider a number of "odd-ball" unidentified fast X-ray transients from other experiments, to see if we can find traces of some sort of underlying pattern. We concluded these events were too rare and too poorly defined for us to make a strong case for one or another proposed hierarchy of events. However, by comparison with the A-2/A-4 observations of GB780506, we find we clearly can identify none of our fast transients with X-ray counterparts to gamma-ray bursts, and so find a 90% upper limit on the

63

event rate (above gamma-ray fluences of 10^{-9} ergs-cm^{-2}) of less than 1300 per year over the whole sky. Even a conservative comparison with the event rate measured above higher fluences by the A-4 experiment shows this to be a stringent upper limit and a very marked departure from an isotropic distribution, suggesting we are seeing all the way across the Galaxy at fluences of around 10^{-7-8} ergs-cm^{-2}. By using an upper limit on gamma-ray burst recurrence times of ~8 years (Schaefer and Cline 1985), we estimated the total number of gamma-ray burst sources throughout the Galaxy to be $\leq 10^4$.

B. An Aside: A Galactic Overview of Fast X-ray Variability

One of the most telling representations of the Galaxy in X-rays is a seven minute movie, "The X-ray Sky: 1969-1977", made from seven years of 3-12 keV observations by the all-sky monitor mounted on the Vela 5B satellite (Terrell et al. 1982). The detectors had a small area (26 cm^2) and low spatial resolution (~6°x6° FWHM), but monitored the X-ray sky for nearly a decade. The data were processed in 10 day skymaps, with color indicating the intensity, and put in the form of a time-lapse movie. The movie displays persistently luminous X-ray binaries of all types changing in brightness (by factors of 2-10) on timescales of weeks to months, with high mass binaries dotting the Galactic plane, and low mass binaries (or "Galactic bulge sources") clustered about the Galactic center (Priedhorsky private communication). More dramatic than these bright persistent sources, the movie representation of the X-ray sky exhibits the classical X-ray transients becoming among the brightest sources in the X-ray sky as they turned on (on timescales of days to weeks), then decaying in

intensity on timescales of weeks to months. Not all transients faded in that manner: two prominent transients near the Galactic center (QV Nor, a hard eclipsing pulsar, and QX Nor, a soft transient that is now a persistent X-ray burst source) have remained luminous since their turn-on.

Persistently luminous binaries containing accreting neutron stars with high magnetic fields (identified by their pulsations and generally harder spectra) more often have younger, high mass companions found along the plane of the Galaxy; while binaries containing neutron stars with magnetic fields less than $\sim 10^{10}$ gauss (which tended to exhibit soft spectra and X-ray bursts) most often have older, late-type companions, or are found in Globular Clusters, and are spread in a "Pop II" halo about the Galactic center (Cowley et al. 1987; White, Kaluzienski, and Swank 1984; White and Marshall 1983; Lewin and Joss 1981). Rapid, irregular variability (no pulsations or X-ray bursts), and an "ultra-soft" spectrum when the intensity was high, were two suggested X-ray hallmarks of both high and low mass systems containing black holes. White, Kaluzienski, and Swank (1984) have argued that the dramatically variable (on time-scales of weeks to months) classical X-ray transient systems fall into similar categories as the persistently bright sytems, save that the average accretion rate is probably lower.

As prominent as these classical X-ray transients appeared when viewed with an integration time of 10 days, their rise and decay were not events which stood out when one viewed the X-ray sky at fast transient time-scales, such as through the 1-10^4 s filter of the HEAO 1 A-2 all-sky fast transient survey. With this "filter", one

Table 3.1: Sources Excluded From the All-Sky Survey

Source	Galactic Coordinates	Type (a)	Comments on Variability
X0155+634	125.9, 1.0	TBe	Transient, pulsar
X0900-403, Vela X-1	263.1, 3.9	PBHM	Eclipsing, flares, pulsar
X1119-603, Cen X-3	292.1, 0.3	PBHM	Eclipsing, pulsar
X1258-613, GX304-1[b]	304.1, 1.2	PBe	Transient, pulsar
X1455-314, Cen X-4[b]	332.2, 23.9	XNova	Transient, burster
X1516-569, Cir X-1	322.1, 0.0	PBHM	Transient[c], rapid irregular
X1538-522, QV Nor	327.4, 2.1	TBe, PBHM	Transient, eclipsing pulsar
X1608-522, QX Nor	330.9, -0.9	XNova, PBLM	Transient, burster
X1617-155, Sco X-1	359.1, 23.8	PBLM	Irregular
X1642-455, GX340+0	339.6, -0.1	PBLM	Irregular
X1656+354, Her X-1	58.2, 37.5	PBLM[d]	Eclipsing, pulsar
X1702-43 [e]	343.9, -1.3	PBLM	Burster
X1705-440[e]	343.3, -2.3	PBLM	Irregular, dipper, burster
X1705-250, Nova Oph	358.6, 9.1	XNova	Transient
X1813-140, GX17+2	16.4, 1.3	PBLM	Irregular, burster
X1908+005, Aquila X-1	35.7, -4.1	XNova	Transient, burster
X1956+350, Cyg X-1	71.3, 3.1	PBHM	Rapid irregular
X2030+407, Cyg X-3	79.9, 0.7	PBLM	4.8h eclipsing(?), irregular

a) All are thought to be binaries. We have not distinguished between neutron star systems and those thought to contain black holes. We used PBHM (persistently bright high mass X-ray binary) to designate X-ray binaries with high mass companions, where the compact object is X-ray bright, $L_x > 10^{36}$ ergs-s^{-1}, due to continuous accretion from either a strong wind (for massive supergiants) or Roche-lobe overflow; and PBLM (persistently bright low mass X-ray binary) for low mass binaries persistently bright in X-rays due to continuous accretion onto the compact object. "Xnova" designates the 'soft transients', low mass X-ray binaries observed to give X-ray nova (often accompanied by optical or radio outbursts), with rise and decay times on the order of tens to hundreds of days (White, Kaluzienski, and Swank 1984; White and Mason 1985; Bradt and McClintock 1983). "TBe" designates 'hard transients', high mass (O-B II-Ve) transient systems that have been observed to give irregular outbursts, with peak luminosities $> 10^{36}$ ergs-s^{-1}, and rise and decay times of tens of days;

66

Table 3.1: Sources Excluded From the All-Sky Survey, Continued

or equally bright quasi-periodic outbursts with durations on the order of a day (Bradt and McClintock 1983; Van den Heuvel and Rappaport 1986; Stella, White, and Rosner 1986); while "PBe" designates fainter ($L_x < 10^{36}$ ergs-s^{-1}), persistent high mass systems that are less dramatically variable ($L_{MAX}/L_{MIN} \sim 10$).

b) These sources were included in the original table because they were listed as bright and variable in Bradt and McClintock (1983), but were probably not active when HEAO 1 could observe them.

c) This system exhibits irregular 16 d outbursts, presumably due to binary changes (see Robinson-Saba 1982).

d) Her X-1, with a ~2 solar mass companion, can be categorized as either a high- or low-mass X-ray binary (Bradt and McClintock 1983).

e) These sources were confused (~½° apart). Both can be ~100 millicrabs in intensity, and both have been observed to give X-ray bursts.

viewed not absolute flux levels, but fast variations ($\leq 6\sigma \leq 10^{-10}$ ergs-cm^{-2}-s^{-1}) above an average flux (calculated over 12 hours). As we discussed in Chapter 2, this study focused on new fast transients, and so discarded any event that that could be attributed to known, variable, X-ray sources. In the "source-free" phase of the survey, we accomplished this by searching only portions of the data free of sources brighter than about 1 millicrab. For the "source-full" data, we needed to have a method for identifying and discarding events from known varying sources. As a side benefit, from this second phase of the all-sky survey, we accumulated a summary of short time-scale X-ray variability throughout the Galaxy.

After a preliminary data run netted nearly 100 triggers from the Cygnus region alone, it became clear that we also needed to exclude the brightest, most variable sources before the data were processed through our survey 'trigger' algorithms. We compiled a (somewhat arbitrary) list of eighteen bright sources that varied on our fast transient time-scales. We have displayed these eighteen sources in Table 3.1, and noted the characteristics of each that could cause them to trigger our search (Bradt and McClintock 1983). We chose to use a simple algorithm, which excluded all data when the instrument look-directions were within ±3° (in scan latitude and longitude) of any of these sources. Further, whenever an event triggered while the instruments pointed to within ±3° of a known, variable source (stored in an on-line catalog), we discarded that event. Whenever a source (as identified by this simple algorithm) triggered the fast transient survey six or more times in one 20 day data run, it was automatically added to the table of bright, variable, sources, so that a 36 square

degree region around that source was excluded from processing for the remainder of that run. Although computationally inexpensive, this algorithm could clearly have misidentified events from crowded regions. (For example, all but a handful of the thirty-seven events found in the Magellanic Clouds survey were misidentified, until the more sophisticated position fitting programs of Appendix B were brought to bear.)

Therefore, this summary of discarded events serves not only as a rough overview of Galactic X-ray variability, but as a record of which regions of sky were excluded. (Some future researcher with idle computer time on their hands may find it a worthwhile project to more accurately identify triggers from interesting regions of the sky. However, we decided such a project to be outside the focus of this work.)

In Table 3.2, we have given a rough (and incomplete) measure of $1\frac{1}{2}$ years of 2-20 keV X-ray variability over the whole sky by listing all 155 (out of 170) good events that we attributed to previously studied variable X-ray sources, along with brief indications of the type of source and the type of variable X-ray behavior each source has been seen to exhibit. We found the X-ray sky to be dominated by irregular "flickering" from the persistent, high flux sources, when viewed on $1-10^4$ s time-scales. We noted flickering from high mass X-ray binaries, from low mass binaries, from systems containing neutron stars, and from systems thought to contain black holes. Though a matter of active research for each type of source, the irregular flickering is thought to reflect a turbulent or grainy flow of matter through an accretion disk onto the compact object. These

Table 3.2: Sources That Triggered the All-Sky Survey

Source	Galactic Coordinates	No. of Triggers[a]	Type (b)	Comments on Variability
H0125+07, HD8357	136.5°,-54.6°	1	RSCVn	Flares
4U0352+30, X Per	163.1 ,-17.1	>1	PBe	Pulsar
A0535+26	181.4 , -2.6	2	TBe	Transient, pulsar,
4U0614+09	200.9 , -3.4	4	PBLM	Irregular, burster
4U1145-61	295.6 , -0.2	>8	TBe	Transient, pulsar
4U1223-62	300.1 , -0.0	7	PBHM	Eclipsing, pulsar
A1524-61, KY TrA	320.3 , -4.4	1	Xnova	Transient
4U1626-67, KZ TrA	321.8 ,-13.1	>12	PBLM	Irregular, flares, pulsar
4U1630-47	336.9 , 0.3	6	Xnova	Transient
2S1636-536	332.9 , -4.8	>8	PBLM	Burster
4U1658-48, GX339-4	338.9 , -4.3	2	PBLM	Rapid irregular
4U1702-36, Sco X-2	349.1 , 2.7	>8	PBLM	Irregular
X1724-30, Terzan 2	356.3 , 2.3	1	GlCl	Burster
4U1728-33,Grindlay1	354.3 , -0.2	1	GlCl	Burster
4U1728-24, GX1+4	1.9 , 4.8	>8	PBLM	Pulsar
(also confused with 4U1735-28 and 4U1730-22)				
4U1728-16, GX9+9	8.5 , 9.0	>9	PBLM	Irregular
MXB1730-33 (Rapid Burster)	354.8 , -0.2	>5	GlCl	Burster
2S1735-444	346.1 , -7.0	>9	PBLM	Burster
A1742-289	359.6 , -0.4	>7	Xnova	Transient
4U1744-26, Terzan5	2.3 , 0.8	1	GlCl	Burster
A1745-36, 76 trans	354.1 , -4.2	1	?	Transient
4U1755-33	357.2 , -4.9	2	PBLM	Irregular
4U1758-25, GX5-1	5.1 , -1.0	1	?	Irregular
4U1758-20, GX9+1	9.1 , 1.2	>8	?	Irregular
4U1811-17, GX13+1	13.5 , 0.1	3	?	Irregular
4U1813+50, AM Her	77.9 , 25.9	1	CV	Eclipsing, flickers
4U1820-30	2.8 , -7.9	>6	GlCl	Burster
4U1822-37	356.9 ,-11.3	2	PBLM	Eclipsing

Table 3.2: Sources That Triggered the All-Sky Survey (continued)

Source	Galactic Coordinates	No. of Triggers[a]	Type (b)	Comments on Variability
4U1829-06, Sct X-1	24.5 , -0.2	4	?	Irregular
(Also confused with 1833-076)				
2S1837+049, Ser X-1	36.1 , 4.8	>8	PBLM	Burster
A1847-05, 1850-087	25.4 , -4.3	1	?	Flares, burster
(confused region)				
4U1907+09	43.7 , 0.5	>7	PBe	Eclipsing, flares, pulsar
2S1916-053	31.4 , -8.5	2	?	Dipper, burster
4U1954+31	67.6 , 1.4	5	PBe[c]	Flares, flickers
4U2129+47 V1727 Cyg	108.2 , -32.6	1	PBLM	Eclipsing
4U2142+38, Cyg X-2	87.3 , -11.3	>12	PBLM	Irregular

a) If the software indicated a source was responsible for more than 6 triggers in a row, a $6°x6°$ box around it was excluded from future processing. Therefore some of these numbers are only upper limits. On some occasions a single fast transient event was so bright that the burst search program recorded it as several triggers. The program might then exclude that source from future processing after less than 6 actual bursts or flares.

b) All are thought to be binaries. Sources with only a question mark were unidentified. We have not distinguished between neutron star systems and those thought to contain black holes. We used PBHM (persistently bright high mass X-ray binary) to designate X-ray binaries with high mass companions, where the compact object is X-ray bright, $L_x > 10^{36}$ ergs-s^{-1}, due to continuous accretion from either a strong wind (for massive supergiants) or Roche-lobe overflow; and PBLM (persistently bright low mass X-ray binary) for low mass binaries persistently bright in X-rays due to continuous accretion onto the compact object. "Xnova" designates the 'soft transients', low mass X-ray binaries observed to give X-ray nova (often accompanied by optical or radio outbursts), with rise and decay times on the order of tens to hundreds of days (White, Kaluzienski, and Swank 1984; White and Mason 1985; Bradt and McClintock 1983). "TBe" designates 'hard transients', high mass (O-B II-Ve) transient systems that have been observed to give irregular outbursts, with peak luminosities $>10^{36}$ ergs-s^{-1}, and rise and decay times of tens of days; or equally bright quasi-periodic outbursts with durations on the order of a day (Bradt and McClintock 1983; Van den Huevel and Rappaport 1986; Stella, White, and Rosner 1986); while "PBe" designates fainter ($L_x < 10^{36}$ ergs-s^{-1}), persistent high mass (O-B II-Ve) systems that are less dramatically variable ($L_{MAX}/L_{MIN} \sim 10$). "GlCl" designates a source in a globular cluster (X-ray properties indicate these are low mass

Table 3.2: Sources That Triggered the All-Sky Survey (continued)

X-ray binaries; see Bradt and McClintock 1983; White, Kaluzienski,
and Swank 1984; White and Mason 1985;); "CV" indicates a cataclysmic
variable, a close binary composed of a low mass main sequence star
plus a white dwarf rather than a neutron star or black hole (Patterson
1984); "RSCVn" indicates an RS CVn-like binary, a cool sub-giant with
an active corona locked in a close synchronous orbit with a white
dwarf star (Hall 1984; Bradt and McClintock 1983).
c) Although the X-ray properties of this system seem to indicate
identification as a Be-transient system, it has not yet been optically
identified (Swank 1987 private communication).

persistently luminous sources also have states of high and low (2-20 keV) intensity; when a transition between these two states occurred abruptly (<3 hours), the fast transient survey could have registered it as a rapid variation.

Other types of variability capable of triggering the fast transient survey included eclipse ingresses, eclipse egresses, and slower intensity variations known as "dips" (which have been well modeled as eclipses by a thickened portion of the accretion disk); highly luminous (occasionally super-Eddington) flares from these accreting systems; pulsations from compact objects with strong ($\sim 10^{12}$ gauss) magnetic fields; and, most prominent (because of their high luminosity and high ratio of peak-flux-to-average-flux), X-ray bursts from neutron stars with weak ($< 10^{-10}$ gauss) magnetic fields.

The persistently bright (i.e. high accretion rate) low and high mass X-ray binaries were not the only systems to show these types of variability. As Tables 3.1 and 3.2 illustrate, the classical X-ray transients also exhibited these same kinds of variable behavior. X-ray novae were apt to have soft (kT<15 keV) spectra, X-ray bursts (from binaries with neutron stars, rather than ones though to contain black holes), and were more likely to be associated with an older population of late-type stars. Those with harder spectra (kT>15 keV) tended to show evidence of pulsations, and were more likely to have younger, more massive (O-Be II-V) companions (White, Kaluzienski, and Swank 1984). The classical "soft" X-ray transients had peak luminosities of 10^{37-38} ergs-s^{-1}, as luminous at peak as their persistent counterparts. Outbursts from transient Be-systems had peak luminosities ranging from 10^{36-39} ergs-s^{-1}, and lasted from hundreds

of days to considerably less than a day (Van den Heuvel and Rappaport 1986; Stella, White, and Rosner 1986; see also the LMC Transient in Chapter 4). The "persistent" Be binaries exhibited lower luminosities ($L_x < 10^{36}$ ergs-s^{-1}), flare-like increases by an order of magnitude on time-scales as short as an hour, and larger intensity modulations on time-scales of ~days-months.

There were two more types of systems represented in Table 3.2 that exhibited shorter, less luminous, fast transient events. One event was identified with the eclipsing Cataclysmic Variable, AM Her, a close binary composed of a cool (main sequence) dwarf star plus an accreting white dwarf. (Interestingly, the optical and X-ray light-curves of these dramatically optically variable systems also often exhibited irregular "flickering" on fast transient time-scales.) Another event was identified as a 10^{31-32} erg-s^{-1} flare from the RS CVn-type system HD8357, a cool subgiant plus white dwarf binary, with the flare activity arising from magnetic activity in the corona of the cool subgiant (Garcia et al. 1980). Historically, these fainter types of events were labeled "high latitude transients", and were probably the original "fast transients" (Bradt and McClintock 1983; Pye and McHardy 1983).

Almost all of the sources described in this section were sufficiently bright for HEAO 1 to detect even in quiescence. The new events we describe in the following two sections were fainter, and for the most part the sources were undetectable in quiescence.

C. Results From the Source-Free Sky

We turn to the results of the first phase of the HEAO 1 A-2 all-

sky fast transient survey, covering the "source-free" sky (i.e.
regions of sky free from X-ray sources brighter than about a
millicrab). In this phase, we compared event rates every ~1 and 5 s,
looking for variations of more than ~6σ significance above the average
diffuse sky plus internal detector background counting rate. We
published the results from this initial phase in Connors, Serlemitsos,
and Swank (1986). Out of the equivalent of ~64 continuous days (~10^6
5.12 s intervals) of scanning data, during which at least one out of
four detectors was on (54.6 days each of HED1 and HED3 data, which
viewed adjacent but independent sections of the sky; 41.6 days of
data from MED, and 24.9 days from HED2, which were co-aligned with
HED3), we discovered seven fast transient events, five of them new.
In this section, we have also included an ~80 s event found
serendipitously in HEAO 1 A-2 pointed data by Tennant and Swank
(1983), in a region free from sources brighter than ~1 millicrab.
(This survey encompassed only scanning data.) The events had
durations ranging from ~1 minute to over two hours, and peak fluxes
ranging from ~6 to 150 millicrabs. In what follows, we have detailed
the event properties, then discussed possible identifications. We
argued that all but two were probably hard flares from the active
coronae of cool dwarf stars, but that the remaining two, which showed
evidence of hard spectra and anomalously high intrinsic absorption,
could not be identified as any known type of variable X-ray source.

Table 3.3.a: Events From The "Source-Free" Search

TIMES (a) D.O.Y. 1977	U.T. Duration	POSITIONS (b) R.A., DEC (1950.0)	Galactic l(II), b(II)	INTENSITIES (c) Peak Flux	Varies?	Quiescent Flux	SPECTRA (d) PL	TTB	BB	NOTES (e)
249.36	08:35	57.9°, 64.5°	141.1°, 8.6°	6.9	N	<0.84	...	...	...	(f)
	1≤τ<95						2.6±1.5	>9.0	0.8±0.2	
298.62	14:58	307.5 ,-33.0	10.2 ,-34.7	6.5	N	<0.76	2.7±0.1	3.7±0.9	...	(g)
	τ~35						...	...	...	
343.97	23:15	164.8 , -3.6	258.2 , 49.2	11.	N	<0.56	2.0±0.3	10+15/-4	...	(h)
	1≤τ<175						...	...	...	
370.82	19:41	126.6 ,-65.4	279.8 ,-15.4	4.0	N	<0.51	3.0±1.1	2.6+4/-1	0.8±0.2	(i)
	1≤τ<107						6.0±2.3	0.5±0.4	0.4±0.1	
405.85	20:24	73.13,-55.94	264.3 ,-38.6	120.	Y	(<0.2)	...	12.6+4.4/-2.6	...	‡ (j)
	τ~145						...	...	...	
436.84	20:11	265.7 , 48.4	75.2 , 30.8	13.	N	<0.45	...	...	...	‡
	1≤τ<106						1.3±0.4	>16	1.8±0.4	
623.47	11:21	263.4 , 18.2	41.6 , 24.6	7.6	N	<0.46	1.9±0.8	>3.	1.3±0.3	
	1≤τ<209						3.1+2/-1	2.+4/-1.5	0.8±0.2	
728.15	03:37	319.6 , 54.6	95.5 , 3.6	32.	Y	1.0±0.1	2.0±0.2	9.0+4/-2	...	‡ (k)
	τ~2						...	...	...	

a) Times are in D.O.Y. (1977) followed by hours and minutes (in U.T.), for the start time of each event. The constraints on duration are given in minutes.

b) We listed the best fit positions, in both 1950.0 R.A. and Declination, and Galactic l^{II}, b^{II}, calculated using the position finding program described in Appendix B.

c) The intensities are in units of HED3 cts-s^{-1}. The intensity of the Crab (pulsar + nebula) is about 660 HED3 cts/s ($\sim 3.4 \times 10^{-8}$ ergs-cm^{-2}-s^{-1} from 2-20 keV). To calculate these values we performed least-squares

76

fits of the light curves in Figures 3.1 and 3.2, assuming a constant intensity. For the events for which a constant intensity was a bad fit, which we defined to be when the value for χ^2 was more than twice the number of degrees of freedom, we used the highest intensity 5.12 s data point (that was at least 4σ above zero). We have indicated these events with a 'Y' under the label "Varies?". To measure the quiescent flux, we summed HEAO 1 A-2 scanning MED+HED3 1.5° rates from the six month pass in which the event was detected (although for D728.14 we looked at data from the first two six month passes, as it was detected in pointing data and near the end of the mission). Typically, this meant about six days of scanning data. If χ^2 dropped by at least thirty when two fit parameters (intensity and scan angle) were introduced, we deemed that source to be significant. (Note that the units are "new R15" units, or MED+HED3 cts-s^{-1}, which are different from the units for the peak intensities.)

d) In this column, 'PL' stands for the photon index of a power law model; 'TTB' indicates a thin thermal bremmstrahlung (i.e. exponential plus Gaunt factor) temperature in keV; and BB indicates the temperature for a black body model, in keV. The top row in each triple pair corresponds to fits assuming negligible absorption ($N_H \sim 10^{19}$ cm^{-2}). The second row in each pair requires a column density of $\sim 10^{23}$ cm^{-2}. When the number of degrees of freedom was ten or greater, and if χ^2 for a particular model was greater than twice the number of degrees of freedom, we deemed the model unacceptable and left that entry blank. For events with fewer than ten degrees of freedom, a model was deemed unacceptable when χ^2 exceeded the number of degrees of freedom plus ten. Those events marked with an ‡ may require a changing spectrum and are discussed in more detail in the text.

e) In the footnotes, we listed objects found in the 99% confidence position limits (of Figure 3.1) that belonged to classes of objects associated with variable X-ray emission, and discussed possible identifications.

f) The position error box of this source intersects that of a gamma-ray burst source, 1973 Mar 2 at an R.A., Decl. of 59°,59° with r=5°. Ambruster (private communication) noted a "definite faint source" in A-1 data 16 minutes after this event was observed in A-2 data.

g) Found in HEAO 1 A-2 LED data by Kahn et al. (1979), and attributed to AT Mic. Kahn et al. (1979) showed the LED+MED spectrum to be best fit by a thin thermal bremsstrahlung model, with kT~2.7 keV, plus an iron line. The Ariel V fast transient source AT2030+30 also lies across the center of the error box. Quoted upper limits are consistent with Tsikoudi (1982,1983).

h) Ambruster (private communication) noted weak emission in the A-1 data 16 minutes before and 48 minutes after this event was observed in A-2 data.

i) The position limits intersect that of gamma-ray burst source 1973 Jun 10 at R.A., Decl. of 127.,-64., with r=5°. Contains HD 73834, a 7.9 mag Be star (Wackerling 1970), and one eclipsing Algol-type system, TX Vol (Kukarkin et al. 1974).

j) This event was found in A-2 data by Kaluzienski et al. (1978a,b). We list here the position of the only IPC source (also an EXOSAT CMA source) to fall within our 99% confidence position limits. Griffiths et al.

(1979) identified this source, on the basis of A-3 and A-4 data, with two dMe stars. Their position is consistent with that of the Einstein IPC source.

k)   The spectral parameters for this event come from fits to 10.24 s of MED and HED3 PHA data containing the event peak. A gamma-ray burst error box, 1972 Jan 17 at an R.A. and Decl. of 21^h28^m,+50 with r=5°, overlaps the A-2 position, as does a weak A-2 steady source, and a COS B error box which contains an IPC source (Caraveo 1983). Tennant and Swank (1983) noted a weak persistent source in scanning data, a year before this event. We listed the intensity of this faint source under "quiescent flux".

Figure 3.1 We present 99% confidence position limits ($\chi^2 = \chi^2_{MIN} + 9.21$, for two parameters; Lampton, Margon, and Bowyer 1976) for the eight events from the "source-free" search, generated using the "intensity-independent" fitting procedure described in Appendix B. The light curves presented here are by-products of that process. Except where noted, for the light curves shown here, we used the best-fit values for position, with the position free to vary in the scan direction, but constrained to lie in the scan plane (off-scan angle held fixed at zero), so that the 1σ error bars generated would reflect the uncertainty in the shape of the light curve due to the uncertainty in source scan angle, but not the uncertainty in overall event normalization due to the uncertainty in its off-scan position.

66.000

D249TS.LTP

ORIGINAL PAGE IS
OF POOR QUALITY

80

63.000

54.00

HED3 CTS/$-CM^2-S$

.1

.05

0

-.05

0   20   40   60   80

TIME IN SECONDS

67.(

$\chi^2 =$ 19.4 FOR 16 DOF
P1= 0.143E-01 SIG= 0.164E-02
$\chi^2 =$ 15.9 FOR 15 DOF
P2= 0.185E-03 P3= 0.650E-02

a) We plotted the 99% confidence position limits (in 1950.0 R.A. and Decl.) on the left, and the ~1 minute event light curve (in HED3 cts-cm^{-2}-s^{-1} versus time in seconds) on the right, for the event on D.O.Y. 249.36. Time zero for the light curve is at 8:35:16.488 UT. The center of the error box is at Galactic l^{II},b^{II} ~ 141.1°, 8.6°. We found no identified X-ray sources, no A-1 catalog sources, and no known optically variable objects or emission line stars (Wackerling 1970; Kukarkin et al. 1969; 1971; 1974; 1976) in the field of view. However this A-2 position error box overlaps a large error box for a gamma-ray burst, 1973 Mar 2 at an R.A., Dec of 59°,59° with r=5°.
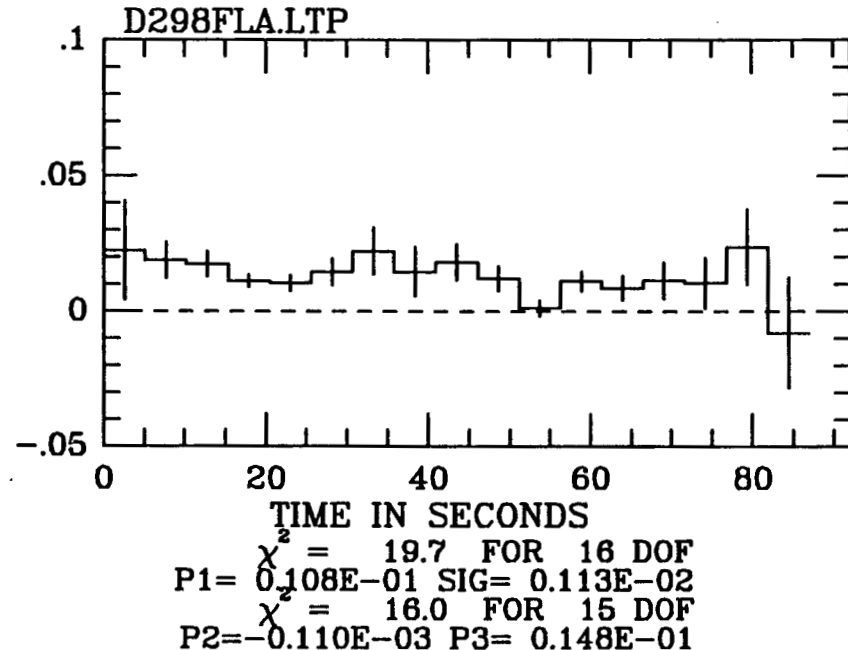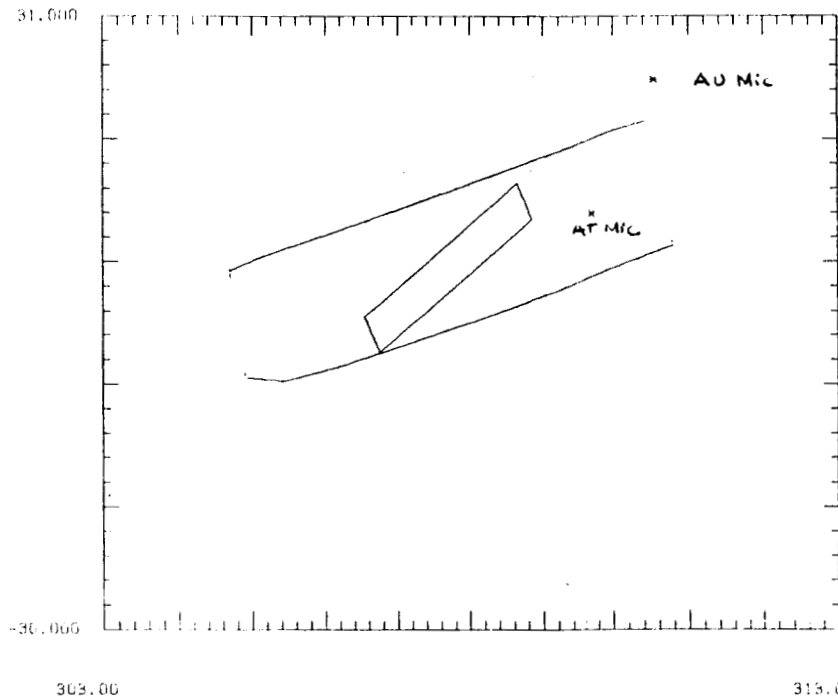
b) Found in HEAO 1 A-2 LED data by Kahn et al. (1979), and attributed to AT Mic. We plotted the 99%
confidence position limits (in 1950.0 R.A. and Decl.) on the left, and the ~1 minute event light curve (in
HED3 cts-cm^{-2}-s^{-1} versus time in seconds) on the right, for the event on D.O.Y. 298.62. Time zero for the
light curve is at 14:57:44.402 UT. The center of the error box is at Galactic l^{II},b^{II} ~ 10.2°, 49.2°. The
HEAO 1 A-2 99% confidence position error box contains both AT Mic and the 230 millicrab repeating Ariel V
transient AT2030-330 (Pye and McHardy 1983). We have also indicated the position of the nearby flare star
AU Mic.

» INDP 99% CONFIDENCE CONTOURS FOR D343.97

-1.000

-6.000

162.00

168.00

D343FL.LTP

.1

.05

0

-.05

HED3 CTS/-CM^2-S

0   20   40   60   80

TIME IN SECONDS

χ^2 =   18.4 FOR 14 DOF
P1= 0.240E-01 SIG= 0.141E-02
χ^2 =   18.0 FOR 13 DOF
P2= 0.466E-04 P3= 0.223E-01

c) We plotted the 99% confidence position limits (in 1950.0 R.A. and Decl.) on the left, and the ~1 minute event light curve (in HED3 cts-cm^{-2}-s^{-1} versus time in seconds) on the right, for the event on D.O.Y. 343.97. Time zero for the light curve is at 23:15:24.281 UT. The center of the error box is at Galactic l^{II},b^{II} ~ 258.2°, 49.2°. We found no identified X-ray sources, no A-1 catalog sources, and no known optically variable stars or emission line stars (Wackerling 1970; Kukarkin et al. 1969; 1971; 1974; 1976) in the field of view.

5FINDP 99% CONFIDENCE CONTOURS FOR 0370.82

-62.000

-69.000

122.00   132.0

D370FL.LTP

HED3 CTS/-CM^2-S

.1

.05

0

-.05

0   20   40   60   80   100

TIME IN SECONDS

$\chi^2 =$ 23.8   FOR   17 DOF
P1= 0.733E-02 SIG= 0.957E-03
$\chi^2 =$ 23.1   FOR   16 DOF
P2=-0.445E-04 P3= 0.935E-02
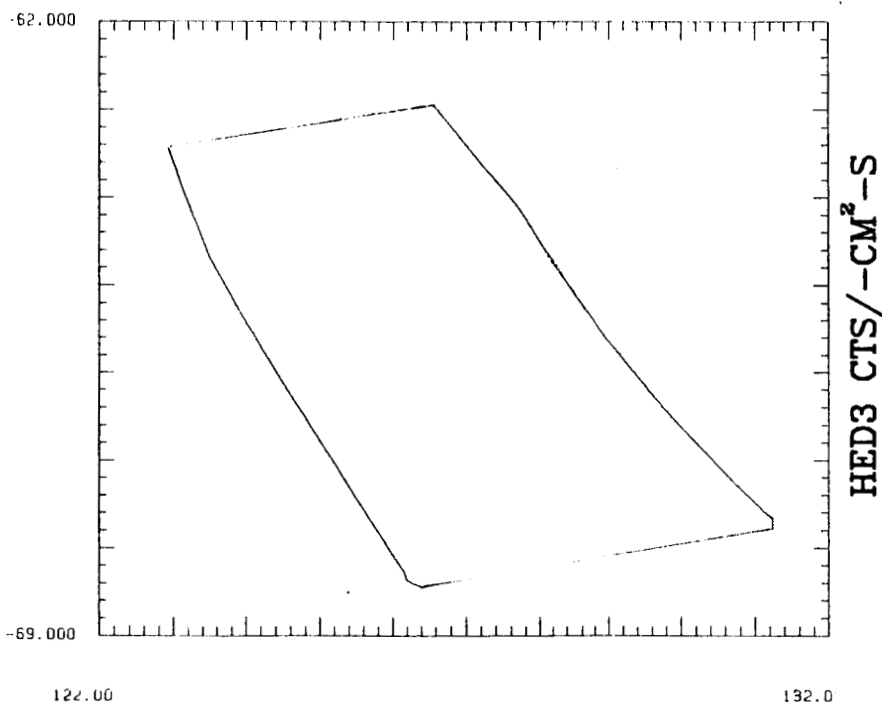
d)   We plotted the 99% confidence position limits (in 1950.0 R.A. and Decl.) on the left, and the ~1 minute event light curve (in HED3 cts-cm^{-2}-s^{-1} versus time in seconds) on the right, for the event on D.O.Y. 370.82.   Time zero for the light curve is at 19:40:36.297 UT. The center of the error box is at Galactic l^{II},b^{II} ~ 279.8°, -15.4°. We found no identified X-ray sources, and no A-1 catalog sources in the field of view. However the error box contains HD 73834, a 7.9 mag Be star (Wackerling 1970), one eclipsing Algol-type system, TX Vol (Kukarkin et al. 1974), and overlapped a large error box for a gamma-ray burst, 1973 Jun 10 at an R.A., Dec of 127°,-64° with r=5°.
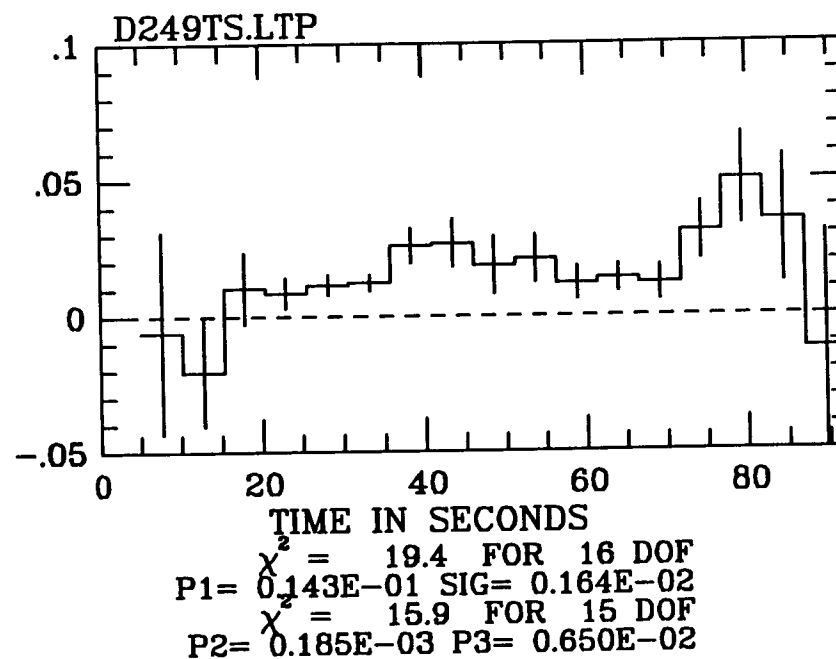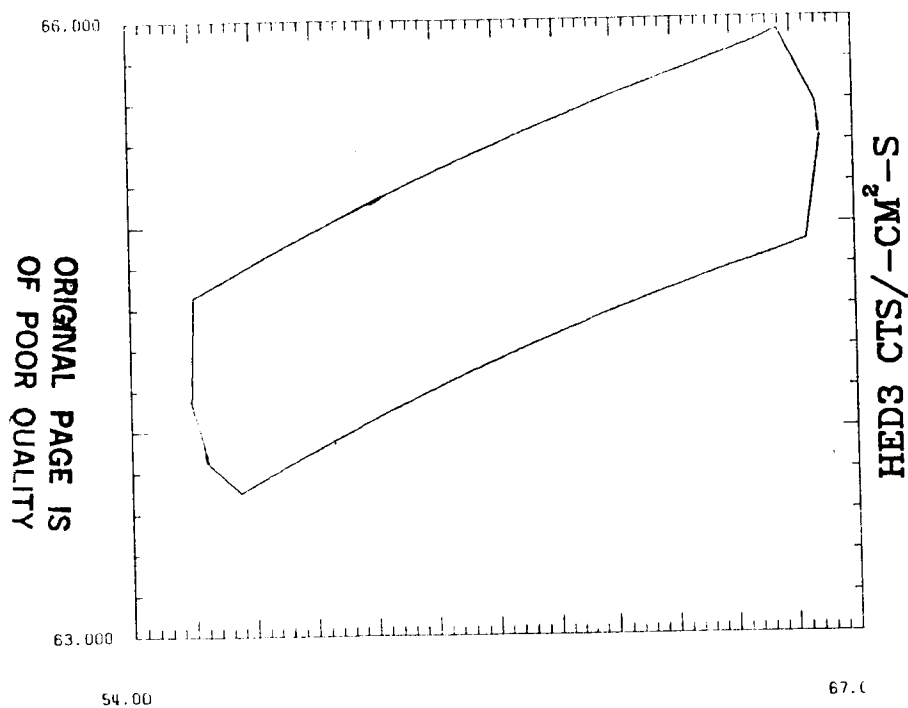
ISFINDP 99% CONFIDENCE CONTOUR FOR D405.85 + LDS 131

D405LDSB.LTP

HED3 CTS/-CM^2-S

TIME IN SECONDS

χ^2 = 7423.2   FOR   47 DOF
P1= 0.982E-01 SIG= 0.134E-02
χ^2 = 1894.1   FOR   46 DOF
P2=-0.529E-04 P3= 0.321E+00
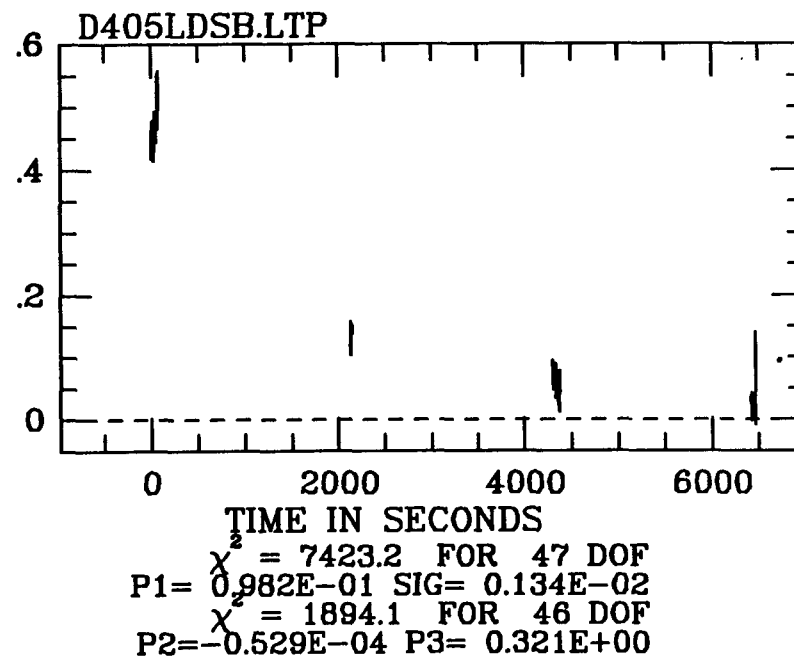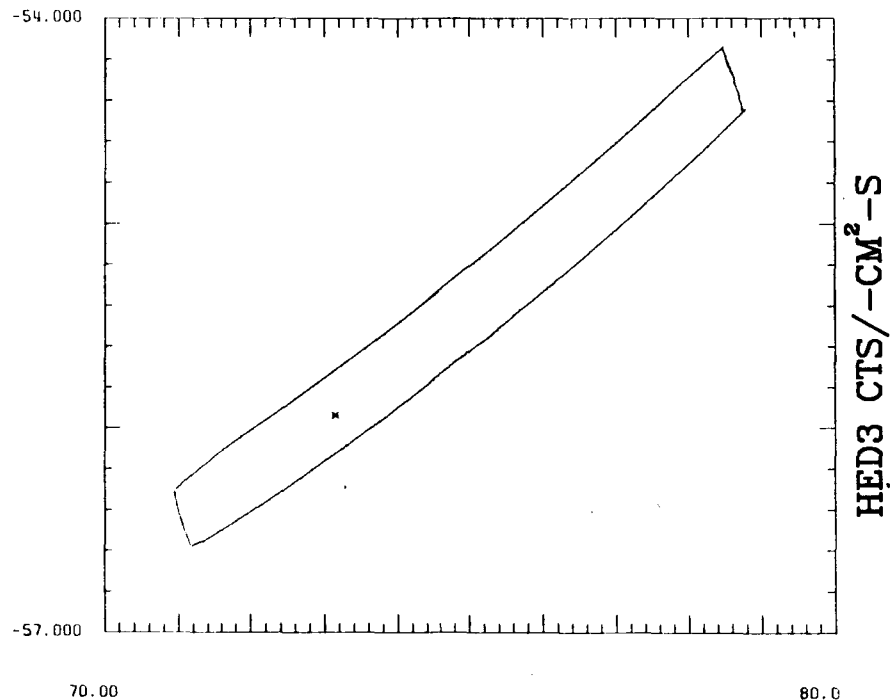
e)   This event was discovered in HEAO 1 A-2 data by Kaluzienski et al. (1978a,b), and identified by Griffiths et al. (1979) with a 10 mag dMe pair, LDS 131. It was detectable for four scans. We plotted the 99% confidence position limits (in 1950.0 R.A. and Decl.) together with the position of the suggested source, followed by the ~2 hour light curve of the event on D.O.Y. 405.85 (in HED3 cts-cm^{-2}-s^{-1} versus time in seconds), requiring the position to be fixed at that of LDS 131. Time zero is at 20:24:17.781 UT. The center of the error box is at Galactic l^{II},b^{II} ~ 264.3°, -38.6°. We found no other identified X-ray sources, no A-1 catalog sources, and no known optically variable stars or emission line stars in the field of view.

· 5 90% CONFIDENCE CONTOURS FOR EVENT D436.84

D436FL.LTP

HED3 CTS/-CM^2-S

TIME IN SECONDS

$\chi^2 = 14.9$ FOR 18 DOF

P1= 0.277E-01 SIG= 0.175E-02
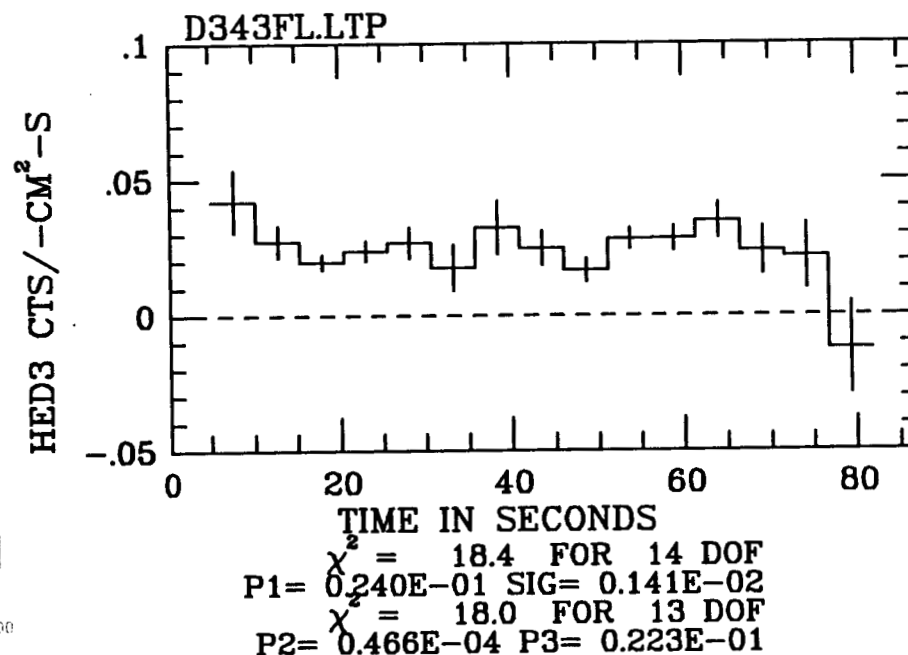
$\chi^2 = 14.8$ FOR 17 DOF

P2=-0.380E-04 P3= 0.300E-01
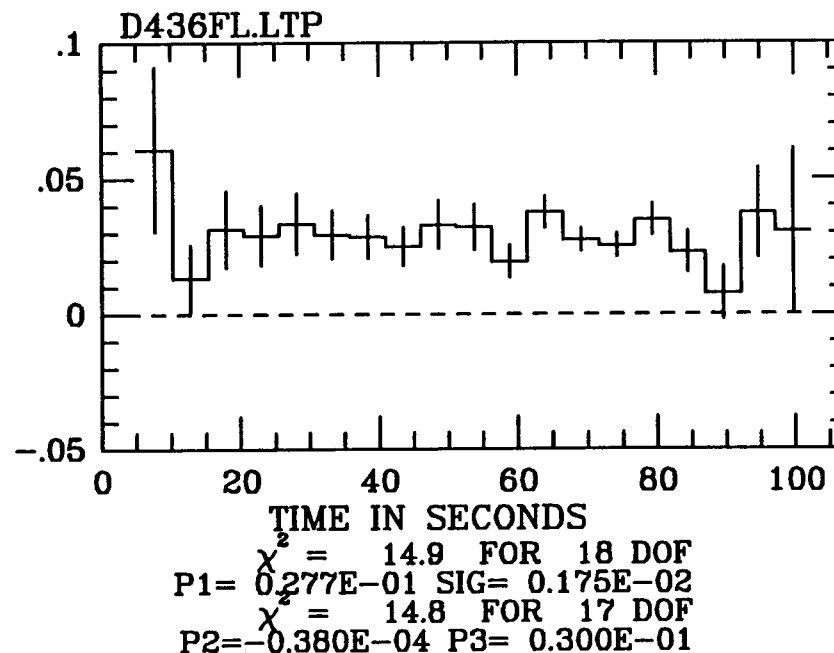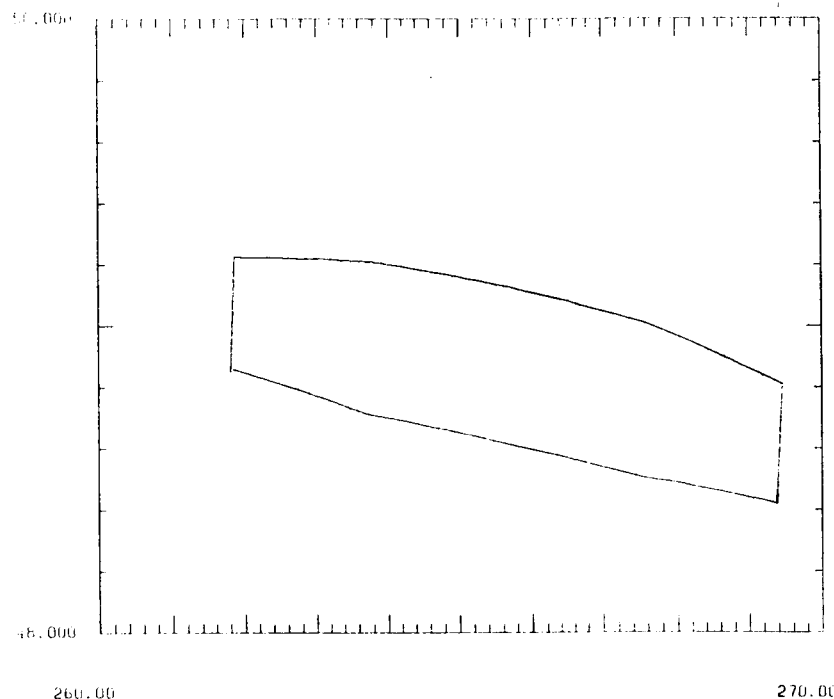
f) We plotted the 99% confidence position limits (in 1950.0 R.A. and Decl.) on the left, and the ~1 minute event light curve (in HED3 cts-cm^{-2}-s^{-1} versus time in seconds) on the right, for the event on D.O.Y. 436.84. Time zero for the light curve is at 20:10:33.516 UT. The center of the error box is at Galactic l^{II}, b^{II} ~ 75.2°, 30.8°. We found no identified X-ray sources, no A-1 catalog sources, no known optically variable stars or emission line stars (Wackerling 1970; Kukarkin et al. 1969; 1971; 1974; 1976), and no gamma-ray source error boxes in the field of view.

86

D623FL.LTP

HED3 CTS/-CM^2-S

TIME IN SECONDS

χ^2 = 13.7 FOR 15 DOF
P1= 0.635E-02 SIG= 0.116E-02
χ^2 = 11.8 FOR 14 DOF
P2=-0.814E-04 P3= 0.949E-02

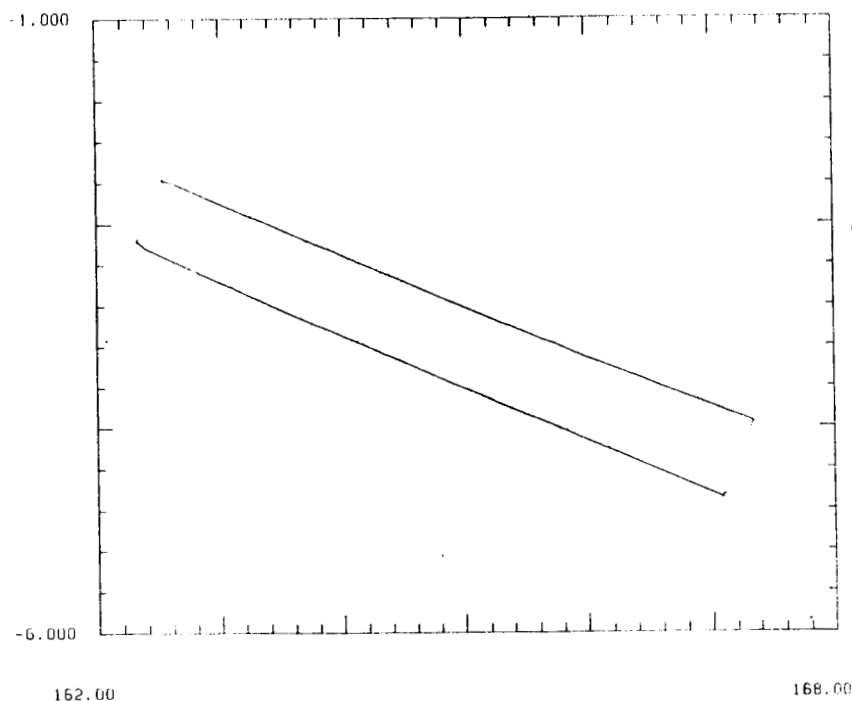g) We plotted the 99% confidence position limits (in 1950.0 R.A. and Decl.) on the left, and the ~1 minute event light curve (in HED3 cts-cm^{-2}-s^{-1} versus time in seconds) on the right, for the event on D.O.Y. 623.47. Time zero for the light curve is at 11:21:19.582 UT. The center of the error box is at Galactic l^{II},b^{II} ~ 41.6°, 24.6°. We found no identified X-ray sources, no A-1 catalog sources, no known gamma-ray source positions, and no known optically variable stars or emission line stars (Wackerling 1970; Kukarkin et al. 1969; 1971; 1974; 1976) in the field of view.

H2120P55.LTP
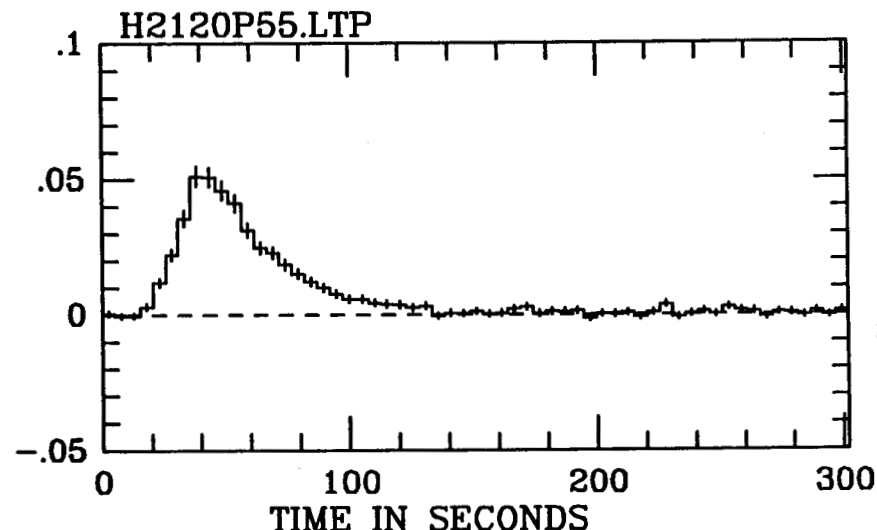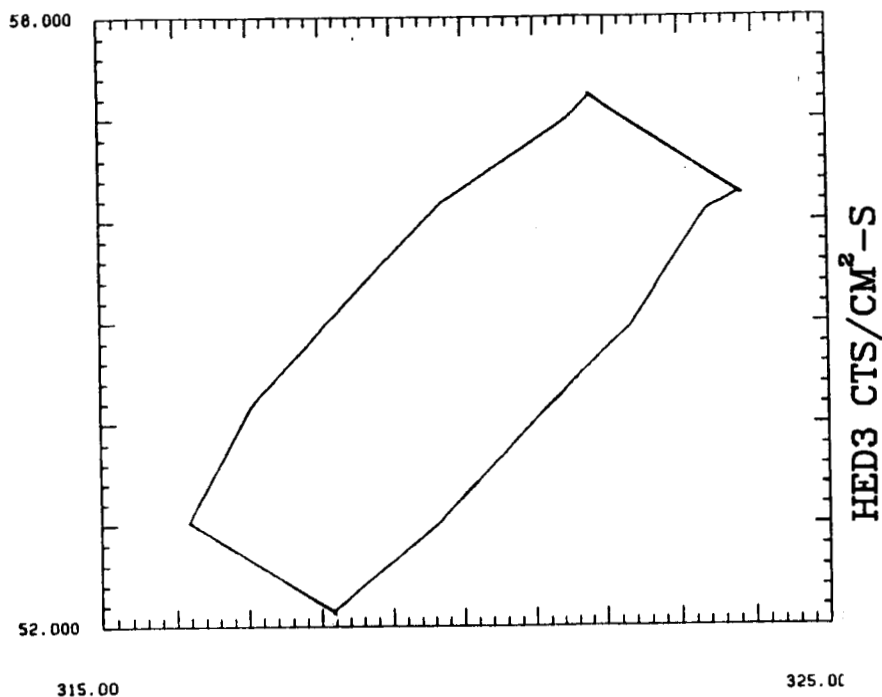
$\chi^2 = 1498.1$ FOR 58 DOF
P1= 0.292E−02 SIG= 0.178E−03
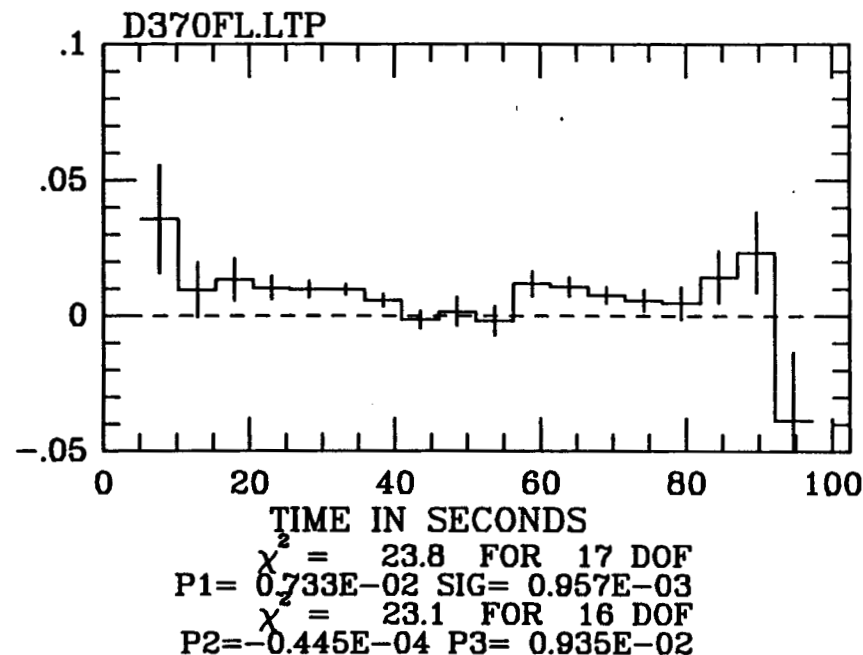$\chi^2 = 1232.4$ FOR 57 DOF
P2=−0.344E−04 P3= 0.881E−02

h) We plotted the 99% confidence position limits (in 1950.0 R.A. and Decl.) on the left, and the ~1 minute event light curve (in HED3 cts-cm^{-2}-s^{-1} versus time in seconds) on the right, for the event on D.O.Y. 728.15. Time zero for the light curve is at 3:36:40.000 UT. Since this was a pointed observation we can display a complete ~100 s light curve for the event. The center of the error box is at Galactic l^{II},b^{II} ~ 95.5°, 3.6°. We found no identified X-ray sources, no A-1 catalog sources, and no known optically variable stars or emission line stars (Wackerling 1970; Kukarkin et al. 1969; 1971; 1974; 1976) in the field of view. However this A-2 position error box overlaps a large gamma-ray burst error box, 1972 Jan 17 at an R.A., Dec of 322°,50° with r=5°, as well as that of a weak A-2 steady source, and a COS B (gamma-ray) error box which contains an IPC source (just outside the 99% confidence position limits).

1. Description of the Events

We have listed the times, positions, intensities, and spectral characteristics of the seven events from the "source-free" survey, plus the one in pointed data from Tennant and Swank (1983), in Table 3.3.a. We calculated the best-fit positions, intensities, and indications of <1 minute variability using the position finding program described in Appendix B. (Essentially, we have compared the count rate minus the background among the overlapping instrument fields of view, each 5 s interval, to constrain the position in an intensity-independent fashion. The event light curves were by-products of this process.) We have presented the corresponding light curves and 99% confidence position error boxes in Figure 3.1. When a fit of a light curve to a constant intensity produced a value for χ^2 that was more than twice the number of degrees of freedom, we indicated that source to be variable in the eighth column of Table 3.3.a. For this source-free phase, only two events showed indications of <100 s variability. One was the event on D405.85, which was also distinguished by its high peak flux (~150 millicrabs), and long duration (exponential decay time ~40 minutes). During the first and brightest pass over the source, the flux was increasing, with an exponential rise time of 7-10 minutes. The only other event in Table 3.3.a showing evidence of <100 s variability was the event on D728.15, the fast transient discovered serendipitously by Tennant and Swank (1983). Since it was observed in pointed data, it was the only event for which we have a complete, uninterrupted light curve. When the satellite was in scanning mode, the detectors spun past each source position at best every ~32 minutes; interruptions of the data, due

88

primarily to Earth occultations and occasional electron contamination, constrained the mean time between viewings to be closer to twice this value. Occasionally, data from the A-1 experiment on the opposite side of the spacecraft could be used to help constrain the durations of the events found in scanning data (C. Ambruster private communication; Ambruster and Wood 1986). Only the event on D298.62 was clearly visible in A-1 data, although there may have been weak indications around the time of the events on D249.36 and D343.97. (The A-1 detectors were turned off during the bright event on D405.85; K. Wood and P. Hertz, private communication.)

Not surprisingly, we found no evidence for associated persistent emission around the time of the event for any of the events found in the source-free transient survey. However Tennant and Swank (1983) noted a weak persistent source consistent in position with the event on D728.15, but occurring a year before that outburst. We have listed 90% upper limits on quiescent flux during roughly a week around the time of each transient in the ninth column of Table 3.3.a. (Note that these values are not in the same units as the peak flux). We found, for all events, the ratio of peak flux to quiescent flux ranges from ≥ 20 (for D249.36) to ~600 (for the brightest event, on D405.85). This already set strong constraints on possible sources for these events. Aside from sources in the Magellanic Clouds, extragalactic objects which flare by over a factor of twenty in less than an hour are very rare, for example.

Further constraints were provided by fits to spectral data. We have listed parameters from fits to three simple models in columns ten through twelve of Table 3.3.a. For most events, we detected

insufficient photons to unambiguously deconvolve the measurements of any possible low energy turnover from those of the temperature (for the black body or thin thermal bremsstrahlung models) or photon index (for a power law model). We therefore reported the best-fit temperatures and power law photon indexes for two different assumed column densities, $N_H \leq 10^{19}$ cm^{-2} and $N_H \sim 10^{23}$ cm^{-2}.

In four cases, we found evidence for negligible absorption. Using HEAO 1 A-2 LED (0.15-3 keV) and MED (2-20 keV) data, Kahn et al. (1979) demonstrated the spectrum of the event on D298.62 (identified as a $\sim 4 \times 10^{30}$ erg-s^{-1} flare from the dM4e star AT Mic) to be well fit by an optically thin thermal bremsstrahlung spectrum (kT$\sim$2.7 keV) plus an iron line. Our best fit MED+HED3 spectra were consistent with their results. In Chapter 5, we presented the spectrum of the brightest event, on D405.85 (Kaluzienski et al. 1978a,b), and noted that it was also well described by a cooling, optically thin, thermal bremsstrahlung plus iron line model, but with a temperature of $\sim$12.6 keV. This event had also been identified by Griffiths et al. (1979) as a flare from a dM3e pair, LDS 131 (in Luyten 1963a; also BPM 17964/17965, in Luyten 1963b; and U98, in Upgren et al. 1972). The spectrum of the event found in pointed data on D728.15 was also well-described by a cooling, optically thin thermal bremsstrahlung model with a temperature at peak of $\sim$9 keV. The column density was constrained to be $<10^{22}$ cm^2 by the MED data. The event on D343.97, though fainter than the events on D405.85 and D728.15, and without low energy information from the LED detectors, was bright enough in MED and HED3 data to constrain the column density to under 10^{22} cm^{-2}.

For two other events, those on D249.36 and D436.85, the spectra

indicated a low energy turnover equivalent to $N_H \geq 10^{22}$ cm^{-2}. During the event on D249.36, the LEDs (0.15-3 keV) were on but showed no appreciable flux increase. This implied a column density $>10^{22}$ cm^{-2} (Nugent et al. 1983). In marked contrast, Kahn et al. (1979) found the AT Mic flare emitted the bulk of its photons in the LED range.

In Figure 3.2, we show the HED2 and (offset) HED1 pulse height spectra with thermal bremsstrahlung fits, for the event on D436.84. The best fit thermal bremsstrahlung models for the three co-aligned detectors all had kT>16 keV and negligible absorption; the best fit power law models had photon indices of 1.3±0.4. The best fit kT for HED1 (which trailed the others by 30 s) was 8 keV (and the photon index ~2.7), with $N_H \sim 10^{23}$ cm^{-2}. The data are thus consistent with a softening spectrum, but, on the other hand, the 90% confidence contours shown in Figure 3.3 are consistent with a constant temperature of ~15 keV for $N_H \sim 2 \times 10^{22}$cm^{-2}. Upper limits on the flux from this event in the 20-120 keV, 0.1-1.1 MeV, and 1.1-6 MeV energy ranges from the A-4 instruments were kindly provided by Geoff Hueter at the University of California, San Diego. They were consistent with our best-fit spectra but did not constrain them beyond requiring a power law photon index of more than 1.

During two of the four faintest events in Table 3.3.a (on D370.82 and D623.47), the LED detectors were off. Evidence on N_H from the higher energy A-2 detectors was ambiguous, but consistent with negligible absorption.

Although for a few events we could exclude black body or power law models, all events had spectra that could be adequately described by thin thermal bremsstrahlung models. The best-fit temperatures of
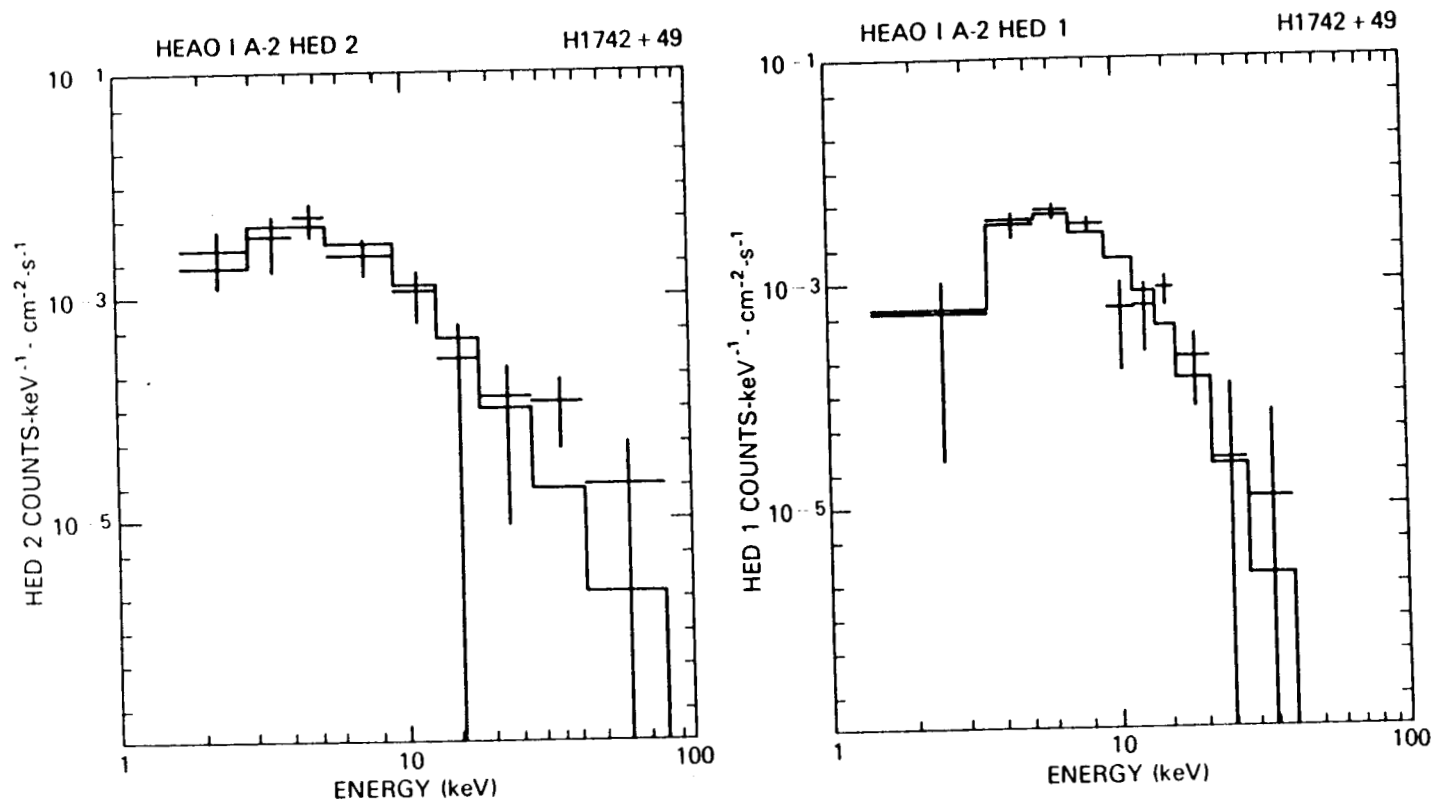
Figure 3.2

a) The HED2 raw spectrum of H1742+49 (event on D436.84) is compared to a thermal bremsstrahlung model with kT = 100keV and negligible absorption.

b) The analogous raw spectrum from the offset detector, HED1, with kT = 8 keV and N_H f 2×10^{22} cm^{-2}. (The two detectors have similar response save below a few keV, where HED1 has a smaller effective area.)

H1742+49 THERMAL BREMSSTRAHLUNG
90% χ^2 CONTOURS
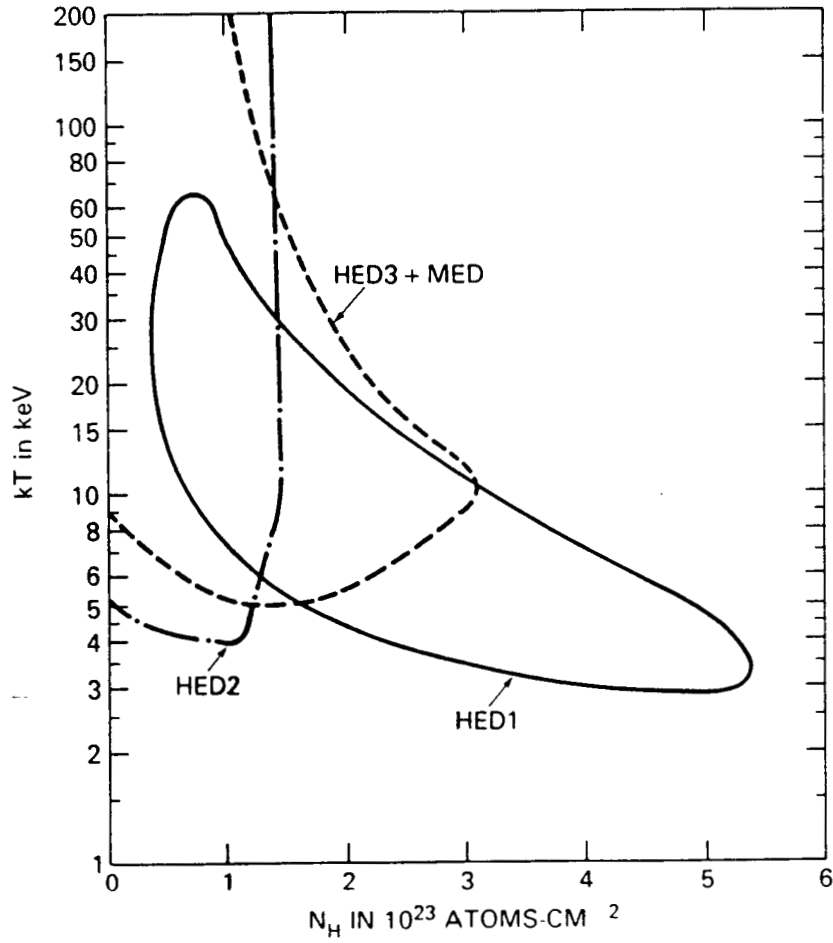
Figure 3.3 90% confidence contours in thermal bremsstrahlung temperature (in keV) versus column density (in 10^{23} cm^2) for HED2, HED3+MED, and HED1 data from the H1742-49 flare.

the events ranged from greater than 16 keV (for the event on D436.84), to on the order of 10 keV (D249.36, D343.97, D405.85, D728.15), or less than 5 keV (D298.62, D370.82, and D623.47).

In the last column of Table 3.3.a, we proffered notes on nearby X-ray sources (Bradt and McClintock 1983; Kahn et al. 1979; Griffiths et al. 1979; Ambruster and Wood 1986) and types of optical objects that may vary in X-rays. For the latter, we used an on-line computer catalog (Mead and Hill 1983). We found the two flare star systems mentioned previously (AT Mic and LDS 131); and one early type emission-line object plus one eclipsing Algol-type system (probably too distant to be the source of the event), within the 99% position contours for the event D370.82, (which had the largest error box due to its low flux). We also listed any gamma-ray burst position error boxes, kindly provided by J. Norris, U. Desai, and T. Cline (private communication), that may have overlapped the position limits of our events.

ii. General Remarks on Identifications

We have limited our discussion to objects within the Galaxy, as extra-galactic objects which flare by over an order of magnitude in less than an hour are quite rare, and we found no such objects within the event (99% confidence) position limits. We have by definition excluded any possible variable objects in the Magellanic Clouds.

In this discussion, we compared the HEAO 1 A-2 fast transient events with well-known types of variable X-ray sources. There is always the possibility that one or more events may represent classes of rare and poorly understood events. That such events do occur is

illustrated in Chapter 5 by the discussion of a singular bright event observed in OSO-8 data (Serlemitsos, Bunner, and Swank 1979), and by puzzling events from other fast transient surveys (Helfand and Vrtilek 1983; Ambruster and Wood 1986; Pye and McHardy 1983).

iii. Luminous Events from Compact Objects

We consider it unlikely that any of these A-2 source-free fast transients were from luminous compact X-ray binaries of the types displayed in Tables 3.1 and 3.2, since both the events and their quiescent counterparts were so faint. One might at first have thought, for example, of distant X-ray burst sources, as an explanation for the events with large turn-overs at low energies. However, in order to have a luminosity near the Eddington limit, as is typical for Type I and II X-ray bursts (Lewin and Joss 1981), a 7×10^{-10} ergs-cm^{-2}-s^{-2} source would have to be more distant than 50 kpc, placing it well outside the Galaxy. For most of the events in Table 3.3 that had acceptable black body fits, if we assumed a source the size of a neutron star, we again inferred distances outside the Galaxy. The exceptions required column densities of $\sim 10^{23}$ cm^{-2}, which were incompatible with measured interstellar values. Local column densities of this magnitude are atypical for X-ray bursts. For the event on D436.84, at (l,b) of (75°,31°), the total line of sight absorption was $\sim 4 \times 10^{20}$ cm^{-2} (Burstein and Heiles 1982), an order of magnitude less than that required by the 90% lower limit on N_H from the offset detector. For the event on D249.36, the average E(B-V) in the direction (l,b) of (141°,8.6°) was ~ 0.4 mag kpc^{-1} (Lucke 1978); one expects an interstellar column density of less than 3×10^{21} cm^{-2}.

(A more plausible model might involve black body emission from a fraction of a neutron star surface, with some intrinsic absorption, implying a distance of less than 2 kpc; see §3.D) Therefore in what follows we concentrated on outbursts from the types of objects we have described in the overview as more X-ray faint, such as coronal flares.

iv. The Case for Identification with Flare Stars

We suggest that 5 of the 7 source free fast transient events, plus the event on D728.15 found in pointed data, may have been stellar flares from ubiquitous (roughly one per 25 pc^3) dMe-dKe stars. Haisch (1983), reviewing the X-ray properties of stellar flares (from nearby stars), noted peak X-ray luminosities from 10^{28} to 10^{31} ergs-s^{-1}, temperatures from ~1 to 9 keV, and durations from a minute to an hour. Five of the events in Table 3.3.a (on D298.62, attributed to AT Mic; D343.97; D370.82; D623.47; and D728.15) fit this description. As illustrated in Chapter 5, the event on D405.85 was slightly hotter and an order of magnitude more luminous. However, in their discussion of a "superflare" from EV Lac (L_V~10^{32} ergs-s^{-1}, E≥10^{36} ergs), Roizman and Shevchenko (1982) suggested that all nearby dMe-dKe stars may be capable of extremely energetic outbursts upon occasion. Ambruster et al. (1983) also made this suggestion when discussing a bright A-1 fast transient, H0547-14 (flux ~ 177 millicrabs, kT ~ 25 keV, quiescent to peak flux ratio of ≥3x10^{-3}).

Two of the events in Table 3.3.a have been attributed to the flare stars AT Mic and LDS 131. A search similar to this one, but using the first six months of HEAO 1 A-1 data found 10 events, three with flare stars in their position error boxes, including the rise and

fall of the event on D298.62 from AT Mic (Ambruster and Wood 1986).
An energetic flare from EV Lac had a peak luminosity of ~5x10^{30}
ergs-s^{-1} (2-20 keV), a total energy of ~10^{34} ergs, and a quiescent-to-
peak-flux ratio of ~2x10^{-2} (Ambruster, Snyder, and Wood 1984). An
event attributed to EQ Vir would have had a peak luminosity of ~7x10^{30}
ergs-s^{-1} (2-20 keV) (Ambruster and Wood 1984).

It is improbable that all four systems fell within the event
position error boxes by chance. The one object that was identified by
optical observations, D405.85, had combined A-3 and A-4 error boxes of
~0.24 deg^2; the expected number of dMe-dKe stars within 20 pc that
would fall in this error box by chance is less than 8x10^{-3}. For the
larger error boxes we searched published catalogs of nearby stars
(Gliese 1969; Woolley et al. 1970; Joy and Abt 1974; Petterson
1976; Gliese and Jahreiss 1979; Gurzadyan 1980; Upgren et al.
1972), as did Ambruster and Wood (1986). Out of 90 dM-dK stars listed
in the literature as having either Hα emission or to have flared, four
(LDS 131= U98, AT Mic, EV Lac, and EQ Vir) were found in the A-1 and
A-2 error boxes, with combined area ~200 deg^2. The expected number if
they are serendipitous is 0.4, so that the probability of finding four
or more in combined HEAO 1 A-1 and A-2 position error boxes is less
than 0.1%.

These lists of active dM-dK stars published in the literature are
not complete. A comparison with Joy and Abt (1974), Allen (1973), and
Bahcall and Soneira (1980) demonstrates that ~70% of the dMe-dKe stars
closer than 5 pc, and less than 4% of those within 25 pc, are
listed. Taking the maximum X-ray flare luminosity to be
10^{32} ergs-s^{-1}, consistent with that measured from the bright flare

from LDS 131 on D405.85, we find that this fast transient survey could have detected flares from dMe-dKe stars as distant as 60-70 pc. Therefore it seems reasonable that uncatalogued active dwarf stars may have been the source of most of the unidentified fast transients.

We compared event rates found in this search with those one expects from all dMe-dKe stars, by extrapolating optical flare rates to X-rays (see Appendix C). Our flare star model predicted an event rate above a flux S to be $R(S) \approx 10^4 (S/S_0)^{-1.5}$ events-yr^{-1} per sky, with S_0 our lowest search threshold of $\sim$ 4 millicrabs ($\sim 10^{-10}$ ergs-cm^{-2}-s^{-1}), and assuming that the frequency of flares goes as L_x^{-1}, and that the maximum flare luminosity in our energy band is $\sim 10^{32}$ ergs-s^{-1}. The normalization, which goes as $\tau^{-1} L_{max}^{\frac{1}{2}}$, where τ is the event duration, is uncertain (1σ) by a factor of $\sim$3 in either direction. From Einstein Observatory results we found an average duration τ of 200-1300 s (Haisch 1983; see Appendix C), implying that decay times of X-ray flares are several times longer than their U-band counterparts (Kahler et al 1982). By analogy with the sun, we speculate that these very energetic X-ray stellar flares may be analogous to solar gradual flares, which originate on quite large ($\geq 4 \times 10^4$ km) magnetic loops (Tsuneta 1984; Sturrock 1985). We consider this further in the discussion of the flares from LDS 131 in Chapter 5.

Next we considered whether this calculated flare rate matches that seen in our data. In this "source-free" phase of our search, out of the equivalent of $\sim$64 days of 'on' time (54.6 days each from HED3 and HED1, which viewed adjacent but independent sections of the sky; 41.6 days of data from MED, and 24.9 days from HED2, which were co-

aligned with HED3), we found five events with spectra consistent with that of stellar flares (D298.62, D343.97, D370.82, D405.85, and D623.47), plus the event from pointed data (on D728.15), or about one per 13 days of good data above our search threshold. Using the expressions for the probability of detecting events developed in Appendix A, for the "source-free" search (which had a constant set of thresholds), the maximum likelihood fit to these six (unabsorbed) events was $R(S) \approx 2 \times 10^4 (S/S_0)^{-1.5}$ events-yr^{-1} over the whole sky, differing only by a factor of two from our predictions based on optical studies and flare rates observed with the Einstein Observatory. The normalization was uncertain (1σ) by about a factor of three. We inferred that these six events from the "source-free" sky could have been flares from dMe-dKe stars.

We performed a similar calculation for the expected number of flares from active dM-dK stars found in the literature, using the properties listed there (Gliese 1969; Woolley et al. 1970; Joy and Abt 1974; Petterson 1976; Gliese and Jahreiss 1979; Upgren et al. 1972). We predicted an average rate of about 1 event found in both the A-1 search and the A-2 all-sky survey, with an uncertainty of an order of magnitude, due chiefly to the uncertainty of the average ratio of X-ray to U-band luminosity, which was assumed to be about 10 (Haisch 1983 and Appendix C). For L_U/L_X of about 2, as suggested by the A-2 "source-free" survey event rates, we predicted ~4 events in the combined A-1 and A-2 all-sky surveys. These estimates were consistent with the observed number of 4 events from flare stars found in the literature.

These event rates raised a related question: could any of the

Ariel V fast transients (Pye and McHardy 1983) have come from the luminous tail of the stellar flare distribution apparently seen by HEAO 1? The mean duration of stellar flares is much briefer than the Ariel V 100 minute integration time, implying that their effective limiting threshold was ~25-100 times that of the HEAO 1 A-2 search. If one compares our maximum likelihood flare star model with the Ariel V logN-logS distribution, one finds that between 1 and 9 of the 29 Ariel v events should have been due to bright stellar flares. As shown in the panel for D298.62 in Figure 3.1, the Ariel V transient source AT2030-330 lies across the center of the D298.62 99% confidence position limits. However, the Ariel V error box is the intersection of four 20° long 95% confidence "lines of position". Ambruster (1984) notes that two of these, from Ariel V events on 1975 December 23 and 1979 November 14, contained AT Mic, while the other two, from a ~200 millicrab event on 1979 November 11, marginally excluded AT Mic but contained the active flare star AU Mic (Petterson 1976; Helfand and Caillault 1982). This suggests that AU Mic may have produced a $>10^{32}$ erg-s^{-1} (2-20 keV) flare, and Ariel V may have detected events from two flare stars. This is consistent with our prediction above.

v. Other Stellar (Coronal) Candidates

Pye and McHardy (1983) suggested that RS CVn-type systems were the source of seven (out of 29) of the Ariel V fast transients. The durations listed range from 310 to 3600 minutes, which is considerably longer than that for the A-2 all-sky events. A typical RS CVn light curve is sharply peaked, with a fast rise time and a slower decay. Could some of the A-2 events have been just the peaks of more distant

RS CVn-type systems? We calculated the event rate expected above the A-2 survey threshold (of ~4 millicrabs), for an isotropic distribution, and assuming the highest normalization allowed by Pye and McHardy's (1983) 90% contour, to have been less than 0.1 flares from RS CVn-like systems in the A-2 all-sky search. We therefore found it unlikely that any of our events came from these sources. This conclusion is further supported by the lack of known RS CVn-like objects in any of our error boxes (Garcia et al. 1980; Scwartz et al. 1981; Walter, Charles, and Bowyer 1978; Hall 1986). (However, as we noted in Chapter 4, we did apparently detect two flares from a nearby RS CVn-type system in our survey of the Magellanic Clouds region.)

Algol (β Persei) and Algol-like systems have been observed giving off flares with total X-ray luminosity as high as 2×10^{31} ergs-s^{-1} (Schnopper et al. 1976; White and Marshall 1983). We noted a total of one Algol-type system in the largest error box. This system was at a distance of greater than 600 pc (Allen 1973; Kukarkin et al. 1969; 1976), implying an X-ray luminosity of more than 10^{34} ergs-s^{-1}. This is roughly three orders of magnitude brighter than the highest previously observed luminosity. We also note that since there are almost 2000 catalogued eclipsing Algol-type systems, there is over a 90% chance of finding one or more in the position error boxes of the 8 events in Table 3.3.a. We therefore considered it unlikely that any of the fast transient events were from Algol-like systems.

EXOSAT observations of contact binary systems (such as W Uma-type stars) showed evidence of coronal X-ray emission, plus soft X-rays from a connecting 'neck' of accreting matter (Vilhua and Heise

1985). However, ratios of X-ray.to bolometric luminosities show them to be not much more active than dMe-dKe stars in general. Like the RS CVn-type systems and Algol-type binaries, the number density of such contact binaries is so much lower than that of dMe-dKe stars that we find them unlikely to have been sources of the A-2 fast transient events.

Not much is known about intense optical flares which have been reported from normal early-type stars (Kunkel 1975b; Schaefer 1988). Although these rare events can be quite intense, their spectra and rates of occurence are very poorly measured. From Einstein Observatory measurements of X-rays from every type of normal star, Pallavicini et al. (1981) have suggested there may be something similar to coronal activity on nearly every type of normal star, including the more massive early-type ones. We therefore cannot completely dismiss coronal flares from early-type stars as sources of these events, chiefly because they are so poorly understood.

vi. Cataclysmic Variables

HEAO 1 data established that cataclysmic variables, systems in which a late-type star interacts in a close binary with a white dwarf, were a class of X-ray sources with luminosities in the range 10^{29-34} ergs-s^{-1}, with several previously unrecognized CVs discovered on the basis of their 2-10 keV X-ray emission (Steiner et al. 1981 and references therein). Mason (1985) classifies these systems roughly by the strength of the magnetic field of the white dwarf, including systems with weak fields (such as SS Cyg), with very soft (~<100 eV black body temperatures) X-ray emission plus harder X-rays (possibly

from transient regions of strong magnetic fields analogous to active regions on cool stars); rotating magnetic stars with stronger 2-20 keV X-ray emission (presumably from the magnetic poles) showing modulation from the rotation period of the star; and phase locked magnetic CVs, such as AM Her, with more complicated light curves featuring several eclipses per cycle. However CVs are often more prominent in soft X-rays than they are above 2 keV; during optical outbursts (novae and dwarf novae outbursts), although one sees an increase in the <0.5 keV X-rays, the harder emission drops in intensity. In general, we find it unlikely that any of the events from this 2-20 keV survey of the sky were from cataclysmic variables. In this energy band, although the flux often varies by factors of 2-5 in irregular flickering and flaring on time-scales of ~1-100 minutes, and although it is possible to observe quite dramatic intensity variations due to eclipses from systems such as AM Her (see §3.B), we note that CV systems with 2-20 keV variations bright enough to have triggered our search also would have been bright enough to have been found as quiescent sources by previous researchers.

vii. Non-Coronal Events: Outbursts from Compact Objects?

We were left with two events, D249.36 and D436.84, which we could not attribute to any coronal source because of the low energy turnover (equivalent to $N_H \geq 10^{22}$ cm^{-2}) which was not due to interstellar extinction. From fits to our data, we infered an event frequency above our threshold (of ~4 millicrabs ~ 10^{-10} ergs-cm^{-2}-s^{-1}) of 3×10^2- 6×10^3 similar events per year over the whole sky, with durations of less than an hour but greater than about 15 minutes. If these events

are distributed like stellar flares, which originate on nearby

(<100 pc) Galactic sources, with peak X-ray luminosities less than

10^{33} ergs-s^{-1}, one expects an isotropic distribution and therefore a

couple more similar events as the HEAO 1 A-2 fast transient survey is

extended to "source-full" regions of sky. If they originate on

Galactic sources containing compact objects, with have peak X-ray

luminosities greater than about 10^{35} ergs-s^{-1}, one may find a disk

distribution in the unexplored "source-full" sections of the data.

D. Results From the "Source-Full" Sky"

In this section we describe fast transient activity from the rest

of the sky, excepting regions around those sources listed in Tables

3.1 and 3.2. For this second phase, rather than comparing ~1 and 5 s

rates with counting rates from the diffuse sky plus internal detector

background, we compared the rates in ~5, 15, and 61 s intervals with

12 hour averages of the corresponding positions on the sky. Although,

as described in Chapter 2, we surveyed the entire database using this

second algorithm, in this section we consider only the additional

events from major frames of data designated as containing sources

brighter than about one millicrab. That is, we have considered only

data not covered by the "source-free" survey, and so have called this

second phase a survey of the "source-full" sky. From Chapter 2, we

noted that the inclusion of source-full regions almost doubled the

amount of data surveyed, but that the "source-full" data incorporated

a greater proportion of data with higher average count-rates, so that

on average the search threshold was slightly higher. In this second

pass through all the scanning data, using the "all-sky" search

algorithm, we did not trigger on two of the faintest events from the

survey of the "source-free" sky (on D370.82 and D623.47), although we did again trigger on all five other events.

Out of the equivalent of an additional ~59 days of scanning data ($\sim 10^6$ 5.12 s intervals) during which at lest one out of four detectors was on (50.3 days each of HED1 and HED3 data, which viewed adjacent but independent sections of the sky; plus 38.4 and 22.9 days of data from MED and HED2, respectively, which were co-aligned with HED3), we uncovered eight more fast transient events, seven of them new. The eighth was identified by Hueter (1987) as a 1.3×10^{-5} erg-cm^{-2} gamma-ray burst incident through the sides of the detectors. The events ranged in peak flux from ~5 to 15 millicrabs. Three of the events, occurring within 3½ days of each other, probably originated from the same source. The two brighter of these three events showed indications of <100 s variability and may have lasted less than 30 s. Below, we have described the characteristics of these events in detail, and then discussed possible identifications. We have argued that three events have light curves and spectra consistent with those of stellar coronal flares, which is consistent with the number predicted based on results from the "source-free" survey. The other four events were found near the Galactic plane and exhibited harder spectra. We have suggested they may be representatives of a proposed new class of faint hard variable sources along the Galactic plane, and suggested that one event from the "source-free" survey may also have been from this class. We find $\sim 10^{2-3}$ Be-neutron star binaries scattered throughout the Galactic plane to be a plausible identification for these events.

Table 3.3.b: Events From The "Source-Full" Search

TIMES (a)		POSITIONS (b)		INTENSITIES (c)			SPECTRA (d)			NOTES
D.O.Y. 1977	U.T. Duration	R.A., DEC (1950.0)	Galactic l(II), b(II)	Peak Flux	Varies?	Quiescent Flux	PL	TTB	BB	(e)
268.67	16:03 $1 \leq \tau < 176$	90.0 ,-48.6	255.9 ,-28.0	6.8	N	<0.43	2.1±1.6 4.3±1.6	7.+20/-4 >7.0	1.5±0.8 1.1±0.5	(f)
311.65	15:39 $1 \leq \tau < 175$	151.0 , 47.6	169.5 , 52.2	8.2	N	<0.35	1.9±1.6 2.4+4/-2	>4.0 >1.0	>0.4 >0.4	(g)
342.12	02:55 $1 \leq \tau < 175$	132.2 ,-53.3	271.6 , -6.0	4.9	N	<0.60	1.6±0.9 2.1±1.0	>6.0 >3.8	>1.5 2.4±1.1	(h)
343.23	05:34 $\tfrac{1}{2} \leq \tau < 35$	134.7 ,-54.4	273.4 , -5.6	6.3	Y	<0.56	1.6±0.5 2.2±0.7	>9.5 11+35/-6.4	2.3±0.7 2.0±0.6	(h)
345.62	14:51 $1 \leq \tau < 105$	134.6 ,-53.4	272.6 , -5.0	7.6	Y	<0.45	0.8±0.5 1.2±0.6	>42. >16.	>2.5 >2.1	(h)
454.44	10:41	... ...	... ...	9.6	Y	...	...	...	...	(i)
494.15	03:35 $1 \leq \tau < 246$	302.2 , 36.3	73.7 , 1.6	9.2	N	<2.6	1.1±1.0 <3.1	>10. >2.	>2. >1.7	(j)
586.70	16:48 $1 \leq \tau < 141$	75.7 ,-57.1	265.5 ,-37.0	5.6	N	<0.33	1.9±0.5 3.4±1.1	10+34/-5 2.7+5/-1.4	1.5±0.5 0.9±0.4	(k)

a) Times are in D.O.Y. (1977) followed by hours and minutes (in U.T.), for the start time of each event. The constraints on duration are given in minutes.
b) We listed the best fit positions, in both 1950.0 R.A. and Declination, and Galactic l^{II}, b^{II}, calculated using the position finding program described in Appendix B. For these events, from the "source-full" search, we first subtracted a 12 hour average flux for each position, and then proceeded with the fits for positions. For the event on D454.44, a gamma-ray burst incident through the sides of the detector (Heuter

1987), this procedure was not appropriate, and no position was listed.

c) The intensities are in units of excess HED3 cts-s^{-1} above the appropriate 12 hour averages. The intensity of the Crab (pulsar + nebula) is about 660 HED3 cts/s ($\sim$3.4x10^{-8} ergs-cm^{-2}-s^{-1} from 2-20 keV). To calculate these values we performed least-squares fits of the light curves in Figures 3.1 and 3.2, assuming a constant intensity. For the events for which a constant intensity was a bad fit, which we defined to be when the value for χ^2 was more than twice the number of degrees of freedom, we used the highest intensity 5.12 s data point (that was at least 4σ above zero). We have indicated these events with a 'Y' under the label "Varies?". To measure the quiescent flux, we summed HEAO 1 A-2 scanning MED+HED3 1.5° rates from the six month pass in which the event was detected. Typically, this meant about six days of scanning data. If χ^2 dropped by at least twenty when two fit parameters (intensity and scan angle) were introduced, we deemed that source to be significant. The exception was D494.15, which was very close to a bright source, which can cause systematic errors: we listed only upper limits, even though, formally, χ^2 dropped by over thirty when two fit parameters were introduced. (Note that the units are "new R15" units, or MED+HED3 cts-s^{-1}, which are different from the units for the peak intensities.)

d) Unlike for most of the "source-free" events, for these spectra, we first subtracted a 12 hour average appropriate for that position on the sky. We then used "color" rates (available every 5.12 s) rather than the more reliable, more carefully calibrated PHA spectra (often available only every 41 s). See Chapters 2 and 4 for discussions of the systematic uncertainties this method may introduce. In this column, 'PL' stands for the photon index of a power law model; 'TTB' indicates a thin thermal bremmstrahlung (i.e. exponential plus Gaunt factor) temperature in keV; and BB indicates the temperature for a black body model, in keV. The top row in each triple pair corresponds to fits assuming negligible absorption ($N_H \sim 10^{19}$ cm^{-2}). The second row in each pair requires a column density of $\sim 10^{23}$ cm^{-2}. When the number of degrees of freedom was ten or greater, and if χ^2 for a particular model was greater than twice the number of degrees of freedom, we deemed the model unacceptable and left that entry blank. For events with fewer than ten degrees of freedom, a model was deemed unacceptable when χ^2 exceeded the number of degrees of freedom plus ten. Those events marked with an $\ddagger$ may require a changing spectrum and are discussed in more detail in the text. We did not attempt any spectral fits of D454.44.

e) In the footnotes, we listed objects found in the 99% confidence position limits (of Figure 3.1) that belonged to classes of objects associated with variable X-ray emission, and discussed possible identifications. We also mentioned X-ray sources from the A-1 catalog (Wood et al. 1984) if they were very nearby but formally excluded, because variability could have introduced systematic errors in the calculation of the A-1 positions, which were calculated under the assumption of constant intensity.

f) The A1 Catalog source 1H0553-480 lies just outside the 99% confidence position error box.

g) The A-1 Catalog source 1H013+498 is nearby, but formally excluded.

h) These three events probably come from the same source. There are two interesting stars that are in all 3 99% confidence error boxes: CQ Vel, a classiscal GK Per type nova (in 1940, m=9-16; Kukarkin et al. 1969);

and HD299794, an 8.6 m_v early-type emission-line star of "unknown spectral type" (Wackerling 1970). All three events are near (~½° away) the unidentified variable source H0845-53. However, the formal A-1 Catalog 1H0846-534 position error box is outside all three event error boxes in the scan direction.

i) Heuter (1987) identifies this as a moderately intense (fluence~1.5×10^{-5} ergs-cm^{-2}) gamma-ray burst, which came through the sides of the detector at roughly an angle of 31° to the main detector axis.

j) The position of this event falls squarely on one of the more crowded regions of the sky, the Cygnus region. The 99% confidence position contours contain 58 early-type emission-line objects (Wackerling 1970); 7 eclipsing Algol types that are probably too distant to give a flare of this flux; 4 eclipsing beta Lyrae type variables with m_p>8, probably indicating that they are too distant; and 1 U Gem type dwarf nova (m_p=15-18; probably also too far; Kukarkin et al. 1969; 1971; 1974). The position error box for this event overlaps the A-1 error box for the X-ray source H2018+37. The close proximity of the bright source Cyg X-1 made the measurement of persistent flux highly uncertain.

k) One corner of the A-1 Catalog source 1H0524-552 intersects the northeast edge of the event error box.

Figure 3.4 We present 99% confidence position limits ($\chi^2 = \chi^2_{MIN} + 9.21$, for two parameters; Lampton, Margon, and Bowyer 1976) for the eight events from the "source-free" search, generated using the "intensity-independent" fitting procedure described in Appendix B. The light curves presented here are by-products of that process. Except where noted, for the light curves shown here, we used the best-fit values for position, with the position free to vary in the scan direction, but constrained to lie in the scan plane (off-scan angle held fixed at zero), so that the 1σ error bars generated would reflect the uncertainty in the shape of the light curve due to the uncertainty in source scan angle, but not the uncertainty in overall event normalization due to the uncertainty in its off-scan position.

a) We plotted the 99% confidence position limits (in 1950.0 R.A. and Decl.) on the left, and the ~1 minute event light curve (in HED3 cts-cm^{-2}-s^{-1} versus time in seconds) on the right, for the event on D.O.Y. 268.67. Time zero for the light curve is at 16:03:21.648 UT. The center of the error box is at Galactic l^{II},b^{II} ~ 225.1°,-29.0°. We found no identified X-ray sources and no known optically variable stars or emission line stars (Wackerling 1970; Kukarkin et al. 1969; 1971; 1974; 1976) in the field of view. However the A-1 catalog source 1H0553-480 lies just outside (unidentified; Wood et al. 1984).

111
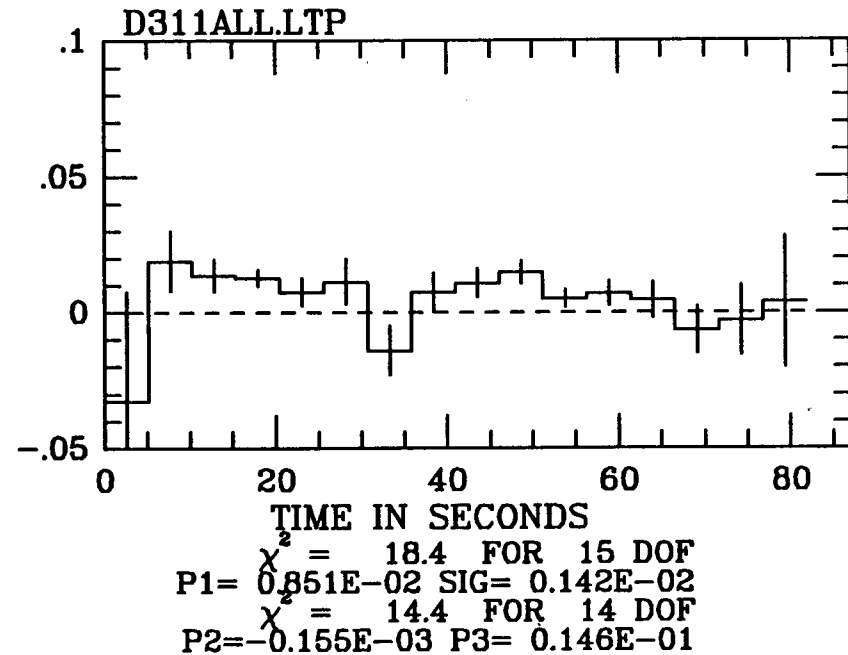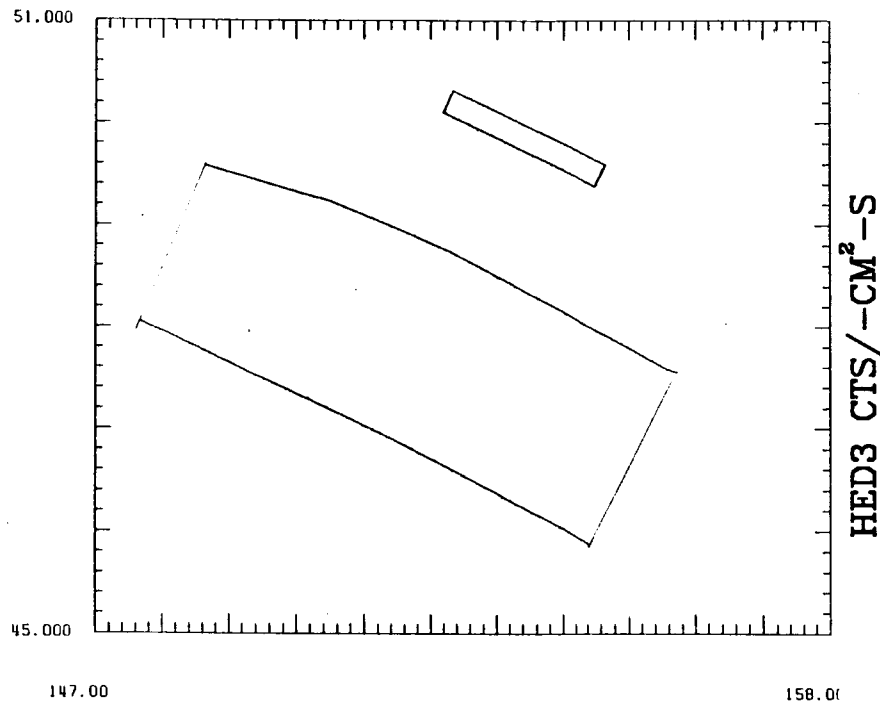
b) We plotted the 99% confidence position limits (in 1950.0 R.A. and Decl.) on the left, and the ~1 minute event light curve (in HED3 cts-cm^{-2}-s^{-1} versus time in seconds) on the right, for the event on D.O.Y. 311.65. Time zero for the light curve is at 15:39:22.988 UT. The center of the error box is at Galactic l^{II},b^{II} ~ 165.1°,52.9°. We found no identified X-ray sources and no known optically variable stars or emission line stars (Wackerling 1970; Kukarkin et al. 1969; 1971; 1974; 1976) in the field of view. Although the A-1 catalog source 1H013+498 is nearby, it is formally excluded.

D342ALL.LTP

HED3 CTS/-CM^2-S

TIME IN SECONDS

χ^2 = 8.0 FOR 12 DOF
P1= 0.870E-02 SIG= 0.129E-02
χ^2 = 8.0 FOR 11 DOF
P2=-0.118E-04 P3= 0.898E-02

c) We plotted the 99% confidence position limits (in 1950.0 R.A. and Decl.) on the left, and the ~1 minute event light curve (in HED3 cts-cm^{-2}-s^{-1}, above a 12 hour average, versus time in seconds) on the right, for the event on D.O.Y. 342.12. Time zero for the light curve is at 2:55:08.305 UT. The center of the error box is at Galactic l^{II},b^{II} ~ 271.6°,-6.3° . This is the first of three events, occurring within 3½ days, with overlapping position limits. We found two optically variable stars within the intersection of all three 99% contours: CQ Vel, a classical DQ Her-type nova; and HD299794, an 8.6 m_v early type emission line star of "unknown spectral type" (Wackerling 1970; Kukarkin et al 1969; 1971; 1974; 1976). The formal A-1 catalog source 1H0845-53 is very close but formally excluded.

-49.000

-57.000

127.00

140.00

D343ALL.LTP

HED3 CTS/-CM^2-S

.1

.05

0

-.05

0   20   40   60   80

TIME IN SECONDS

χ^2 =   53.1   FOR   14 DOF
P1= 0.735E-02 SIG= 0.113E-02
χ^2 =   23.3   FOR   13 DOF
P2= 0.341E-03 P3=-0.191E-02

d) We plotted the 99% confidence position limits (in 1950.0 R.A. and Decl.) on the left, and the ~1 minute event light curve (in HED3 cts-cm^{-2}-s^{-1}, above a 12 hour average, versus time in seconds) on the right, for the event on D.O.Y. 343.23. Time zero for the light curve is at 5:34:27.342 UT. This event varies appreciably as the A-2 instruments scan over the source. The center of the error box is at Galactic l^{II},b^{II} ~ 271.6°,-6.3°. This is the second of three events, occurring within 3½ days, with overlapping position limits. We found two optically variable stars within the intersection of all three 99% contours: CQ Vel, a classical DQ Her-type nova; and HD299794, an 8.6 m$_V$ early type emission line star of "unknown spectral type" (Wackerling 1970; Kukarkin et al 1969; 1971; 1974; 1976). The formal A-1 catalog source 1H0845-53 is very close but formally excluded.

113

345HOS 99% FASE INCP LIMITS +1H0839-558+1H0846-534+1H0918-54

D345HOS.LTP

HED3 CTS/-CM^2-S

TIME IN SECONDS
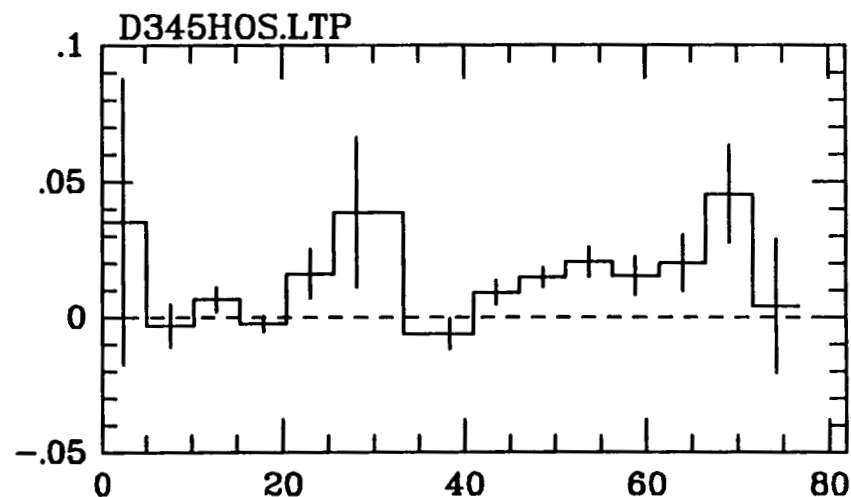
χ^2 =   37.8   FOR   13 DOF
P1= 0.681E-02 SIG= 0.156E-02
χ^2 =   19.0   FOR   12 DOF
P2= 0.390E-03 P3=-0.623E-02

114

e) We plotted the 99% confidence position limits (in 1950.0 R.A. and Decl.) on the left, and the ~1 minute event light curve (in HED3 cts-cm^{-2}-s^{-1}, above a 12 hour average, versus time in seconds) on the right, for the event on D.O.Y. 345.62. Time zero for the light curve is at 14:51:05.117 UT. The event clearly varies during the ~1 minute the source is in the A-2 detector fields of view. The center of the error box is at Galactic l^{II},b^{II} ~ 271.6°,-6.3°. This is the third of three events, occurring within 3½ days, with overlapping position limits. We found two optically variable stars within the intersection of all three 99% contours: CQ Vel, a classical DQ Her-type nova; and HD299794, an 8.6 m$_V$ early type emission line star of "unknown spectral type" (Wackerling 1970; Kukarkin et al 1969; 1971; 1974; 1976). The A-1 catalog source 1H0845-53 is very close but formally excluded.
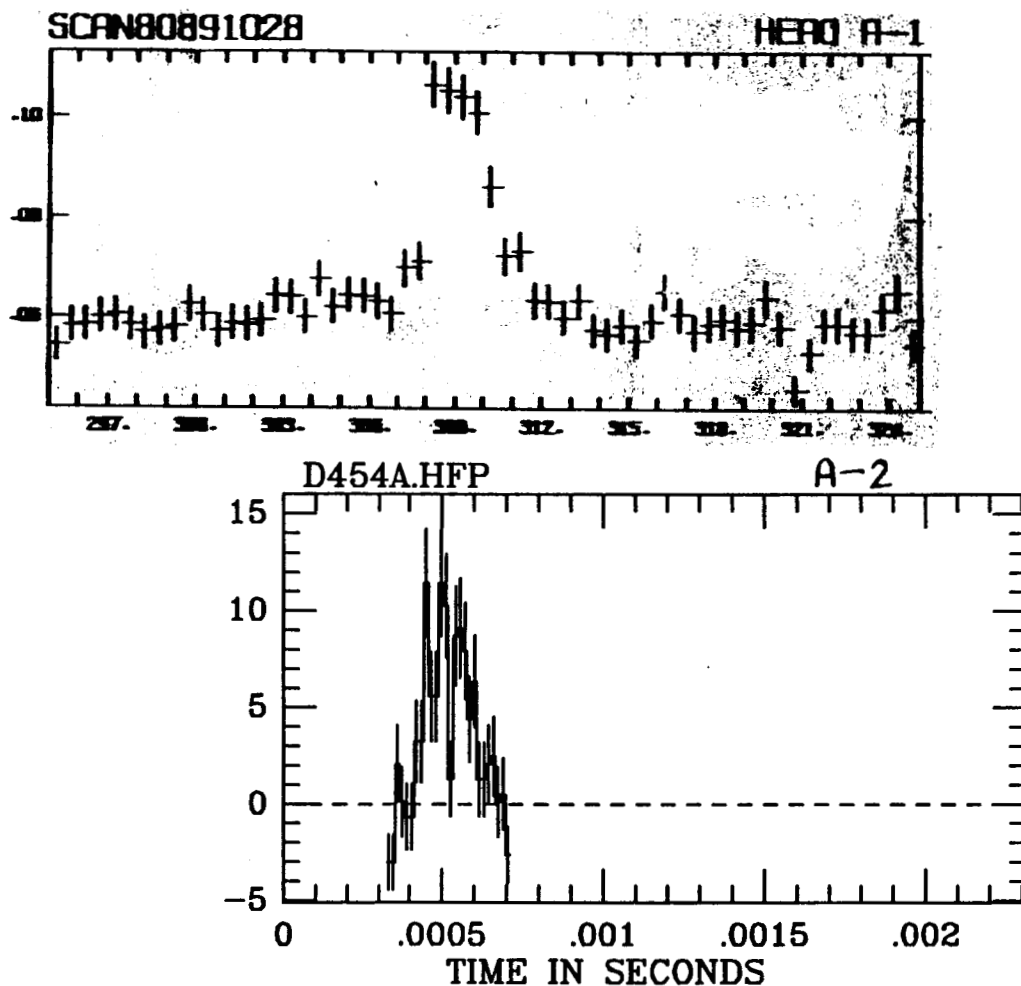
f) This event was identified by Hueter (1987) as a gamma-ray burst incident (at an angle of ~31°) through the sides of the detector. We display here both the A-2 light curve (in HED3+HED1 cts-s^{-1}), and the A-1 count rate, kindly provided by P. Hertz of NRL. Time zero for the light curves is at 10:41:00 U.T.

116

38.000

33.000

291.00

306.00

D494HOS.LTP

HED3 CTS/$-CM^2-S$

.1

.05

0

-.05

0   10   20   30   40   50

TIME IN SECONDS
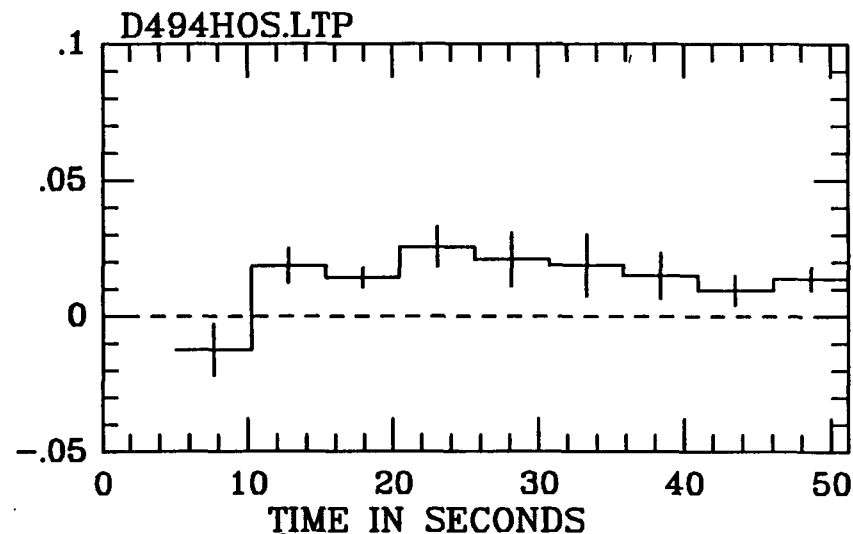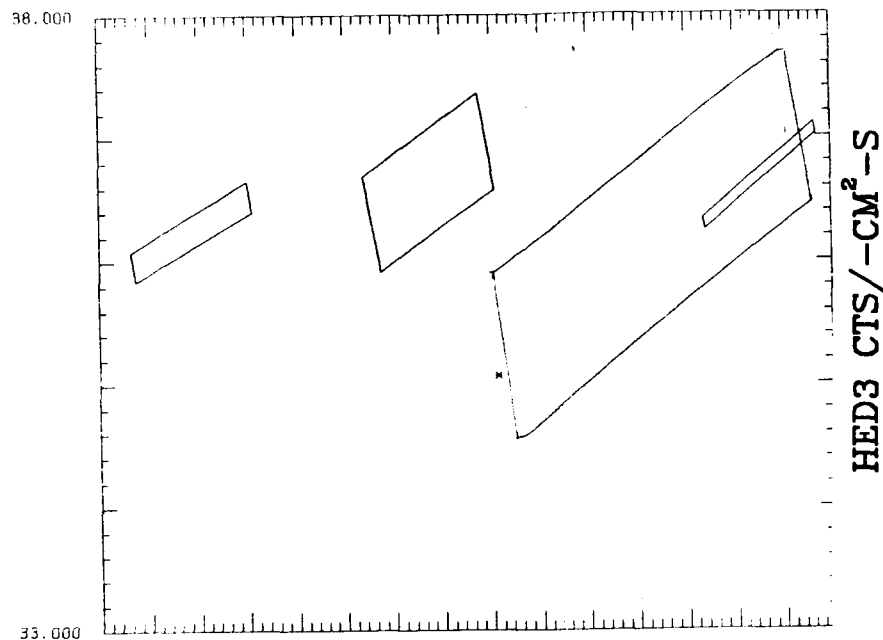
χ^2 =   12.0 FOR   8 DOF
P1= 0.140E−01 SIG= 0.200E−02
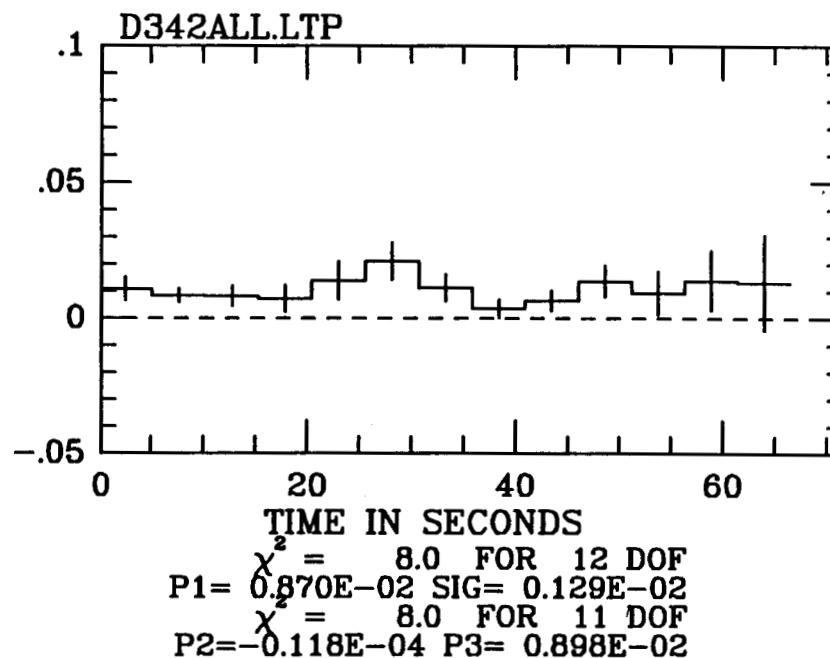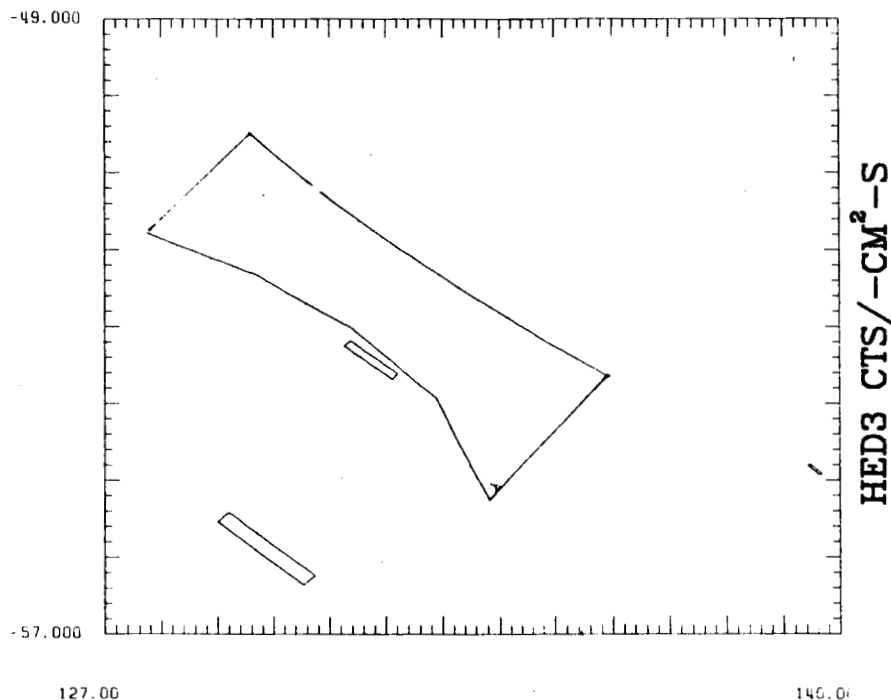χ^2 =   12.0 FOR   7 DOF
P2= 0.169E−04 P3= 0.135E−01

g) We plotted the 99% confidence position limits (in 1950.0 R.A. and Decl.) on the left, and the ~1 minute event light curve (in HED3 cts-cm^{-2}-s^{-1}, above a 12 hour average, versus time in seconds) on the right, for the event on D.O.Y. 494.15. Time zero for the light curve is at 3:34:48.300 UT. The center of the error box is at Galactic l^{II},b^{II} ~ 73.7°, 1.6°. The position of this event falls squarely on one of the more crowded regions of the sky. We have plotted the position of the luminous, highly variable, high mass X-ray binary Cyg X-1 which fell just outside the A-2 detector collimators during this event. The position error box for this event overlaps that of an A-1 catalog source, H2018+366, a (disputed?) SNR (Wood et al. 1984), which we have also plotted. Also in the field of view, but excluded as a source of the transient, is the A-1 error box for the Be-star X-ray source X1950+37. However we deemed the region too crowded to plot all the interesting optical sources. Within the A-2 99% confidence position limits we found 58 early-type emission line objects (Wackerling 1970), 7 eclipsing Algol type systems that are probably too distant to give a flare of this intensity (Kukarkin et al 1969; 1971; 1974; 1976; White and Marshall 1983), 4 eclipsing β Lyrae type variables with m_p>8, and 1 U Gem type dwarf nova with m_p=15-18, probably indicating they are also too distant.
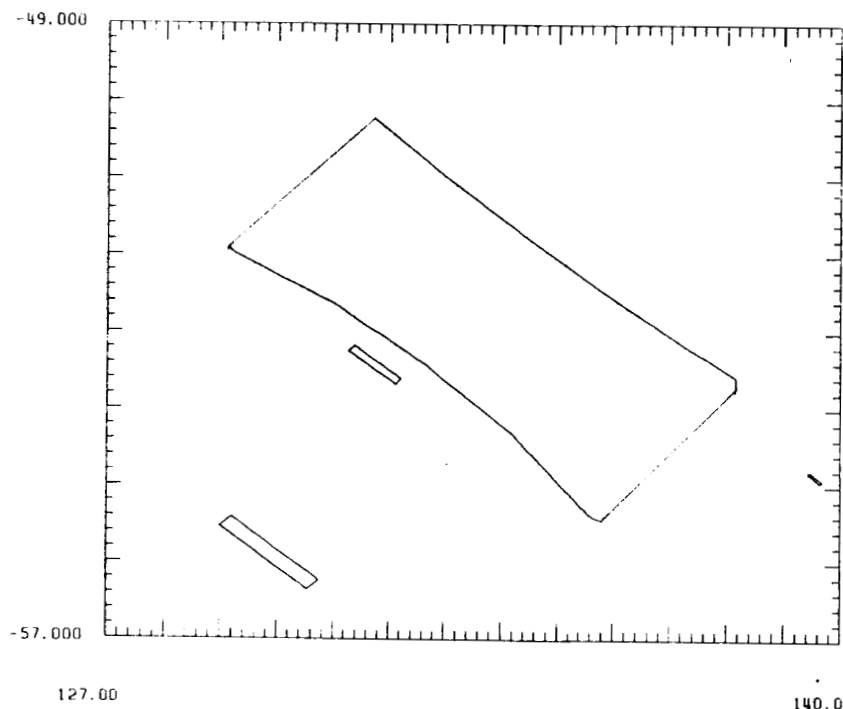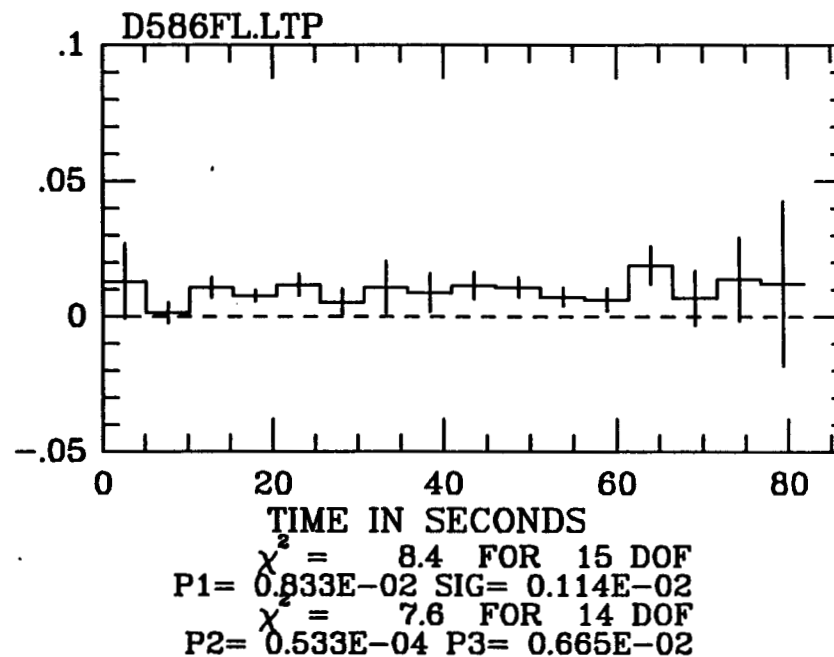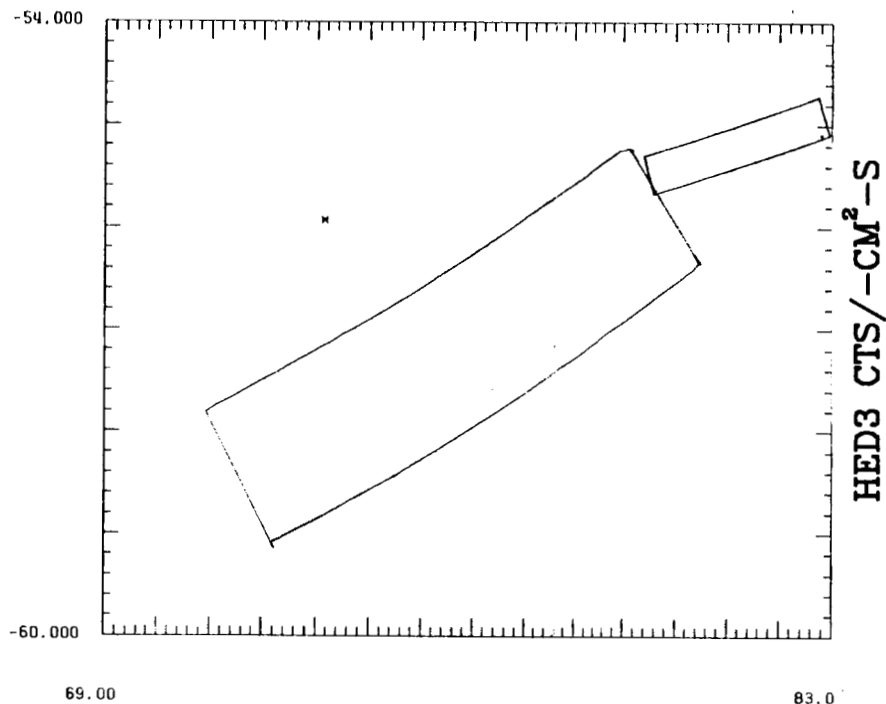
h) We plotted the 99% confidence position limits (in 1950.0 R.A. and Decl.) on the left, and the ~1 minute event light curve (in HED3 cts-cm^{-2}-s^{-1} versus time in seconds) on the right, for the event on D.O.Y. 586.70. Time zero for the light curve is at 8:23:32.457 UT. The center of the error box is at Galactic l^{II},b^{II} ~ 265.5°, -37.0°. Our 99% A-2 position limits very slightly overlap those for the A-1 source 1H0524-552 (Wood et al. 1984). Since it is nearby, we have also plotted the position of the dMe pair LDS 131 (that flared 6 months earlier). We found no other identified X-ray sources, no A-1 catalog sources, and no known optically variable stars or emission line stars (Wackerling 1970; Kukarkin et al. 1969; 1971; 1974; 1976) in the field of view.

i. Description of the Events

We have listed the eight events from the HEAO 1 A-2 survey of the "source-full" sky in Table 3.3.b. We calculated the best-fit positions, intensities, and indications of <1 minute variability using the position fitting program described in Appendix B, as in Table 3.3.a, save that we first subtracted the 12 hour mean flux at each position on the sky. (For extremely variable sources, it was possible for this to produce apparently negative count-rates. As mentioned in Chapter 2, this does not affect the accuracy of the position limits, but it can skew an event light curve, and eventually the inferred spectrum, when the spectrum is measured from rough 'color rates' that were also calculated by first subtracting a time-averaged mean for each position.) We have presented the corresponding light curves and 99% confidence position limits in Figure 3.4.

The position of the event on D494.15 fell so close to Cygnus X-1 that there was some question whether or not it was real. If Cygnus X-1 were radiating at its maximum luminosity, and if, further, the spacecraft positions were off by about 0.02° (which is the usual systematic error associated with determining the spacecraft position), then Cyg X-1 could have been the source of this event, although formally it lay just outside the detector collimators at the time. Since we had no evidence from the other HEAO 1 instruments that Cyg X-1 was outstandingly bright (R. Remillard private communication, P. Hertz private communication), we have provisionally accepted this event.

Three of the events, on D342.12, D343.23, and D345.62, had overlapping position error boxes and occurred within 3½ days of each

118

other, suggesting they may have come from the same source. We calculated that the probablity of one or two of the seven event error boxes overlapped by chance to be quite small - less than 0.2%, even if one assumes first that all three have fallen on the Galactic plane. We inferred that it was likely that these three events were indeed related.

For three events (including GB780330 on D454.44) a fit to a constant intensity gave a value for χ^2 that was greater than twice the number of degrees of freedom. We have indicated these sources with a 'Y' in the eighth column. The other two variable events, on D343.23 and D345.62, showed an increase in flux as the detectors spun over the source, and there were slight indications in the brighter event of ~20-30 s substructure. (We found reduced χ^2 for a linear fit to be ~1.7 for the event on D343.23.) As in Table 3.3.a, data from the A-1 detectors could be used to help constrain the durations of the other five events. None were detected as lasting longer than an hour.

The positions of the three repeating events fell very near an unidentified, variable source H0845-53 (~0.6° away). However we think the three fast transient events probably came from a separate source, as 99% confidence limits on the scan angle for the hard, variable, ~2 millicrab source H0845-53 (calculated assuming a constant source intensity, using 8 days of summed HED3 plus MED data from the 1.5° fields of view) did not overlap those for any of the three events (D342.12, D343.23, and D345.62). This is illustrated in Figure 3.4.c-e, where we have plotted 99% position limits for the three events and the A-1 catalog error box for 1H0846-531 (=H0845-53).

As for the events from the source-free phase, we found no

significant of quiescent flux, and have listed 90% upper limits on persistent emission in the 9th column of Table 3.3.b. The ratio of peak-flux-to-quiescent-flux ranged from above 20:1, for events on D268.67, D311.65, and D586.70, to almost 20:1 for the three events on D342-D345, to less than 10:1 for the event in the Cygnus region on D494.15. The close proximity of Cygnus X-1 made measurements of persistent emission highly uncertain for this event.

Again, we listed parameters from fits to three simple models in columns ten through twelve of Tables 3.3.b. Unlike for some of the events found in "source-free" data, we could not rule out any of the models, and we could not constrain the column densities for any of the events. In part, this may be because we relied on fits to the "color" rates, for which it was possible to subtract an appropriate 12 hour average and therefore the contributions of nearby sources, rather than the better calibrated PHA spectra, for which this was not possible. For optically thin thermal bremsstrahlung models, with negligible column densities, we found events with temperatures ranging from greater than 9.5 keV (D342.12, D345.62, D494.15) to consistent with 3-10 keV (D268.67, D311.65, D586.70). For the gamma-ray burst GB780330 incident through the sides of the detectors, on D454.44, spectral fits would have been meaningless and so were not performed.

In the last column of Table 3.3, we listed notes on nearby X-ray sources, from the A-1 Catalog (Wood et al. 1984), Bradt and McClintock (1983); and types of optical objects that may vary in X-rays. For the latter, we used an on-line computer catalog (Mead and Hill 1983). In some cases, we included the positions of nearby A-1 catalog sources, even if they were formally excluded, as variability could have skewed

solutions for the positions of theses sources, which were calculated under the assumption of constant intensity (Wood et al. 1984). We found 59 early type emission-line objects (58 within the 99% position contours for D494.15, and one in the intersection of the position error boxes for D342.12, D343.23, and D345.62); and one classical DQ Her type nova (in the intersection of the 99% contours of the three repeating events). The error box for the event on D494.15 that fell in the crowded Cygnus region also contained seven eclipsing Algol-type systems, all probably too distant to be the source of this event; four eclipsing beta Lyrae type variables and one U Gem type dwarf nova, again probably too distant to be likely sources of the X-ray event. We also listed any gamma-ray burst position error boxes, kindly provided by J. Norris, U. Desai, and T. Cline (private communication), that may have overlapped the position limits of our events.

ii. General Remarks on Identifications

As was the case for the events from the "source-free" sky, we again found it improbable that any of the events from the "source-full" sky survey would have originated on extragalactic objects. We found no known rapidly variable AGNs in any of the position error limits. The one event for which the peak-flux-to quiescent-flux ratio was allowed to be less than 10:1 (the event on D494.15) came from a direction on the sky crowded with interesting and possibly X-ray variable Galactic sources, while for the other events this ratio was again constrained to be greater than 20:1 in under an hour, even for the two events exhibiting evidence of persistent emission.

121

We find the events in Table 3.3.b to be divided into three natural categories. The event on D454.44 formed a class by itself, as it was identified by Hueter (1987) as a ~20 s, 1.3×10^{-5} erg-cm^{-2} gamma-ray burst, GB780330, with a moderately hard spectrum (power law photon index ~1.8), incident through the sides of the detectors at an angle of ~31° from the main detector axis. The four events exhibiting the hardest best-fit spectra (three apparently from the same direction) all came from low Galactic latitudes, and two exhibited evidence of <100 s variability. We suggest these four events probably were not coronal flares, and probably originated on systems containing compact objects. The remaining three events all had spectra consistent with thin thermal bremsstrahlung models with temperatures of 5-10 keV, and probably represent flares from active stellar coronae.

iii. Coronal Transients: Flare Stars Revisited

We suggest three of the events from the source-full search, those not occurring within 10° of the Galactic plane and constrained to have peak-to-quiescent-flux ratios >20 (D268.67, D311.65, and D586.70), were probably coronal flares from cool dwarf stars. In the first phase, we suggested that five out of seven events were flares from dMe-dKe stars. In this second phase, we covered nearly twice as much data (92% more), but the effective threshold of this second search algorithm, which compared 5, 15, and 61 s rates with 12 hour means for corresponding positions, was slightly higher. This is illustrated by our results when we re-surveyed the source-free sky data with this second algorithm: we triggered on five (D249.14, D298.62, D343.97,

122

D405.85, and D436.84) out of the original seven source-free events, but not the two faint events that we suggested originated on dMe-dKe stars (D370.82 and D623.47). That is, using this second algorithm, we found three events that probably originated on cool dwarf stars in the source-free regions of data, and three more in the additional ~92% of data from the "source-full" sky. Therefore we measured roughly the same event rates in both sections of the data, finding the rate of three new events from the source-full sky (D268.67, D311.65, and D586.70) to also be consistent with the rates of flares expected from dMe-dKe stars calculated in §3.C.iii and Appendix C.

iv. Luminous Events From Compact Objects Revisited

It is unlikely that any of the events could have originated on strongly accreting, persistently luminous, high- or low- mass X-ray binaries, with average luminosities on the order of the Eddington limit, as these would be detectable in quiescence clear across the Galaxy at levels of several millicrabs or more in the 2-20 keV energy band. If we let h_{100} represent the height of a source above the plane of the Galaxy in units of 100 pc, then the upper limits on 2-20 keV quiescent emission range from less than $(h_{100})^2 \cdot 10^{35}$ ergs-s^{-1}, for the event from the Cygnus region on D494.15; to less than $(h_{100})^2 \cdot 2 \times 10^{33}$ ergs-s^{-1}, for the three events on the other side of the Galactic plane on D342.12, D343.23, and D345.62; and $(h_{100})^2 \cdot 6 \times 10^{31}$ ergs-s^{-1} for the three events that probably were coronal flares (on D268.27, D311.65, and D586.70). Upper limits on the event luminosities are roughly a factor of five greater, for the event on D494.15, and an order of magnitude larger, for the events on D342.12,

123

D343.23, and D345.62, and are therefore well under the Eddington luminosity unless one allows distances above the disk of greater than 500 pc or 2 kpc, respectively. We note that it is therefore unlikely that any of the events we observed were classic Type I or Type II X-ray bursts.

In their detailed summary of what is understood of the geometry of low-mass X-ray binaries, White and Mason (1985) describe the decrease in observed source intensity that occurs when the observer's line of sight lies close to the plane of the accretion disk. The flared and irregular accretion disk can obscure the X-ray bright compact object in the center, so that one observes only radiation scattered from material (an accretion disk corona) that is outside the plane of the disk. The observed X-ray luminosity is on the order of 3×10^{35} ergs-s^{-1}, with variations in intensity by factors of ~2-5, due to obscurations by differing portions of the irregular rim of the thick accretion disk as the system rotates (irregular dippers such as X1822-371). White and Mason (1985) note that it is possible to observe higher ratios of peak flux to quiescent flux from systems tilted in such a way that the X-ray bright point source in the center is directly visible, but can be briefly occulted in each orbit by a thick accretion column; however for these systems the average observed X-ray luminosity is higher (on the order of 10^{36-37} ergs-s^{-1} for periodic but irregular dippers such as XB1916-050). Therefore we can rule out luminous low mass binaries viewed edge-on through an irregular accretion disk (dippers) as an explanation for all the fast transient events save the event on D494.15. We point out that it seems unlikely that we should have observed only one significant

variation in intensity from this source, if it is a dipper, as such dips tend to occur quasi-periodically, but we cannot exclude the possibility.

Similarly, it is unlikely that any of the A-2 fast transient events originated from a close binary containing a very massive optical companion (giant or supergiant), as the average luminosity would be too bright. However, sources containing only moderately massive companions (O-B II-Ve) are a varied lot. Some have been observed to be transient sources lasting for weeks or months with peak luminosities on the order of the Eddington limit; some Be transients exhibit quasi-periodic outbursts (coincident with periastron of the binary cycle) lasting for hours to days and with peak luminosities from apparently super-Eddington to orders of magnitude fainter (cf. the LMC Transient in Chapter 4; see also van den Heuvel and Rappaport 1986; Stella, White, and Rosner 1986). There are also less luminous Be-neutron star binaries ($L_x < 10^{35}$ ergs-s^{-1}), which can flare by an order of magnitude in about an hour and show indications of incoherent variations on time-scales of minutes (Steiner et al. 1984; Koenigsberger et al. 1983; White, Swank, Holt, and Parmar 1982). Over 50% of these systems show evidence of pulsations, and many have hard pulsar spectra (power law ~1 plus an exponential cutoff above 10-20 keV), although there is considerable variation in hardness. We consider these varied systems as sources of the harder, Galactic plane, A-2 fast transient events in the following section.

v.   The Be Star-Neutron Star Binary Hypothesis

In this section, we argue that the four events that occurred

within 10° of the Galactic plane (D342.12, D343.23, D345.62, and D494.15, and possibly D249.36) probably represent a class of hard, variable sources identified with wide, less luminous, Be-neutron star binaries. These events were faint. Since they were found in scanning data, we viewed them for less than 100 s each. The four Galactic plane events we discuss here came by definition from regions of sky prone to source confusion. Therefore our conclusions, though plausible, cannot be definitive, and should be considered as a working hypothesis in need of further testing.

We cannot rule out a coronal flare as the source of the event from the Cygnus region on D494.15, and that its position in the middle of a Cygnus OB association is simply by chance (probability ~2%), although we do not consider it the most likely explanation. Of the other three events on the Galactic plane, an optically thin thermal bremsstrahlung temperature constrained to be above 42 keV, for the event on D345.62, seems to rule out a stellar flare origin. Since we have argued that the other two events (on D342.12 and D343.23) probably originated from the same source, they were also unlikely to have been stellar coronal flares. For all these sources, the quiescent luminosity was constrained to be less than 10^{36} ergs-s^{-1}, if they were to be contained in the Galaxy, and the ratio of maximum to minimum luminosity was on the order of 5-10:1, or greater. The two brightest of the repeating events showed evidence of variability on time-scales of ~minutes. We note that two events from the source-free phase of the fast transient survey, on D249.36 and D728.15, also came from within 10° of the Galactic plane, but that the spectrum of the latter event was so well fit by a cooling optically thin thermal

bremsstrahlung spectrum that a stellar coronal flare was the preferred explanation. However the event on D249.36, which exhibited strong evidence of high intrinsic absorption, had a limit on peak-to-quiescent-flux ratio of 12:1 or greater, and so we include it in this discussion of Galactic plane fast transients.

To the consideration of these events, we added some investigations done for a completely different project: looking for persistent emission from a gamma-ray burst, GB780506, viewed in pointed data, that happened to fall in the Galactic plane in a region free of sources with average fluxes less than about a millicrab (Connors, Hueter, and Serlemitsos 1988). We investigated both three six hour points and 2½ days of scanning data along the region. We divided it into ¼ day intervals, and looked for significant persistent emission with the position finding program described in Appendix B. We assumed the sources were constant over the 3-6 hour intervals we studied. As described earlier, a source was considered significant if χ^2 dropped by at least 30 when a single constant source. We apparently found at least three separate sources, all with hard spectra consistent with what one expects from Be stars. These sources only glowed for 3-12 hours at a time, but were as bright as 5-15 millicrabs. We found at least one of these sources to be in the field of view 30% of the time. One of these few-hour variable sources contains within it 99% position contours an A-1 source, suggested by Buckley et al (1988) to be identified with a recently discovered Be star. We present the 99% confidence position contours in Figure 3.5, calculated using the position finding programs of Appendix B, along with the positions of nearby A-1 catalog sources (Wood et al. 1984)

Figure 3.5 Two maps of confidence position limits of sources in the region containing GB780506, centered at Galactic longitude and latitude of ~256°,-9°, plotted in 1950.0 R.A. (abcissa) and Dec. (ordinate). The criteria for the existence of a source was that χ^2 drop by at least twenty when two parameters, describing the source scan-angle and intensity, were introduced.
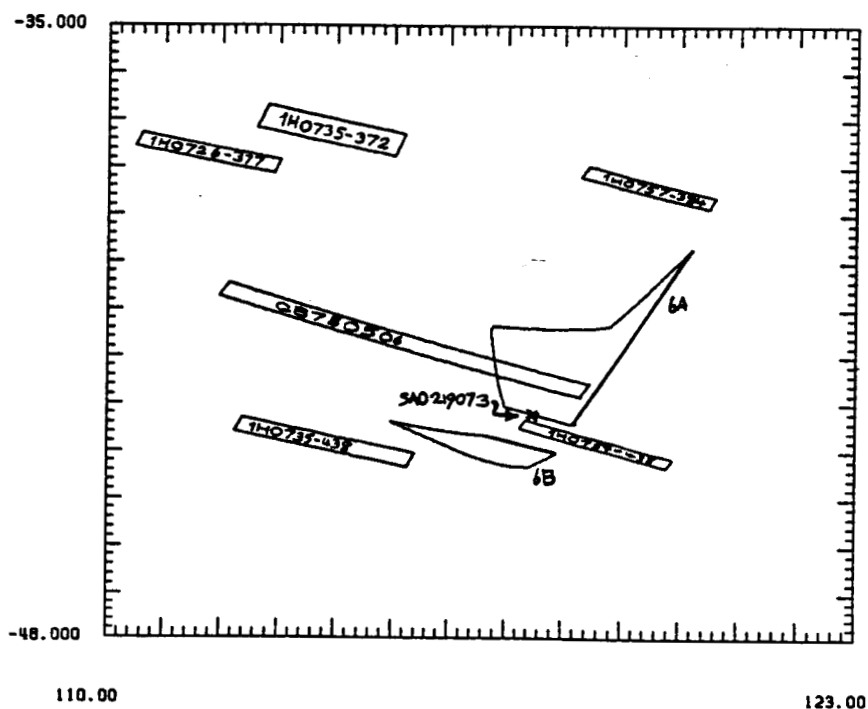
a) We show here the gamma-ray burst 99% confidence error box and 90% confidence limits on the positions of two weak sources of persistent emission, labeled '6A' and '6B', visible during the point on May 6, 1978 (D491). We have also plotted the positions of nearby A-1 catalog sources (Wood et al. 1984), one of which has been tentatively suggested to be a recently identified Be star, SAO219073 (Buckley et al. 1988).

-35.000

-46.000

110.00

123.00

8C   8D

SAO 219073

8A

9A
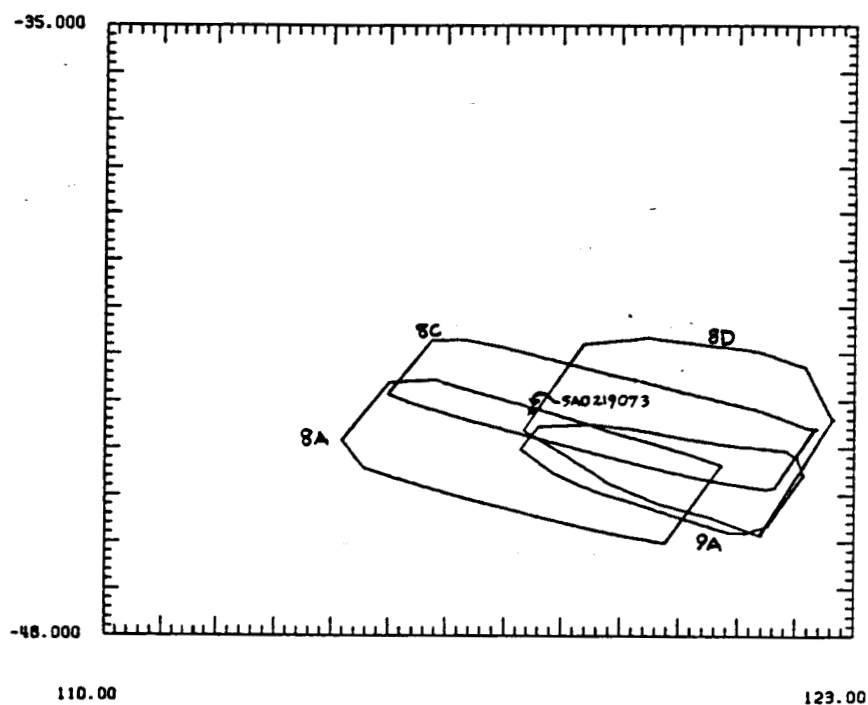
b) We display 99% confidence position limits for four more variable
sources ('8A' on May 8, 1978, 0-6 hrs UT., with a flux of f6
millicrabs; '8C' on May 8, 1978, 12-18 hrs UT., with a flux of f4
millicrabs; '8D' on May 8, 1978, 18-24 hrs UT., with a flux of f2
millicrabs; and '9A' on May 9, 1978, 0-6 hrs UT., with a flux of
f13 millicrabs), plus the Be star of Buckley et al. (1988), which
we think may be the source of all but two of the sources of hard
emission.

and the newly identified Be star (SAO 219073). We have plotted the positions of the sources seen in the pointed data (including that of GB780506) seperately from those discerned in the following three days of scanning data. (However, when one summed the data over one or more days, only one of these sources turned out to be significant, leading us to conclude a probability of ~8% of chance association with a weak source of persistent emission visible on >12 hour timescales. We suggest the faint persistent source in the direction of the event on D728.15 but visible a year earlier may have been one of these variable Galactic plane sources, and possibly also the hard variable source H0845-53.)

From five careful scanning observations of the Galactic plane with the Japanese satellite GINGA, Koyama et al (1988) have discovered four hard, 2-10 millicrab sources, visible for 1-3 days, but erratically variable during that time. One of these sources was subsequently shown to be a 413 s pulsar (Tawara et al. 1988).

The simplest interpretation of these disparate observations is that all are evidence of a single class of hard, variable, sources along the Galactic plane, with peak fluxes $<10^{36}$ ergs-s^{-1}, and average quiescent luminosities of over an order of magnitude fainter. Widely seperated Be-neutron star binaries are therefore a natural source population for this proposed class, as their characteristics (L_x~10^{33-35} ergs-s^{-1}; L_x/q_x~1; power law 'pulsar' spectra with photon index ~1; both coherent and incoherent variability on time-scales of minutes; longer intensity variations on time-scales of days to months; and tight Galactic plane distribution) match all of the observed properties. Calculations by Rappaport and van den Heuvel (1982)

suggested there may be on the order of 10^{2-3} such systems throughout the Galaxy. It is certainly the obvious identification for the event on D494.15 that had 58 early-type emission line objects (two, HD194335 and 28 Cyg, with $m_v<5$, and so probably as close as 1-2 kpc) in its error box (Wackerling 1970; Allen 1973). There is also at least one object identified by Wackerling (1970) as an early-type emission line star of unknown spectral type (HD299794, with $m_v \sim 8.6$) in the intersection of the 99% position limits for the events on D342.12, D343.32, and D345.62. Also, the identification by Buckley et al. (1988) of SAO 219703 as an emission-line object illustrates that not all O-B II-V emission-line stars have been identified. Although the A-2 position error boxes are probably too large to make direct optical identifications feasible, we think the finding of pulsations in these proposed Be-neutron star binaries would constitute strong indirect evidence in favor of this hypothesized identification.

However, although we think this the simplest explanation, it is not the only possible explanation. First, we may be being fooled by small statistics into hypothesizing a single category when we may have actually observed a handful of disparate, rare, types, only a few of which may turn out to be Be-neutron star binaries. For example, the brightest high intrinsic absorbtion event from the source-free phase of the survey (on D436.84) was not well fit by this explanation (as the average quiescent flux was constrained to be less than 5×10^{31} ergs-s^{-1}, the ratio of peak-flux-to quiescent-flux to be greater than 40:1, and we saw no evidence of recurring outbursts); neither was the singular bright 6-Nov-77 event observed by OSO-8 and discussed in Chapter 5.

Also, in their report on a flux-limited survey of the Galactic plane using data from the IPC instrument of the Einstein Observatory, Hertz and Grindlay (1984) found 71 sources above their threshold of ~0.02 millicrabs in 275 deg^2. They found roughly 46% of their sources to be due to coronal emission from main sequence stars (assuming all systems with $\log(L_x/L_V) < -1$ were coronal sources), ~31% to be from extragalactic sources, and 23% that were "neither coronal nor extragalactic". They attributed this last class of sources to accreting white dwarfs, such as those in cataclysmic varible systems with X-ray luminosities of ~10^{31}-10^{32} ergs-s^{-1}, but with luminosites closer to those of a proposed class of systems in globular clusters with luminosities of ~10^{34}-10^{35} ergs-s^{-1}, in part because these systems exhibited high ratios of X-ray to optical luminosity. In contrast, the Be-neutron star systems we considered above should been visible both in soft X-rays and optically (unless they were heavily absorbed), with $L_x/L_{opt} < 1$; Hertz and Grindlay (1984) noted that they could have mislabeled neutron star systems with Be companions as 'coronal' sources, because of this relatively low ratio of X-ray to optical flux.

This illustrates that many questions, suggested by this hypothesis of a class of hard, variable sources along the Galactic plane, remain unanswered. Assuming a duration on the order of an hour, we calculate a total event rate over the whole sky of ~300 events per year above our threshold of ~4 millicrabs (~10^{-10} ergs-cm^{-2}-s^{-1}), with an uncertainty (1σ) of nearly an order of magnitude. If the peak luminosity is ~10^{35} ergs-s^{-1}, we detected these events only out to about 4 kpc, and calculate an event rate of

~4000 per year tover the whole Galaxy. If the tentative calculation of ~100-1000 such Be-neutron star systems throughout the Galaxy was correct, we infer an average recurrence time of 4-40 outbursts per year per system.

E. Constraints on Gamma-Ray Bursts

We think it unlikely that any of the sixteen HEAO 1 A-2 fast transient events listed in Table 3.3 were "Soft Gamma-ray Repeaters" (or SGRs). This term was coined to decribe hard (kT~20-40 keV, with a dramatic low energy turnover below 5 keV), very short (durations on the order of 0.1 s, with rise and decay times often two orders of magnitude faster), repeated outbursts, from two sources on the plane of the Galaxy, and possibly one more in the direction of the supernova remnant N49, with observed fluences of ~5-40x10^{-7} ergs-cm^{-2}, and peak fluxes inferred to be on the order of 10^{-5} ergs-cm^{-2}-s^{-1} (Atteia et al. 1987; Laros et al. 1986). None of the A-2 fast transients varied on these extremely short time-scales, and although two showed evidence for a low energy turnover, and none were spatially coincident with any of the three suggested SGR sources.

X-ray observations of "classic" gamma-ray bursts indicate that although the emission in ~2-20 keV X-rays exhibits less rapid variability than is characteristic at higher energies, the X-ray emission is still characterized by dramatic, hard-to-soft spectral variablity (Connors, Hueter, and Serlemitsos 1988); the X-ray emission has in general rise and decay times 2-5 times longer than that seen at higher energies; and that an event that lasts 10s >30 keV may have an X-ray duration of more than a minute. From comparing

the spectra alone of D249.36 and D436.84 to that of the only gamma-ray

burst seen through the front of the A-2 detectors (GB780506), we see

that the 2-60 keV spectra of these two events resemble the spectrum of

the softening tail of GB780506 (Connors, Hueter, and Serlemitsos

1988). However, A-4 data (kindly provided by G. Hueter at U.C.S.D.,

and Hueter 1987) showed no evidence of gamma-ray emission prior to or

around the times of the A-2 detections of these events. If they were

from gamma-ray bursts similar to GB780506, the fluence in gamma-rays

should have been above 10^{-6} ergs-cm^{-2}, easily observable by A-4

(Hueter 1987). We therefore inferred that the HEAO 1 A-2 all-sky

survey saw no gamma-ray bursts down to our flux level of ~4

millicrabs.

By comparing the observed X-ray flux and duration with the

calculated gamma-ray fluence for the one gamma-ray burst observed

through the front of a HEAO 1 A-2 detector (Connors, Hueter, and

Serlemitsos 1988) we find that a 7×10^{-7} ergs-cm^{-2} gamma-ray burst has

a 2-20 keV flux about 200 times our search threshold of 4 millicrabs,

and lasts for about a minute. This event was soft for a gamma-ray

burst, so we calculated that our all-sky X-ray search threshold

corresponded roughly to a gamma-ray fluence of ~10^{-8}-10^{-9} ergs-cm^{-2};

a measurement of no gamma-ray bursts (through the front of the

detectors) in ~104. days of 'on' time corresponds to a 90% upper limit

of 1300 gamma-ray bursts over the whole sky per year above 10^{-8}-10^{-9}

ergs-cm^{-2}. Even if one considers that there are large systematic

errors in comparing fluences observed in different experiments

(Jennings 1987), when considering only the bursts observed by HEAO 1

satellite (Hueter 1987), this rough calculation seems to indicate a

difference of over 5 orders of magnitude between what one calculates assuming an $S^{-1.5}$ distribution and our crude constraint on the number observed above fluences of 10^{-8} ergs-cm^{-2}. If systematic errors do not invalidate this estimate, it seems likely that the gamma-ray burst logN-logS curve does indeed turn over somewhere around 10^{-7} ergs-cm^{-2}, suggesting that the sources of gamma-ray bursts may be within a few hundred parsecs. From stringent upper limits placed on the apparent magnitude of optical counterparts on some of the brighter gamma-ray bursts ($m_V \leq 22$; Schaefer and Cline 1985) one is led to infer an absolute visual magnitude on the order of 12 or more. If the sources of gamma-ray bursts are neutron star binaries, this seems to suggest their companions should be cool red dwarf stars or degenerate stars such as white dwarfs.

Chapter 4: Looking Towards the Magellanic Clouds

A. Overview

If one considers the geometry of the sky seen by HEAO 1 as laid out in the sky and coverage maps of Chapter 2, one sees that by excluding the Magellanic Clouds from our all-sky search, we excluded a fair proportion of the sky. First, because of the geometry of the sky: the Magellanic Clouds are understood to be small sister galaxies in orbit at ~53 and 69 kpc from our larger Milky Way. The Large Magellanic Cloud, about 1/10 the mass of the Milky Way, subtends a solid angle of ~10° in diameter; the Small Magellanic Cloud has a mass about a fifth less (1/50 that of the Milky Way) and subtends an angle about half the size. Second, from the geometry of the satellite orbit: as HEAO 1 moved in Ecliptic coordinates it passed frequently over the North and South Ecliptic poles. While sources along the plane of the Ecliptic were only observed for about 6 days at a time, some of the sources in the direction of the Magellanic Clouds were visible to HEAO 1 A-2 as long as 100 days (per 6 month pass) because of their proximity to the South Ecliptic pole. Therefore the HEAO 1 data affords a particularly rich sample of data on the X-ray sources in these nearby dwarf galaxies. This effort focuses on just one small area out of many possible areas of investigation. We consider the question, what would one expect to find if the mass of the Milky Way were reduced by a factor of 10, and viewed in 2-20 keV X-rays, from a distance of half a megaparsec, through the 'filter' of the HEAO 1 fast transient search algorithm? Does what one expects match what this search has found?

We reemphasize that this fast transient survey only considered

variations above a twelve hour average. One should not expect this search to trigger on a bright 1 - 14 day outburst of the LMC Transient (A0538-66), for example, even though this is "fast but not unheard of" (Johnston et al. 1979) by classic X-ray transient standards. Also, the Magellanic Clouds region is more crowded and more prone to source confusion than the areas around most of the "all-sky" triggers in Table 3.1, so the peculiarities of dealing with only the excess flux above a 12 hour mean will be more evident. For example, when fitting the positions of most events, we have fit this excess above the 12 hour average to a model of a variable point source plus a constant background. If the source(s) in the field of view at the time of this excess flux varied appreciably during the scans within the 12 hours, although the position contour would not have been affected, the light curve inferred from the excess flux may not have been indicative of the true fast transient light curve and may have included negative count rates. The spectral fits we infer from the relative intensities of the excess counts in several energy bands (called 'color rates') could have been skewed by this effect: to avoid source confusion problems and because of the large number of events, we relied on fits of the 'color' rates' minus the 12 hour background to give us an indication of the spectrum. Since these excess color rates were available every 5.12 s rather than every 40.96 s (as was the case for the generally more reliable PHA spectra), we could also use them as an indication of the hardness, or temperature versus time, as the detectors spun past a source. However useful as this was for indicating hardening or softening trends, spectral fits of these color rates are not as well calibrated and in general were not as clean an

indicator of the absolute value of spectral parameters as were fits to PHA data (Marshall private communication; Swank private communication). One should be wary, also, of possible biases introduced by subtracting a 12 hour mean that may include a spectrally varying source. (We consider that this may have been particularly a problem for the bright pulsing flares from LMC X-4 discussed later.)

From work by Cowley et al. (1984) we first draw a static map of the X-ray sources in the Magellanic Clouds. This is from a survey undertaken with the IPC and HRI instruments of the Einstein Observatory in 0.3-3 keV X-rays (Long, Helfand, and Grabelsky 1981) revealing ~100 X-ray sources found in 37 deg^2 towards the Magellanic Clouds. Cowley et al. (1984) suggest a ratio of ~25 interlopers (including stars with active coronae such as cool dwarfs and RS CVn-like variables; clusters of galaxies; and AGN) to 10 LMC members. They expect ~70% of the LMC X-ray sources to be supernovae remnants which should not contribute events to the fast transient search. They suggest a total of 4-11 of the remainder may be Population I massive binaries (LMC X-1, LMC X-3, LMC X-4, the LMC Transient (A0538-66), plus Columbia Astrophysical Laboratory sources CAL 8, CAL 9, and CAL 37, and 4 unidentified point sources). They point out only two possible Population II low-mass X-ray binaries, LMC X-2 and CAL 83. Cowley et al. (1984) conclude that although the total number of X-ray binaries per unit mass is consistent with being the same in both the Milky Way and the Magellanic Clouds, the LMC Pop I sources appeared more luminous than their Milky Way counterparts, and there may have been a dearth of moderate luminosity Pop II low-mass binaries in the Magellanic Clouds.

The fast transient search required a minimum increase in flux of about 10^{-10} ergs-cm^{-2}-s^{-1} (2-20 keV) over ~ 1-10^3 s. (This is equivalent to ~ 0.007 HED3 cts-cm^{-2}-s^{-1}, or ~ 4 millicrabs.) At a distance of 55 kpc, that corresponds to a minimum increase in luminosity, above a 12 hr mean, of $\sim 4 \times 10^{37}$ ergs-s^{-1} (2-20 keV) (or $\sim 6 \times 10^{37}$ ergs-s^{-1} at 69 kpc, the distance of the SMC). From our survey of the Galaxy in the preceding chapter, we see that a similar search of the Magellanic Clouds could expect to trigger only on the brightest types of events from close X-ray binaries with compact objects, including: luminous flares; rapid 'flickering'; abrupt transitions between high and low intensity states; Type I and II X-ray bursts; and (possibly) X-ray counterparts to gamma-ray events like those observed after March 5, 1979 from the direction of the LMC SNR N49.

In the equivalent of ~ 6 continuous days of clean data from the direction of the Magellanic Clouds, our survey found 37 good events. We found none from the direction of the North Ecliptic pole, over which the HEAO 1 satellite had similar coverage. We have attributed two to a foreground star identified by Cowley et al. (1984) as an RS CVn type system at ~ 70 pc (that happens to be 0.4° from N49). We identified two with the low mass binary LMC X-2, and five with bright 'flickers' from the high mass binary (and black hole candidate) LMC X-1. Eight were consistent in phase and position with an origin on the LMC Transient. Interestingly, we suggest nineteen of the remaining twenty events to have been bright flares from the (high mass) pulsar system LMC X-4, and we think it likely the last event was a trigger on an eclipse egress of this ~ 1.4 day binary system. Many of these events were apparently super-Eddington. We found no events

from the direction of the Small Magellanic Cloud, including none from the black hole candidate SMC X-1. We also detected none from the black hole candidate LMC X-3. We found no events that we could plausibly attribute to sources invisible to the CAL HEAO 2 survey (hidden either by high column densities or long term variability). In particular, we detected no events that we identified as classic X-ray bursts. As we discuss in the final section, this may suggest a lack of moderate luminosity Pop II low mass binaries of the sort responsible for the majority of the X-ray bursts in the Milky Way.

B. The Hunt for Identifications

We first constrained the possible sources of the 37 events by plotting 99% confidence position limits (in 1950 R.A. and Decl.) for each on a map of the X-ray sources in the Magellanic Clouds region, as identified by Cowley et al. (1984). The 37 events fell naturally into several categories. The position limits of two (on D.O.Y. 1977 365.35 and 550.58) were consistent only with N49 and that of the RS CVn-type system HD36705. Two more (on D.O.Y. 1977 290.62 and 653.78) contained only the (Pop II) low mass binary LMC X-2 and the nearby candidate Pop I massive binary systems, CAL 8 and CAL 9. Five events that occurred within eight days of each other (D.O.Y. 1977 303.98-311.59) evinced position limits containing only the massive binary systems LMC X-1 and CAL 37. The positions of the remaining twenty-eight events clustered about the corner of the Large Magellanic Cloud that contained the LMC Transient (A0538-66), the pulsar system LMC X-4, the proposed low mass binary CAL 83, and the super nova remnant and suggested gamma-ray burst source N49. One of these 99% confidence error boxes contained

only the LMC Transient; four others contained only LMC X-4. We display all these position contours in Figure 4.1, in groups of two to five based on spatial and/or temporal proximity. We have labeled each position contour with the Day of Year 1977 on which it occurred.

We next compared the times of our events with long-term light curves of LMC sources from other observations. Skinner et al. (1980) had investigated LMC X-4 and the LMC Transient using data from the first six months of HEAO 1 A-1 and A-3 observations. They corroborated the results of Johnston et al. (1979) who found the LMC Transient to have outbursts on roughly a 16.7 day cycle. Seven of the A-2 LMC fast transients were identified by comparison with Skinner et al. (1980) to be outbursts from the LMC Transient. We identified one more as an LMC Transient outburst, based on its position constraints and occurrence at the proper phase of the 16.7 day outburst cycle.

None of our events coincide exactly in time with the events identified by Skinner et al. (1980) as originating on LMC X-4. (However, one, on D.O.Y. 1977 328.34 is very close.) Since bright flares from LMC X-4 may last 20-40 minutes (Kelley et al. 1983), and their data was from the A-1 instrument, which was on the opposite side of the spinning spacecraft from A-2, this is not surprising. Kelley et al. (1983) point out that these flares (during which the source is seen to pulse with a 13.5 s pulse period) may occur preferentially in the week following the peak of LMC X-4's 30.5 day cycle. From HEAO 1 A-4 data, Lang et al. (1981) have mapped out a long-term light-curve for LMC X-4 which clearly displays this 30.5 day cycle. By comparing the times of our events with this long term light curve, we find, as illustrated in Figure 4.2, all but one of the remaining twenty LMC

fast transients fall at the same phase of the 30.5 day cycle, about 1-7 days after the peak. We therefore suggest these nineteen events may be flares from the pulsar system LMC X-4. The remaining event, falling on D.O.Y. 1977 530.57, contains only LMC X-4 within its 99% position limits. It also coincides in time with a local peak of Lang et al.'s LMC X-4 light curve, so it seems plausible to identify this last event with LMC X-4 as well. This was the event we identified as a trigger on eclipse egress, after considering its phase with respect to the ~1.4 day binary period.

We have listed these 37 events, in order of their occurrence, in Table 4.1. We listed the times in Days of Year 1977; the excess count rates in HED3 cts/s (the Crab nebula + pulsar is about 660 HED3 cts/s); the X-ray sources found within each position error box; plus our suggested identification for each event and the information on which each suggested identification was based. We displayed, in Figure 4.3, a short term (~80 s) light curve and an indication of the hardness or color temperature as a function of time, for all the events. Below, we discuss some of the characteristics of the events from each source.

i. HD36705 / N49

The events on D.O.Y. 1977 365.35 and 550.58 contained only the SNR and suspected gamma-ray burst source N49, and the suggested RS CVn-type system HD36705, a seventh magnitude K1 IIIp star. Although it would be exciting to find bursts from N49 prior to the massive March 5, 1979 gamma-ray burst, we find, because of the lack of variability and the apparent unevolving, ~10 keV (thin thermal

143

bremsstrahlung) spectra of these events, that they were unlikely to be gamma-ray bursts. However both the temperature and lack of variations on time-scales of seconds are what one expects from flares from the active coronae of a cool star. If they are flares originating on the foreground RS CVn-like system HD36705, which is at a distance of ~70 pc, we find luminosities of $1-5 \times 10^{32}$ ergs-s^{-1}. This is again what one expects for flares from an RS CVn-type system. Ambruster (1984) finds a flare rate of 1 events with luminosities ~10^{32}ergs-s^{-1} or greater per five days of scans over HD8357, which is also a seventh magnitude sub-giant at a distance of ~70 pc and of similar spectral type to HD36705. (Ambruster notes that there were actually two flares from this system, but they occurred so close in time that they may have come from the same active region on the star and so were not independent events. In Chapter 3, we noted that the A-2 fast transient search had triggered on the brighter of the two flares from this system, which was originally identified from A-3 data as coming from HD8357 (Garcia et al. 1980). Given that the HEAO A-2 coverage of HD36705 was about an order of magnitude higher than that of HD8357, but because of differing collimator sizes the A-1 coverage was about twice that of A-2, it seems reasonable that this search should have detected two separate events from HD36705. We therefore consider HD36705 a much more likely source than N49 for these two events.

ii. <u>LMC X-2 / CAL 8 or CAL 9</u>

There were two events with positions consistent with that of LMC

X-2. The first of these events, on D.O.Y. (1977) 290.62, also

contained the faint proposed high mass X-ray binaries CAL 8 and

CAL 9. In Figure 4.4, we display ~12 hour light curves and plots of

softness ratios (MED/HED3) versus time around the time of each

event. The light curve for the event on D.O.Y. (1977) 653.78 seems to

show a ~6-8 hour transition from a low intensity state to one of

higher intensity. Interestingly, the spectrum of the source also

changed at this time, from a thin thermal bremsstrahlung temperature

of ~6 keV, to ~10 keV, as the source intensity increases. This change

is illustrated by the plot of softness ratio versus time accompanying

the light curve in Figure 4.4.b This is characteristic of the

behavior one finds in similar Galactic low mass X-ray binaries when

one considers the hardness of a source as a function of its intensity

(Parmar, Stella, and White 1985).

For the first event, on D.O.Y. (1977) 290.62, Figure 4.4.a

illustrates a different behavior. The PHA spectra indicate that the

source is apparently in an ~8.4 keV (thin thermal bremsstrahlung)

'soft' state, and one sees evidence of 'flickering' at least on

timescales as short as an hour. The spectrum of the 'flare' on which

the fast transient search triggered is harder than the average LMC X-2

spectrum at this time, with kT~10 keV. (There is a corresponding

slight dip in the plot of softness ratio versus time that accompanies

the light curve in Figure 4.4.a). However (Parmar, Stella, and White

1985), this is also behavior characteristic of low mass X-ray binaries

similar to LMC X-2. We therefore think it plausible to identify both

145

of these events with the low mass binary LMC X-2, rather than the faint Pop I candidates CAL 8 or CAL 9, or with any previously undetected source of X-rays.

iii. LMC X-1 / CAL 37

Five events in eight days occurred around the vicinity of LMC X-1 and the proposed high mass binary CAL 37. However, the 99% position limits for three exclude CAL 37. All five occurred at times when LMC X-1 was most visible during this pass (although, interestingly, the search found no corresponding variability during the second and third passes six and twelve months later). In Figure 4.5, the 13 day light-curve shows flickering on time-scales of ~1 hour to ~ 1 day. From the accompanying plot of softness ratio as a function of time, we see interesting spectral variability, including an indication of slight hardening during the brightest flare; but there is no obvious overall pattern of spectral change related to the other four fast transient events. From comparison of the PHA spectrum of the brightest events with the average spectrum, it appears there may be a slight increase in the emission measure of the hotter component of the soft, 'black-hole-like' spectrum (White, Kaluzienski, and Swank 1984) during these events. Despite the apparently regular spacing of these events, like investigators before us (White and Marshall 1983) we found no evidence of periodicity. Also, we find no evidence of the kind of rapid intensity and temperature variations one typically finds in Type I or II X-ray bursts, which can have outbursts that appear semi-regular but that show no periodicities. Therefore we find it most likely that our fast transient program triggered on the peaks of the sorts of variability one expects from such high mass binaries, and we identify

146

all five of these events with LMC X-1.

iv.   The LMC Transient (A0538-66)

This high mass X-ray binary (B2 IVp + compact object; Johnston et al. 1979) has been observed to give X-ray and optical outbursts that last from a few hours to (in one case) ~14 days (White and Carpenter 1978; Johnston et al. 1979; Skinner et al. 1980). Although White and Carpenter (1978) noted a spectrum consistent with a thin thermal bremsstrahlung model with kT of 6.5 keV and negligible absorption, Johnston et al. (1979) found that the hardness ratios were roughly constant throughout each outburst, but that there was an increase in hardness for the n=8 peak equivalent to a change in power law photon index of 1.5 to 0.3.

Following Skinner et al. (1980) and Johnston et al. (1979), we number the outbursts of the LMC Transient so that n = 0 falls on D.O.Y. (1977) 180.46. By comparing the times of the A-2 events to the A-1 and A-3 light curves of Skinner et al. (1980) and Johnston et al. (1979), we attributed eight of the A-2 LMC fast transients to the LMC Transient during five of its outburst cycles. We list these eight events in Table 4.2, along with intensities and rough spectral information. Since our database of 12 hour averages started on D.O.Y (1977) 232, we did not observe outbursts prior to n = 3 (on D.O.Y. 1977 230.46).

The n = 3 outburst was of unusually long duration; the peak occurred ~1.6 days after the predicted time and excess emission was observed for ~14 days (Skinner et al. 1980). The A-2 fast transient survey found significant variability (above the 12 hour mean) three

times during this long outburst. All three triggers occurred on the falling edge of the event, 1-2 days after the peak. During one of these events, on D.O.Y. (1977) 233.82, we detected significant short term variability (x^2 was greater than twice the number of degrees of freedom when we assumed the source was constant during the ~80 s it was in the fields of view). From power law fits to the average color rates exhibited in Table 4.2, one sees that the spectra of all three of these events was evidently quite hard.

The outburst at n = 6 (D.O.Y 1977 260.43) was roughly twice as bright at peak as at n = 3, but was of much shorter duration (~6 hrs FWHM). In this cycle the A-2 fast transient survey triggered on the peak of the outburst itself, rather than on shorter term variability on the rise or tail. During the ~8 hour (FWHM) n = 8 outburst, the A-2 survey triggered twice, once on the rising edge just prior to the peak (D.O.Y 1977 313.75), and once on the peak itself (D.O.Y. 1977 313.79). During the former we again found evidence for significant variability during the ~80 s the source was in the fields of view of the A-2 detectors. Again, we infer from the power law fits to the excess color rates that the trigger on the rising edge appeared slightly harder than that on the peak. Finally, the A-2 survey indicates one faint trigger each on the peaks of the faint, few hour duration, n = 11 and n = 12 outbursts. (Neither Skinner et al. 1980 nor Johnston et al. 1979 detected the faint n = 12 outburst.) The color rates of both indicated power law (photon) indexes of 1.8-2.4, consistent with the softer values found by Johnston et al. (1979).

The A-2 fast transient survey found no events during the short outbursts of cycles 4, 5, 7, 9, or 10. We also found no events later

than the n = 12 outburst that we attribute to the LMC Transient.
Overall, it may be true that we measured a softer spectrum when
triggering on the peak of an outburst than when triggering on shorter
term variability on the rising or falling edges. However this does
not appear consistent with Johnston et al. (1979) finding the average
spectrum of the n = 8 outburst significantly harder than those at
n = 3 and n = 4.

v. The Flares from LMC X-4

LMC X-4 has been identified as an O8 III + $1.6M_0$ neutron star in
a ~1.4 day eclipsing binary system (Hutchings, Crampton and Cowley
1978; Li, Rappaport, and Epstein 1978; Kelley et al. 1983). Lang et
al. (1981) also observed a clear ~30.48 day cycle in 13-125 keV
X-rays. We noted earlier that all twenty of the remaining events fell
within 1-2 weeks of the peak of this 30.5 day cycle. All but one fell
within phases 0.2-0.48, about one to nine days just after the peak.
We calculate the probability of this clustering in phase happening by
chance to be ~0.001%, and therefore think it probable that all these
events originated on LMC X-4, despite having other variable sources
within 16 out of 20 of the 99% confidence position limits displayed in
Figure 4.1.

White (1978) displays in his Figure 1 a 1.7-17 keV light curve
for LMC X-4, covering five days of data, from roughly phase 0.2 to 0.4
of the ~30.5 day cycle. It illustrates several features of the
shorter term (<30 day) light curve. Most prominent are the bright
flares, lasting ~20-45 minutes, with L_x ~ 10^{39} ergs-s^{-1} (Epstein et
al. 1978; Li, Rappaport, and Epstein 1978; Kelley et al. 1983).

149

Kelley et al. (1983) noted that these flares are seen about 1 to 6 days after the peak of the ~30.5 day cycle (phase ~0.2-0.4), and detected ~13.5 s pulsations only during these flares, with the pulsed fraction of ~30%. Also visible in Figure 1 of White (1978) are the X-ray eclipses, ~1.408 days apart, and lasting for ~5 hours. From his Figures 1 and 2, eclipse ingress and egress appear to last ~20 minutes to an hour each. During the eclipses, the X-ray flux sinks from its average value of ~8-10 millicrabs to consistent with zero. This is roughly an order of magnitude smaller change in flux than that seen during the luminous flares.

Theoretically, this A-2 fast transient survey could trigger on the eclipses as well as the brighter flares. If one of the half-days over which the 12 hour mean was calculated happened to include most of the zero flux portion of an eclipse, it was possible for the A-2 fast transient search program to trigger on the greater amount of emission during eclipse ingress or egress. We find only one event that matches this scenario. The event on D.O.Y. (1977) 530.57 occurs at phase ~0.06, during eclipse egress, and its corresponding 12 hour mean included the ~5 hour eclipse. This was also the only event (out of twenty) that did not occur between phases 0.2 to 0.48 of the ~30.5 day cycle. From Table 4.3, we note the apparently soft spectrum (power law photon index of ~1.9) and short term variability evident during this event.

We calculate the respective trigger rates one expects for the two types of variability (eclipses and flares), assuming that Figure 1 of White (1978) is a reasonable representation of the 2-20 keV LMC X-4 light curve. During this ~1/3 of the 30.48 day cycle (phase 0.2-0.5),

the flares occurred four times in five days and last for ~20 minutes
to an hour (if our identification of the events on D.O.Y. 1977 354.24,
354.26, and 354.28 was correct). The eclipses occur with roughly the
same frequency as the flares (once every ~1.4 days), and eclipse
ingress and egress appear to last about as long (~20 minutes to an
hour). However the flares are only visible during this third of the
~30.5 day cycle; from Lang et al (1981) it appears that the X-ray
flux goes to zero during roughly another third of this cycle (during
which neither the flares nor the eclipses should be visible). That
suggests, overall, that there are roughly four times as many eclipse
ingresses and egresses as luminous flares. From Appendix A we note
that for events which last appreciably longer than a minute, the
probability of triggering on an event of intensity S, when the trigger
threshold is S_0, goes roughly as $(1-S_0/S)$. Since one sees about an
order of magnitude greater change in luminosity from the bright flares
than from the eclipses, there is roughly twice the probability of
triggering on a bright flare than on an eclipse ingress or egress,
assuming they occur with equal frequency, and assuming the minimum
possible trigger threshold S_0 of ~4 millicrabs. Moreover, when
passing over this portion of the sky, the threshold level ranged from
this minimum level to ~20 times that; it was only low enough to
trigger on an eclipse during ~15% of the triggers. Combining these
three factors, we calculate an expected ratio of ~0.6 triggers on
eclipse ingress or egress per twenty triggers on bright flares. This
is consistent with our identification of only one event as a trigger
on an LMC X-4 eclipse egress. This identification of a low number of
events with LMC X-4 eclipses is further supported by the apparent

151

random distribution of all the LMC X-4 events with respect to the phase of the ~1.408 day binary period. (Had a greater proportion of the events been from triggers on eclipse ingress or egress, one would expect a clustering around binary phases of ~0.06 and ~0.94.)

There is one discrepancy apparent with this identification of the event on D.O.Y. (1977) 530.57: it is about five times more luminous than the eclipse ingresses and egresses shown in White (1978). Had every eclipse evinced a change in X-ray flux of this magnitude, the A-2 fast transient search should have triggered on nearly equal numbers of flares and eclipses. That it did not suggests this event was unusual. We leave this interesting question of apparent changes in the profile of the binary period to future researchers.

We have identified the remaining 19 events with luminous flares from LMC X-4, with durations of 20 minutes to an hour, and detected only during phases 0.2-0.48 of the ~30.5 day cycle. The fluxes detected above a 12 hour mean implied excess luminosities of ~0.1-6x10^{39} ergs-s^{-1}. The mass of the neutron star in LMC X-4 has been fairly well determined to be ~1.6 solar masses, so these flares apparently frequently exceed the Eddington luminosity (of ~10^{38} ergs-s^{-1} for hydrogen and twice that for helium). The spectral parameters listed in Table 4.3 range from very hard (power law photon index of ~0.2) to very soft (power law photon index of ~2.4), with no apparent correlation among intensity, variability, and hardness. This differs from the conclusion of Epstein et al. (1978), who suggested that the bright flares have generally harder spectra (power law photon index of ~0.5) than the lower intensity state (power law photon index of ~1.2). However, as indicated in the introduction, the absolute

152

values of spectral parameters determined from fits to excess color

rates may not have been very reliable, and the systematic errors

inherent in this approach were difficult to quantify. A better

understanding of the spectral variability of these events may have to

wait for a careful study of the full LMC X-4 light curve over the year

and a half HEAO 1 was aloft, a project which is beyond the scope of

this thesis.

vi. Upper Limits on X-ray Bursts from the LMC

We identified none of the 37 fast transient events as typical

Type I (or II) X-ray bursts. This conclusion is independent of our

finding that all 37 events most probably originated on known, varying,

sources. None of the 37 events in Table 4.1 exhibited the typical

X-ray burst light curve of sharp rise and exponential decay within

~10 s; neither did any show evidence for a black-body spectrum cooling

on the ~10 s time-scales typical of classic X-ray bursts. (Indeed,

the events that showed evidence of spectral variability on time-scales

of less than a minute seemed to be hardening rather than softening.)

In our Galaxy, Cowley et al. (1984; 1987) estimate there are

about 75 accreting low mass X-ray binaries, about half of which they

expect to be hidden by strong interstellar absorption as one looks

towards the Galactic plane and Galactic center. If these are

considered in terms of their X-ray burst properties, one can divide

them into three categories (with about a third in each category):

high luminosity ($\sim 10^{37-38}$ ergs-s^{-1}) sources, with the X-ray bursts

infrequent due to an inferred high accretion rate; low luminosity

sources (such as those found in globular clusters with $L_x \sim 10^{33}$-

153

10^{35} ergs-s^{-1}) with infrequent bursts due to a low accretion rate; and moderate luminosity sources of the sort responsible for the majority of X-ray bursts. The burst rate of the last type of source is typically once every ~3 hours, during the ~1 month per year when the source is bursting, for a mean yearly rate of 0.5 per day per source (Swank private communication; Bradt and McClintock 1983). The mean burst rate per source, when averaged over all three types of low mass sources found in our galaxy, is then expected to be something like 0.34 per year.

To compare this rate with the limits on X-ray bursts from the LMC, following Cowley et al. (1984), we assume the number of Pop II binaries scales as the total mass, so that one expects ~7-8 Pop II binaries in the LMC. For ease of calculation, we had divided the Magellanic Clouds region into 14 bins (not of equal area), 3° in Ecliptic latitude and longitude on a side, and calculated trigger probabilities as a function of the time-averaged count-rate in each bin. On average one expects 0.5 Pop II sources per bin. Although the Magellanic Clouds survey incorporated a total of ~5.6 continuous days of data, since the expected luminosity of an X-ray burst was only ~4 times the minimum search threshold if the source of the burst was at the distance of the Magellanic Clouds, we found our measured rate of no X-ray bursts in 3 days of 'on' time to be equivalent to a 90% upper limit of a mean burst rate of less than 1 per source in ~0.43 days. Although this 90% upper limit is consistent with the Galactic mean rate estimated in the paragraph above, it still supports the suggestion in the Einstein survey work of Cowley et al. (1984) that there may be a lack of moderate accretion rate Pop II sources in the

Magellanic Clouds.

C. <u>Summary</u>

In this HEAO 1 A-2 fast transient survey of the Magellanic Clouds, out of ~6 days of coverage of the region, we found 37 good events, all from the direction of the Large Magellanic Cloud. We detected none from the Small Magellanic Cloud. We attribute this in part to the smaller number of sources in the SMC (which has ~1/5 the mass of the LMC), in part to the slightly lower coverage of the SMC region (due to its greater distance from the South Ecliptic pole), and in part to the greater distance of the SMC (~70 kpc versus 55 kpc for the LMC), so that to have the same probability of triggering our search algorithm as an event from the LMC, a fast transient from the SMC would need to be almost twice as bright.

We identified two of the thirty-seven events with a foreground object, an RS CVn-type system at ~70 pc. We attributed the remaining thirty-five events to four of the five brightest X-ray binaries in the LMC. Interestingly, we found no events we could plausibly attribute to the high mass binary and black hole candidate LMC X-3. We attributed two (one year apart) to the low mass binary LMC X-2. The first we identified with 'flickering' on time-scales of ~hours; and the second with an abrupt transition from a low intensity state to a state of high intensity. We attributed five events to flickering of the luminous high mass X-ray binary LMC X-1. The events from both sources appeared similar to those from luminous high and low mass Galactic X-ray binaries discussed in Chapter 3. We identified eight events with outbursts from the high mass binary A0538-66, the LMC

Transient. This system exhibited a pattern of (super-luminal)
intensity increases, lasting from hours to weeks, on a ~16.7 day cycle
attributed to its eccentric orbit. For these events, when we
triggered on the peak of an outburst the spectrum appeared softer than
when we triggered on a rising or falling edge.

We attributed the remaining twenty events to the high mass
eclipsing binary LMC X-4. This system exhibits both ~5 hour eclipses
in its ~1.4 day binary period, and overall intensity modulation on a
~30.5 day cycle, as well as bright flares that exhibit ~13.5 s
pulsations (Li, Rappaport, and Epstein 1978; White 1978; Kelley et
al 1983; Lang et al. 1981). We suggested that one event out of the
twenty was a trigger on the change in X-ray flux during eclipse
egress, although that event was abnormally bright. We identified the
remaining nineteen events, with 20-60 minute long highly luminous
flares ($\Delta L_x/L_{Edd}$ ~ 0.5-20), which all occurred between phases 0.2 and
0.5 of the 30.5 day cycle.

We found no events that may be typical Type I (or II) X-ray
bursts (Lewin and Joss 1981). This conclusion was independent of our
identifying all thirty-seven events with known luminous X-ray sources,
and was based on the shape of the ~1 minute light curves and the lack
of characteristic burst cooling seen during each event. (Using these
criteria we could not have ruled out an identification of some of the
events, such as the brightest one from LMC X-1 and LMC X-2, with
unusually long X-ray bursts like those detected from some Galactic
sources. However, for these events, the PHA spectra seemed to
indicate that black body models were not a good fit to the excess
emission.) We calculate a 90% upper limit on the average number of

bursts per source per year from the LMC of < 1 per 0.43 days. This is consistent with the average rate of ~0.34 per year seen from the Milky Way; however, it is interesting to note that no observer has yet detected any 'moderate luminosity', moderate accretion rate Pop II X-ray binaries in the LMC, of the sort responsible for the majority of X-ray bursts in our Galaxy. In fact, this survey found no events from sources invisible to the Columbia Astrophysical Laboratory Einstein LMC survey, hidden either by high column density or long term variability. Cowley et al. (1984) point out that they detected one bright Pop II X-ray binary (LMC X-2), and one faint candidate Pop II binary that is not in a globular cluster - i.e. it apparently does not belong to the oldest population of low-mass X-ray binaries visible in the Milky Way.

Table 4.1
EVENTS FROM THE MAGELLANIC CLOUDS

Time in D.O.Y. 1977	Flux in HED3 cts/s (> 12 hr mean)	Sources in Error Box:	Suggested I.D.	Based On:
233.55	16.4	4, T	LMC Trans	Skinner et al.
233.82	6.3	" "	" "	" " "
234.45	9.2	" "	" "	" " "
280.51	38.1	T	" "	" " "
290.62	8.3	2, 8, 9	LMC X-2	Spectrum, light curve seem plausible; slightly better position fit
303.98	7.9	1, 37	LMC X-1	Same here
306.11	21.5	" "	" "	" "
307.50	5.2	"	" "	" "
311.47	7.1	" 37	" "	" "
311.59	8.9	"	" "	" "
313.75	17.7	4, T	LMC Trans	Skinner et al.
313.79	22.8	" ", 83	" "	" " "
321.29	7.6	4, T, 83	LMC X-4	Phase of 30.5d cycle
321.41	18.5	N, H, 4, T, 83	" "	" " " "
328.34	10.4	4, T, 83	LMC X-4	Skinner et al.
351.57	7.1	4, T, 3, N, H	LMC X-4	Phase of 30.5d cycle
354.23	33.9	4	LMC X-4	Position and phase
354.26	7.9	4, T, 3	" "	Phase of 30.5d cycle
354.28	5.6	" " ", 83	" "	" " " "
355.30	15.0	" " " "	" "	" " " "
357.55	17.9	" " "	" "	" " " "
357.90	15.7	" " ", N, H	" "	" " " "
358.56	9.8	" " "	" "	" " " "

Table 4.1 <u>EVENTS FROM THE MAGELLANIC CLOUDS</u>, continued

Time in D.O.Y. 1977	Flux in HED3 cts/s (> 12 hr mean)	Sources in Error Box:	Suggested I.D.	Based On:
363.64	12.9	4, T, 3, 83	LMC Trans	Skinner et al.
365.35	24.5	N, H	HD36705	Position & spectrum
381.03	5.5	4, T	LMC Trans	Position and phase of 16.6d cycle
420.58	8.7	4	LMC X-4	Position and phase of 30.5d cycle
530.57	28.4	4	LMC X-4	Position
536.52	53.1	4	" "	Position and phase
539.24	43.4	"	" "	Position and phase
540.14	9.2	" T	" "	Phase of 30.5d cycle
541.18	15.1	" " 3	" "	" " " "
543.04	6.9	" " "	" "	" " " "
550.58	9.5	N, H	HD36705	Position & spectrum
573.51	8.5	N, H, 4, T, 3	LMC X-4	Phase of 30.5d cycle
602.64	12.0	4, T	" "	" " " "
653.78	7.8	2	LMC X-2	Position; light curve and spectrum

Above, we designated the brightest X-ray sources by their X-ray source number, e.g. '1' represents LMC X-1, '2' LMC X-2, '3' LMC X-3, and '4' LMC X-4. We designated the supernova remnant N49 by 'N', the LMC Transient (A0538-66) by 'T', and the RS CVn-type variable HD36075 by 'H'. There are four faint sources suggested by Cowley <u>et al</u>. (1984) to be X-ray binaries; we labeled them with their Columbia Astrophysical

Laboratory Einstein LMC Survey number, so that CAL 8, CAL 9, CAL 37, and CAL 83 are designated by '8', '9', '37', and '83', respectively. We did not list the positions of any of the active dwarf stars found by Cowley et al. (1984) to be in the field of view, as they are too distant (>50 pc) to have given the events recorded here. We also did not include X0544-665 in this short list of objects in each error box.

"Skinner et al" stands for Skinner et al. (1980). The 30.5d cycle of LMC X-4 is from Lang et al. (1981). Kelley et al. (1983) discuss those 20-40 min flares from LMC X-4 that occur about 1-7 days after a peak in the 30.5 day cycle.

Table 4.2

Fast Events From The LMC Transient

Time in D.O.Y. 1977	Outburst Cycle Number[a]	Intensity HED3 cts/cm^2-s (> 12 hr mean)[b]	Varies? (x^2>2DOF) (c)	Rough Spectrum: Mean power law Photon Index[d]
233.55	3	0.361±0.04		0.5±0.2
233.82	"	0.211±0.04	Y	0.5±0.3
234.45	"	0.213±0.03		0.7±0.3
280.51	6	0.683±0.04		1.8±0.2
313.75	8	0.120±0.02	Y	0.6±0.3
313.79	"	0.339±0.02		1.3±0.2
363.64	11	0.093±0.02		2.4±0.5
381.03	12	0.016±0.01		1.4±0.5

a. Following Skinner et al. (1980) and Johnston et al. (1979) we have numbered each outburst cycle so that n = 0 begins at D.O.Y. (1977) 180.46.

b. We performed a least-squares fit to a constant value to the ~80 s light curve for each event (displayed in Table 4.3), assuming the position of the LMC Transient. In this column we listed the best fit values and 1σ errors in HED3 cts/cm^2-s. The intensity of the Crab Nebula + pulsar (about 3.4×10^{-8} ergs-cm^{-2}-s^{-1} from 2-20 keV) is ~1.64 HED3 cts/cm^2-s.

c. When x^2 was greater than twice the number of degrees of freedom for the fit described above, we indicated that the source varied on timescales ≤80 s with a 'Y' in the fourth column.

d. We have fit the excess color rates (above the 12 hr mean) to a model power law spectrum, with the column density held fixed at 10^{21} cm^{-2}, the value appropriate for an origin in the LMC. Here we have listed the best fit power law (photon) index, and 1σ errors.

Table 4.3

Fast Events From LMC X-4

| Time in D.O.Y. 1977[a]	Phase of: 30.5d cycle[b]	1.41d cycle[c]	Intensity HED3 cts/cm^2-s (> 12 hr mean)[d]	Varies? (e)	Rough Spectrum: Mean power law Photon Index[f]	Varies?
321.294	0.21	0.457	0.069±0.02	Y	2.3±0.6	
321.415	0.21	0.546	0.378±0.07	Y	0.9±0.4	
328.338	0.44	0.462	0.106±0.02		1.4±0.5	
351.569	0.20	0.957	0.072±0.01	Y	1.5±0.7	
354.235	0.29	0.850	0.525±0.07	Y	2.8±0.2	Y
354.260	"	0.868	0.062±0.01		1.2±0.4	Y
354.284	"	0.885	0.080±0.01	Y	0.8±0.5	
355.305	0.32	0.610	0.047±0.02	Y	1.4±0.3	
357.545	0.40	0.200	0.031±0.01	Y	0.2±0.2	
357.902	0.41	0.454	0.063±0.01	Y	0.6±0.3	
358.557	0.43	0.919	0.057±0.01		1.1±0.5	
420.581	0.47	0.960	0.357±0.04		1.6±0.4	
530.567	0.07	0.058	0.189±0.01	Y	1.9±0.2	
536.520	0.27	0.285	0.122±0.01	Y	2.3±0.2	
539.244	0.36	0.219	0.207±0.01	Y	3.7±0.3	
540.144	0.39	0.858	0.088±0.01		1.7±0.6	
541.180	0.42	0.593	0.109±0.01		0.9±0.2	
543.036	0.48	0.911	0.068±0.01		0.6±0.4	Y
573.514	0.48	0.553	0.126±0.03		2.5±0.8	
602.644	0.44	0.237	0.191±0.05	Y	0.3±0.2	Y

a. Julian Days = D.O.Y. (1977) + 2,443,144.500.

b. We calculate the phase of the 30.5 day cycle from Lang et al. (1981). A phase of zero corresponds to the end of the cycle minimum; the X-ray peak begins at roughly phase 0.2. We estimate a systematic error in phase of roughly ±0.02.

c. We calculate the phase with respect to the ~1.41 day binary period using Kelley et al. (1983). A phase of zero corresponds to the center of the eclipse, which lasts about 5 hours (ϕ = ±0.08). We calculate a systematic error in phase of roughly ±0.02.

d. We performed a least-squares fit to a constant value to the ~80 s light curve for each event (displayed in Table 4.3), assuming the position of LMC X-4. In this column we listed the best fit values and 1σ errors in HED3 cts/cm^2-s. The intensity of the Crab Nebula + pulsar (about 3.4×10^{-8} ergs-cm^{-2}-s^{-1} from 2-20 keV) is ~1.64 HED3 cts/cm^2-s.

e. When χ^2 was greater than twice the number of degrees of freedom for the fit described above, we indicated that the source varied on timescales ≤80 s with a 'Y' in the fourth column.

f. We have fit the excess color rates (above the 12 hr mean) to a model power law spectrum, with the column density held fixed at 10^{21} cm^{-2}, the value appropriate for an origin in the LMC. Here we have listed the best fit power law (photon) index, and 1σ errors.

Figure 4.1 We present the 99% confidence position limits for the 35
LMC fast transient events in Table 4.1. We have labeled each with the
D.O.Y. (1977) on which it occurred. They are superposed on a map of
variable X-ray sources from Bradt and McClintock (1983) and Cowley et
al. (1984). A key to these X-ray sources precedes the plots of these
position error boxes. We designated the brightest X-ray sources by
their X-ray source number, e.g. '1' represents LMC X-1, '2' LMC X-2,
'3' LMC X-3, and '4' LMC X-4. We designate the supernova remnant N49
by 'N', the LMC Transient (A0538-66) by 'T', and the RS CVn-type
variable HD36075 by 'H'. There are four faint sources suggested by
Cowley et al. (1984) to be X-ray binaries; we labeled them with their
Columbia Astrophysical Laboratory Einstein LMC Survey number, so that
CAL 8, CAL 9, CAL 37, and CAL 83 are designated by '8', '9', '37', and
'83', respectively. We have not plotted the positions of any of the
active dwarf stars found by Cowley et al. (1984) to be in the field of
view, as they are too distant (>50 pc) to have given the events
recorded here.

FIGURE 4.1 KEY TO X-RAY SOURCES IN THE DIRECTION OF THE LMC
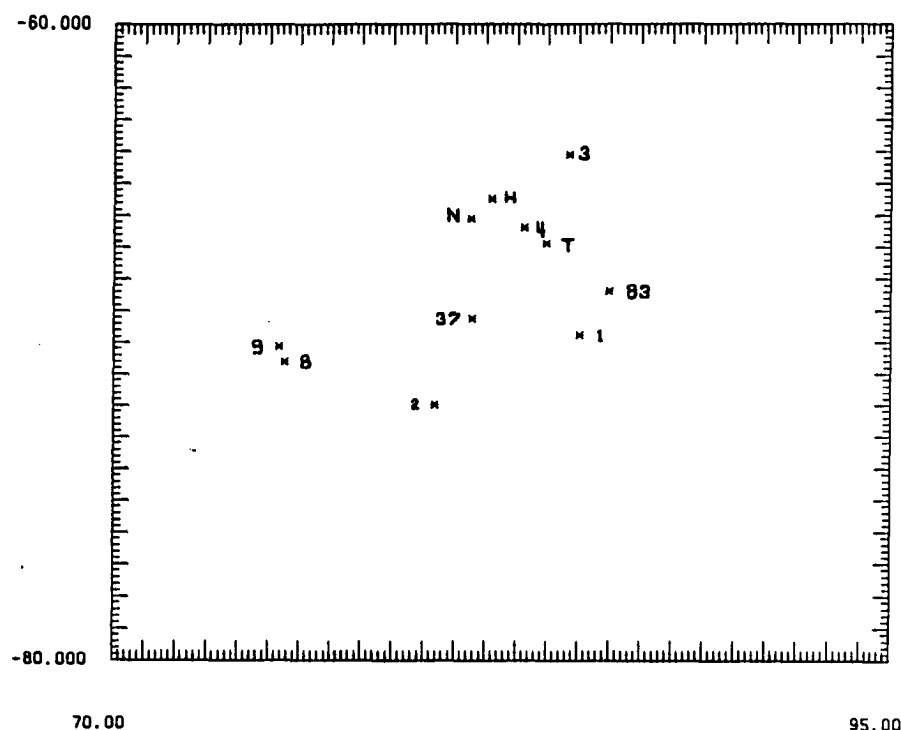
a)   We have plotted 99% confidence position limits for two events,
     ~180 days apart, on D.O.Y. (1977) 365.35 and 550.58. They contain
     only the RS CVn-like system HD36705, and the supernova remnant and
     suggested gamma-ray burst source N49.

FIGURE 4.1.A   (LMCRSCVN.BOX)

70.00   95.00

165
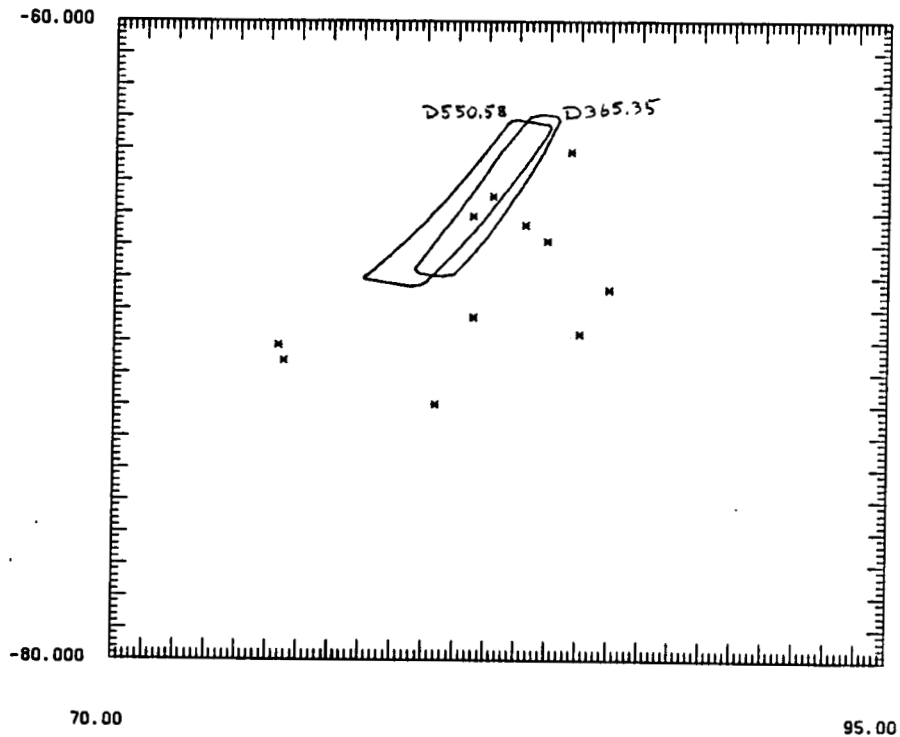
b) We plot here two 99% confidence position limits that contain the low-mass X-ray binary LMC X-2. They are from the events on D.O.Y. (1977) 290.62 and 653.78 (almost exactly one year apart). The first also contains the high mass X-ray binary candidates CAL 8 and CAL 9.

FIGURE 4.1.8   (LMCX2.BOX)

166
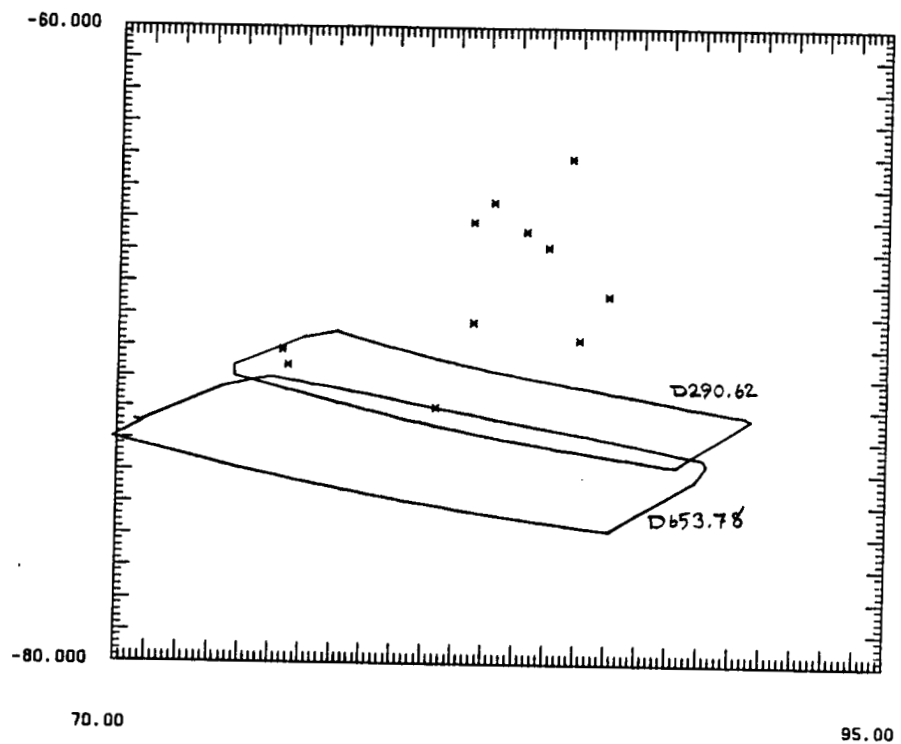
c) There are five events (from D.O.Y. 1977 303.98, 306.11, 307.50, 311.47, and 311.59) with 99% confidence limits that contain LMC X-1. Three of them also contain the suggested high mass binary CAL 37.

FIGURE 4.1.C   (LMCX1.BOX)
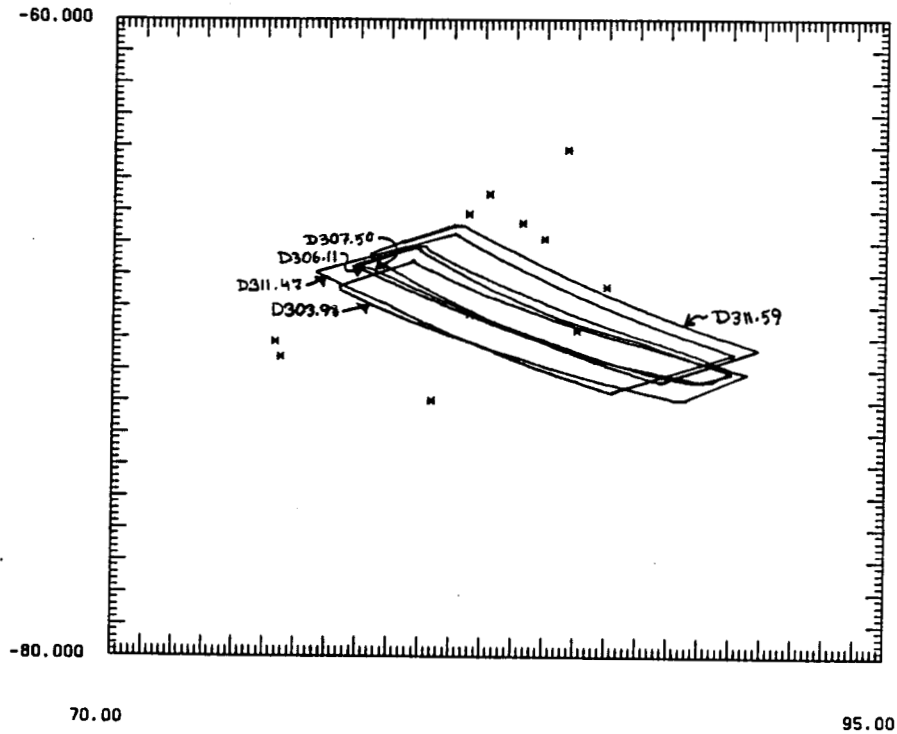
d) We plot here our 99% confidence limits for four events identified by Skinner et al. (1980) as originating from the LMC Transient (A0538-66). These position limits are all consistent with this identification.

FIGURE 4.1.0   (LMCTRANSO.BOX)
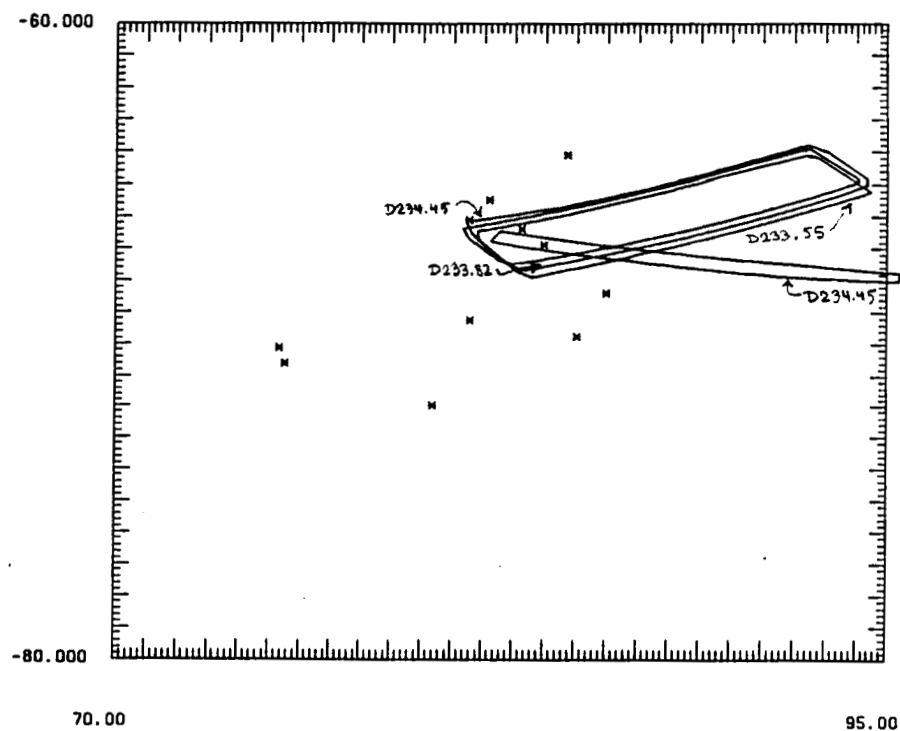
e) We plot here 99% confidence limits for four more events that we attribute to the LMC Transients. Three were identified originally by Skinner et al. (1980), and one we identify with the LMC Transient on the grounds that it occurred at the same phase of the system's 16.6 day cycle, (at n=12, in Skinner's notation) as the other outbursts recorded by Skinner et al. (1980) and Johnston et al (1979). All our position limits are consistent with this identification, although other variable sources in the position error boxes include LMC X-4 and CAL 83.

FIGURE 4.1.E   (LMCTRANSE.BOX)
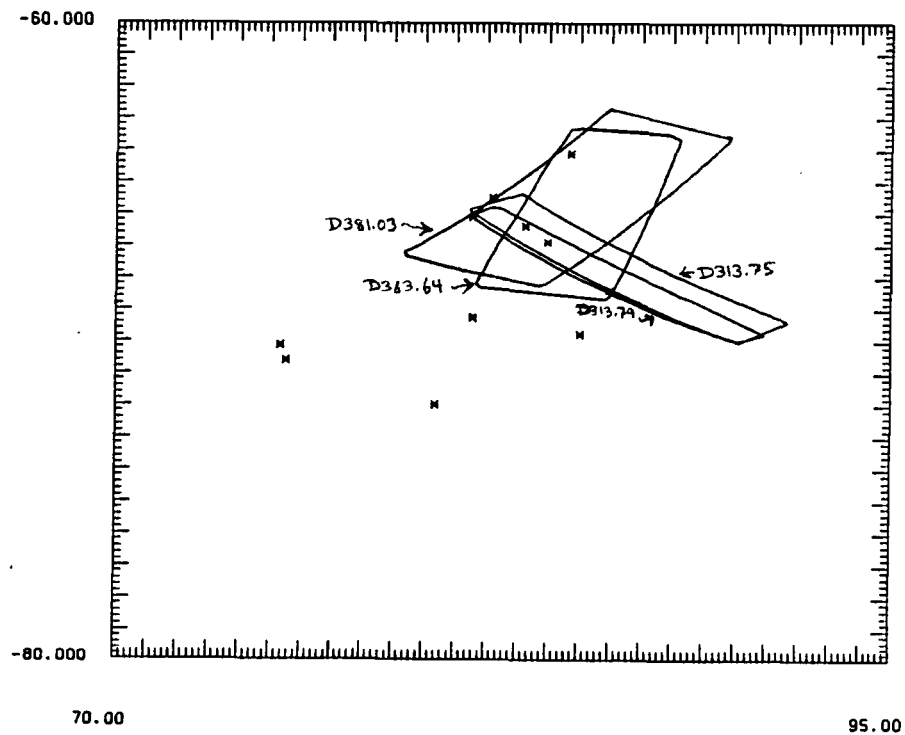
f) The 99% confidence limits for the first three events we attributed to LMC X-4 (on D.O.Y. 1977 321.29, 321.42, and 328.34). They occurred at phases 0.21-0.44 of the 30.5 day cycle.

FIGURE 4.1.F   (LMCX4F.BOX)
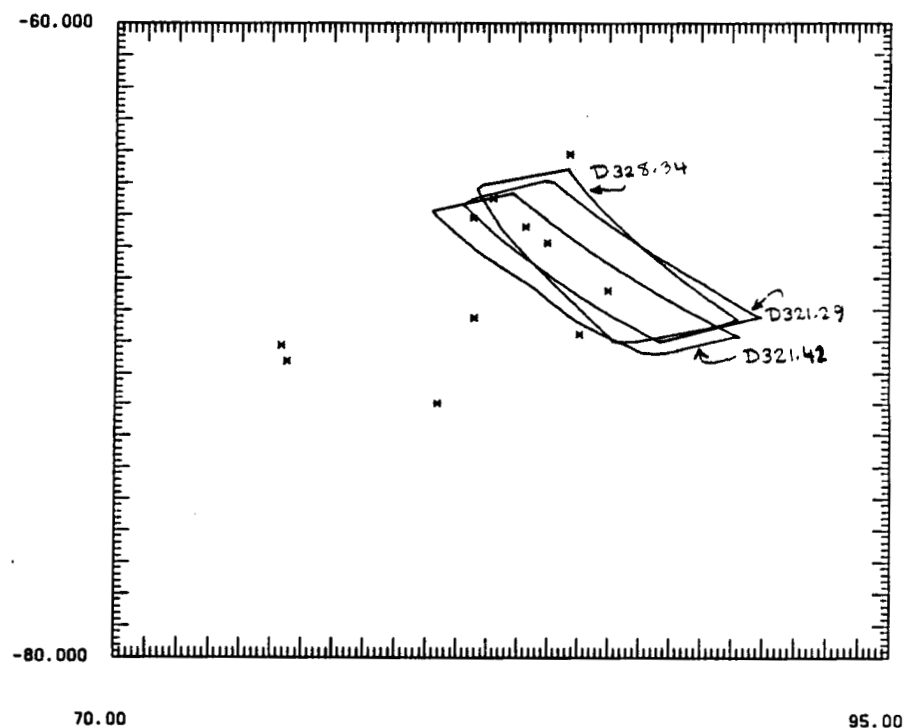
g) The 99% confidence limits for the three events (on D.O.Y 1977 354.24, 354.26, and 354.28) that triggered during three successive spacecraft revolutions (~30 minutes apart) and so were likely to have been three triggers on a single long flare from LMC X-4. The first was extremely bright; the only known X-ray source inside its position limits is LMC X-4. The position limits for the two following events are centered on LMC X-4, but also include the supernova remnant and gamma-ray burst source N49; the RS CVn-type system HD36705; the LMC Transient; and LMC X-3.

FIGURE 4.1.G   (LMCX4G.BOX)
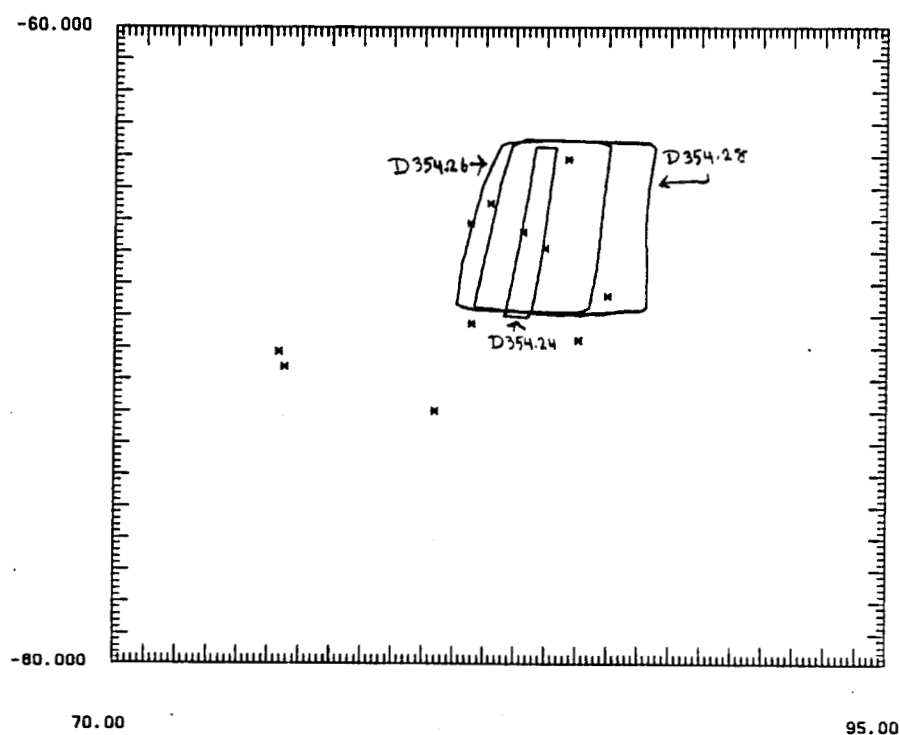
h) The 99% confidence limits for the other five events we attribute to LMC X-4 (on D.O.Y. 1977 351.57, 355.30, 357.55, 357.90, and 358.56) that occurred during this same 30.5 day cycle, with phases ranging from 0.20 to 0.43.

FIGURE 4.1.H   (LMCX4H.BOX)
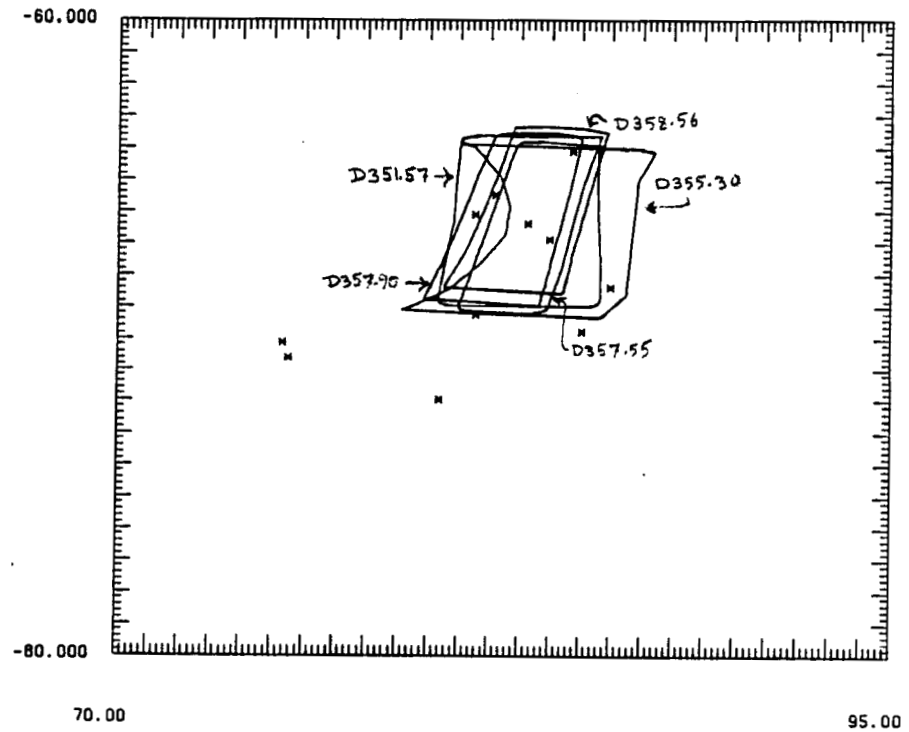
i) This bright event (on D.O.Y. 1977 420.58) occurred two 30.5 day
    cycles after the previous group, at a phase of 0.47.

FIGURE 4.1.1   (LMCX4I.BOX)
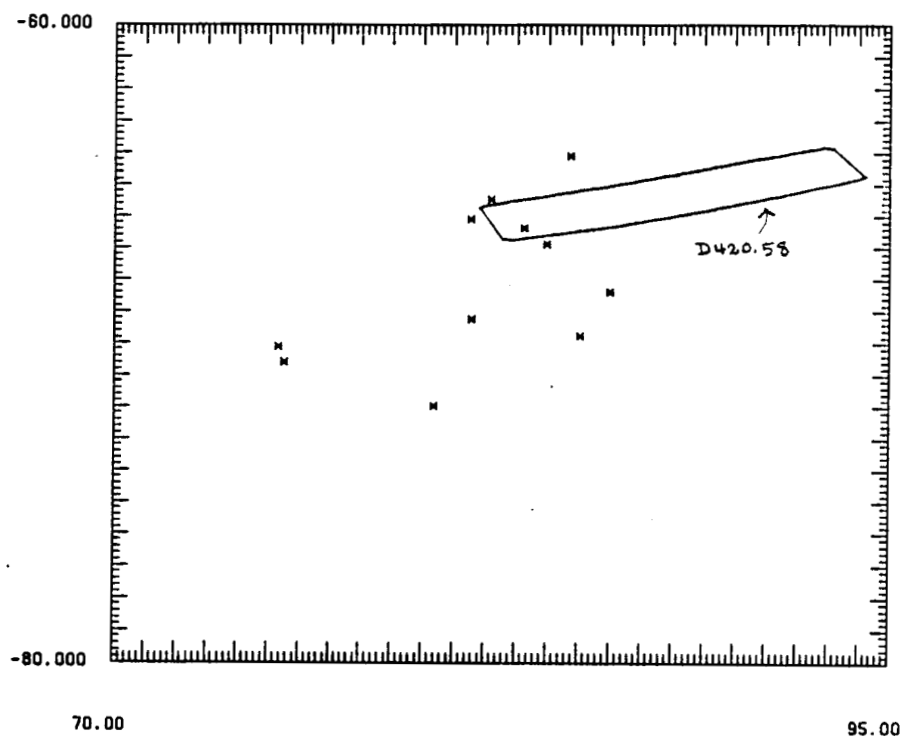
j) This event, on D.O.Y. (1977) 530.57, occurred about 3½ 30.5 day
    cycles (at phase 0.07) after the previous event, and at phase 0.06
    of the 1.408 day binary period (during eclipse egress). Of the
    events apparently from LMC X-4, it is the only one we identified
    as a trigger on an eclipse rather than a trigger on a bright
    flare.

FIGURE 4.1.J   (LMCX4J.BOX)
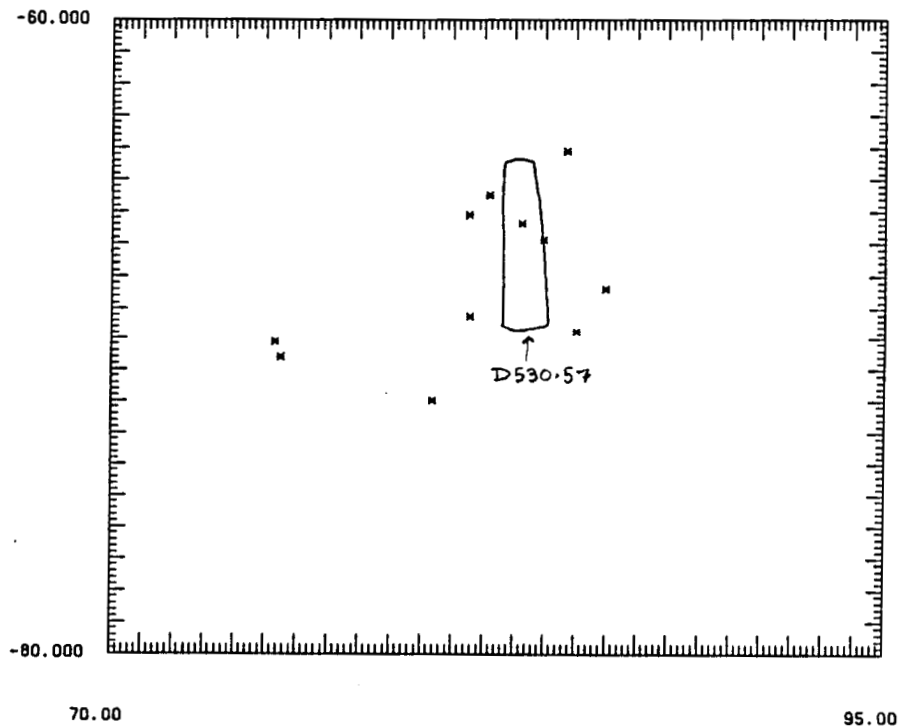
k) These five events (on D.O.Y. 1977 536.52, 539.24, 540.14, 541.18, and 543.04) occurred one to two weeks after the last event, at phases 0.27 to 0.48 of the 30.5 day cycle of LMC X-4.

FIGURE 4.1.K   (LMCX4K.BOX)
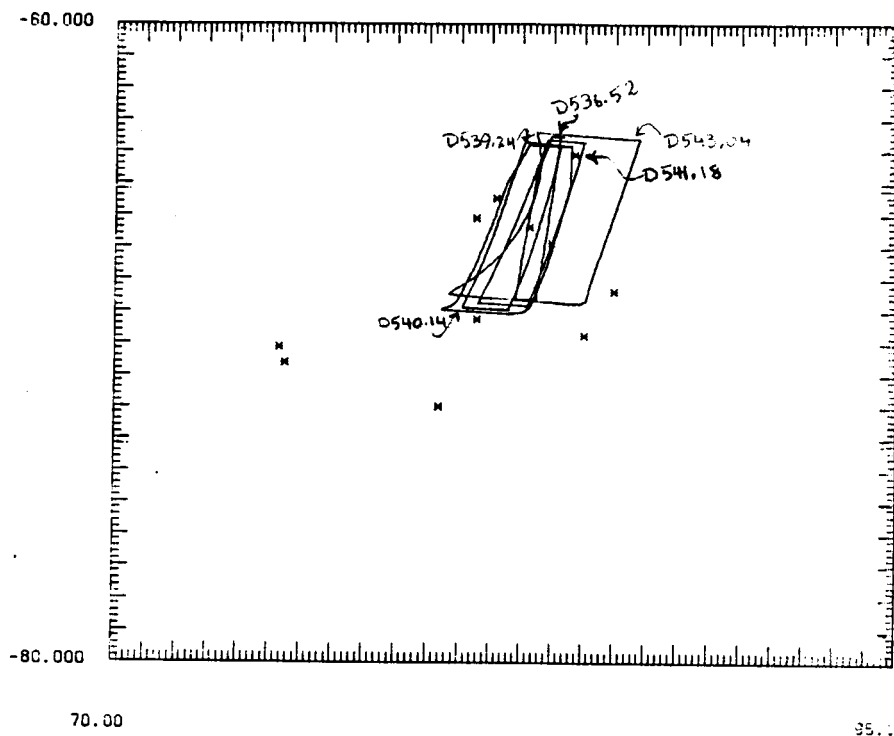
1) The 99% confidence position limits for the last two events (on
    D.O.Y 1977 573.51 and 602.64), which occurred one and two cycles
    after those on the previous plot, at phases 0.48 and 0.44 of the
    30.5 day cycle of LMC X-4.

FIGURE 4.1.L   (LMCX4L.BOX)
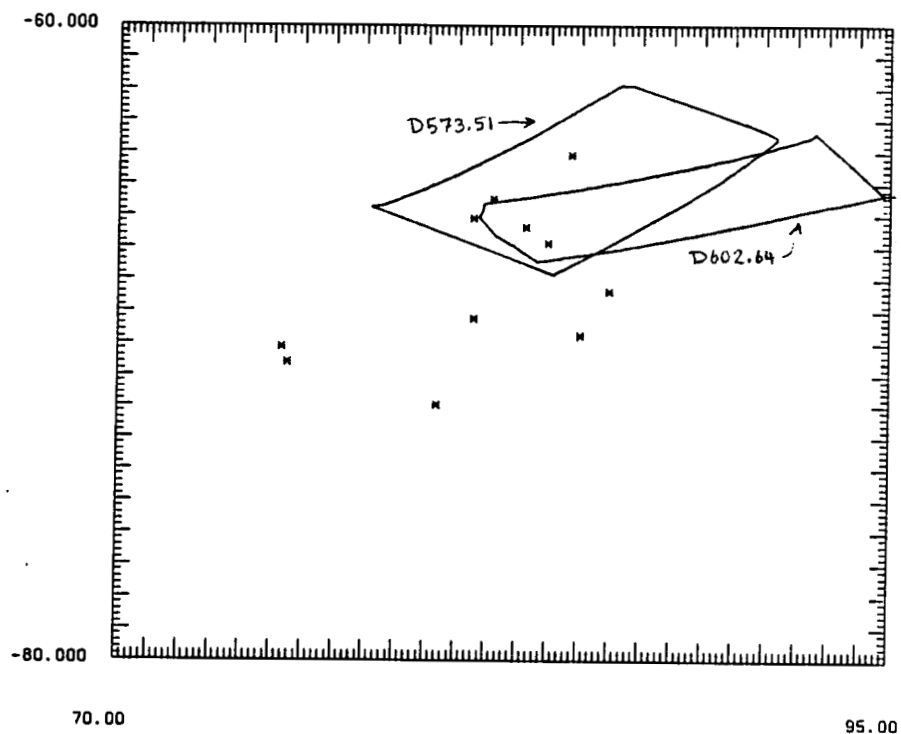
Figure 4.2 We have plotted the intensities (in excess HED3 cts-s^{-1}) versus time (in D.O.Y. 1977) for the twenty events we suggest may have originated on LMC X-4. (The intensity of the Crab nebula + pulsar is about 660 HED3 cts-s^{-1}) Below it, we have reproduced the long-term A-4 (13-100 keV) LMC X-4 light-curve of Lang et al. (1981), which clearly shows the 30.5 day cycle. All save one of these twenty events occurred within 1-7 days after the peak of the 30.5 day cycle. The remaining event, on D.O.Y. (1977) 530.57, seems to coincide with a local maximum just before the peak, and we identified it as a trigger on egress from the binary eclipse.
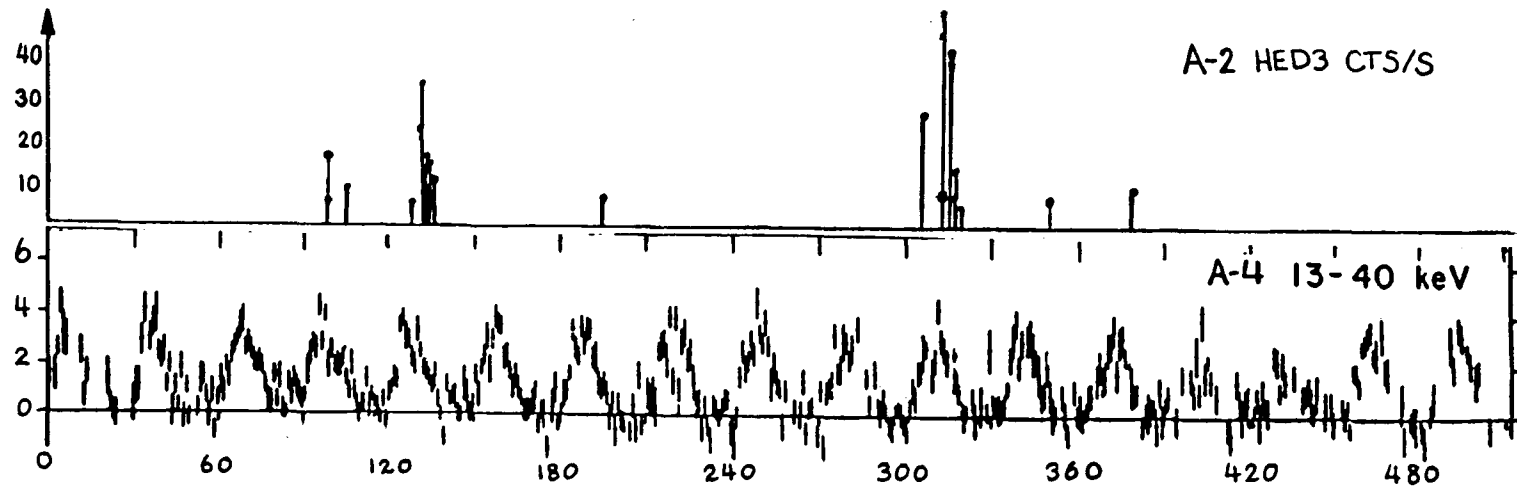
Figure 4.3 In this figure, for every LMC fast transient event, we plot an ≤ 80 s light curve (of the excess HED3 cts-cm^{-2}-s^{-1} above the 12 hour average) while the event was in the combined A-2 fields of view. (One millicrab is ~3.4x10^{-11} ergs-cm^{-2}-s^{-1}, and corresponds to about 0.0016 HED3 cts-cm^{-2}-s^{-1}.) Except where noted, during the fits which produced these light curves, we held the offscan angle fixed at zero, but allowed the scan angle to vary freely, so that the light-curve error bars would reflect the uncertainty in position (but not the uncertainty in the overall normalization). The exceptions either were events identified by someone else (Skinner et al. 1980; Johnson et al. 1979), or were events with no more than one bright X-ray transient within the 99% confidence position limits.

These light-curves are accompanied by plots of the power law photon index as a function of time. To obtain these plots, we fit the excess (above the 12 hour mean) 'color' rates, every 5.12 s, to a power law model with the column density held fixed at the average value to the Magellanic Clouds (N_H ~ 10^{21} cm^{-2}). On each plot we show the results of least squares fits to both a constant and to a straight line. If χ^2 was greater than twice the number of degrees of freedom, that event was designated 'variable' in Tables 4.2 and 4.3. In each graph, the line with the lowest χ^2 was plotted with the data.

a) Plots for the event on D.O.Y (1977) 233.55. Time zero is at 13:08:05 U.T. The position was held fixed at that of the LMC Transient, A0538-66.

LMC1UNK.LTP

$\chi^2 = 14.1$ FOR 13 DOF
P1= 0.687E-01 SIG= 0.596E-02
$\chi^2 = 8.9$ FOR 12 DOF
P2=-0.783E-03 P3= 0.940E-01

LMC1UNK.DP1

$\chi^2 = 1.7$ FOR 5 DOF
P1= 0.528E+00 SIG= 0.234E+00
$\chi^2 = 1.4$ FOR 4 DOF
P2= 0.243E-01 P3= 0.134E+00
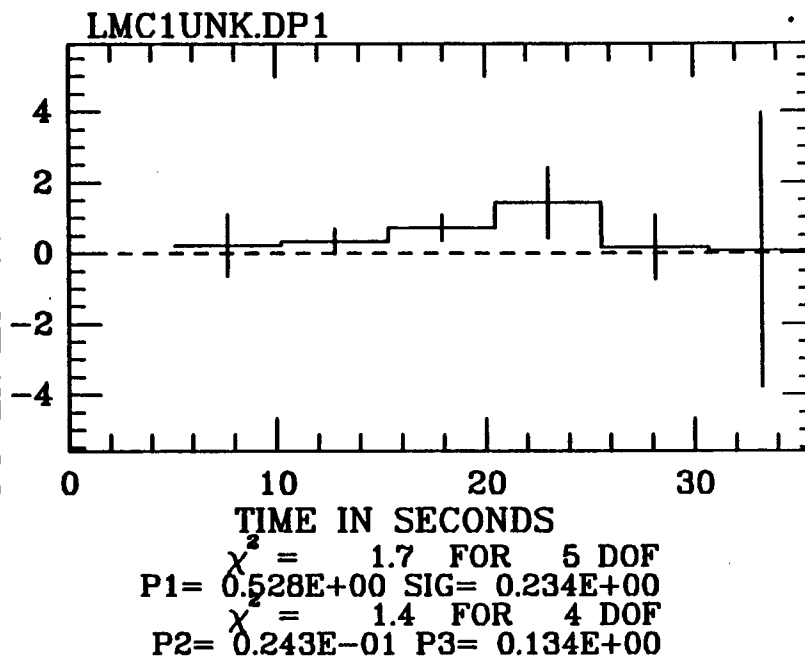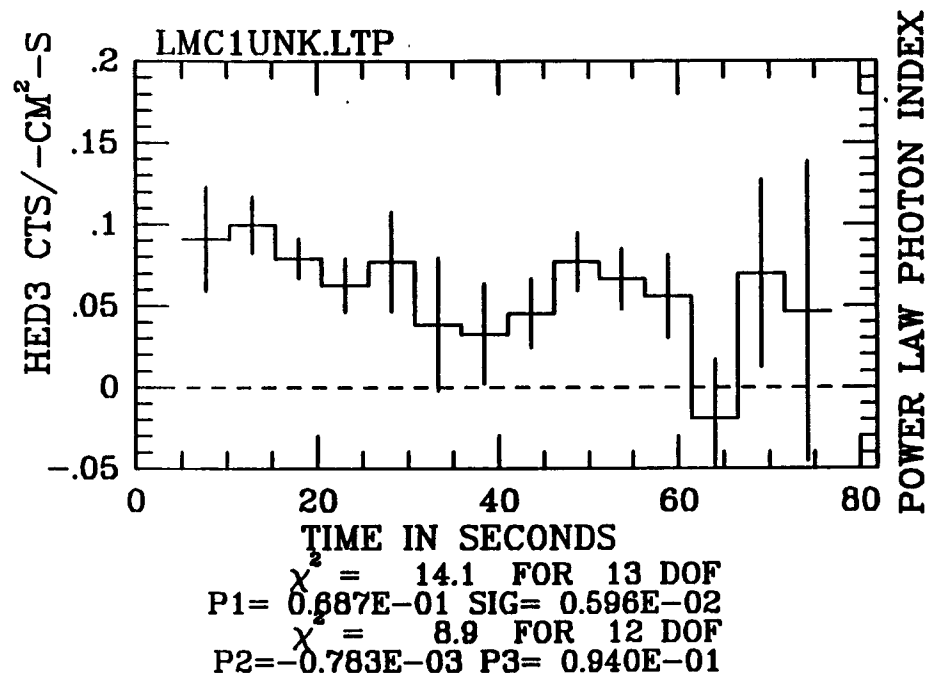
b) Plots for the event on D.O.Y (1977) 233.82. Time zero is at 19:48:33 U.T. The position was held fixed at that of the LMC Transient, A0538-66.

HED3 CTS/-CM^2-S

LMC2UNK.LTP

TIME IN SECONDS
χ^2 = 25.7 FOR 14 DOF
P1= 0.382E-01 SIG= 0.565E-02
χ^2 = 23.9 FOR 13 DOF
P2= 0.405E-03 P3= 0.244E-01

LMC2UNK.DP1

POWER LAW PHOTON INDEX

TIME IN SECONDS
χ^2 = 6.3 FOR 5 DOF
P1= 0.522E+00 SIG= 0.281E+00
χ^2 = 5.7 FOR 4 DOF
P2= 0.245E-01 P3= 0.321E-01
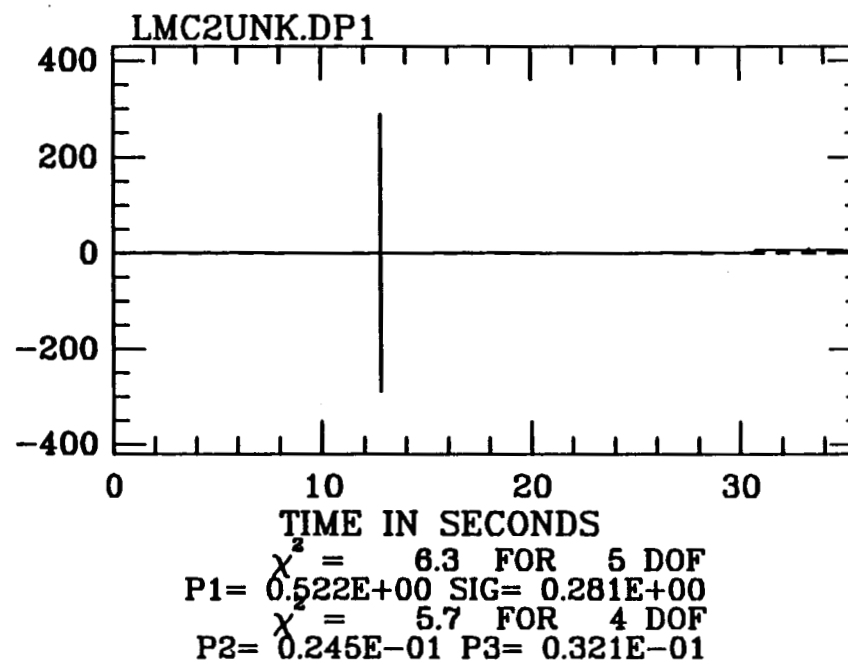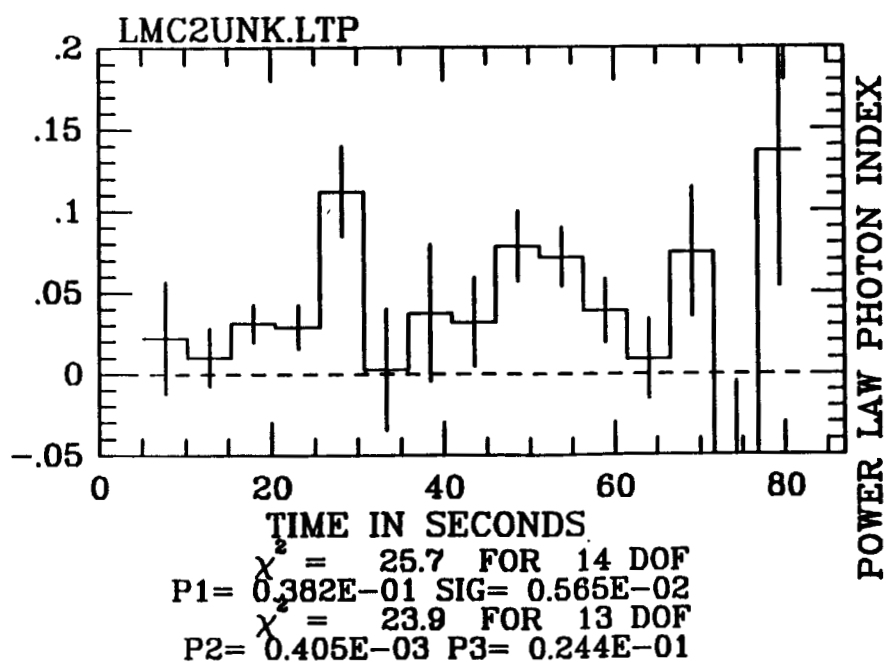
c) Plots for the event on D.O.Y (1977) 234.45. Time zero is at 10:48:59 U.T. for the light curve and 10:49:19 U.T. for the spectral variability plot. The position was held fixed at that of the LMC Transient, A0538-66.

HED3 CTS/$-$CM^2$-$S

LMC3UNK.LTP

.2
.15
.1
.05
0
$-$.05

0   20   40   60   80

TIME IN SECONDS

χ^2 =   16.7 FOR 16 DOF
P1= 0.457E$-$01 SIG= 0.445E$-$02
χ^2 =   12.3 FOR 15 DOF
P2=$-$0.518E$-$03 P3= 0.699E$-$01

POWER LAW PHOTON INDEX

LMC3UNK.DP1

3
2
1
0

0   10   20   30

TIME IN SECONDS

χ^2 =   3.2 FOR   4 DOF
P1= 0.670E+00 SIG= 0.303E+00
χ^2 =   2.6 FOR   3 DOF
P2= 0.387E$-$01 P3= 0.719E$-$01
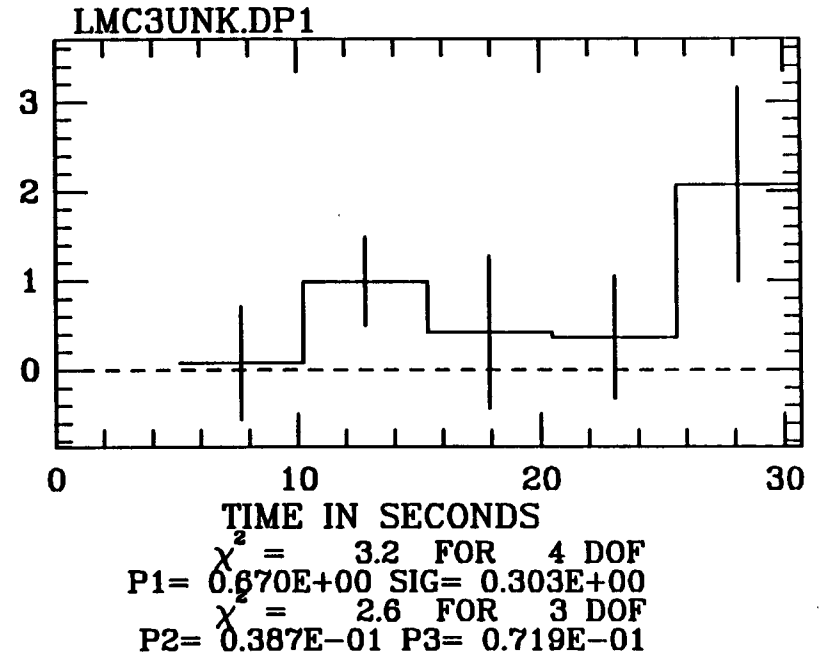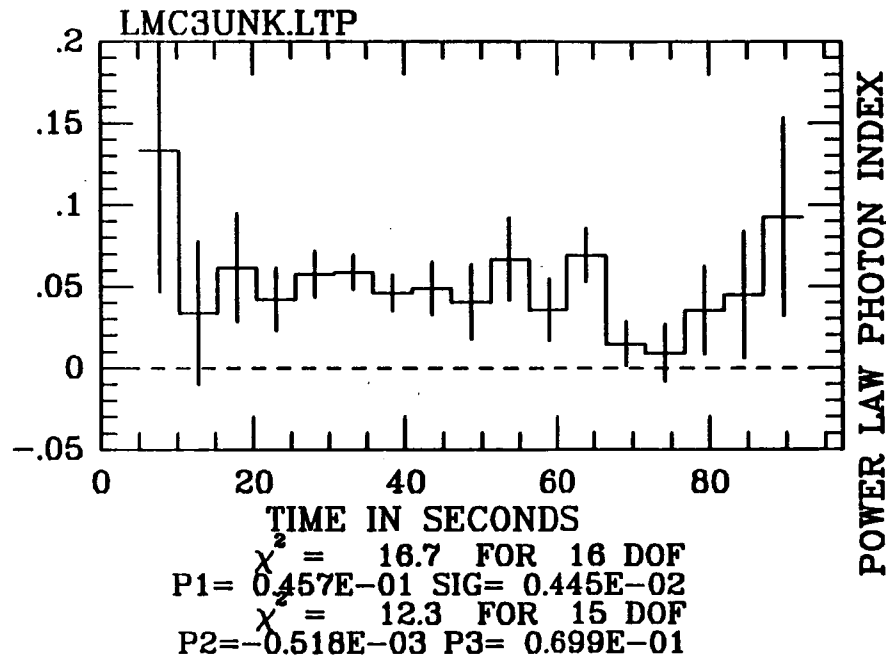
d) Plots for the event on D.O.Y (1977) 280.51. Time zero is at 12:10:59 U.T. The position was held fixed at that of the LMC Transient, A0538-66.

HED3 CTS/$-$CM^2$-$S

LMC4UNK.LTP

TIME IN SECONDS

$\chi^2 = 14.5$ FOR 13 DOF
P1= 0.139E+00 SIG= 0.533E$-$02
$\chi^2 = 9.1$ FOR 12 DOF
P2=$-$0.681E$-$03 P3= 0.157E+00

POWER LAW PHOTON INDEX

LMC4UNK.DP1

TIME IN SECONDS

$\chi^2 = 1.7$ FOR 4 DOF
P1= 0.180E+01 SIG= 0.181E+00
$\chi^2 = 0.8$ FOR 3 DOF
P2=$-$0.388E$-$01 P3= 0.231E+01

e) Plots for the event on D.O.Y (1977) 290.62. Time zero is at 15:00:02 U.T. for the light curve and 15:00:17 U.T. for the spectral variability plot. The position was held fixed at that of LMC X-2.

HED3 CTS/-CM^2-S

LMC5X2.LTP

TIME IN SECONDS

$\chi^2 = 3.9$ FOR 10 DOF
P1= 0.121E-01 SIG= 0.172E-02
$\chi^2 = 2.9$ FOR 9 DOF
P2=-0.131E-03 P3= 0.173E-01

LMC5X2.DP1

POWER LAW PHOTON INDEX

TIME IN SECONDS

$\chi^2 = 11.4$ FOR 4 DOF
P1= 0.645E+00 SIG= 0.314E+00
$\chi^2 = 3.5$ FOR 3 DOF
P2=-0.145E+00 P3= 0.416E+01

f) Plots for the event on D.O.Y (1977) 303.98. Time zero is at 23:32:38 U.T. for the light curve and 23:32:53 U.T. for the spectral variability plot. The position was held fixed at that of LMC X-1.

HED3 CTS/−CM^2−S

LMC7X1.LTP

χ^2 =   39.2   FOR   17 DOF
P1= 0.127E−01 SIG= 0.142E−02
χ^2 =   18.3   FOR   16 DOF
P2= 0.353E−03 P3=−0.230E−02

TIME IN SECONDS

LMC7X1.DP1

POWER LAW PHOTON INDEX

χ^2 =   2.6   FOR   5 DOF
P1= 0.248E+01 SIG= 0.552E+00
χ^2 =   2.5   FOR   4 DOF
P2=−0.295E−01 P3= 0.307E+01

TIME IN SECONDS

g) Plots for the event on D.O.Y (1977) 306.11. Time zero is at 02:41:54 U.T. The position was held fixed at that of LMC X-1.

HED3 CTS/-CM^2-S

LMC8X1.LTP

χ^2 =   44.4 FOR 15 DOF
P1= 0.192E-01 SIG= 0.190E-02
χ^2 =   22.3 FOR 14 DOF
P2=-0.453E-03 P3= 0.344E-01

POWER LAW PHOTON INDEX

LMC8X1.DP1

χ^2 =   7.3 FOR   6 DOF
P1= 0.153E+01 SIG= 0.284E+00
χ^2 =   4.8 FOR   5 DOF
P2=-0.650E-01 P3= 0.279E+01

TIME IN SECONDS

h) Plots for the event on D.O.Y (1977) 307.50. Time zero is at 12:07:30 U.T. for the light curve and 12:07:50 U.T. for the spectral variability plot. The position was held fixed at that of LMC X-1.

HED3 CTS/-CM^2-S

LMC9X1.LTP

χ^2 = 5.7 FOR 18 DOF
P1= 0.794E-02 SIG= 0.130E-02
χ^2 = 4.0 FOR 17 DOF
P2=-0.872E-04 P3= 0.120E-01

LMC9X1.DP1

χ^2 = 13.3 FOR 5 DOF
P1= 0.108E+01 SIG= 0.415E+00
χ^2 = 10.4 FOR 4 DOF
P2=-0.103E+00 P3= 0.306E+01
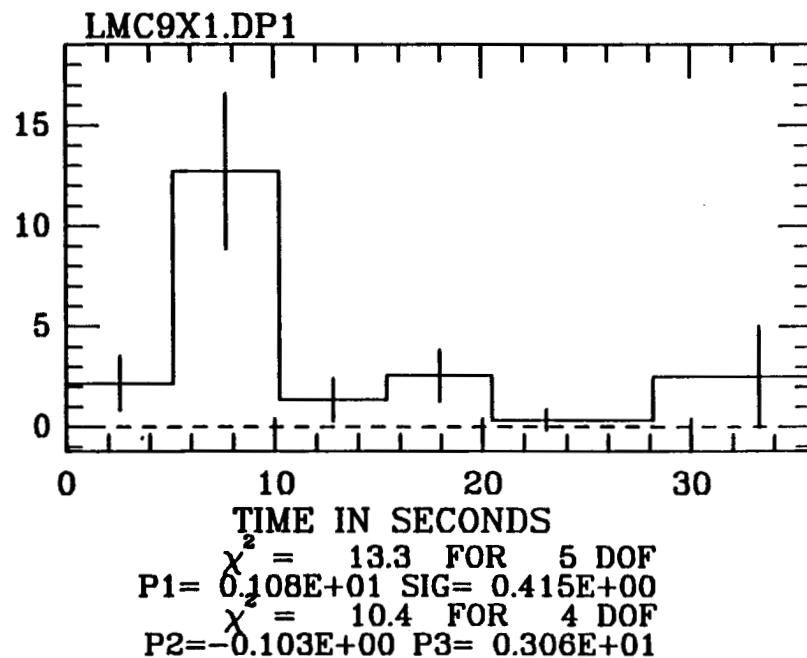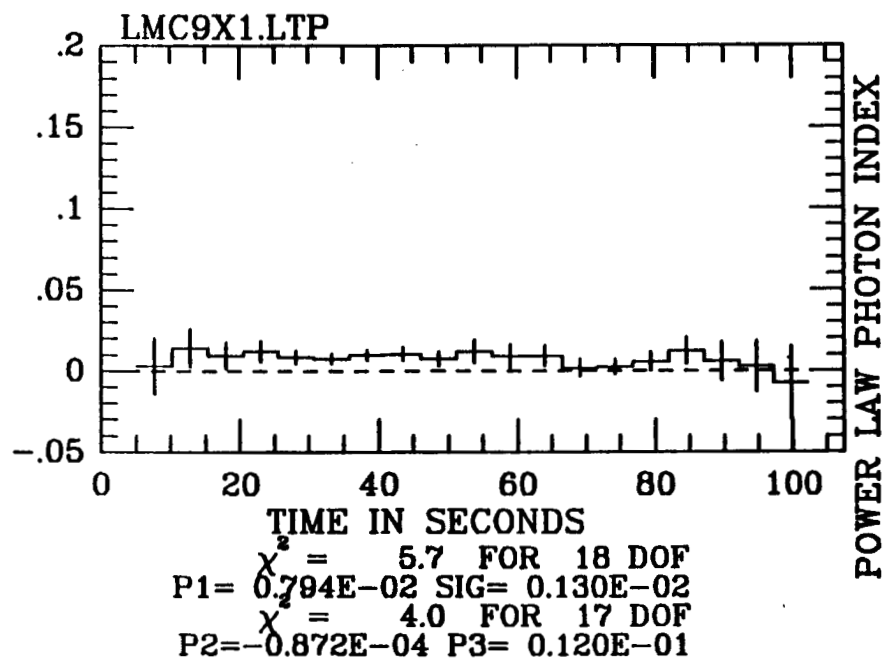
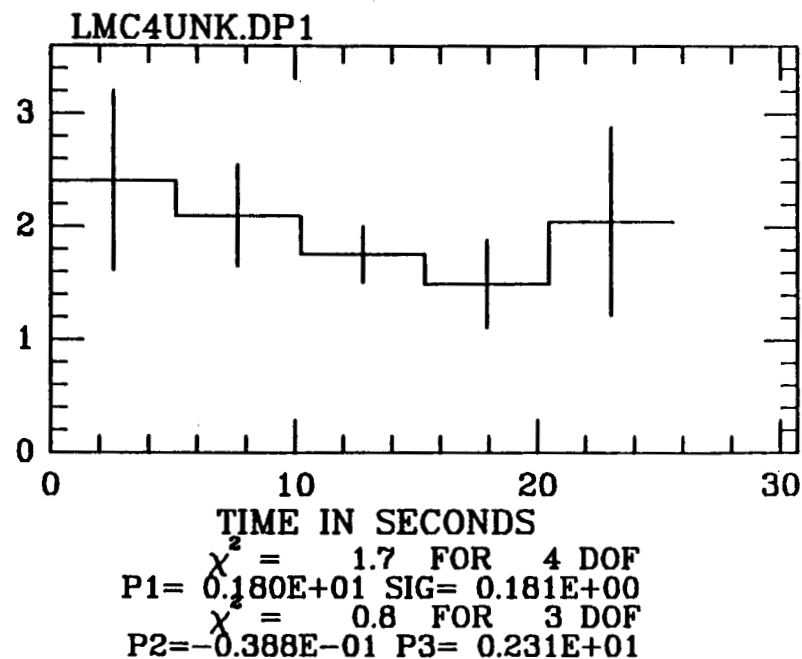i) Plots for the event on D.O.Y (1977) 311.47. Time zero is at 11:11:10 U.T. for the light curve and 11:11:15 U.T. for the spectral variability plot. The position was held fixed at that of LMC X-1.

HED3 CTS/$-$CM^2-S

LMC11X1.LTP

χ^2 =   30.6 FOR   14 DOF
P1= 0.134E$-$01 SIG= 0.199E$-$02
χ^2 =   26.6 FOR   13 DOF
P2= 0.225E$-$03 P3= 0.585E$-$02

LMC11X1.DP1

χ^2 =   3.3 FOR   4 DOF
P1= 0.120E+01 SIG= 0.386E+00
χ^2 =   2.8 FOR   3 DOF
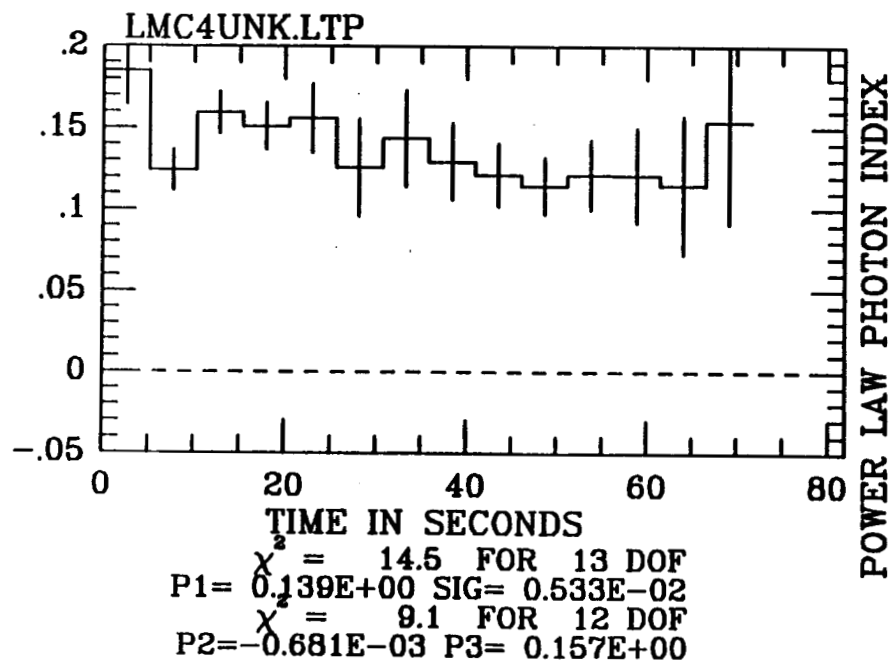P2= 0.599E$-$01 P3= 0.193E+00

TIME IN SECONDS

POWER LAW PHOTON INDEX
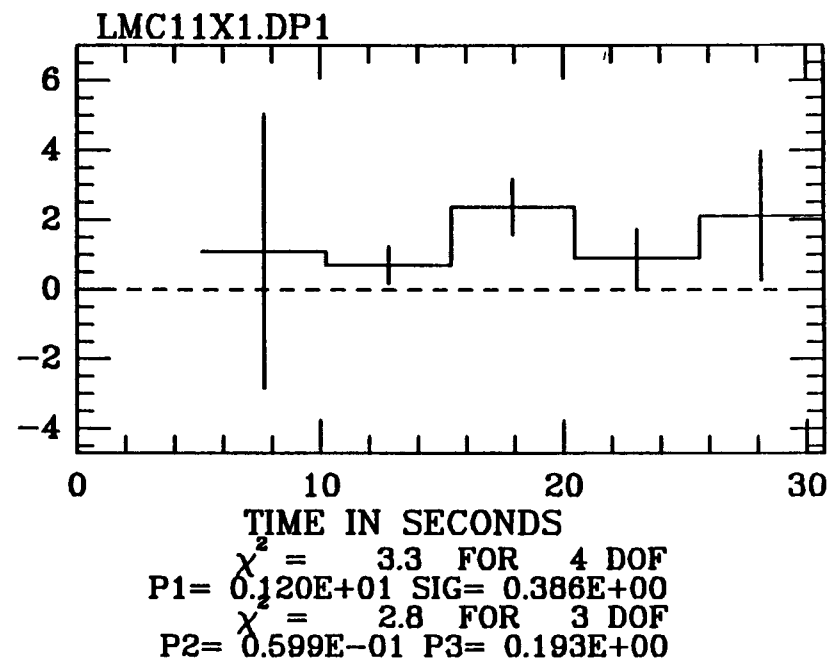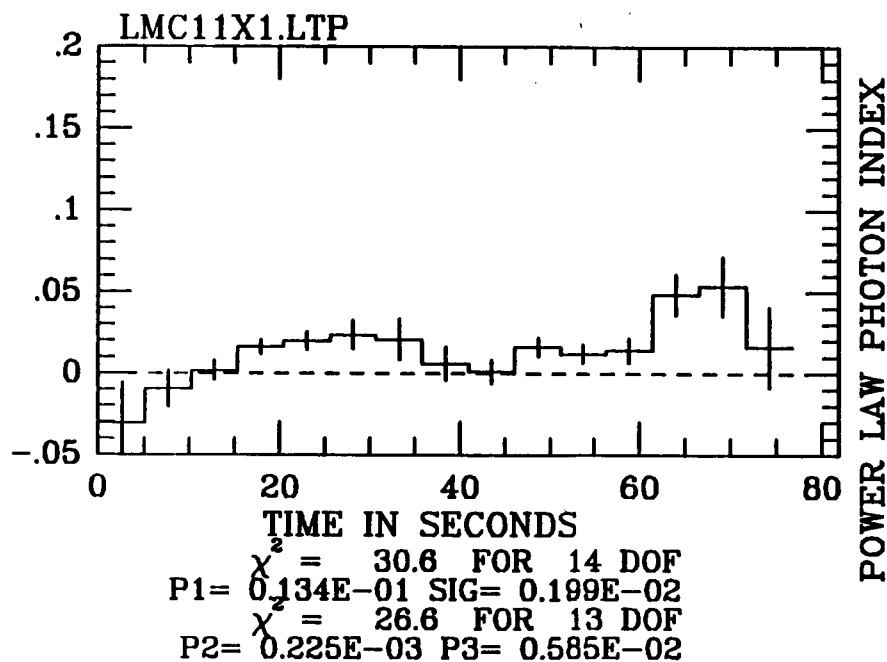
j) Plots for the event on D.O.Y (1977) 311.59. Time zero is at 14:05:56 U.T. for the light curve and 14:06:17 U.T. for the spectral variability plot. The position was held fixed at that of LMC X-1.

HED3 CTS/-CM^2-S

LMC12X1.LTP

TIME IN SECONDS

χ^2 = 17.5 FOR 18 DOF
P1= 0.164E-01 SIG= 0.174E-02
χ^2 = 12.5 FOR 17 DOF
P2= 0.202E-03 P3= 0.674E-02

LMC12X1.DP1

POWER LAW PHOTON INDEX

TIME IN SECONDS

χ^2 = 5.0 FOR 4 DOF
P1= 0.233E+01 SIG= 0.628E+00
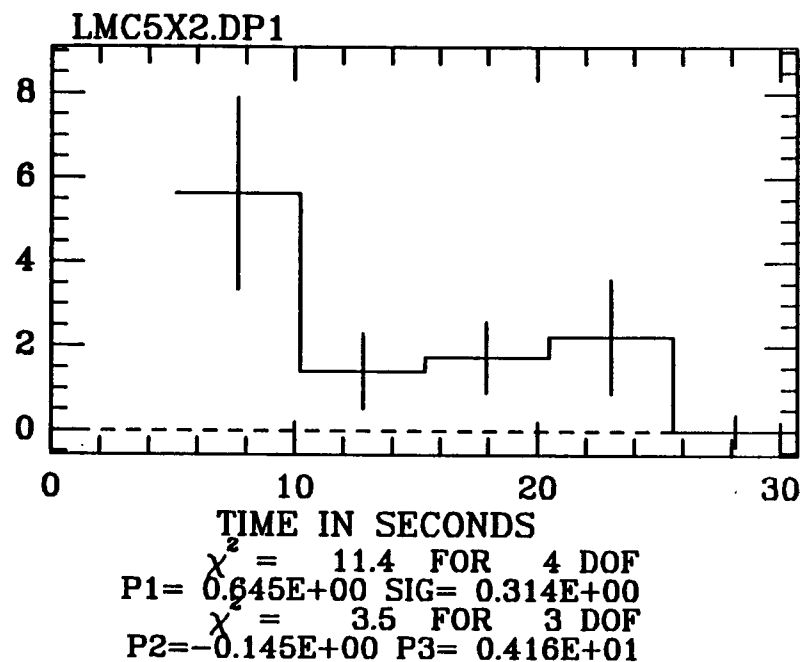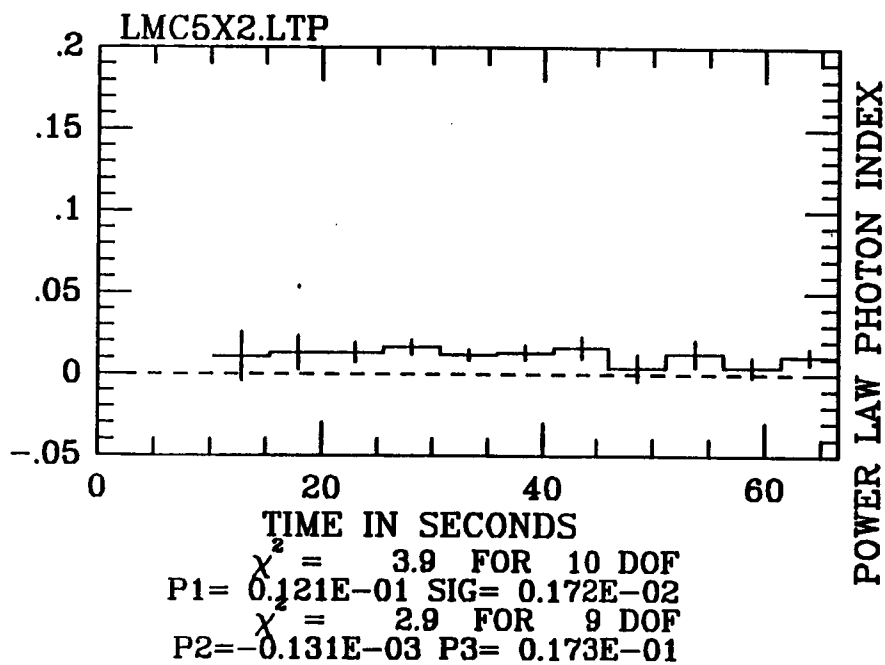χ^2 = 1.5 FOR 3 DOF
P2=-0.188E+00 P3= 0.581E+01
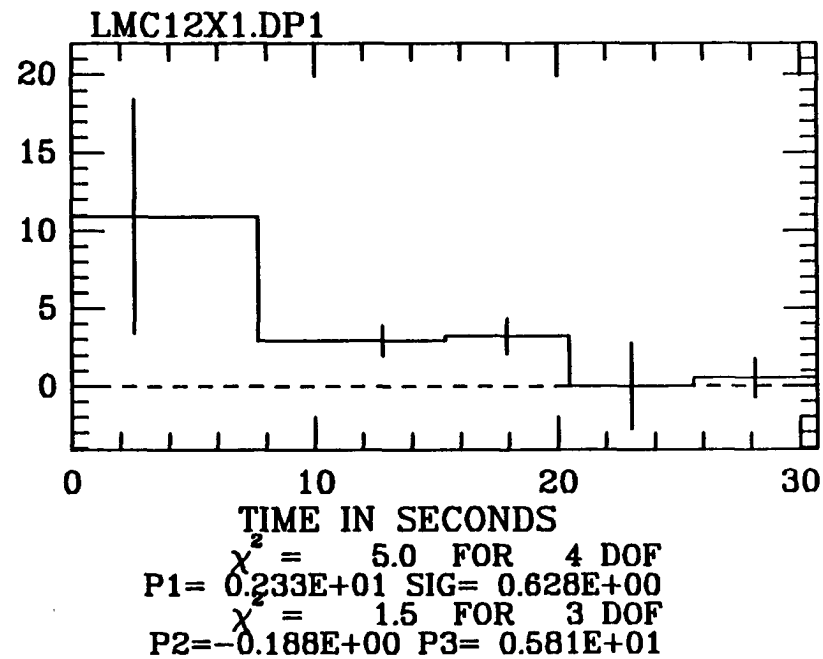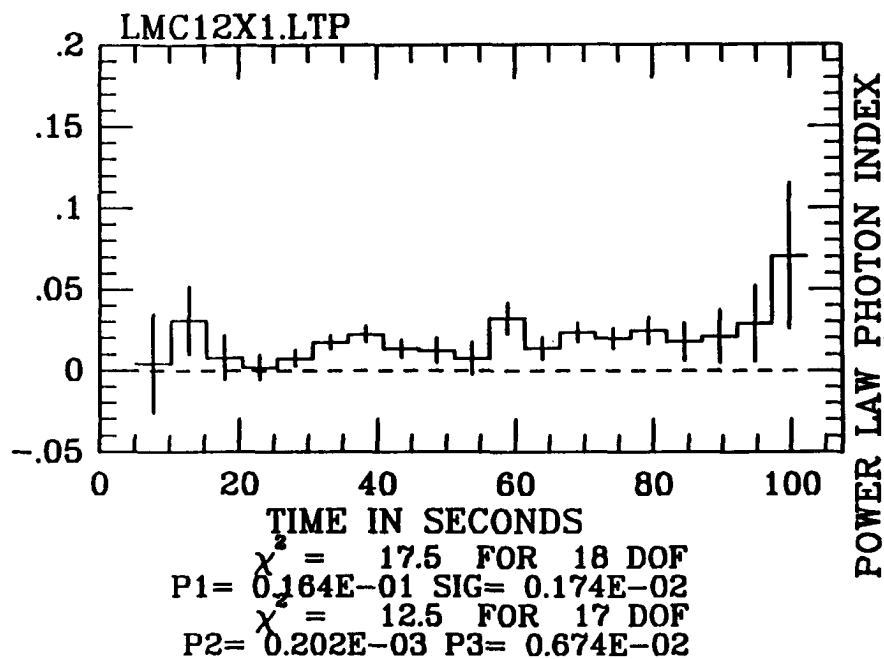
k) Plots for the event on D.O.Y (1977) 313.75. Time zero is at 17:55:44 U.T. The position was held fixed at that of the LMC Transient, A0538-66.
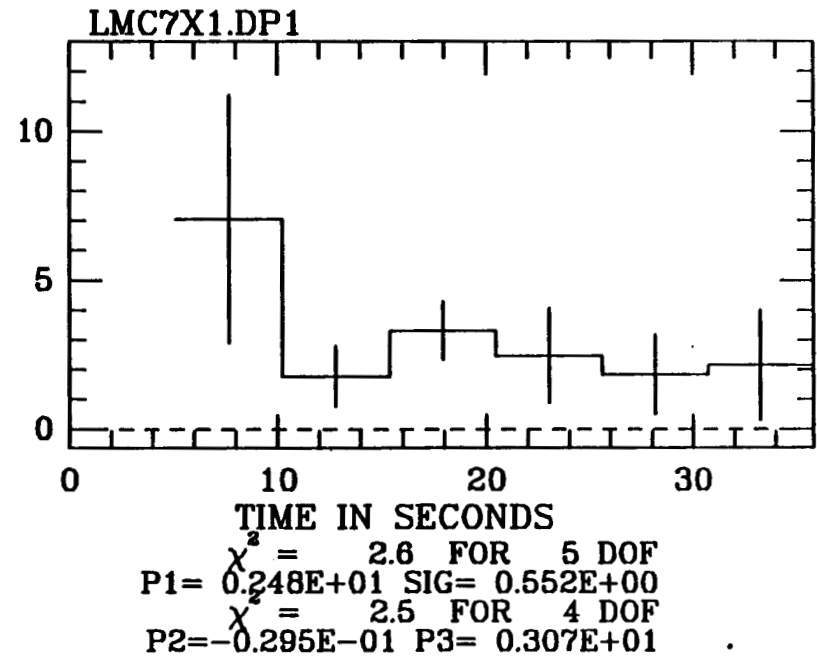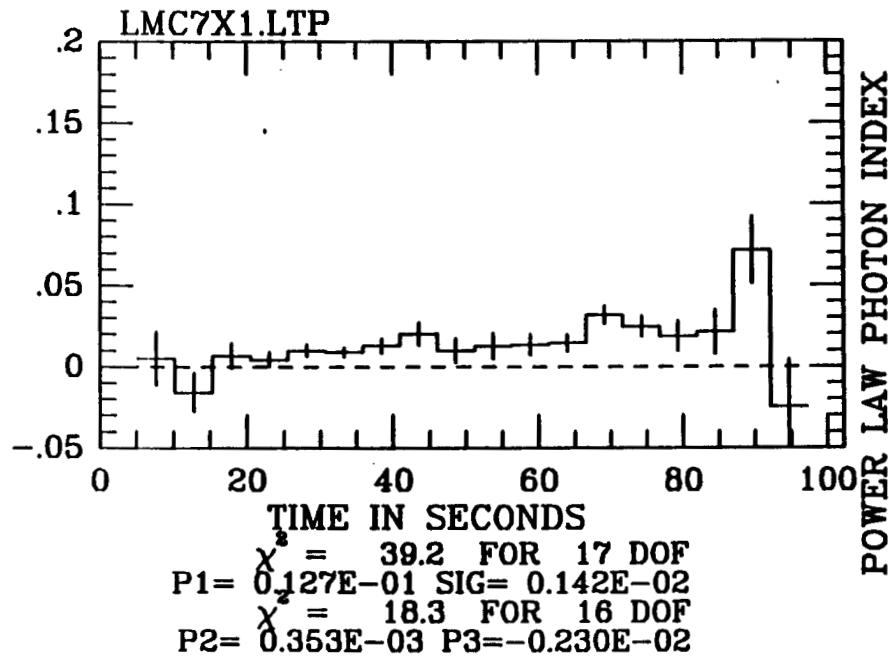
HED3 CTS/-CM^2-S

LM13C83.LTP

$\chi^2 = 84.3$ FOR 15 DOF
P1= 0.241E-01 SIG= 0.313E-02
$\chi^2 = 24.0$ FOR 14 DOF
P2=-0.123E-02 P3= 0.690E-01

TIME IN SECONDS

LM13C83.DP1

POWER LAW PHOTON INDEX

$\chi^2 = 4.6$ FOR 5 DOF
P1= 0.566E+00 SIG= 0.259E+00
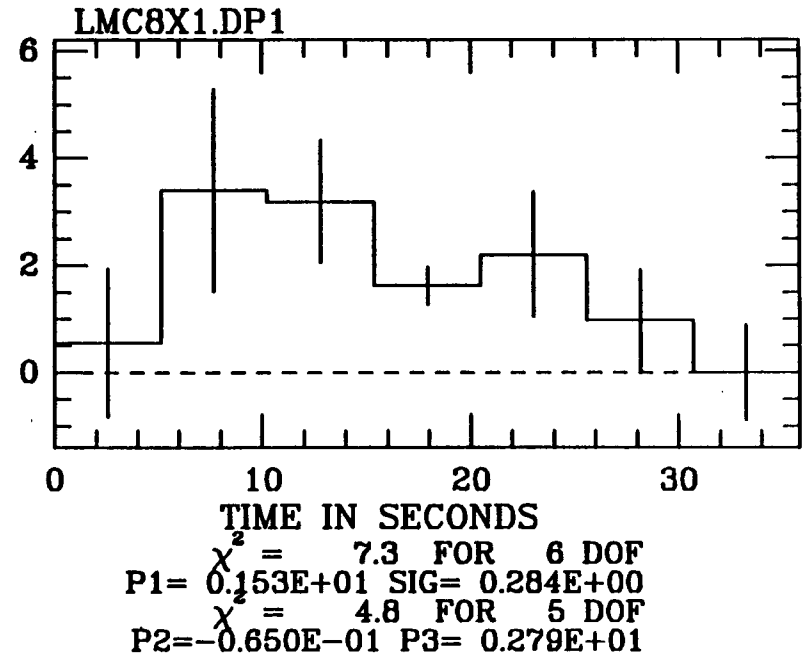$\chi^2 = 4.5$ FOR 4 DOF
P2= 0.171E-01 P3= 0.317E+00

TIME IN SECONDS
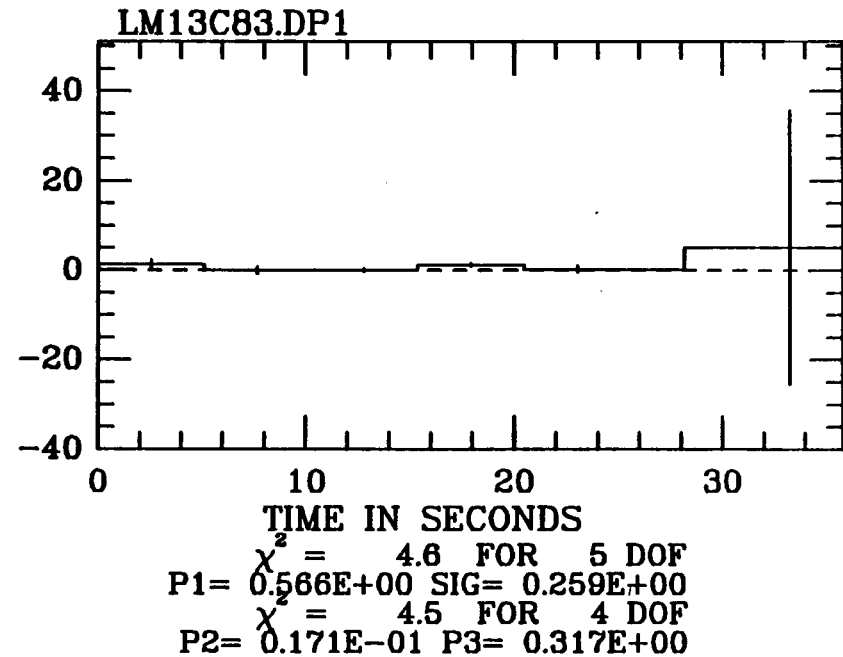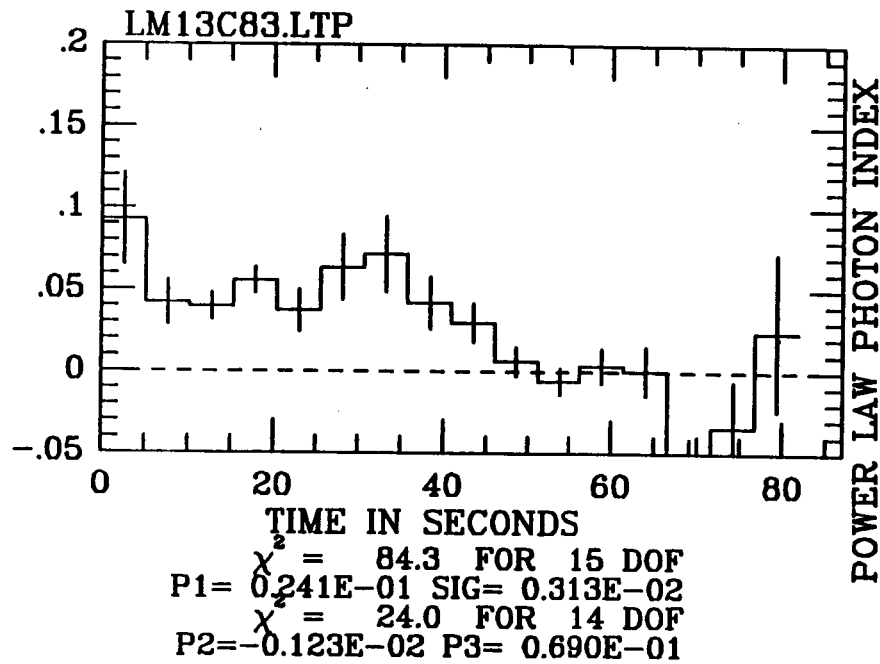
1) Plots for the event on D.O.Y (1977) 313.79. Time zero is at 19:05:17 U.T. for the light curve and 19:05:32 U.T. for the spectral variability plot. The position was held fixed at that of the LMC Transient. A0538-66.

HED3 CTS/–CM^2–S

LM14C83.LTP

χ^2 = 15.4 FOR 15 DOF
P1= 0.671E-01 SIG= 0.342E-02
χ^2 = 14.0 FOR 14 DOF
P2=-0.232E-03 P3= 0.769E-01

TIME IN SECONDS

LM14C83.DP1

POWER LAW PHOTON INDEX

χ^2 = 7.9 FOR 5 DOF
P1= 0.126E+01 SIG= 0.206E+00
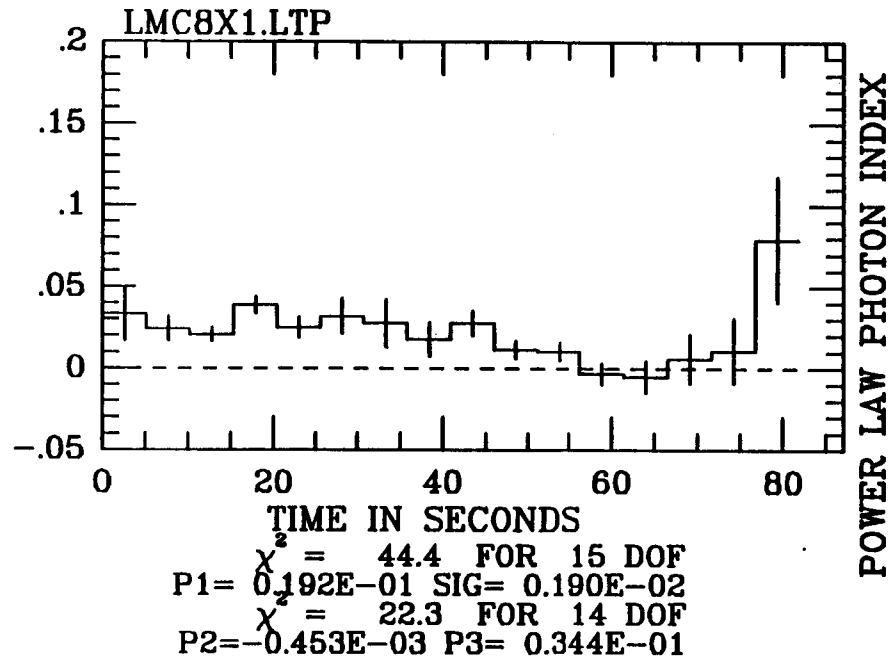χ^2 = 7.9 FOR 4 DOF
P2= 0.131E-02 P3= 0.124E+01

TIME IN SECONDS
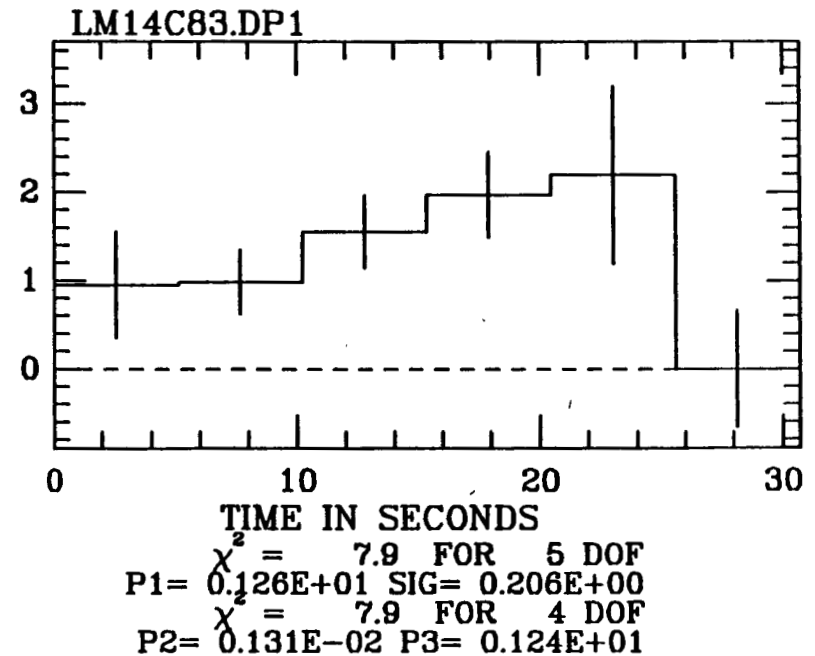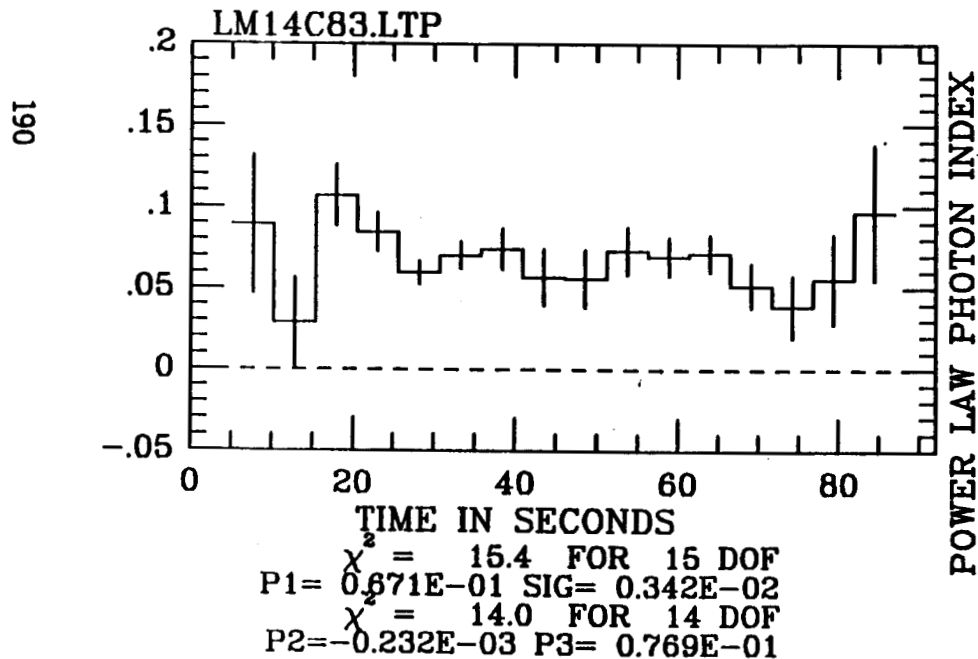
m) Plots for the event on D.O.Y (1977) 321.29. Time zero is at 07:02:51 U.T. for the light curve and 07:03:17 U.T. for the spectral variability plot.

HED3 CTS/-CM^2-S

LM15C83.LTP

TIME IN SECONDS

χ^2 = 30.9 FOR 18 DOF
P1= 0.696E-02 SIG= 0.127E-02
χ^2 = 27.8 FOR 17 DOF
P2=-0.122E-03 P3= 0.137E-01

POWER LAW PHOTON INDEX

LM15C83.DP1

TIME IN SECONDS

χ^2 = 0.9 FOR 5 DOF
P1= 0.227E+01 SIG= 0.595E+00
χ^2 = 0.4 FOR 4 DOF
P2= 0.136E+00 P3= 0.229E+00

n) Plots for the event on D.O.Y (1977) 321.41. Time zero is at 09:57:37 U.T.

HED3 CTS/$-$CM^2$-$S

LMC16X1.LTP

TIME IN SECONDS

$\chi^2 = $ 19.9 FOR 8 DOF
P1= 0.255E$-$01 SIG= 0.418E$-$02
$\chi^2 = $ 13.8 FOR 7 DOF
P2=$-$0.523E$-$03 P3= 0.398E$-$01

POWER LAW PHOTON INDEX

LMC16X1.DP1

TIME IN SECONDS

$\chi^2 = $ 0.6 FOR 1 DOF
P1= 0.936E+00 SIG= 0.356E+00
$\chi^2 = $ 0.0 FOR 0 DOF
P2= 0.162E+00 P3= 0.474E+00

192

o) Plots for the event on D.O.Y (1977) 328.34. Time zero is at 08:06:36 U.T.

HED3 CTS/-CM²-S

LM17C83.LTP

χ^2 = 12.4 FOR 12 DOF
P1= 0.200E-01 SIG= 0.231E-02
χ^2 = 12.3 FOR 11 DOF
P2= 0.420E-04 P3= 0.191E-01

LM17C83.DP1

χ^2 = 0.2 FOR 2 DOF
P1= 0.139E+01 SIG= 0.537E+00
χ^2 = 0.1 FOR 1 DOF
P2= 0.501E-01 P3= 0.119E+01

TIME IN SECONDS

POWER LAW PHOTON INDEX

193

p) Plots for the event on D.O.Y (1977) 351.57. Time zero is at 13:38:12 U.T. for the light curve and 13:38:28 U.T. for the spectral variability plot.

HED3 CTS/$-$CM^2$-$S

LM18TRN.LTP

TIME IN SECONDS

$\chi^2 = $ 24.7 FOR 16 DOF
P1= 0.119E$-$01 SIG= 0.150E$-$02
$\chi^2 = $ 18.6 FOR 15 DOF
P2= 0.196E$-$03 P3= 0.308E$-$02

LM18TRN.DP1

POWER LAW PHOTON INDEX

TIME IN SECONDS

$\chi^2 = $ 6.3 FOR 4 DOF
P1= 0.147E+01 SIG= 0.722E+00
$\chi^2 = $ 6.0 FOR 3 DOF
P2= 0.713E$-$01 P3= 0.526E+00
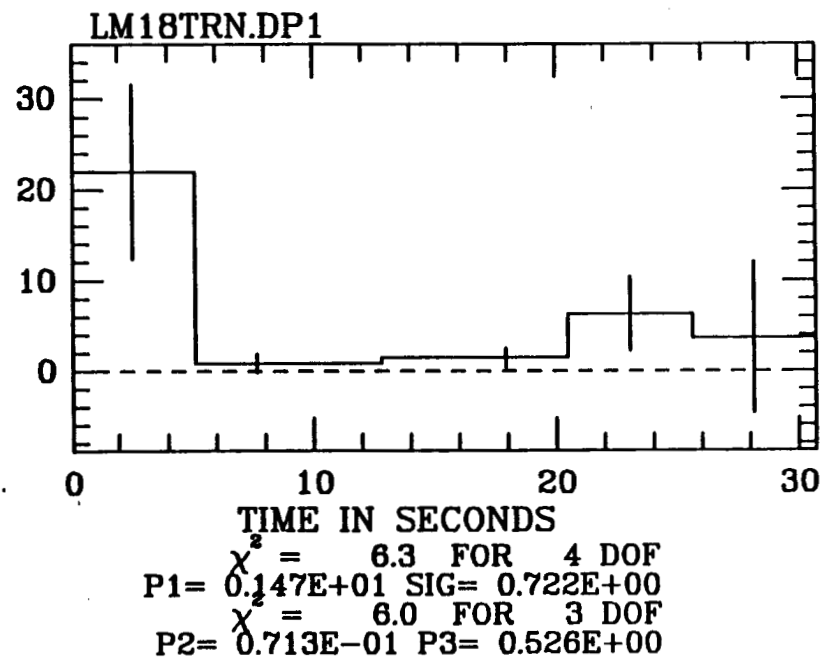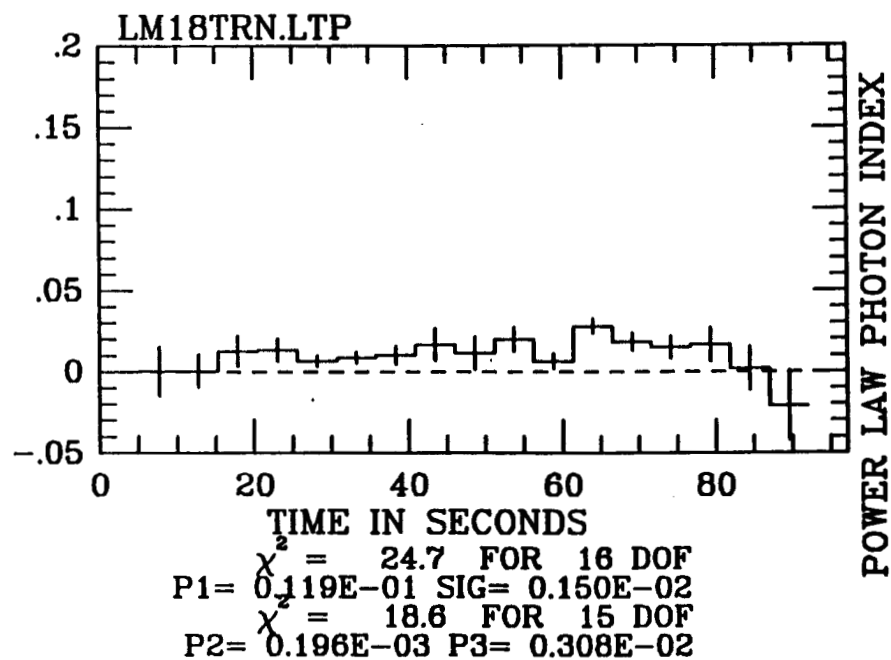
q) Plots for the event on D.O.Y (1977) 354.24. Time zero is at 5:38:07 U.T. for the light curve and 5:38:38 for the spectral variability plot.

HED3 CTS/-CM^2-S

LM19TRN.LTP

TIME IN SECONDS
χ^2 = 1047.4 FOR 15 DOF
P1= 0.103E+00 SIG= 0.268E-02
χ^2 = 392.9 FOR 14 DOF
P2= 0.359E-02 P3=-0.102E-01

POWER LAW PHOTON INDEX

LM19TRN.DP1

TIME IN SECONDS
χ^2 = 10.1 FOR 8 DOF
P1= 0.277E+01 SIG= 0.145E+00
χ^2 = 8.9 FOR 7 DOF
P2= 0.148E-01 P3= 0.241E+01

r) Plots for the event on D.O.Y (1977) 354.26. Time zero is at 06:13:42 U.T. for the light curve and 06:13:57 U.T. for the spectral variability plot.

HED3 CTS/$-$CM^2$-$S

LM20TRN.LTP

.2
.15
.1
.05
0
-.05

0   20   40   60
TIME IN SECONDS

χ^2 =   14.9   FOR   10 DOF
P1= 0.915E-02 SIG= 0.124E-02
χ^2 =   13.3   FOR   9 DOF
P2= 0.122E-03 P3= 0.477E-02

POWER LAW PHOTON INDEX

LM20TRN.DP1

15
10
5
0

0   10   20   30
TIME IN SECONDS

χ^2 =   9.2   FOR   3 DOF
P1= 0.122E+01 SIG= 0.445E+00
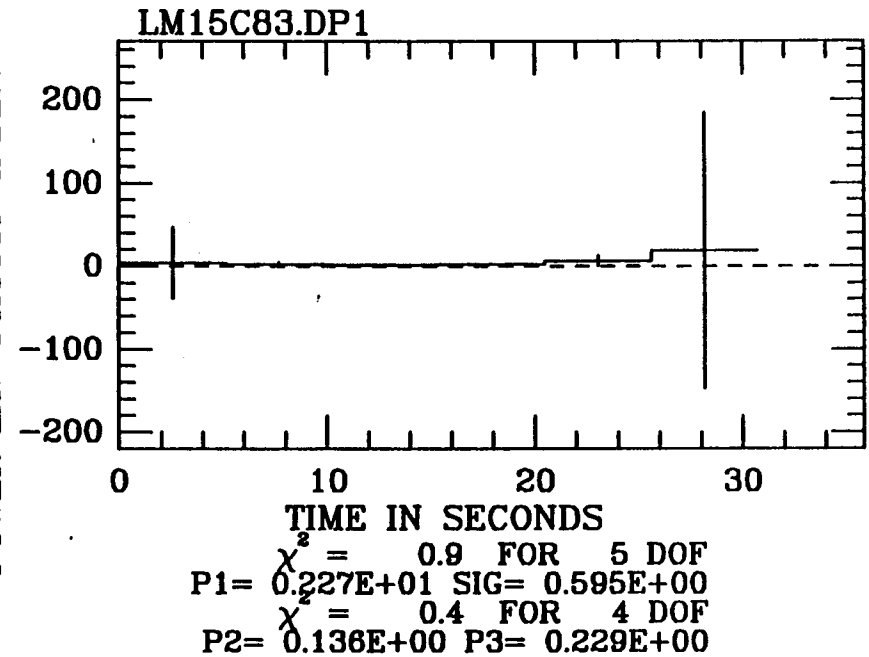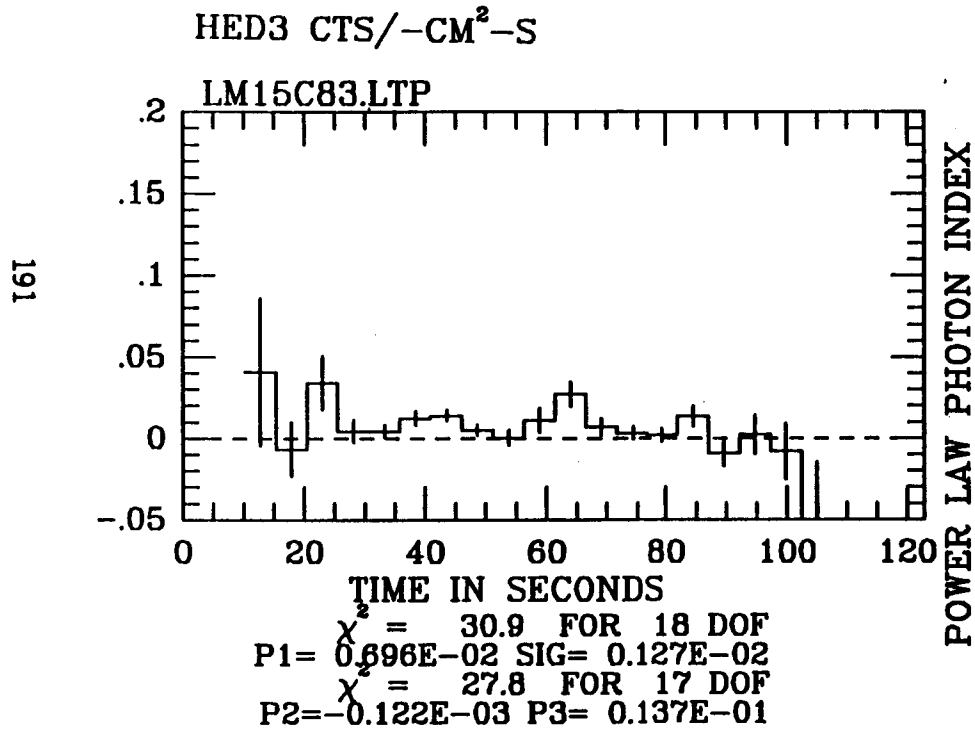χ^2 =   4.1   FOR   2 DOF
P2= 0.262E+00 P3=-0.306E+01

s) Plots for the event on D.O.Y (1977) 354.28. Time zero is at 06:48:36 U.T. for the light curve and 06:48:57 U.T. for the spectral variability plot.

HED3 CTS/-CM^2-S

LM21TRN.LTP

TIME IN SECONDS
$\chi^2 = $ 36.0 FOR 16 DOF
P1= 0.465E-02 SIG= 0.124E-02
$\chi^2 = $ 27.5 FOR 15 DOF
P2=-0.203E-03 P3= 0.136E-01

POWER LAW PHOTON INDEX

LM21TRN.DP1

TIME IN SECONDS
$\chi^2 = $ 7.7 FOR 4 DOF
P1= 0.776E+00 SIG= 0.483E+00
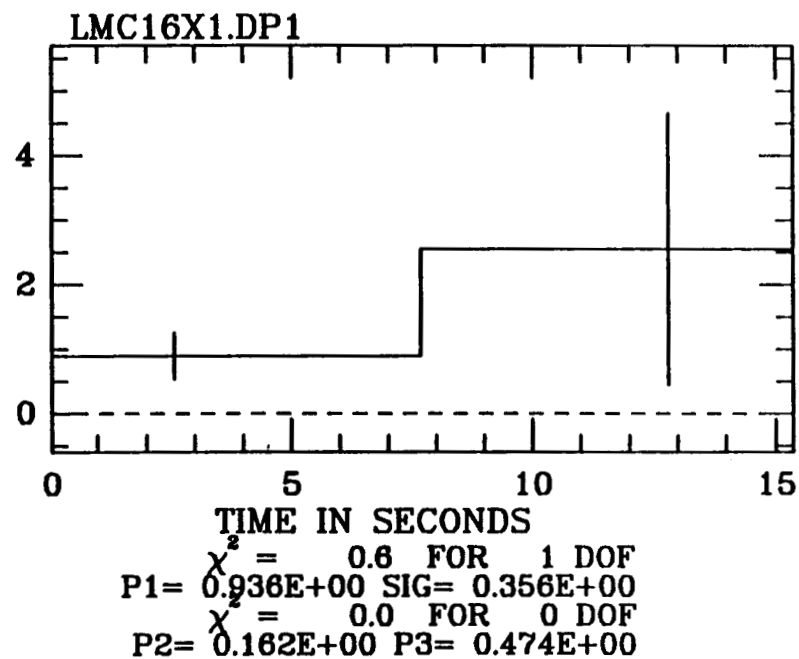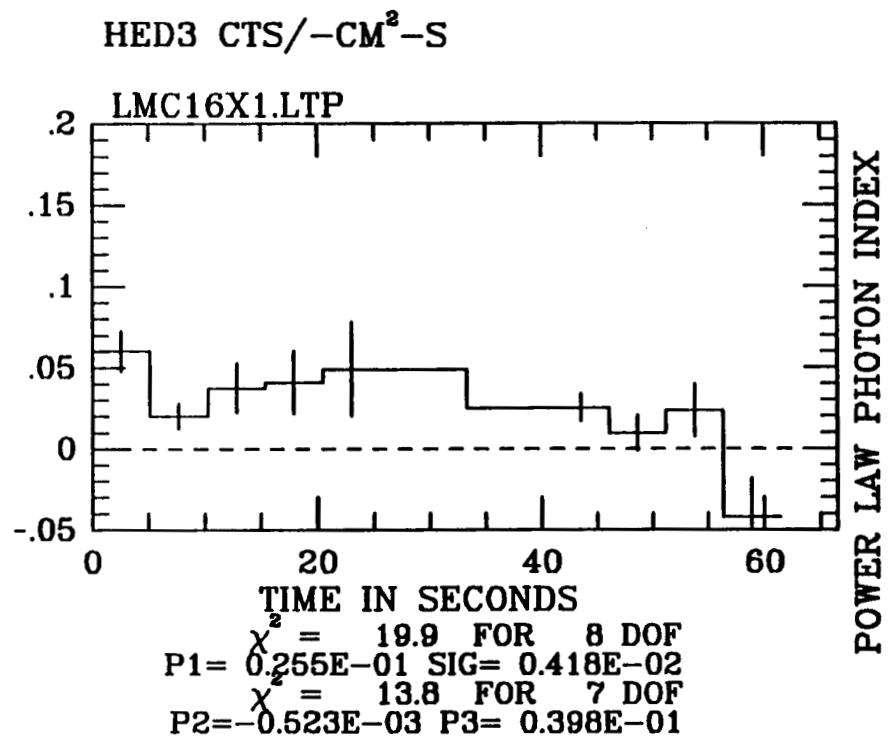$\chi^2 = $ 3.7 FOR 3 DOF
P2= 0.166E+00 P3=-0.345E+00

t) Plots for the event on D.O.Y (1977) 355.30. Time zero is at 07:18:38 U.T. for the light curve and 07:18:49 U.T. for the spectral variability plot.

HED3 CTS/-CM^2-S

LM22TRN4.LTP

χ^2 =   33.7   FOR   16 DOF
P1= 0.129E-02 SIG= 0.641E-03
χ^2 =   30.6   FOR   15 DOF
P2= 0.595E-04 P3=-0.101E-02

TIME IN SECONDS

LM22TRN.DP1

POWER LAW PHOTON INDEX

χ^2 =   3.8   FOR   5 DOF
P1= 0.138E+01 SIG= 0.294E+00
χ^2 =   2.9   FOR   4 DOF
P2= 0.384E-01 P3= 0.106E+01

TIME IN SECONDS

u) Plots for the event on D.O.Y (1977) 357.55. Time zero is at 13:04:45 U.T. for the light curve and 13:05:06 U.T. for the spectral variability plot.
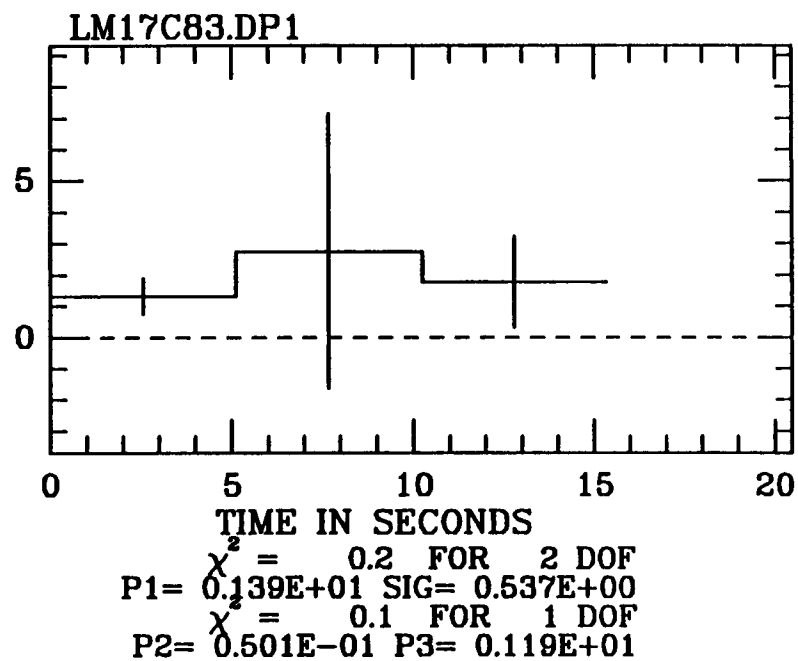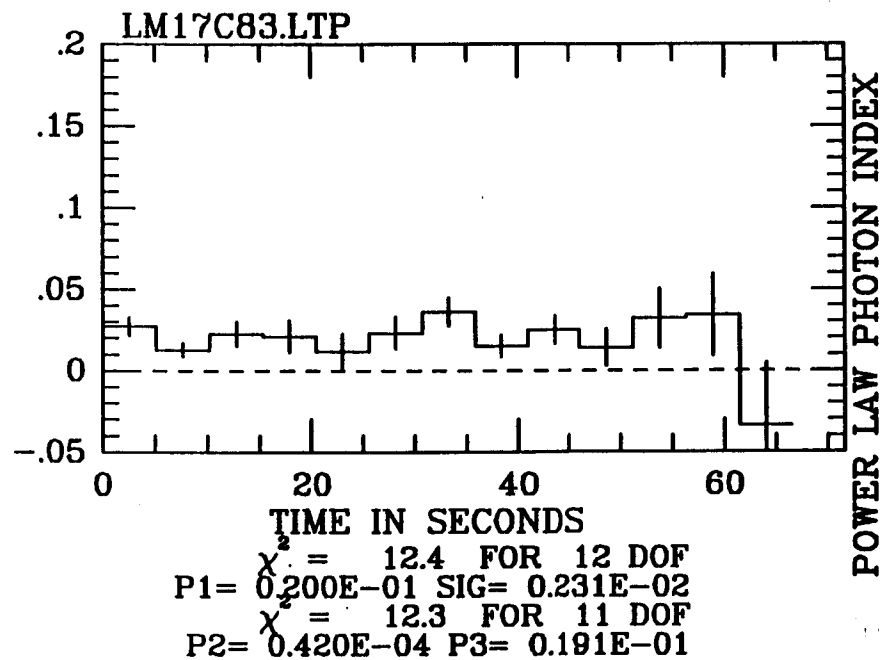
HED3 CTS/–CM^2–S

LM23TRN.LTP

TIME IN SECONDS

χ^2 = 86.7 FOR 18 DOF
P1= 0.694E–02 SIG= 0.143E–02
χ^2 = 44.4 FOR 17 DOF
P2=–0.492E–03 P3= 0.340E–01

LM23TRN.DP1

POWER LAW PHOTON INDEX

TIME IN SECONDS

χ^2 = 4.8 FOR 4 DOF
P1= 0.216E+00 SIG= 0.181E+00
χ^2 = 3.1 FOR 3 DOF
P2= 0.626E–01 P3=–0.611E+00

v) Plots for the event on D.O.Y (1977) 357.90. Time zero is at 21:39:03 U.T. for the light curve and 21:39:08 U.T. for the spectral variability plot.
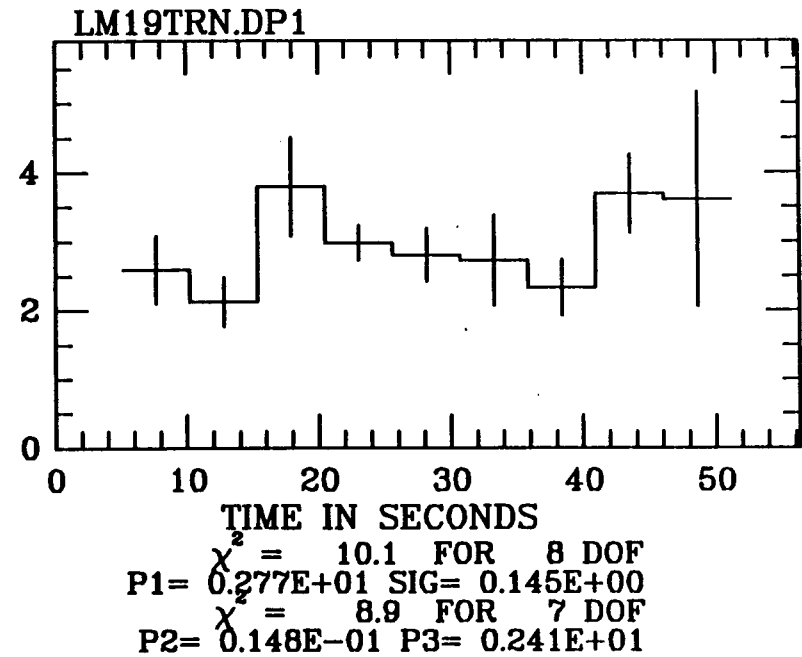
HED3 CTS/–CM^2–S

LM24TRN.LTP

TIME IN SECONDS

χ^2 = 39.0 FOR 14 DOF
P1= 0.106E–01 SIG= 0.178E–02
χ^2 = 21.5 FOR 13 DOF
P2=–0.409E–03 P3= 0.284E–01

POWER LAW PHOTON INDEX

LM24TRN.DP1

TIME IN SECONDS

χ^2 = 0.7 FOR 2 DOF
P1= 0.642E+00 SIG= 0.328E+00
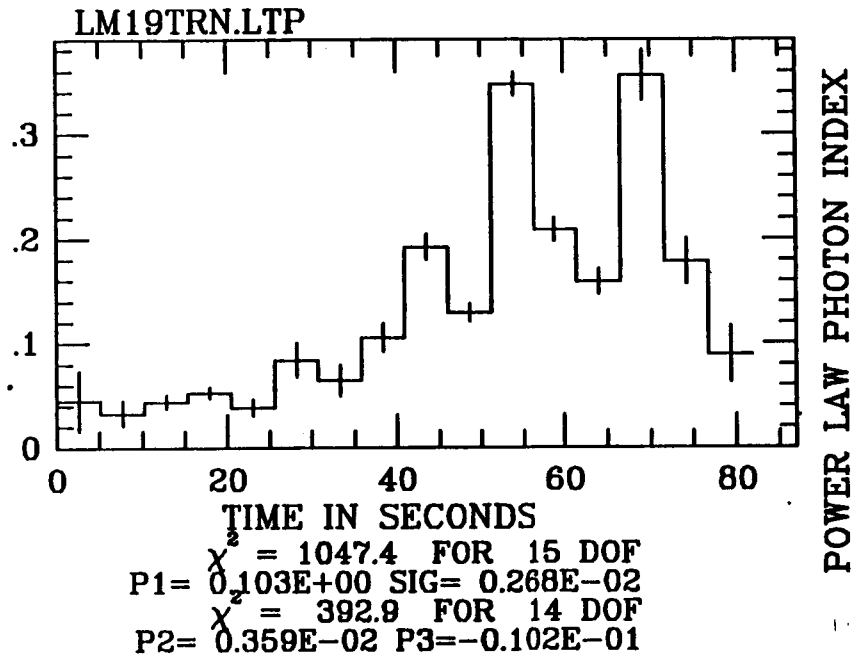χ^2 = 0.6 FOR 1 DOF
P2=–0.257E–01 P3= 0.114E+01

w) Plots for the event on D.O.Y (1977) 358.56. Time zero is at 13:21:49 U.T. for the light curve and
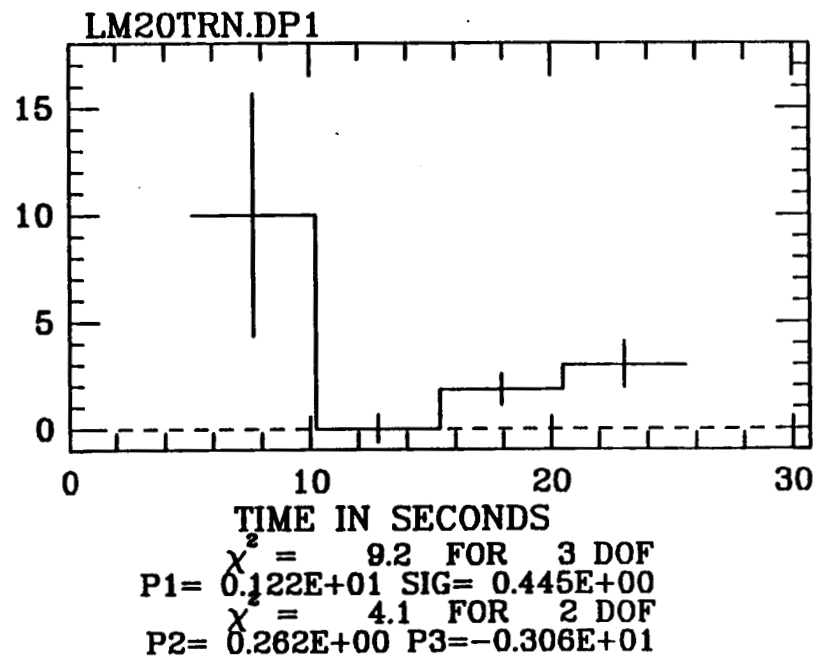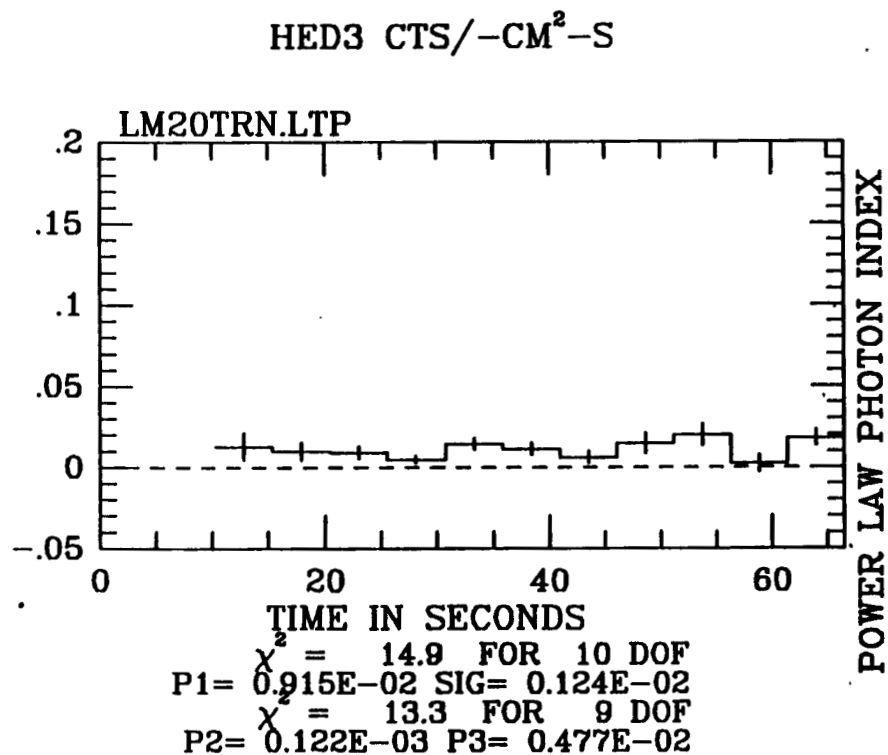   13:21:59 U.T. for the spectral variability plot.

HED3 CTS/$-$CM^2-S

LM25TRN.LTP

TIME IN SECONDS

$\chi^2 = 10.1$ FOR 16 DOF
P1= 0.976E-02 SIG= 0.159E-02
$\chi^2 = 9.2$ FOR 15 DOF
P2=-0.861E-04 P3= 0.134E-01

POWER LAW PHOTON INDEX

LM25TRN.DP1

TIME IN SECONDS

$\chi^2 = 1.7$ FOR 2 DOF
P1= 0.109E+01 SIG= 0.550E+00
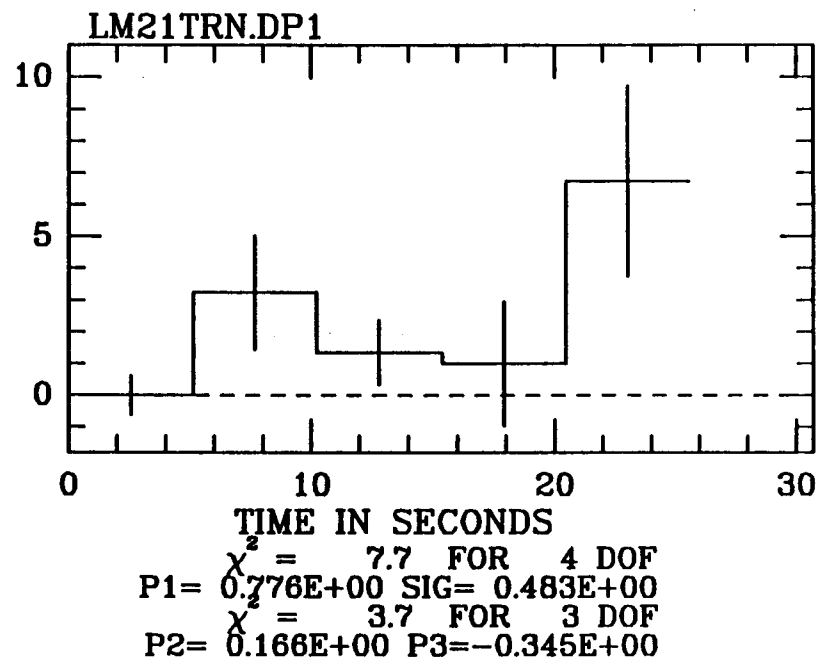$\chi^2 = 1.4$ FOR 1 DOF
P2=-0.799E-01 P3= 0.219E+01
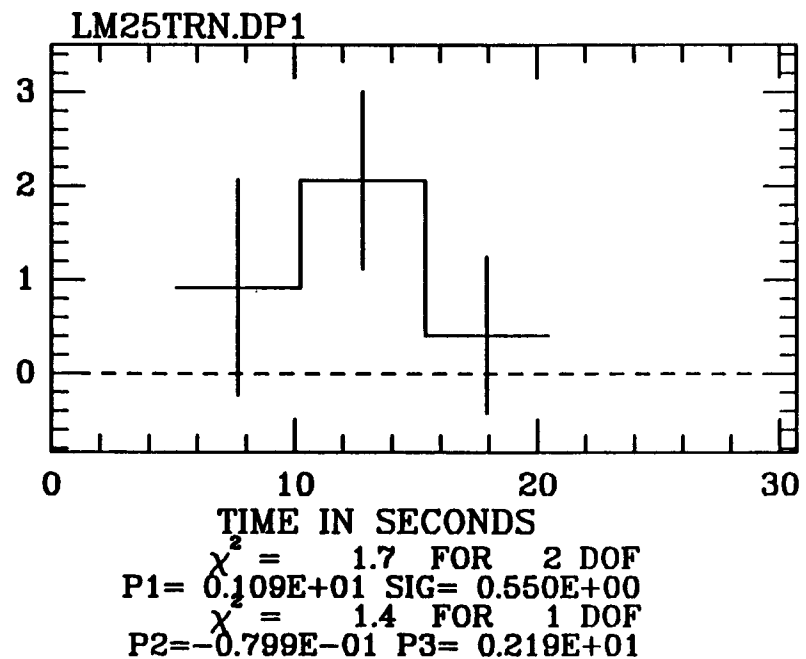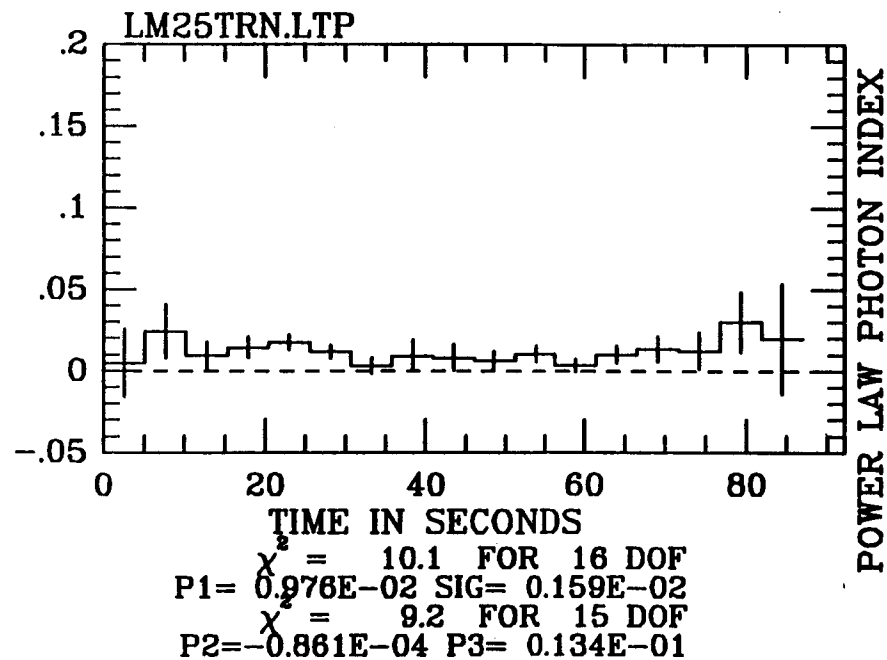
x) Plots for the event on D.O.Y (1977) 363.64. Time zero is at 15:25:08 U.T. for the light curve and 15:25:28 U.T. for the spectral variability plot. The position was held fixed at that of the LMC Transient, A0538-66.

HED3 CTS/$-CM^2$-S

LM26TRN.LTP

TIME IN SECONDS

χ^2 = 38.3 FOR 15 DOF
P1= 0.186E-01 SIG= 0.247E-02
χ^2 = 33.9 FOR 14 DOF
P2=-0.273E-03 P3= 0.330E-01

LM26TRN.DP1

POWER LAW PHOTON INDEX

TIME IN SECONDS

χ^2 = 1.9 FOR 5 DOF
P1= 0.240E+01 SIG= 0.478E+00
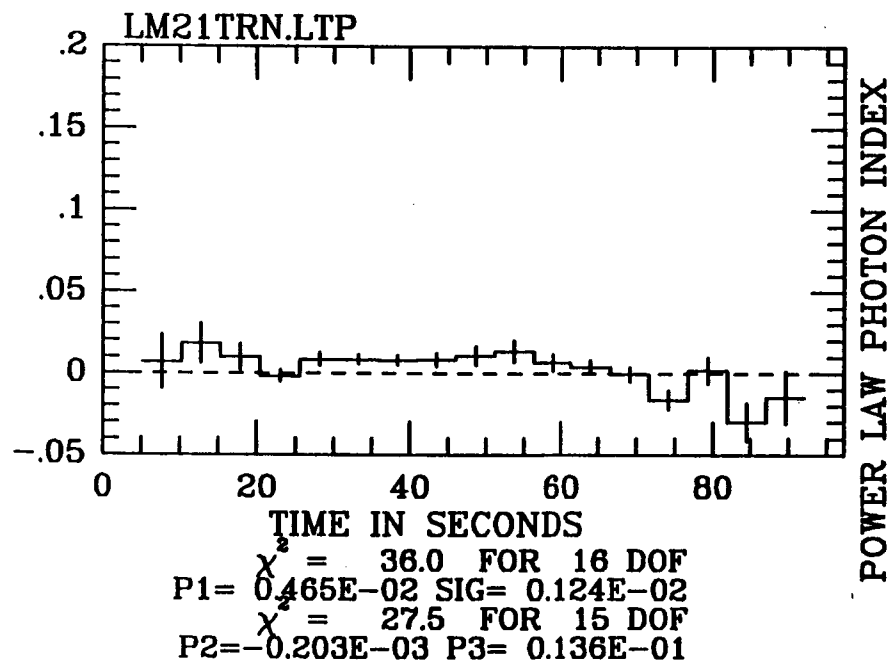χ^2 = 0.6 FOR 4 DOF
P2= 0.129E+00 P3= 0.130E+00
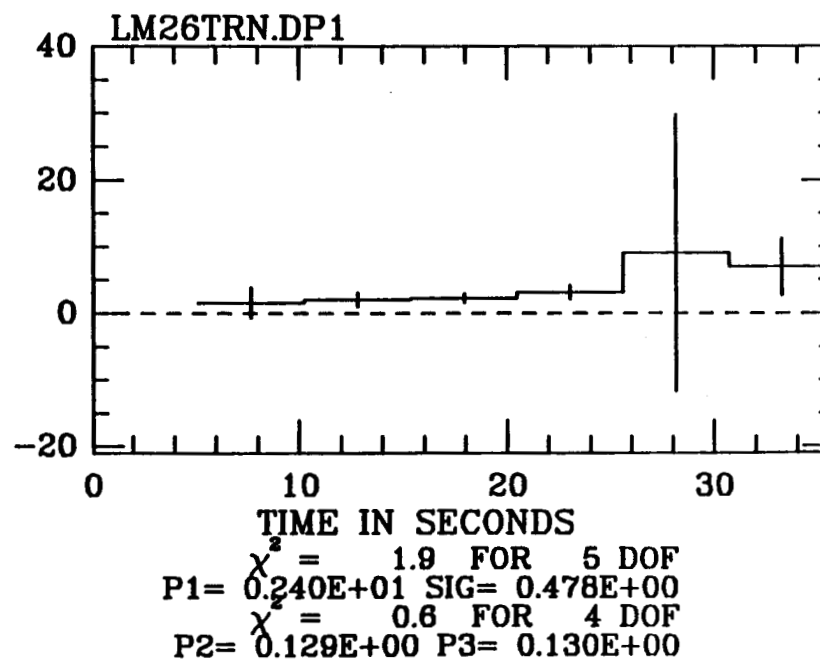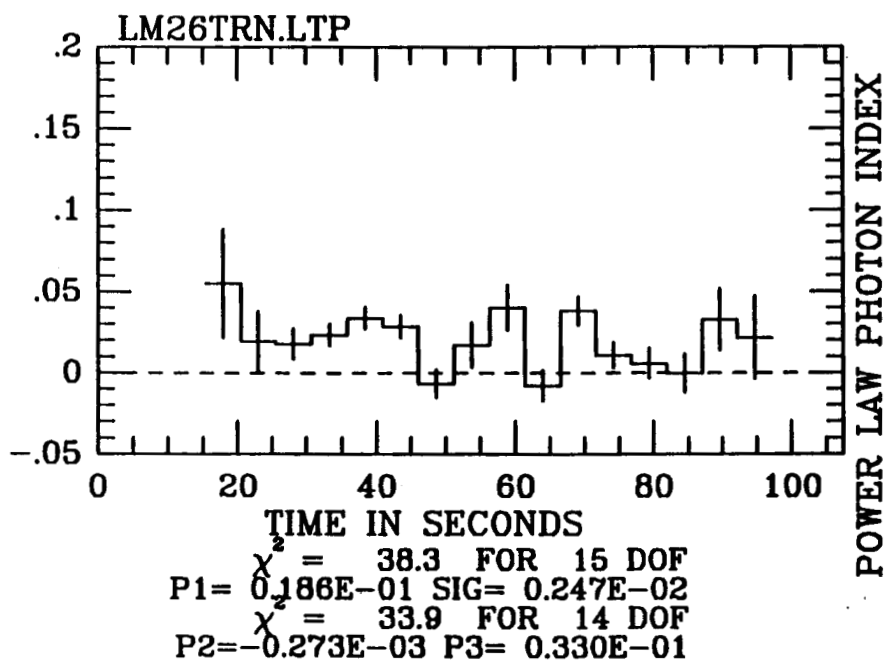
y) Plots for the event on D.O.Y (1977) 365.35. Time zero is at 08:29:54 U.T. for the light curve and 08:30:04 U.T. for the spectral variability plot.
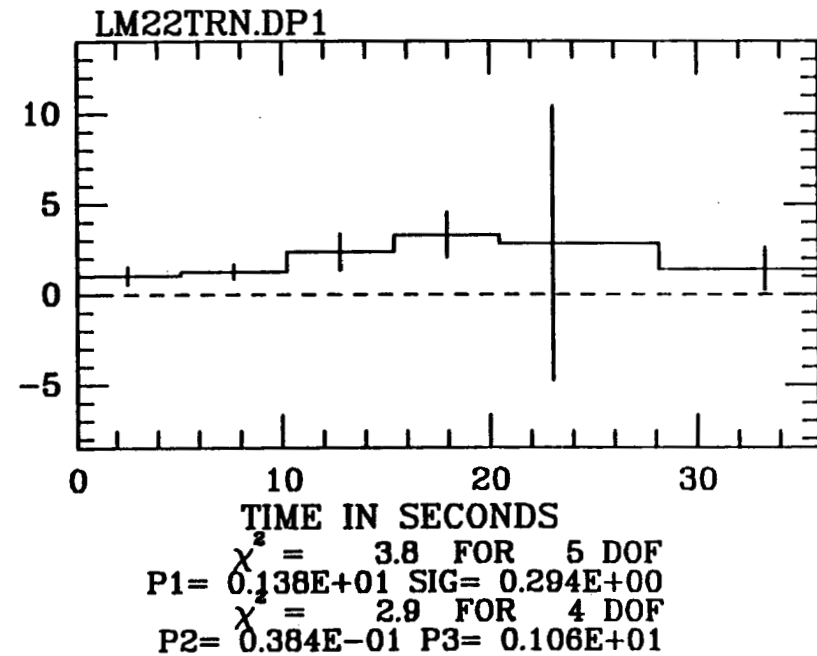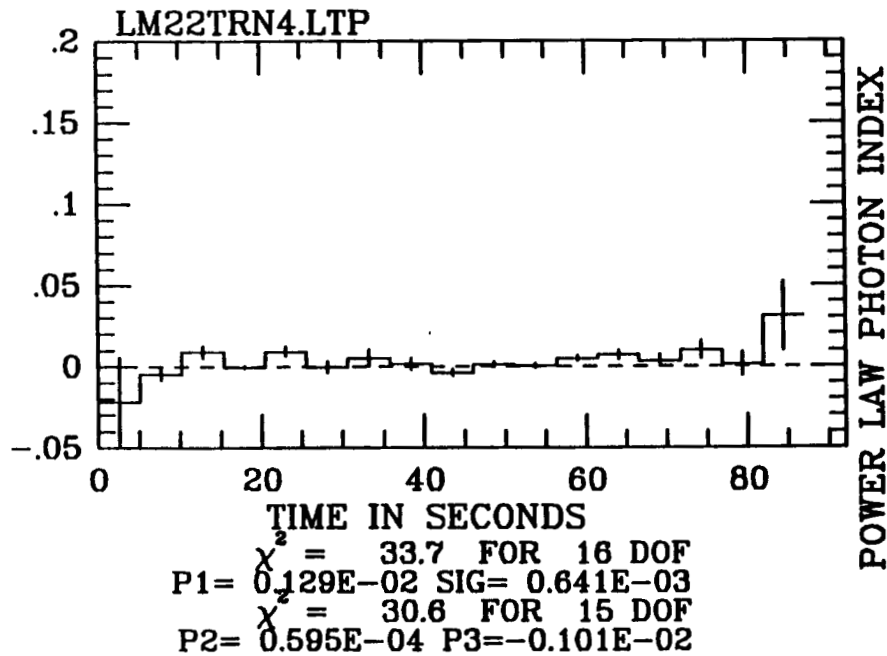
HED3 CTS/—CM^2—S

LM27N49.LTP

TIME IN SECONDS

χ^2 =   11.9 FOR   17 DOF
P1= 0.334E—01 SIG= 0.149E—02
χ^2 =   9.2 FOR   16 DOF
P2= 0.129E—03 P3= 0.280E—01

POWER LAW PHOTON INDEX

LM27N49.DP1

TIME IN SECONDS

χ^2 =   2.7 FOR   5 DOF
P1= 0.214E+01 SIG= 0.262E+00
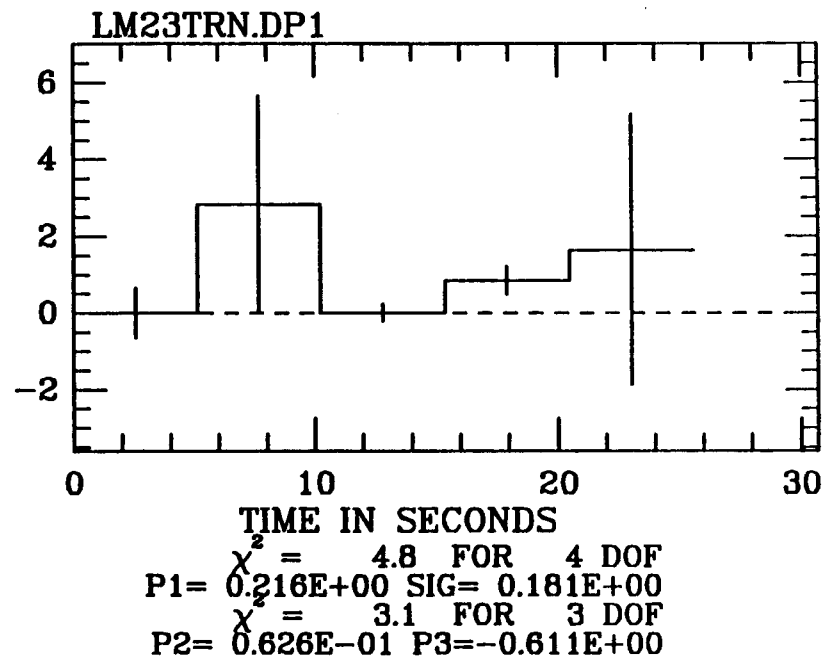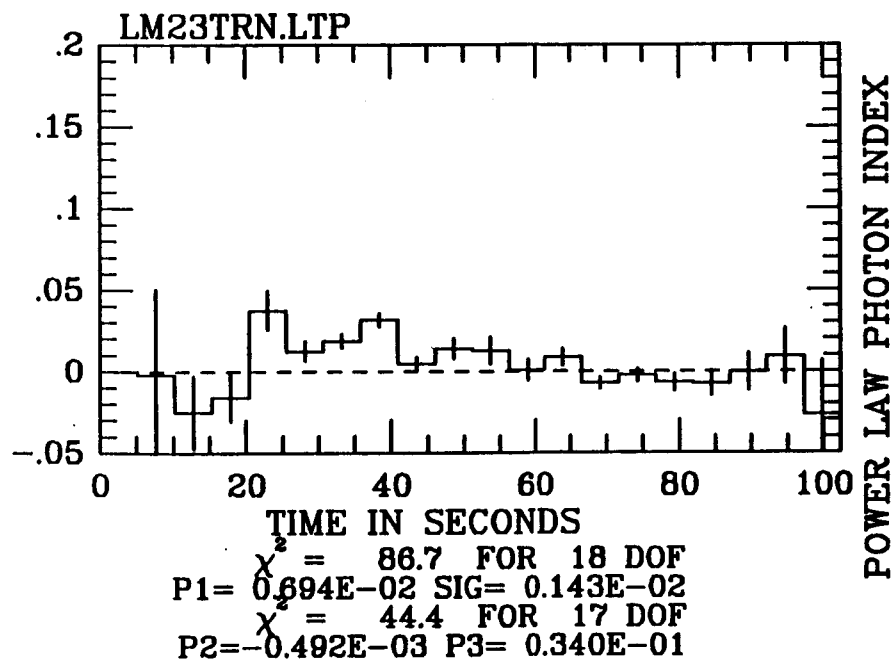χ^2 =   2.7 FOR   4 DOF
P2= 0.500E—02 P3= 0.205E+01
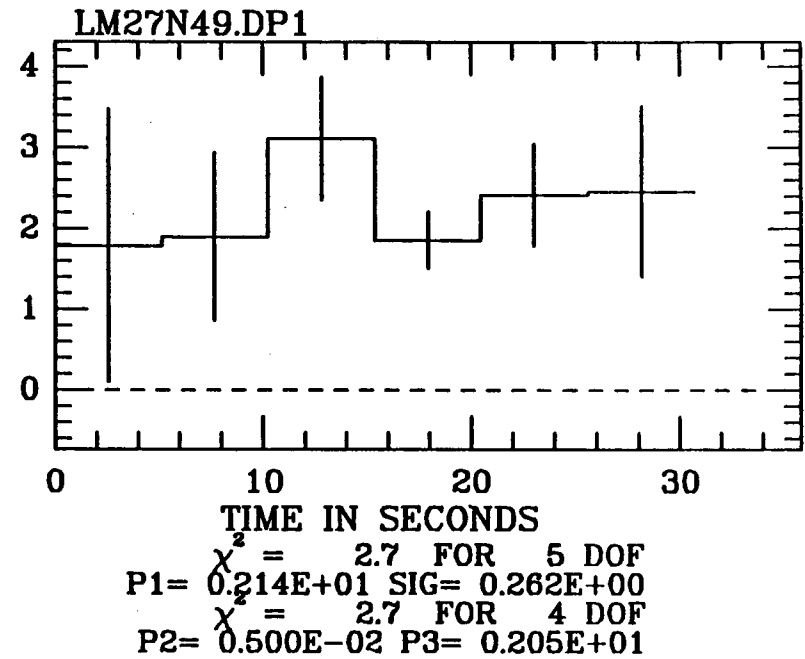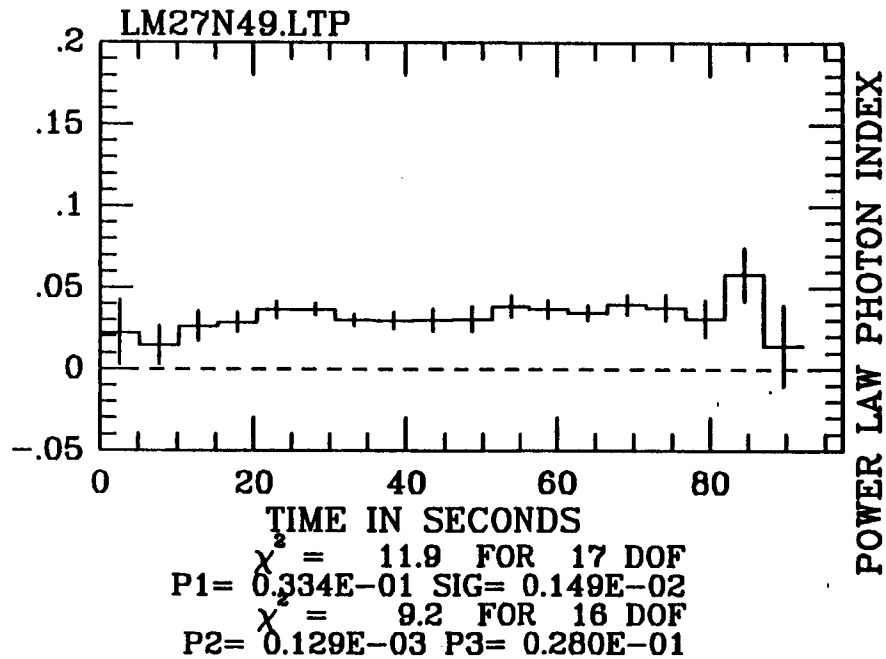
z) Plots for the event on D.O.Y (1977) 381.03. Time zero is at 00:44:08 U.T. for the light curve and 00:44:28 for the spectral variability plot.

HED3 CTS/$-$CM^2$-$S

LMCIB.LTP

χ^2 =   5.5 FOR   15 DOF
P1= 0.156E-01 SIG= 0.269E-02
χ^2 =   5.5 FOR   14 DOF
P2=$-$0.466E-05 P3= 0.158E-01

LMCIB.DP1

χ^2 =   1.7 FOR   4 DOF
P1= 0.140E+01 SIG= 0.417E+00
χ^2 =   0.1 FOR   3 DOF
P2=$-$0.227E+00 P3= 0.644E+01

TIME IN SECONDS

POWER LAW PHOTON INDEX

aa) Plots for the event on D.O.Y (1977) 420.58. Time zero is at 13:56:27 U.T. for the light curve and
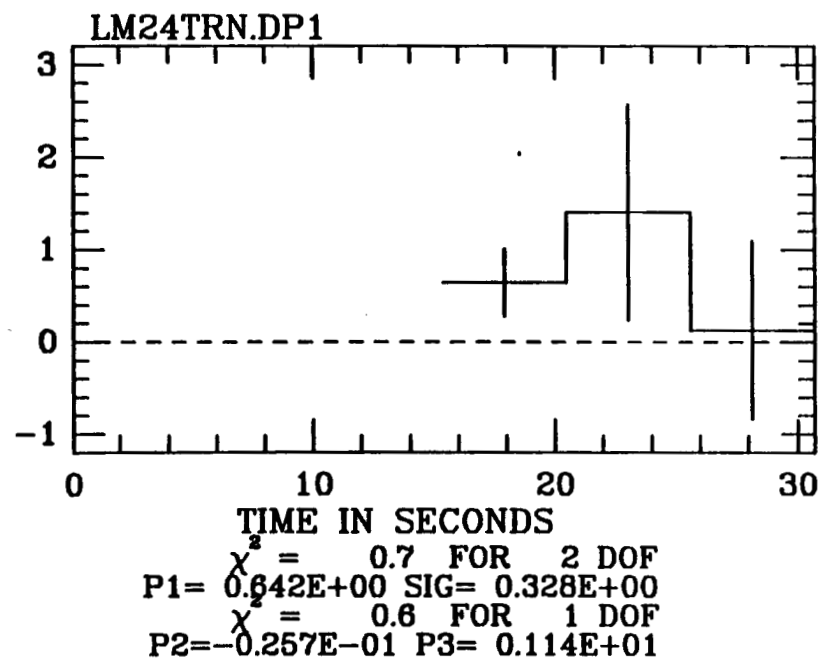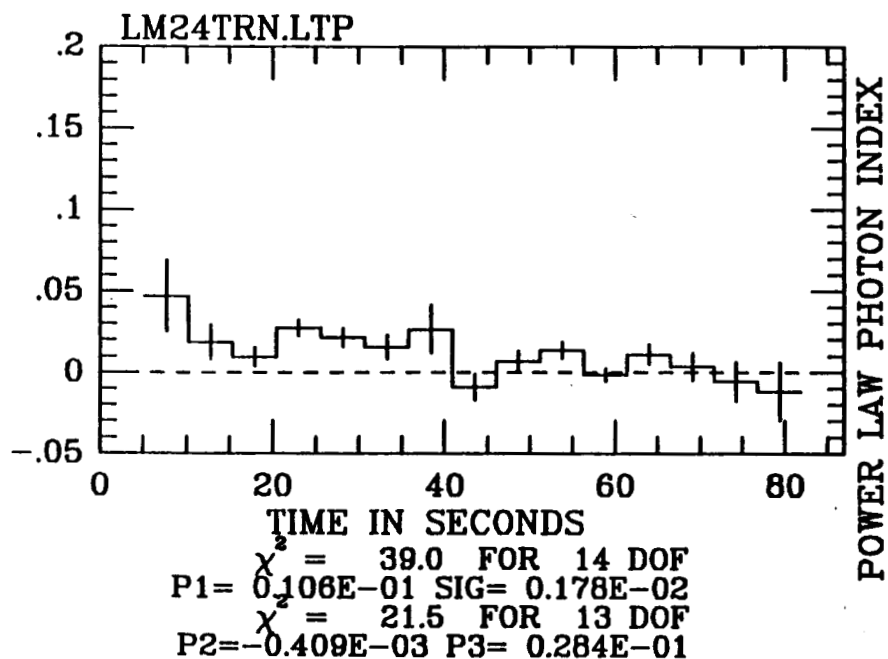
13:56:42 U.T. for the spectral variability plot.

HED3 CTS/-CM^2-S

LM29UNK.LTP

TIME IN SECONDS
χ^2 =   28.2 FOR   16 DOF
P1= 0.711E-01 SIG= 0.661E-02
χ^2 =   27.3 FOR   15 DOF
P2=-0.336E-03 P3= 0.866E-01

POWER LAW PHOTON INDEX

LM29UNK.DP1

TIME IN SECONDS
χ^2 =   0.6 FOR   3 DOF
P1= 0.164E+01 SIG= 0.419E+00
χ^2 =   0.4 FOR   2 DOF
P2=-0.441E-01 P3= 0.237E+01

bb) Plots for the event on D.O.Y (1977) 530.57. Time zero is at 13:35:43 U.T.

HED3 CTS/-CM^2-S

LM30TRN.LTP

.2
.15
.1
.05
0
-.05

0   20   40   60   80

TIME IN SECONDS

χ^2 =   47.7 FOR 13 DOF
P1= 0.377E-01 SIG= 0.201E-02
χ^2 =   35.4 FOR 12 DOF
P2=-0.376E-03 P3= 0.510E-01

POWER LAW PHOTON INDEX

LM30TRN.DP1

4
3
2
1
0
-1

0   5   10   15   20   25

TIME IN SECONDS

χ^2 =   5.3 FOR   4 DOF
P1= 0.185E+01 SIG= 0.223E+00
χ^2 =   4.8 FOR   3 DOF
P2=-0.305E-01 P3= 0.231E+01

206
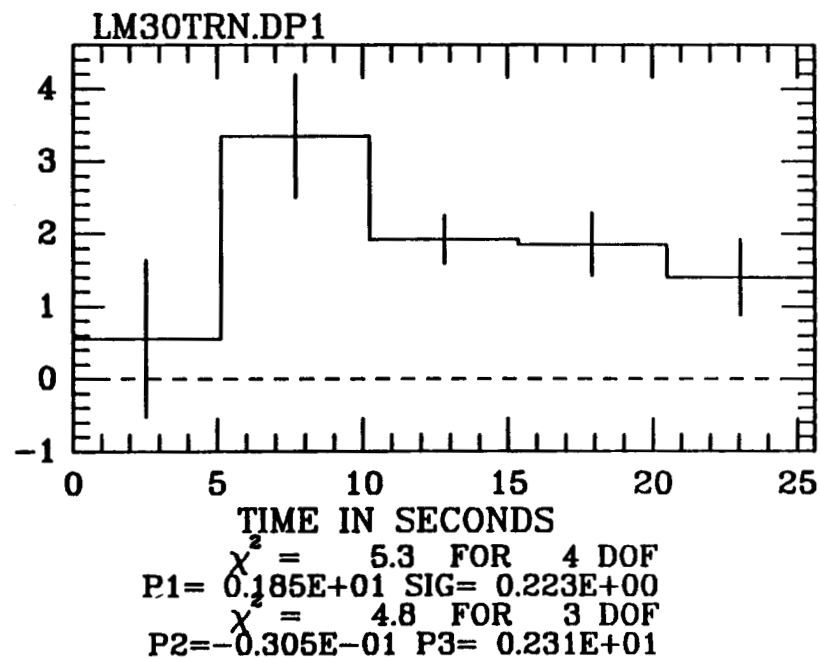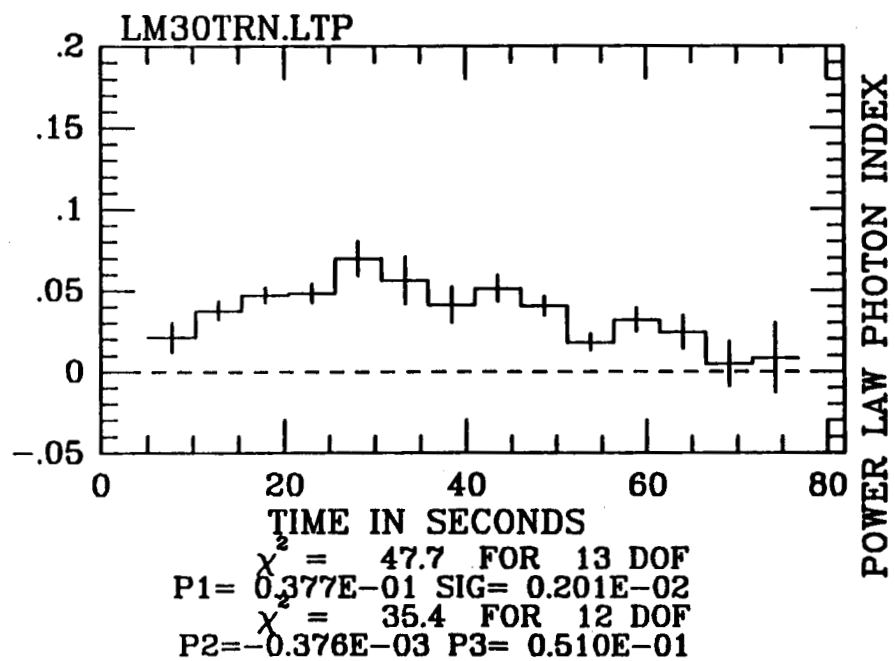
cc) Plots for the event on D.O.Y (1977) 536.52. Time zero is at 12:29:09 U.T.

HED3 CTS/-CM^2-S

LM31UNK.LTP

LM31UNK.DP1

TIME IN SECONDS

χ^2 =   60.3 FOR   2 DOF
P1= 0.122E+00 SIG= 0.626E-02
χ^2 =   6.2 FOR   1 DOF
P2=-0.170E-01 P3= 0.320E+00

POWER LAW PHOTON INDEX

TIME IN SECONDS

χ^2 =   6.1 FOR   2 DOF
P1= 0.232E+01 SIG= 0.151E+00
χ^2 =   0.7 FOR   1 DOF
P2= 0.984E-01 P3= 0.151E+01

dd) Plots for the event on D.O.Y (1977) 539.24. Time zero is at 05:50:44 U.T.

HED3 CTS/−CM²−S

LM32TRN.LTP

χ^2 =   71.1 FOR 14 DOF
P1= 0.399E−01 SIG= 0.208E−02
χ^2 =   33.1 FOR 13 DOF
P2=−0.710E−03 P3= 0.670E−01

LM32TRN2.DP1

POWER LAW PHOTON INDEX

TIME IN SECONDS

χ^2 =   1.3 FOR   5 DOF
P1= 0.368E+01 SIG= 0.321E+00
χ^2 =   0.2 FOR   4 DOF
P2=−0.508E−01 P3= 0.442E+01
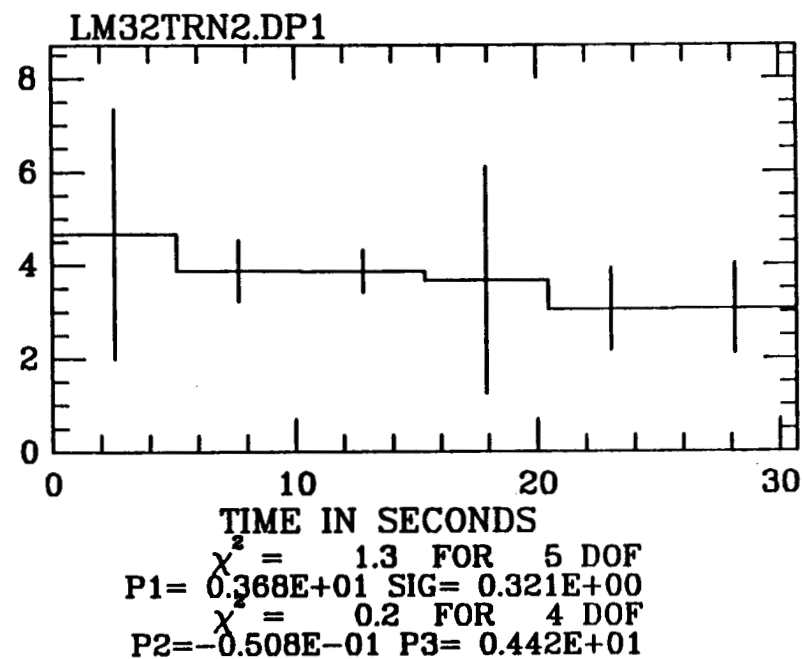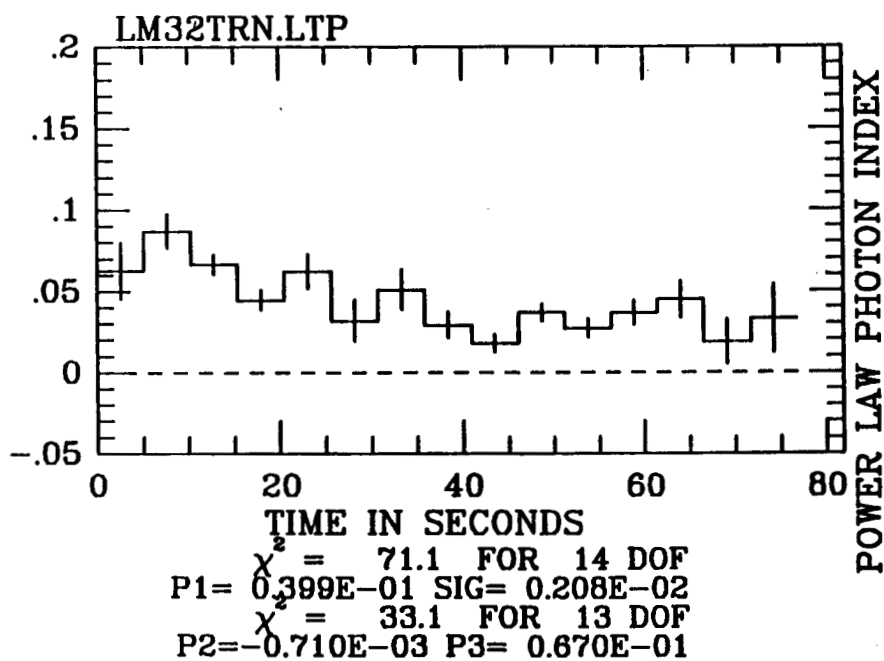
ee) Plots for the event on D.O.Y (1977) 540.14. Time zero is at 03:27:33 U.T.

HED3 CTS/-CM^2-S

LM33TRN.LTP

.2
.15
.1
.05
0
-.05

0   20   40   60   80

TIME IN SECONDS

χ^2 =   14.8 FOR 14 DOF
P1= 0.172E-01 SIG= 0.152E-02
χ^2 =   14.1 FOR 13 DOF
P2= 0.661E-04 P3= 0.150E-01

POWER LAW PHOTON INDEX

LM33TRN.DP1

6
4
2
0
-2

0   5   10   15   20

TIME IN SECONDS

χ^2 =   0.4 FOR   2 DOF
P1= 0.168E+01 SIG= 0.566E+00
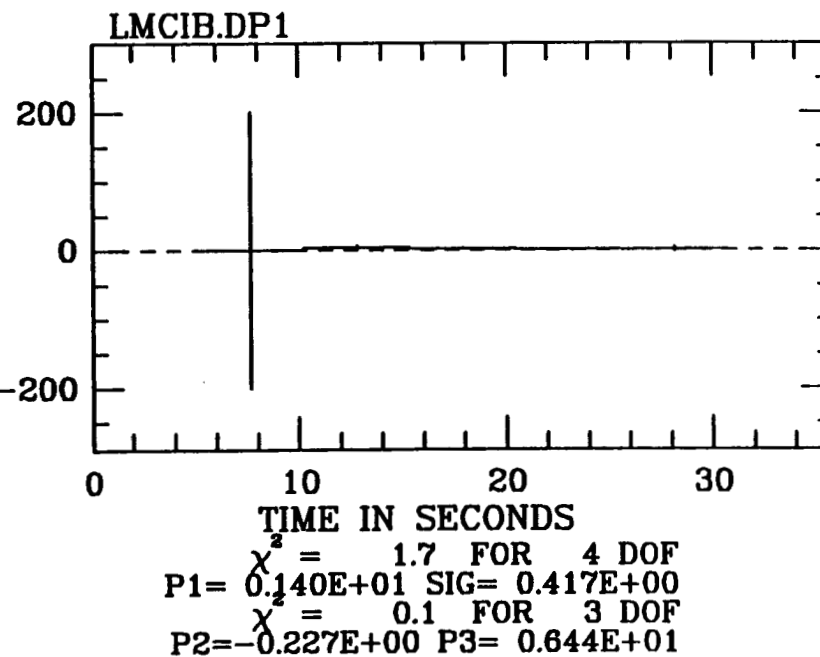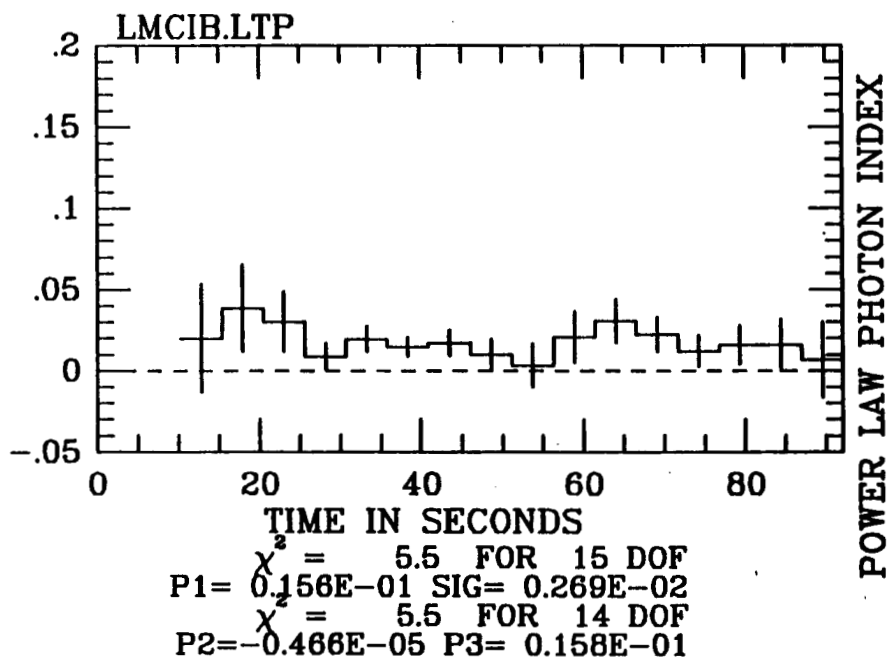χ^2 =   0.1 FOR   1 DOF
P2=-0.102E+00 P3= 0.222E+01
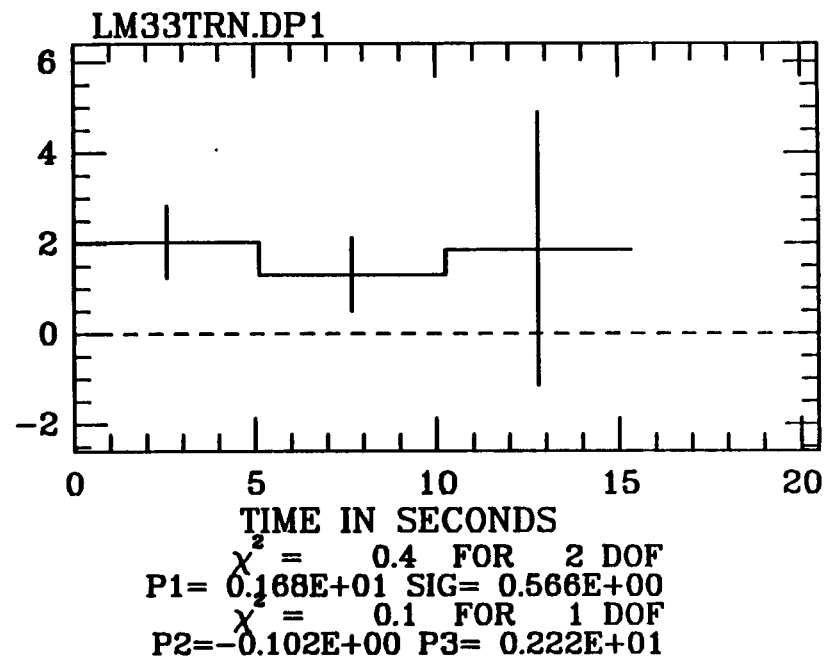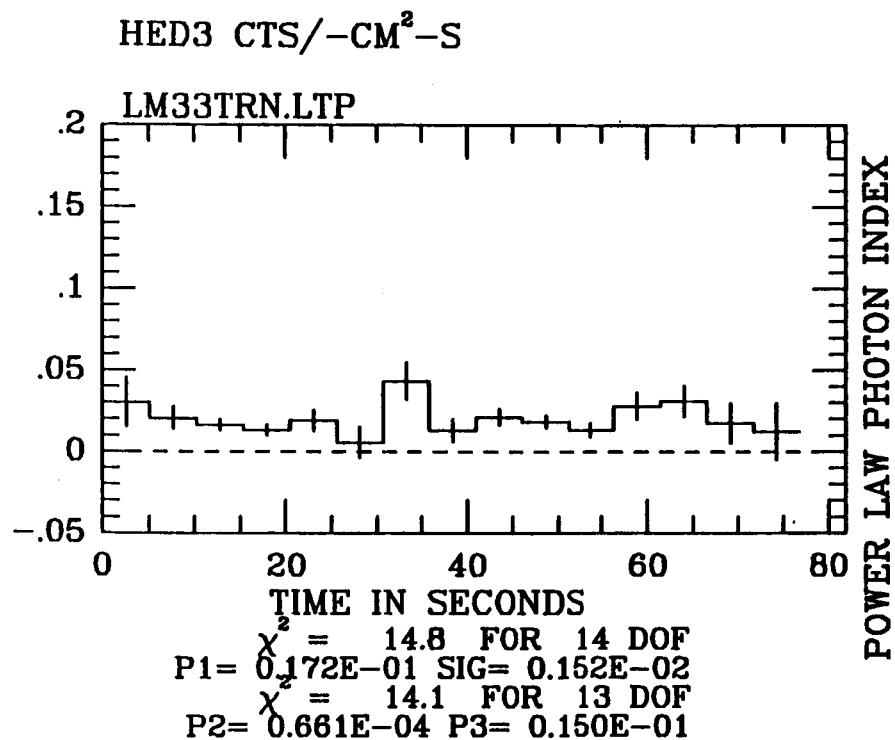
ff) Plots for the event on D.O.Y (1977) 541.18. Time zero is at 04:19:05 U.T. for the light curve and
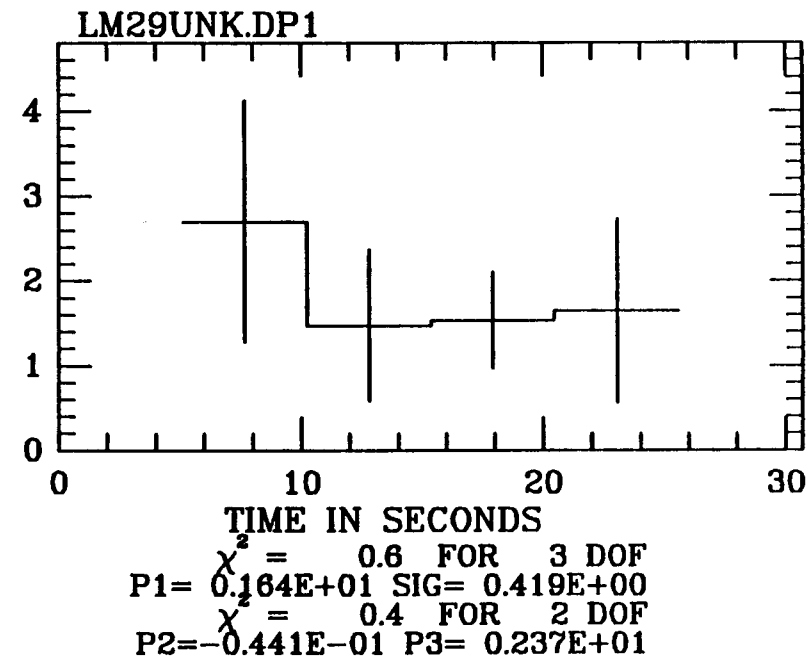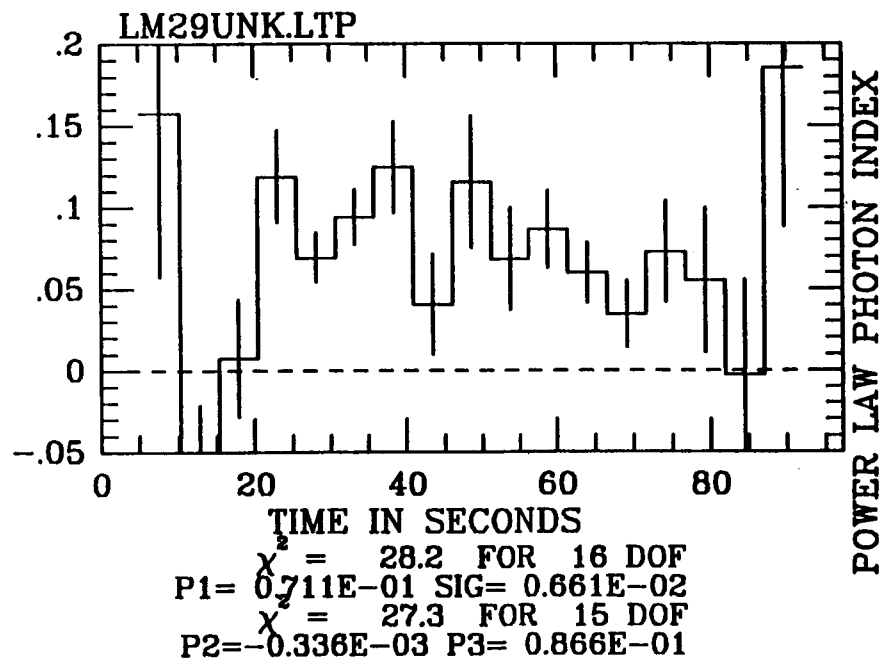04:19:20 U.T. for the spectral variability plot.

HED3 CTS/-CM^2-S

LM34TRN.LTP

TIME IN SECONDS
χ^2 =   15.2 FOR 16 DOF
P1= 0.216E-01 SIG= 0.154E-02
χ^2 =   12.8 FOR 15 DOF
P2=-0.130E-03 P3= 0.280E-01

LM34TRN.DP1

POWER LAW PHOTON INDEX

TIME IN SECONDS
χ^2 =   0.9 FOR   5 DOF
P1= 0.839E+00 SIG= 0.241E+00
χ^2 =   0.9 FOR   4 DOF
P2= 0.222E-02 P3= 0.800E+00

Plots for the event on D.O.Y (1977) 543.04.   Time zero is at 00:50:57 U.T.

HED3 CTS/$-$CM^2-S

211

LM35UNK.LTP

.2
.15
.1
.05
0
$-$.05
0   20   40   60   80
TIME IN SECONDS
χ^2 =   22.7   FOR   14 DOF
P1= 0.109E$-$01 SIG= 0.146E$-$02
χ^2 =   10.3   FOR   13 DOF
P2= 0.284E$-$03 P3= 0.310E$-$02

POWER LAW PHOTON INDEX

LM35UNK.DP1

8
6
4
2
0
0   10   20   30
TIME IN SECONDS
χ^2 =   12.4   FOR   4 DOF
P1= 0.616E+00 SIG= 0.406E+00
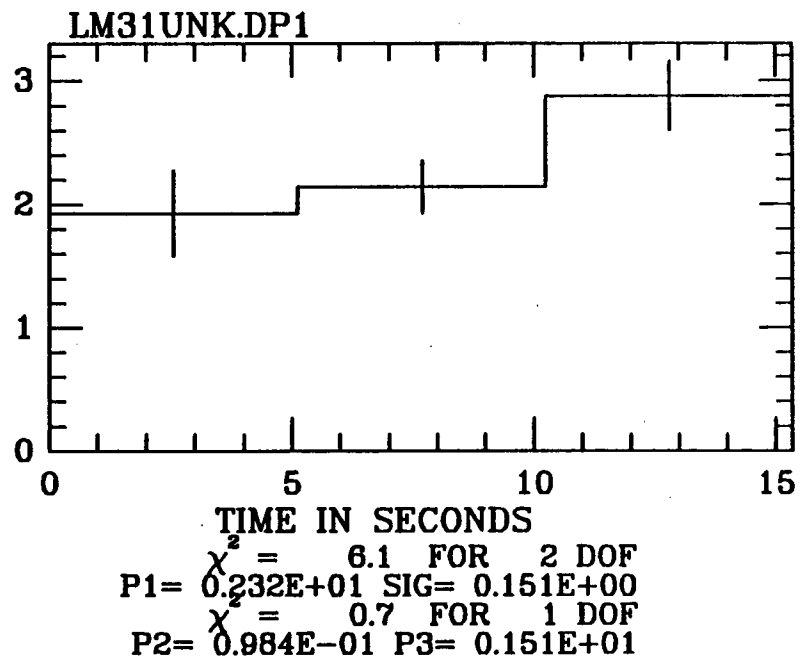χ^2 =   11.9   FOR   3 DOF
P2= 0.436E$-$01 P3= 0.107E+00
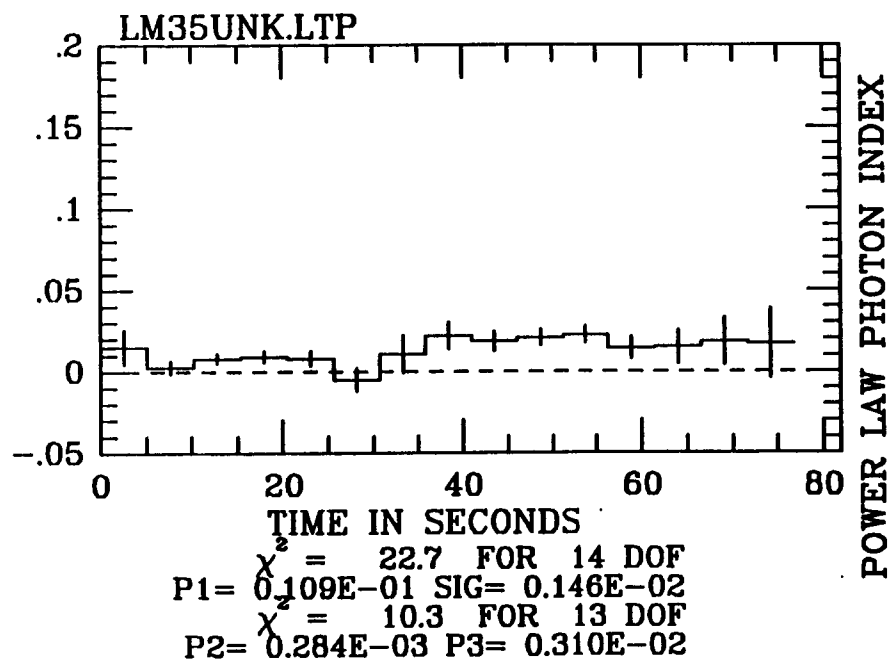
hh) Plots for the event on D.O.Y (1977) 550.58. Time zero is at 14:01:24 U.T.

HED3 CTS/-CM^2-S

LM36N49.LTP

TIME IN SECONDS
χ^2 =   4.1   FOR   16 DOF
P1= 0.163E-01 SIG= 0.118E-02
χ^2 =   3.9   FOR   15 DOF
P2=-0.315E-04 P3= 0.175E-01

LM36N49.DP1

POWER LAW PHOTON INDEX

TIME IN SECONDS
χ^2 =   2.6   FOR   4 DOF
P1= 0.187E+01 SIG= 0.371E+00
χ^2 =   2.5   FOR   3 DOF
P2= 0.343E-01 P3= 0.125E+01
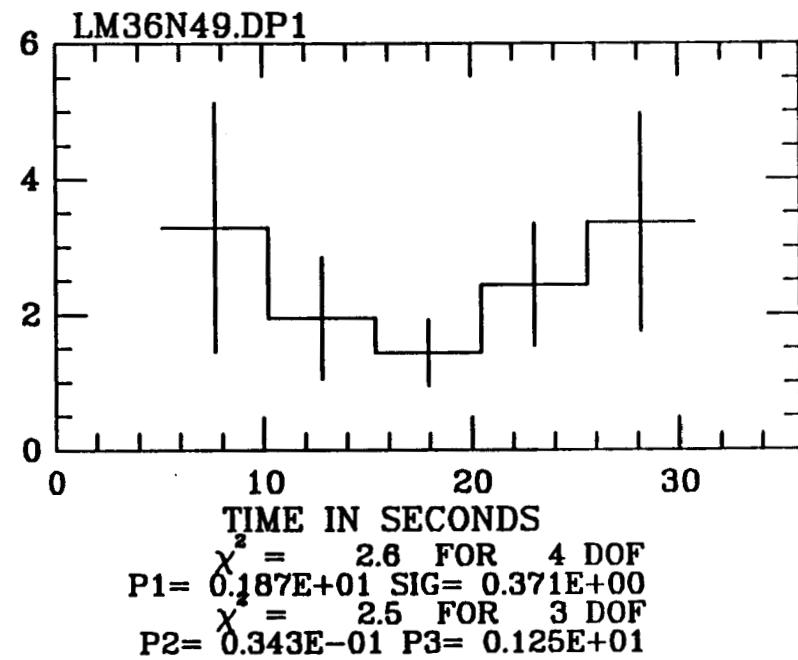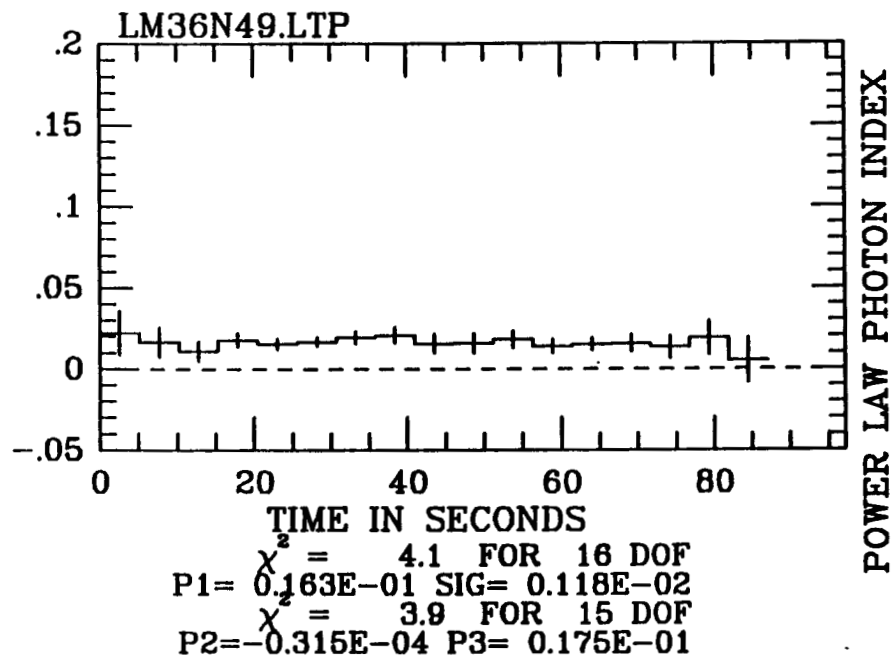
ii) Plots for the event on D.O.Y (1977) 573.51. Time zero is at 12:19:15 U.T. for the light curve and 12:19:26 U.T. for the spectral variability plot.
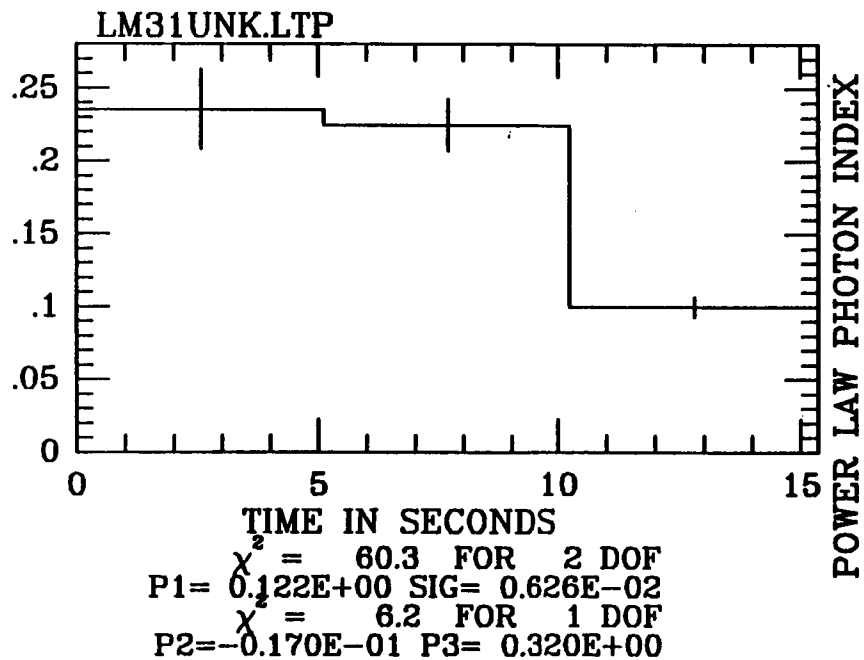
HED3 CTS/-CM^2-S

LM37UNK.LTP

TIME IN SECONDS

χ^2 = 8.7 FOR 14 DOF
P1= 0.770E-02 SIG= 0.148E-02
χ^2 = 8.3 FOR 13 DOF
P2= 0.509E-04 P3= 0.607E-02

LM37UNK.DP1

POWER LAW PHOTON INDEX

TIME IN SECONDS

χ^2 = 2.8 FOR 3 DOF
P1= 0.249E+01 SIG= 0.792E+00
χ^2 = 2.8 FOR 2 DOF
P2= 0.421E-01 P3= 0.190E+01

213
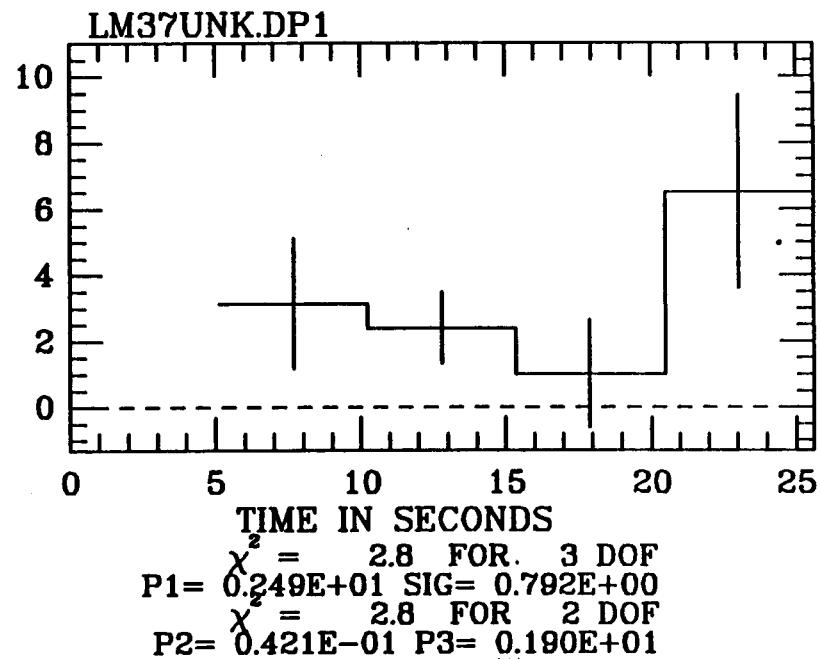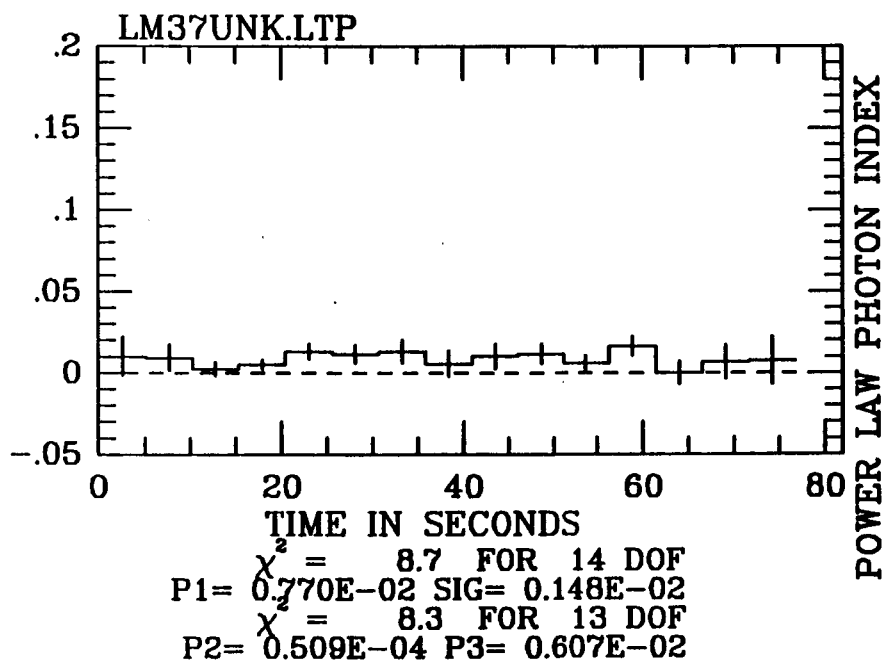
jj) Plots for the event on D.O.Y (1977) 602.64. Time zero is at 15:27:10 U.T.

HED3 CTS/-CM^2-S

LM38UNK.LTP

TIME IN SECONDS
χ^2 =   33.3   FOR   13 DOF
P1= 0.401E-02 SIG= 0.151E-02
χ^2 =   16.5   FOR   12 DOF
P2=-0.363E-03 P3= 0.162E-01

POWER LAW PHOTON INDEX

LM38UNK.DP1

TIME IN SECONDS
χ^2 =   18.1   FOR   5 DOF
P1= 0.305E+00 SIG= 0.192E+00
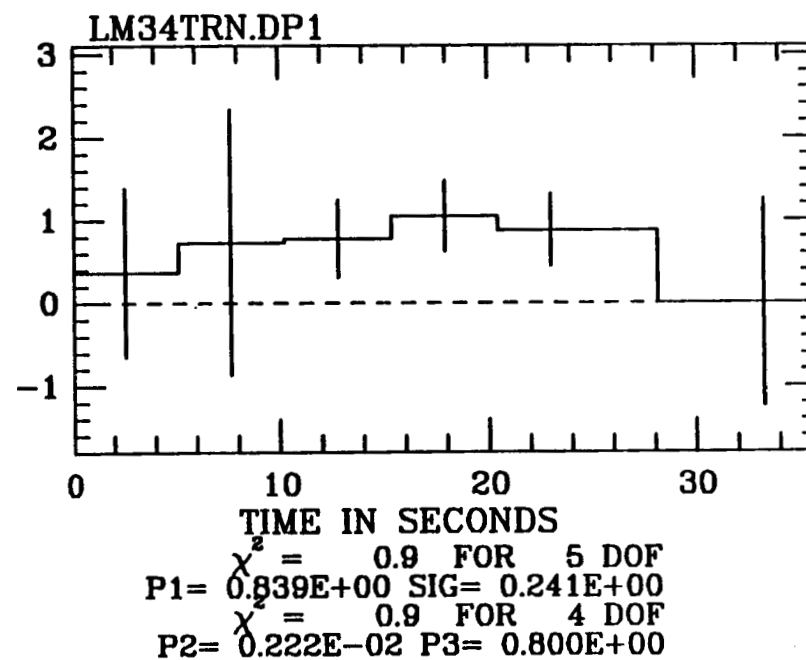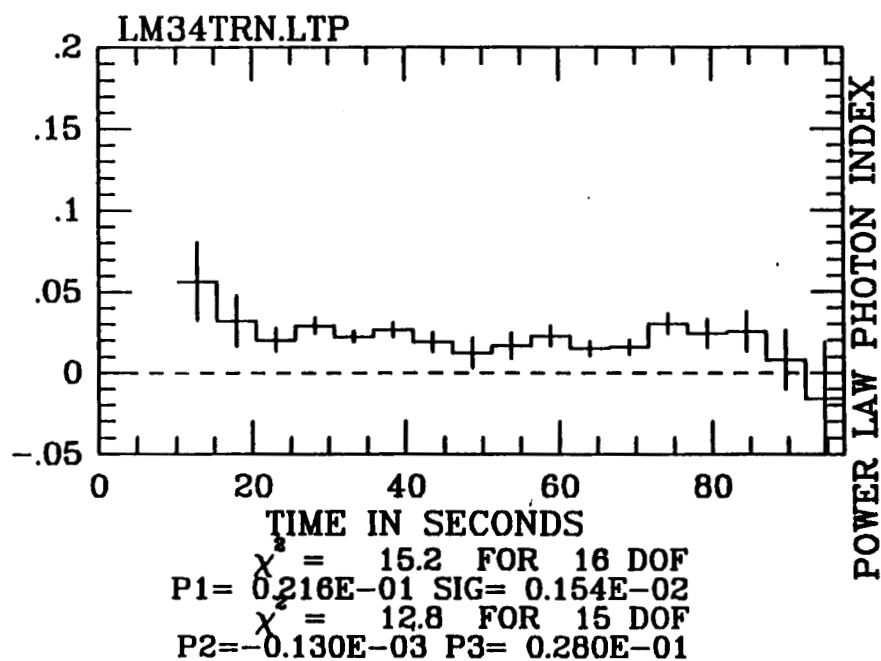χ^2 =   9.1   FOR   4 DOF
P2=-0.153E+00 P3= 0.368E+01

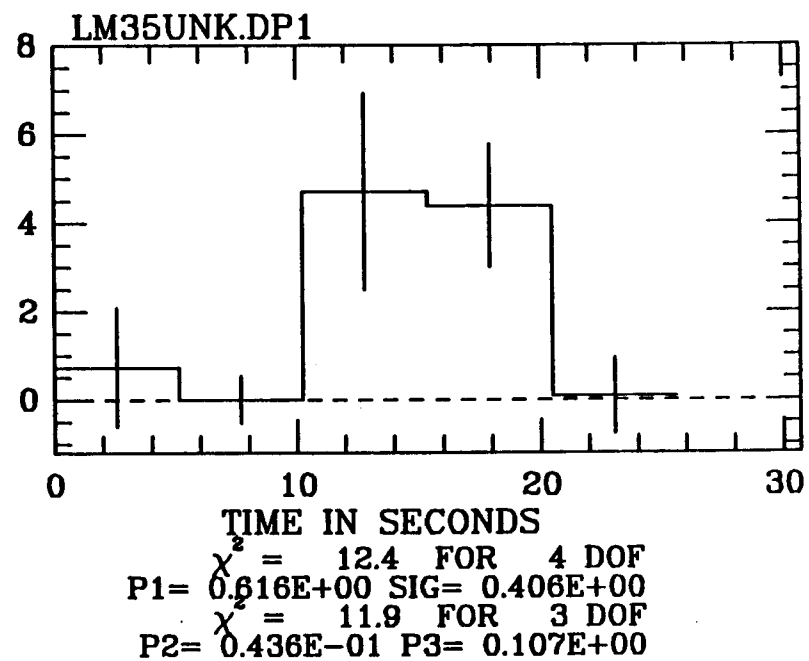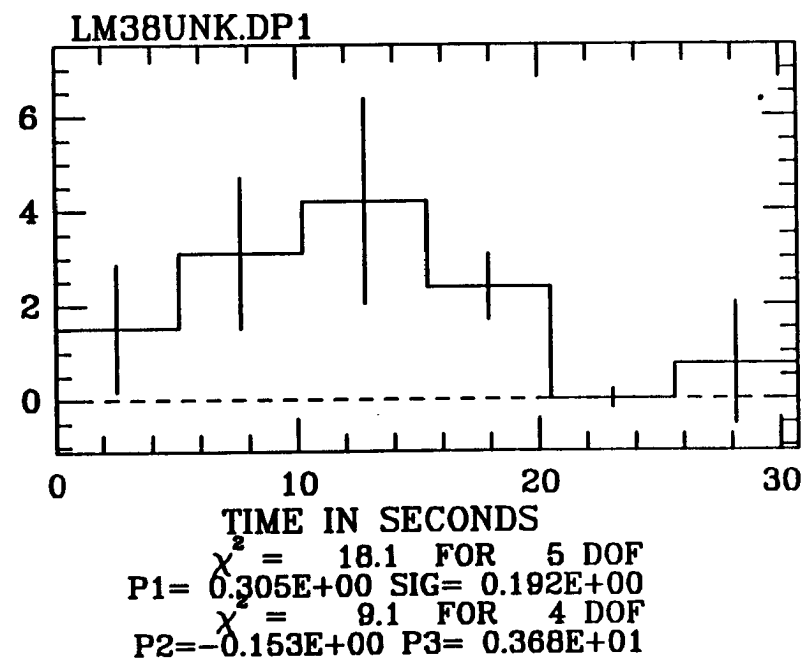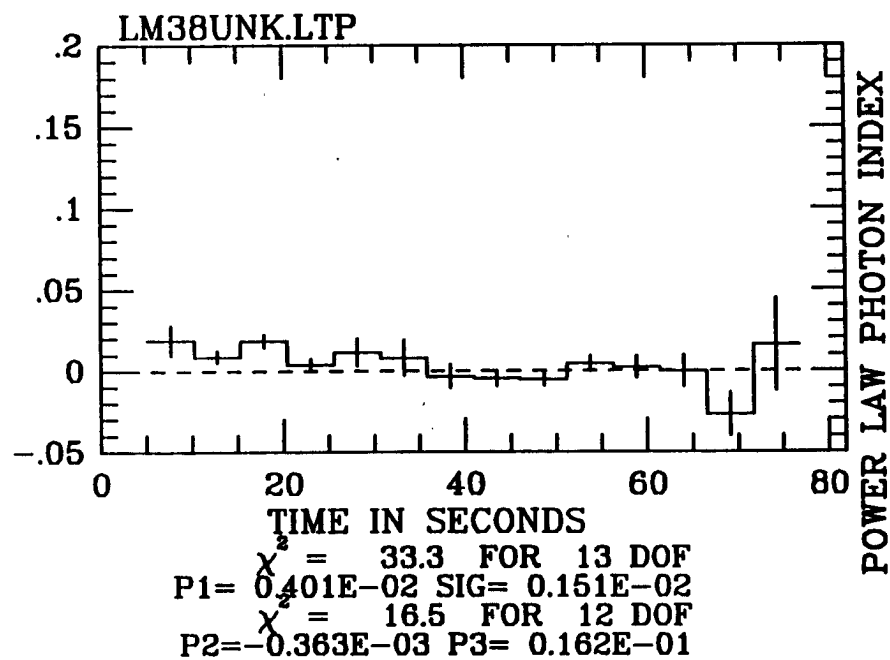kk) Plots for the event on D.O.Y (1977) 653.78. Time zero is at 18:41:18 U.T. for the light curve and 18:41:33 U.T. for the spectral variability plot. The position was held fixed at that of LMC X-2.

HED3 CTS/-CM^2-S

LMC39X2.LTP

$\chi^2 = 17.1$ FOR 16 DOF
P1= 0.755E-02 SIG= 0.170E-02
$\chi^2 = 14.8$ FOR 15 DOF
P2=-0.150E-03 P3= 0.140E-01

LMC39X2.DP1

$\chi^2 = 5.3$ FOR 4 DOF
P1= 0.610E+00 SIG= 0.424E+00
$\chi^2 = 1.6$ FOR 3 DOF
P2=-0.119E+00 P3= 0.338E+01
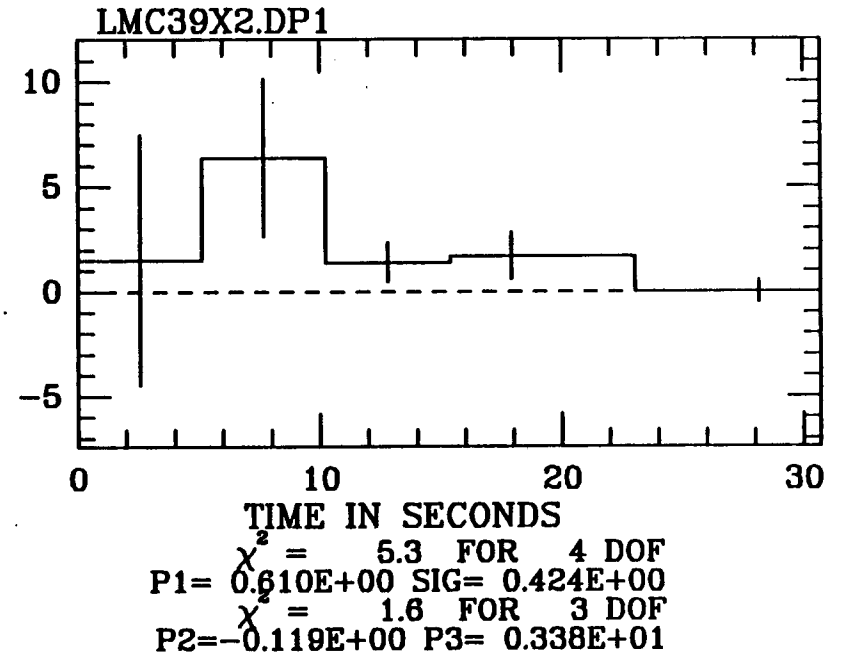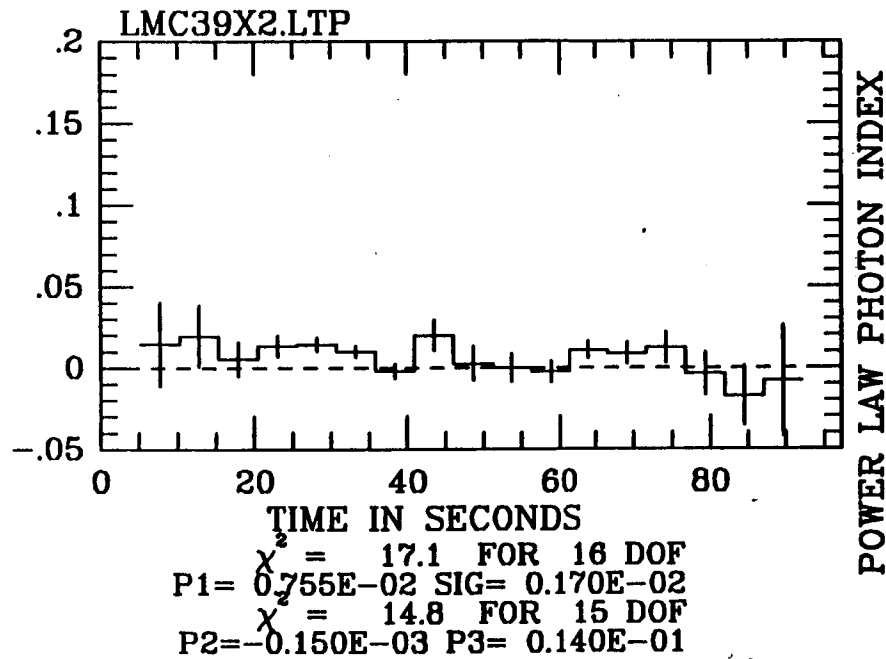
Figure 4.4 Here we have plotted one day light curves and softness ratios (MED/HED3) as a function of time for the two events we attribute to LMC X-2. The light-curves are in units of summed MED + HED3 cts-cm^{-2}-s^{-1} versus time in days. (One millicrab, which is about 3.4×10^{-11} ergs-cm^{-2}-s^{-1}, corresponds to $\sim 3.5 \times 10^{-3}$ MED+HED3 cts-cm^{-2}-s^{-1}. For the Crab Nebula plus pulsar, MED/HED3 ~ 1.14, in these units.)

a) This is the (MED+HED3) light curve and accompanying softness ratios (MED/HED3) for the two twelve hour periods around the event on D.O.Y. (1977) 290.62. We have marked the time of the trigger with an arrow.

HED3 CTS/-CM^2-S

LMC5X2B.HFP

TIME IN DAYS

χ^2 = 31.9 FOR 14 DOF
P1= 0.290E-01 SIG= 0.911E-03
χ^2 = 31.5 FOR 13 DOF
P2=-0.218E-02 P3= 0.299E-01

LMC5X2B.HFP

SOFTNESS RATIO

TIME IN DAYS

χ^2 = 17.7 FOR 14 DOF
P1= 0.110E+01 SIG= 0.452E-01
χ^2 = 16.4 FOR 13 DOF
P2=-0.227E+00 P3= 0.120E+01
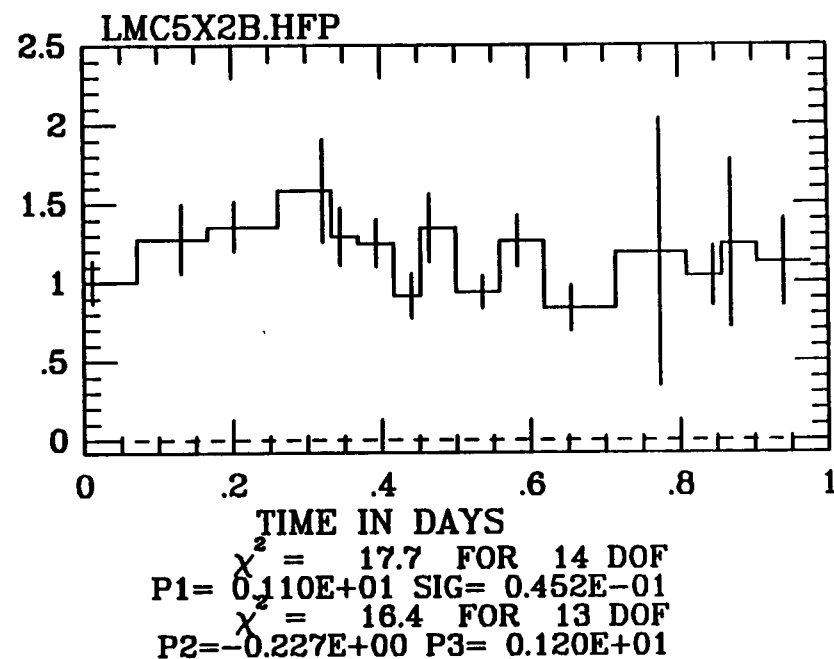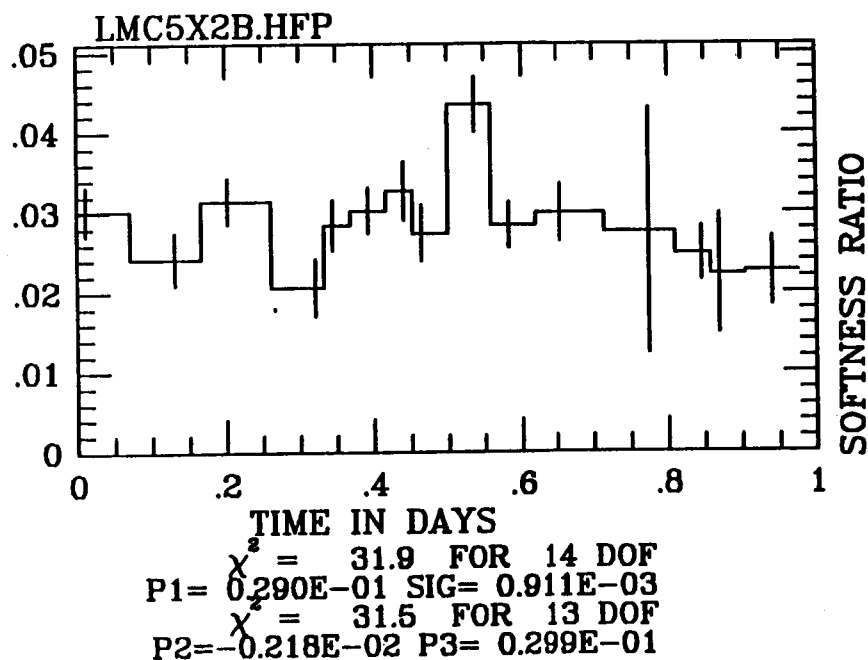
b) This is the (MED+HED3) light-curve and accompanying softness ratios (MED/HED3) for the two twelve hour periods around the event on D.O.Y (1977) 653.78. Again, we have indicated the time of the trigger with an arrow.

HED3 CTS/$-$CM^2$-$S

LM39X2B.HFP
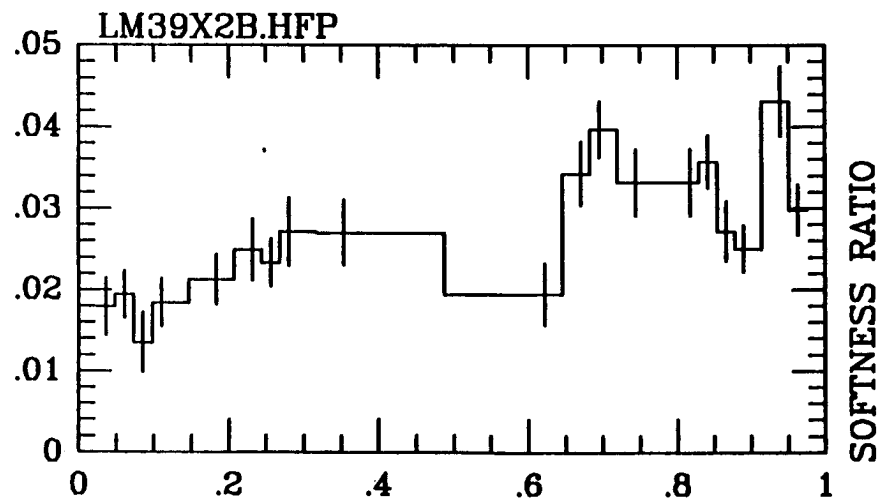
$\chi^2 = 87.5$ FOR 18 DOF
P1= 0.262E$-$01 SIG= 0.798E$-$03
$\chi^2 = 38.8$ FOR 17 DOF
P2= 0.163E$-$01 P3= 0.183E$-$01

TIME IN DAYS

LM39X2B.HFP
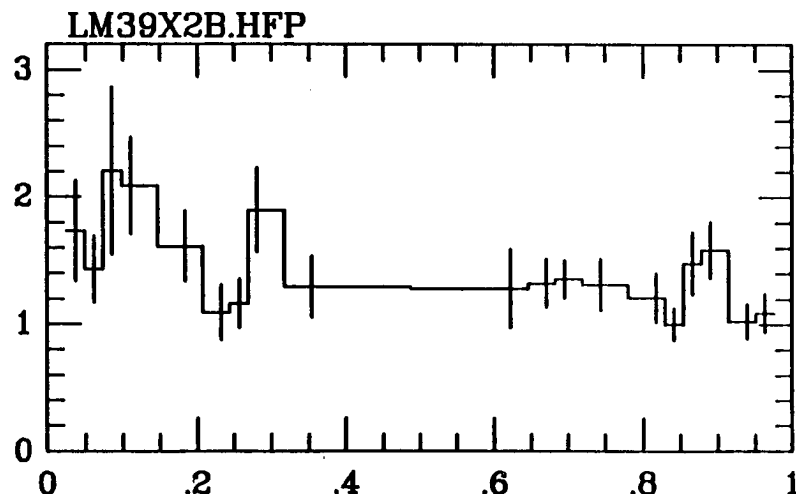
SOFTNESS RATIO

$\chi^2 = 26.6$ FOR 18 DOF
P1= 0.126E+01 SIG= 0.474E$-$01
$\chi^2 = 19.8$ FOR 17 DOF
P2=$-$0.428E+00 P3= 0.154E+01

TIME IN DAYS

Figure 4.5   Here we present a 13 day (MED+HED3) light curve, and the corresponding softness ratios (MED/HED3) as a function of time. (One millicrab, which is about 3.4×10^{-11} ergs-cm^{-2}-s^{-1}, corresponds to ~ 3.5×10^{-3} MED+HED3 cts-cm^{-2}-s^{-1}. For the Crab Nebula plus pulsar, MED/HED3 ~ 1.14, in these units.) The times of the five events we attribute to LMC X-1 have been marked with an arrow.

HED3 CTS/-CM^2-S

LM712X1C.HFP
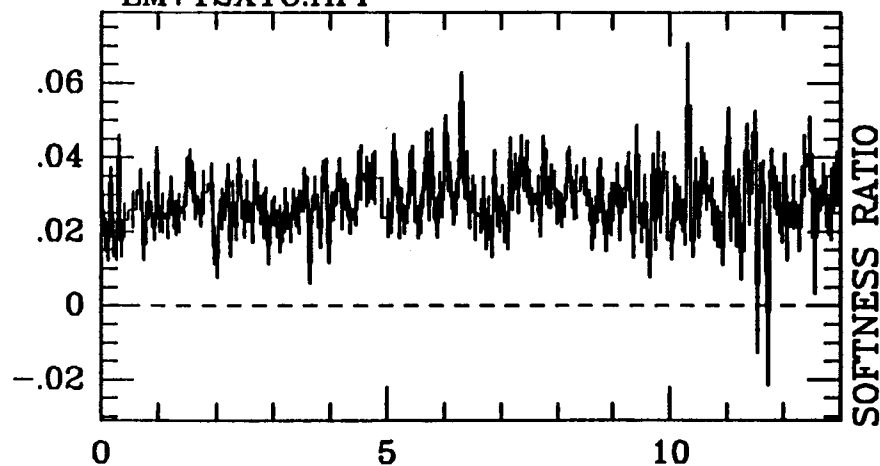
TIME IN DAYS

$\chi^2 = 338.9$ FOR 228 DOF
P1= 0.276E-01 SIG= 0.343E-03
$\chi^2 = 326.3$ FOR 227 DOF
P2= 0.349E-03 P3= 0.255E-01

SOFTNESS RATIO

LM712X1C.HFP
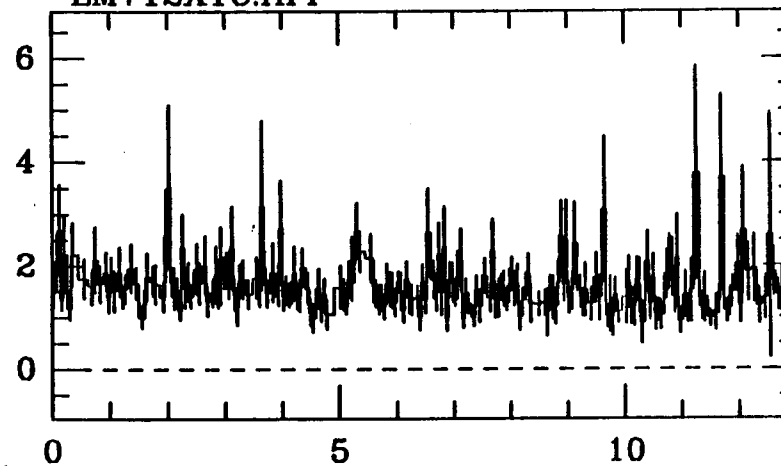
TIME IN DAYS

$\chi^2 = 176.4$ FOR 210 DOF
P1= 0.143E+01 SIG= 0.230E-01
$\chi^2 = 165.6$ FOR 209 DOF
P2=-0.221E-01 P3= 0.157E+01

219

Chapter 5

Two Special Cases: LDS 131 and 6-Nov-77 OSO-8 Event

A. Overview

In this chapter we present data on two very different bright fast
transients, representing the two classes of fast transient events
discussed in Chapter 3. One was a prototypical coronal transient, the
energetic bright stellar X-ray flare source LDS 131. The other
represents the incompletely understood class of rare events that
probably originate on compact objects. It was a bright, highly
variable, unidentified, 12 minute event observed by the OSO-8
satellite on November 6, 1977, from the direction of Cygnus, near the
Galactic plane.

The identification of the event on D405.85 with LDS 131 seemed
unexpected because it was so bright, with $L_x \sim 10^{32}$ ergs-s^{-1} and $E_x \sim 10^{35}$
ergs (Kaluzienski et al. 1978a,b; Griffiths et al. 1979). Those only
slightly familiar with stellar flares may not realize that the
measured distribution of event rate with flare size follows a power
law rather than a Gaussian form, with an ill-defined mimimum and
maximum flare size (Lacy, Moffet, and Evans 1976; Kunkel 1975a;
Gershberg 1972; see Appendix C; and Ambruster, Sciortino, and Golub
1987 on microflaring). For example, although the most frequently
observed flare sizes are on the order of 10^{31-32} ergs, this is not
necessarily the mean flare size; and it is more probable to get
flares with sizes far from the mean than one expects assuming a normal
distribution.

In §5.B we present detailed data of this bright flare observed by
HEAO 1. We show that the identification of this event with the 10th

magnitude dM3e pair LDS 131 is highly probable (>99.9%), and discuss
follow up observations of this active dwarf star system. Although
some have used the term 'superflare' to denote events of this
magnitude (Roizman and Shevchenko 1982; Ambruster, Snyder, and Wood
1984), we find the dM3e pair to be normal active dwarf stars, and the
bright flare itself to differ from more common events mainly in the
inferred size (and overall emission measure) of the coronal magnetic
loops thought to confine the 10^8 K plasma during the flare.

The bright 6-Nov-77 OSO 8 event, on the other hand, is shown to
be atypical of any of the classes of X-ray fast transients discussed
earlier (including the 'hard transients' of Chapter 3, because of its
inferred Eddington luminosity). In §5.C we summarize data from the
event itself, and from attempted follow-up observations. It was
detected once, at a flux of 1.5×10^3 millicrabs, but not detected again
despite coverage of the region by several X-ray satellites.
Constraints on position show that it originated from the crowded
Cygnus region (not far from the event on D494.15), but in that
direction lie several heavily absorbing clouds (the "Cygnus rift"), so
that constraints on optical emission were difficult.

B. The Bright Coronal Flare from LDS 131

i. History and Overview

Kaluzienski et al. (1978a,b) reported detecting an X-ray
transient event in the quick-look data from HEAO 1 A-2, on Feb 9, 1977
at 20^h24^m U.T. (or D405.85), with a peak flux $>8 \times 10^{-9}$ ergs-cm^{-2}-s^{-1},
making it one of the brightest 'high latitude transients'. The event
was visible for several scans, decaying in intensity with a time

constant of about 40 minutes (see Figure 3.1.e). It was given the X-ray designation H0449-55, since the center of the original A-2 error box lay at a 1950.0 R.A. and Dec. of 04^h 49^m, -55°. Optical observations of the combined A-4 and A-3 position error boxes resulted in the identification of the source with one of two dM3e stars with similar optical spectra, at a 1950.0 R.A. and Dec. of 04h 52m 31.5s, -55° 56' 27" (Griffiths et al. 1979). The brighter was about 10th magnitude, and the other, 8.5" due NW of the first, was about half a magnitude fainter. This pair was designated LDS 131 in the double star catalog of Luyten (1963a), and BPM 17964 and 17965 in the Bruce Proper Motion Catalog (Luyten 1963b). Measurements of their proper motion [by Tom Morgan of Sidney Observatory] showed the brighter to have μ_α, μ_δ of 0.130±0.004,0.050±0.004, and the fainter to have μ_α, μ_δ of 0.136±0.009,0.058±0.009, implying a distance of about 10 pc (Griffiths private communication). Upgren et al. (1972) noted that the pair, listed as U98, exhibited hydrogen emission lines (although they were listed as a single 9.2 mag object because of the small 8.5" separation).

If this identification is correct, the outburst on D405.85 was both the highest temperature (kT~12 keV) and highest peak luminosity (L_x~6x10^{31} ergs-s^{-1}) flare that has been detected in X-rays from a cool dwarf star. (It may not have been the most energetic; see discussions of a longer event from EV Lac in Ambruster et al 1983). Events of similar duration and intensity have long been observed in the U-band (Kunkel 1975a). The bright flare on D405.85 appears to support the contention of Roizman and Shevchenko (1982) that nearby field flare stars are capable of rare outbursts as violent and

energetic as those observed more frequently from dMe-dKe stars in young associations (Gurzadyan 1980). In Chapter 3 of this work, we used the identification of this event as an energetic stellar flare as a cornerstone in building our argument for the identification of the majority of the A-2 fast transient events with flares from similar systems. This, in turn, supports the current understanding of stellar flares as dramatic manifestations of the coronal magnetic fields thought to determine the structure of the outer atmospheres of cool stars. Flare size and temperature correspond to varying sizes of magnetic loops in the coronae, from small ($\sim 10^6$ cm) loops thought to be associated with soft, kT<1keV, microflares which may be the source of heating in the coronae (Ambruster, Sciortino, and Golub 1987); to large ($\sim 10^{11}$ cm) loops associated with the dramatic outburst from LDS 131.

In the following sub-sections, we present the varied data on H0449-55/LDS 131. Since it is crucial, in §5.B.ii we present the evidence, based primarily on position constraints, for the identification of the bright X-ray flare on D405.85 with LDS 131. We then discuss the properties of the original intense event observed by HEAO 1, and infer some physical parameters, in §5.B.iii. In §5.B.iv we briefly discuss follow up observations of LDS 131 in flares and quiescence with both the Einstein IPC and EXOSAT observatories, and we briefly summarize IUE observations of the dM3e pair.

ii. Constraints on Position and the Identification with LDS 131

In Figure 3.1.e we plotted the new HEAO 1 A-2 99% confidence position limits, produced by the position finding algorithm described in Appendix B, for the bright event on D405.85. The new A-2 position

223

Figure 5.1 The eighteen-day HEAO 1 A-2 light curve of LDS 131, from the six month pass over the source that contained the bright flare. Each point shows the twelve hour average for that time, in units of HED3+MED cts-s^{-1}, versus D.O.Y. 1977.
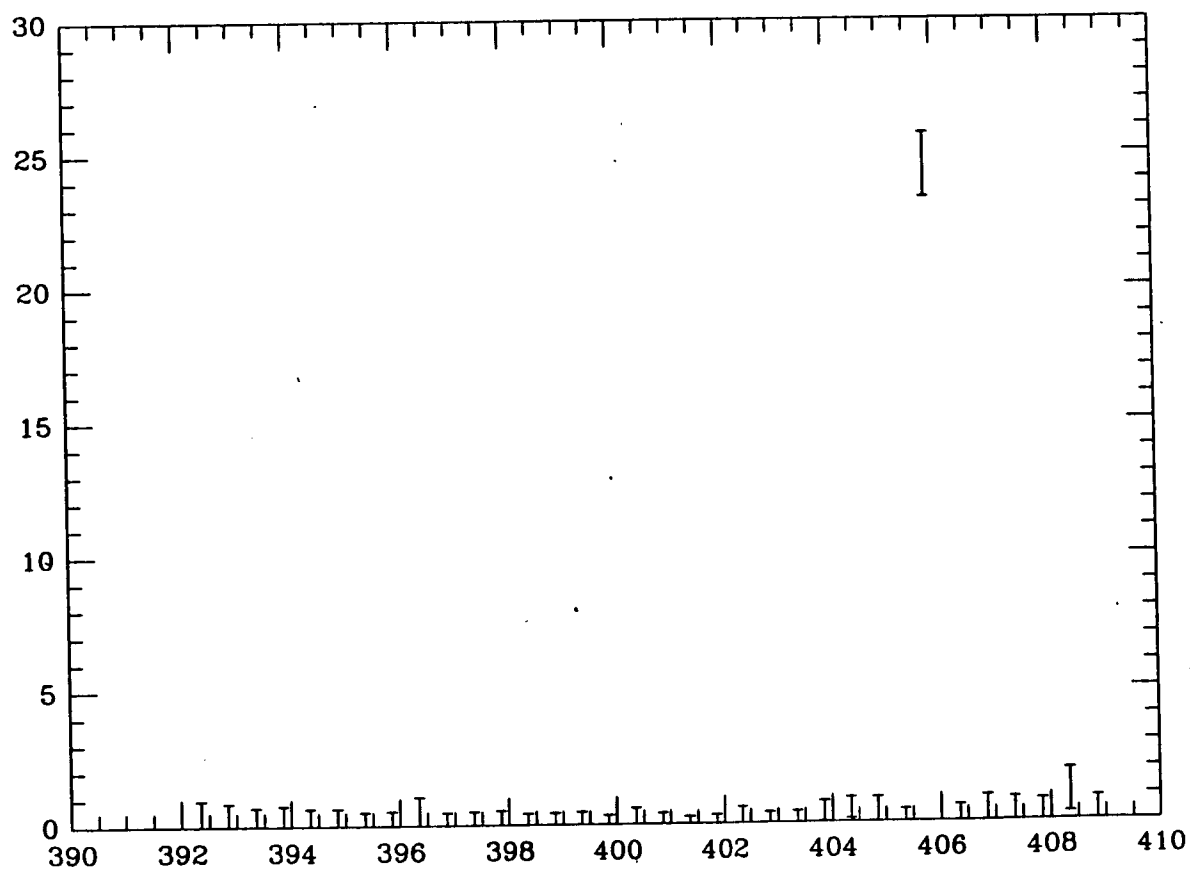
error box eliminated all but 5 of the A-3 position diamonds (Griffiths et al 1979; also Griffiths private communication), and was neatly centered on the dM3e pair LDS 131. The combined error boxes covered an area of about 10^{-3} square degrees. If one also required the source to fall within the A-1 catalog source identified as H0449-55 (Wood et al. 1984), one eliminated all of the A-3 error diamonds save the one with LDS 131 on its edge. The combined error boxes would then cover an area of about 2×10^{-4} square degrees. From Joy and Abt (1974) and Allen (1973), one estimates a space density of dMe-dKe stars of about 0.0394 pc^{-3}. We find the expected number of dMe-dKe stars within 30 pc to fall within the position limits by chance to be about 7×10^{-5}, ignoring the A-1 position limits; and 1×10^{-5}, including them; implying the probability of serendipitously finding one or more dMe-dKe systems within the position limits of less than 0.01%.

Also, as mentioned in the overview, the region around LDS 131 has been observed both by the EXOSAT CMA, with a 2°x2° field of view, and the Einstein Observatory IPC, with a 1°x1° field of view. Not only was LDS 131 the brightest X-ray source in either field of view, but it was also the only one detected within the A-2 99% confidence position limits. Of course, simply because a quiescent X-ray source falls very near a small position error box of a bright transient does not prove it is the source of the bright event; witness the case of the bright OSO-8 transient described in §5.C, where it was probably not physically reasonable to identify the event with the X-ray emitting dK star found just outside the transient error box. However, we find the position constraints for H0449-55 to be quite strong and the identification with a bright stellar flare to be physically

reasonable.

iii. Data from the Bright Flare: Inferring Physical Parameters

HO449-55 was at high Ecliptic latitude (-76.3°), and so was visible by the scanning HEAO 1 A-2 detectors for about 18 days per 6 month pass. In Figure 5.1, we display the 18 day light-curve for the pass containing the bright flare. The data were summed A-2 HED3 and MED 1.5° rates, averaged over twelve hours. The flux was consistent with zero save during the 12 hours centered on the flare on D405.85, when the time-averaged flux rose to roughly 25 cts-s^{-1}. The flux was measured by A-2 to be consistent with zero during the passes 6 months before and after the bright flare. However, the softer bandpass, larger area A-1 instruments measured a weak flux during the ~4 days that LDS 131 was in the center of their fields of view, around D.O.Y. 1977 400 (Wood et al. 1984; P. Hertz private communication). This A-1 flux of ~0.4 millicrabs, 0.15-10 keV, was significantly higher than extrapolations to higher energies from the Einstein and EXOSAT observations described later. If this flux was indeed associated with the cool dwarf pair LDS 131, it suggested a light curve similar to those shown by Ambruster, Snyder, and Wood (1984) for days-long, low level soft X-ray activity around the times of bright stellar flares from EV Lac and EQ Vir. One is struck by the image of a particularly large active stellar active region (or 'star-spot'), giving rise to both enhanced quiescent X-ray flux and the large flare.

In Figure 3.1.e we have displayed the A-2 light curve of just the three hours containing the bright flare. We noted a sharp rise from a quiescent level of less than 2.5 HED3 cts-s^{-1}, to 62 cts-s^{-1} 32

226

Figure 5.2 Two plots of HED3 spectrum, summed over both layers and both 40.96 s time intervals available during the first, brightest, pass. The first plot shows the raw (uninverted) PHA spectrum, in cts-cm^{-2}-s^{-1}-kev^{-1}, as a function of energy in keV, to exhibit the iron line feature at 6.8 keV. The second shows the inverted photon spectrum, assuming the best-fit spectrum, in photons-kev^{-1}.
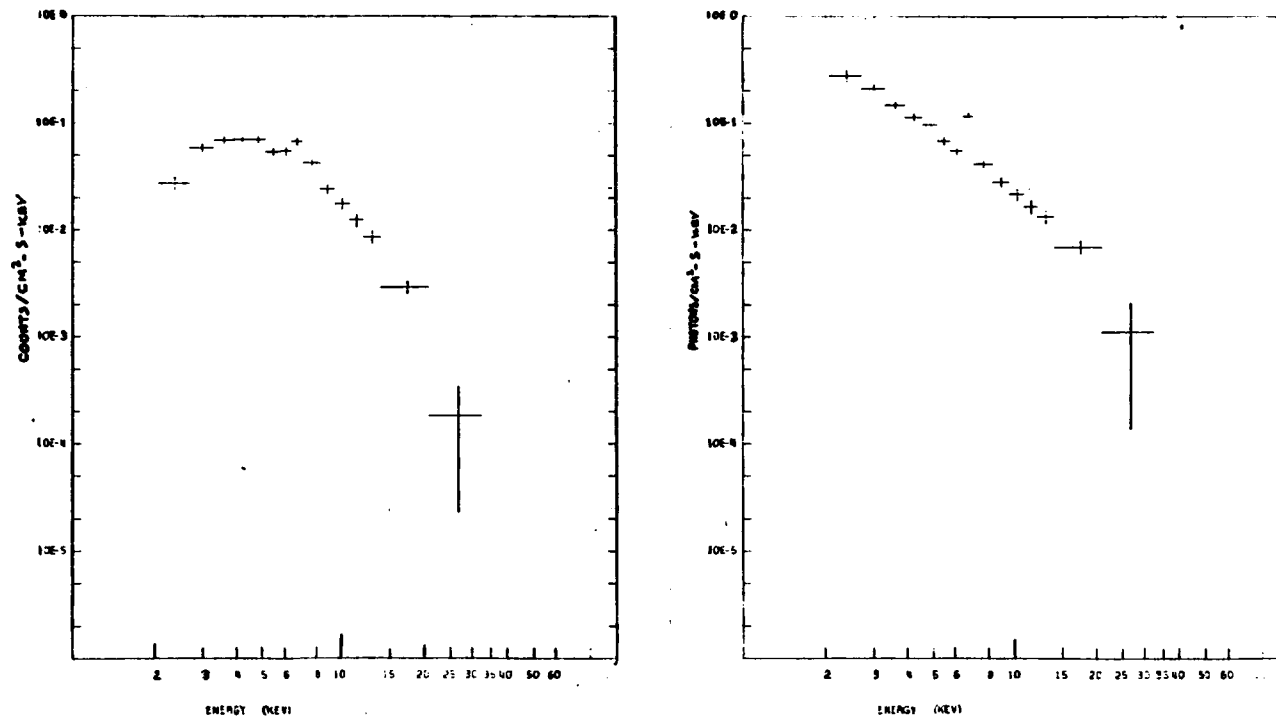
minutes later, implying an exponential rise time of 10 minutes or less. It was interesting that the flux measured during that first brightest pass was also still increasing at about an exponential rise time of 7-10 minutes, implying that the flare may not have reached its peak. The subsequent scans exhibited a slower decay, with a time constant of about 40 minutes.

We first consider the spectra from just the first, brightest, pass. As Kaluzienski et al. (1978b) pointed out, the overall spectrum was well-fit by an optically thin thermal bremsstrahlung model, with a clear Fe line feature visible at 6.8±0.1 keV. To demonstrate the significance of the iron line, we added together all three fields of view during which the flare was visible in the two detectors with the highest signal-to-noise at the energy of the Fe line. As Figure 5.2 demonstrates, the line feature was visible in the raw data. A minimum χ^2 fit to a simple thin thermal bremsstrahlung model (exponential modified by a Gaunt factor and absorption) gave a χ^2 of 25.1 for HED3, and 12.8 for HED2. When two parameters describing the intensity and position of the line feature were added (the line width was held constant at roughly the resolution of the detectors), χ^2 dropped to 12.8 for HED3, and 8.2 for HED2. Both indicated a line at 6.8 keV, with an emission width of 0.8±0.3 keV, which is consistent with predictions for line strengths predicted from (solar abundance) thermal plasmas with kT~11.5 keV from Raymond and Smith (1977). The most stringent limits on low energy absorption came from fits to the MED and HED2 detectors, which had the highest quantum efficiencies below a few keV. Combining the limits from fits to the two detectors, we found a 90% upper limit on N_H of $<3 \times 10^{21}$ cm^2, certainly consistent

Figure 5.3 We plotted three 90% confidence contours of thin thermal bremmstrahlung temperature in keV versus emission measure ($n_e^2 V$) in units of 4.05×10^{54} cm^{-3}. Each contour corresponds to a different ~30 s time interval during the first brightest scan over the flaring source. For T1 and T2 we combined data from the HED3 and HED2 data from the 3°x3° fields of view; for T3 we used data from the 3°x3° field of view of HED1, the offset detector.

TEMPERATURE IN KEV

EMISSION MEASURE IN UNITS OF 4.05×10^{54} CM^{-3}
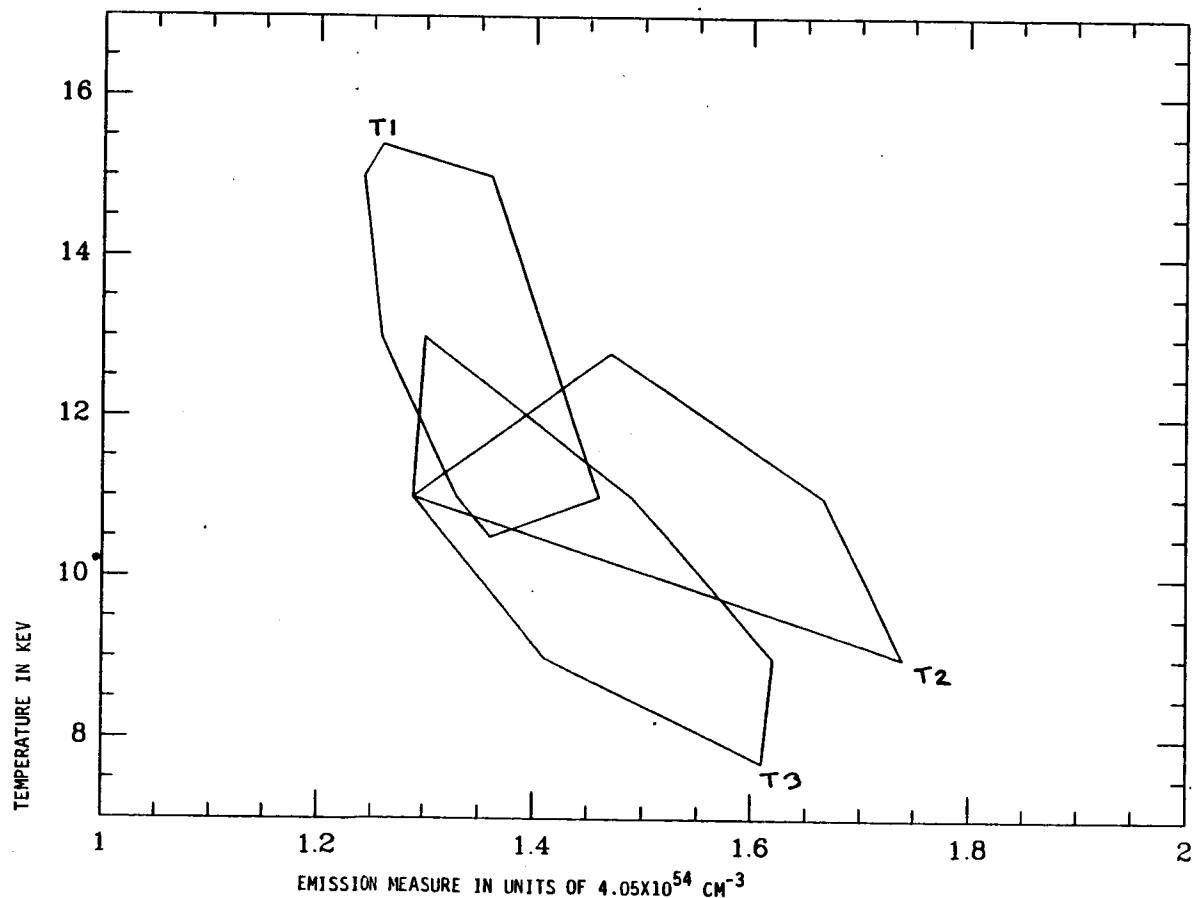
with an estimate of ~1 atom per cm^3 out to 10 pc.

In Figure 5.3, we show the results of fits to the spectra at three different times during this brightest scan, in three 90% confidence contours of flare emission measure versus temperature. We were able to obtain PHA spectra from all 4 detectors (HED3, MED, HED2, and HED1), covering three (disjoint) 41 s intervals (T1, T2, and T3), as the detectors scanned over the source. The light curve indicated that the flux was increasing during the ~90 s the source was in the combined fields of view of the offset and co-aligned detectors, so it is interesting to see whether the temperature or emission measure may have changed as well. We used only the 3°x3° fields of view, which not only had high signal to noise, but did not contain data from overlapping times. The first contour is from combined HED3 (both layers) and HED2 (top layer) at time 'T1' (~20h24.3-24.6m UT); the second from the same detector fields of view at time 'T2' (~20h24.6-24.9m UT); while the third is from the 3° field of view of the offset detector HED1 at time T3 (~20h24.9-25.2m UT). We find, during the 100 s of this brightest pass, the best fit temperatures dropped from kT~13 keV at T1, to ~11 keV at T2, and ~10 keV at T3; while the corresponding best-fit emission measures ($n_e^2 V$) increased slightly from ~5x10^{54} to 6x10^{54} cm^{-3} (for a distance of 10 pc). However all three 90% confidence contours were consistent with a constant temperature of ~11.5±0.5 keV. This is in contrast to what one expects from simple thermal models of flares, where the temperature continues to increase at least as long as the flare intensity increases (e.g. Batchelor et al. 1985 on thermal models). Both the luminosity and emission measure were closer to values more frequently observed from

Figure 5.4 To the three 90% confidence contours of temperature versus emission measure of the brightest
scan from the previous figure, we have added 90% confidence contours, of the same spectral parameters, for
the subsequent two fainter scans (~32 and 64 minutes later). For these fainter scans we used only HED3 data
(from both fields of view). The stars indicate the best-fit temperatures and emission measures.
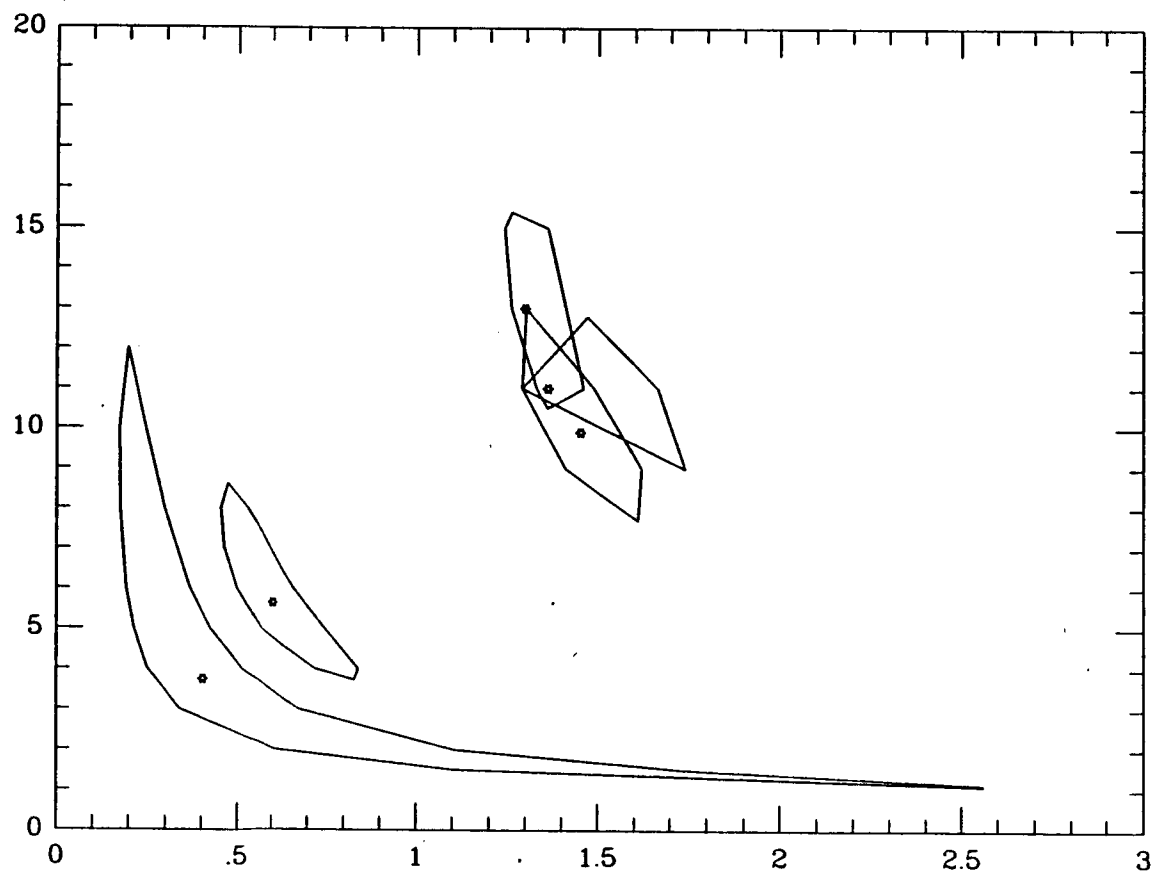
RS CVn-type flares, rather than those from cool dwarf stars.

In Figure 5.4 we compared the temperature and emission measure of the flare during this brightest pass with 90% confidence contours of the spectrum of the two subsequent passes ~32 and ~64 minutes later. (The flux dropped by roughly a factor of 2 each time.) The PHA data were from the HED3 detector, which was on during all three passes. The best-fit temperatures and emission measures fell at a rate roughly the same as the decay rate of the X-ray flux.

For understanding the physical properties of stellar flares, it is reasonable to compare them to flares observed from the active dwarf star closest to us - that is, to flares from the sun. Solar flares have been observed in a bewildering variety of sizes, shapes, and temperatures at all wavelengths from radio to hard gamma-ray; detections of energetic particles have also been correlated with these observations. Recently a delineation into two rough classes of flares has been found to be useful: 'impulsive' flares exhibit <10 keV X-ray flux lasting for an hour or less, associated with >10 keV X-ray emission and microwave emission lasting for less than about 10 minutes, with little or no coronal mass and energetic particles ejected, and apparently occuring on small, low coronal magnetic loops ($<10^9$ cm on the sun); while 'gradual' events are probably associated with coronal mass ejections, with filament eruption perhaps leading to very large loops high in the corona ($>10^9$ cm for the sun), with hard X-ray emission lasting for over ~10 minutes, and <10 keV X-ray emission lasting for over an hour (Sturrock 1986).

Applying models based on the sun to more distant stars, with very different masses, temperatures, radii, suface gravities, and rotation

232

rates, is not straightforward. One obvious difference is that one cannot directly image the structure of stellar coronae, and so must infer the geography of the outer atmosphere from indirect evidence, including photometry and variations in optical and ultraviolet line intensity, or X-ray flux, with time (Bopp and Espenak 1977; Linsky 1980; Linsky et al. 1982; Schrijver 1985); and high resolution spectral work such as mapping of magnetic fields via measurements of Zeeman splitting (Saar and Linsky 1985). During flares, the rise and decay times in differing wave bands or the ratios of key lines formed at different temperatures can be used, with some simple models, to infer temperatures, pressures, and densities as functions of loop geomtries. For this bright flare from LDS 131, none of these methods were readily available, as we were hampered by both an interrupted light curve, and no simultaneous observations at other wavelengths (although quality of X-ray spectra is very good). Therefore we relied on limits from some very simple models, to match the limitations of our data.

In the models used by Batchelor et al. (1985) to describe hard X-ray and microwave emission from 'impulsive' solar flares, the top a coronal magnetic loop is heated, by some unspecified process of annihilation of magnetic flux, possibly through reconnection. The thermal electrons propogate down along the magnetic field lines, in a 'conduction front' traveling at roughly the ion sound speed, to the footpoints of the loop in the denser chromosphere. Cooler material is boiled up from this denser region, still confined by the magnetic field, and fills the whole loop. The X-rays are radiated by thermal bremsstrahlung from this optically thin plasma. In this scenario, the

X-ray rise time is roughly the height of the loop (or loop 'half-length') divided by the ion sound speed, while some other scenarios suggest the Alfven speed to be more appropriate. However, this picture does have grosser features generally in agreement with many other scenarios, including the hardest X-ray emission occuring at the greatest height, and the necessity of continual energy input, from some kind of magnetic field annhilation near the top of the loop, throughout the duration of the flare (Stucker 1986). Since scenarios detailing filament eruption and coronal mass ejection appear more complicated, we shall not consider them here.

From the light curve in Figure 3.1.e, we see the total rise time of this bright X-ray flare must be less than ~30 minutes. Since the ion sound speed, $\sim(kT_e/m_i)^{\frac{1}{2}}$, is ~ 10^8 cm-s^{-1} for kT_e ~ 11.5 keV, we find an upper limit to the loop half-length of ~2×10^{11} cm (or less than several stellar radii). A second crude constraint on the total volume 'V' of the emitting region comes from combining the reasonable assumption that the ratio of thermal energy density to that of the magnetic field is less than one (i.e. this is a low 'β' plasma, with $\beta = (n_e kT)/(B^2/8\pi)$, where n_e is the electron density and B the magnetic field strength), together with the looser assumption that, since the flare was powered by magnetic field annhilation, the total energy emitted in the flare was roughly equal to the energy originally stored in the magnetic field: $E \sim 10^{35}$ ergs ~ $V \times (B^2/8\pi)$. Since we have found the emission measure to be ~5×10^{54} cm^{-3} for a distance of 10 pc, one can solve for an upper limit on the volume. We find $V < 3 \times 10^{30}$ cm^3, which in turn implies an average B > 700 G. This value of the magnetic field is certainly consistent with measurements of magnetic

field strengths in the active regions of stars (Saar and Linsky

1985; Saar, Linsky, and Beckers 1986) and in intense impulsive solar

flares (see, for example, Batchelor et al 1985). The electron density

was inferred to be $n_e > 10^{12}$ cm^{-3}, only slightly higher than that

observed from similar stellar flares (see, for example, a 10^{34} erg

event with similar rise and decay times observed by EXOSAT from EQ

Peg, a dM3.7e star, in Pallavicini, Kundu, and Jackson 1985). In

other words, we found this bright stellar flare observed with HEAO 1

A-2 appeared only slightly larger, denser, and hotter, but otherwise

very similar, to those observed (with high spatial resolution

instruments) from other cool dwarf stars, and so the identification of

this event as a flare from the dMe pair LDS 131 appears physically

reasonable.

iv. Brief Summary of Einstein, Exosat, and IUE Observations

The soft X-ray telescope of the Einstein Observatory pointed in

the direction of HO449-55/LDS 131, with the Imaging Proportional

Counter at its focus, for about 1.1×10^4 s on 1980 Mar 8,

18:29:8.2 U.T., through 1980 Mar 9, 10:42:37.17 U.T. The Einstein IPC

had about a 1°x1° field of view and spatial resolution of 30

arcseconds, which was insufficient to resolve the two proposed

sources, LDS 131 'a' and 'b', or stars 'S' and 'T' of Griffiths et al.

(1979). The band pass of the HEAO B Einstein Observatory telescope

with the IPC was about 0.15-3 keV, with moderate spectral

resolution. As mentioned earlier in this chapter, a soft X-ray source

was observed at the position of the two stars comprising LDS 131, with

a flux of ~0.4 ct-s^{-1}, or ~10^{-11} ergs-cm^{-2}-s^{-1}, implying a combined

quiescent X-ray luminosity of ~10^{29} ergs-s^{-1} and a ratio of X-ray to

Figure 5.5 The X-ray light curve of LDS 131, from the Einstein Observatory IPC observation, in IPC cts-s^{-1} versus time in 10^3 s, for hard and soft rates.

236
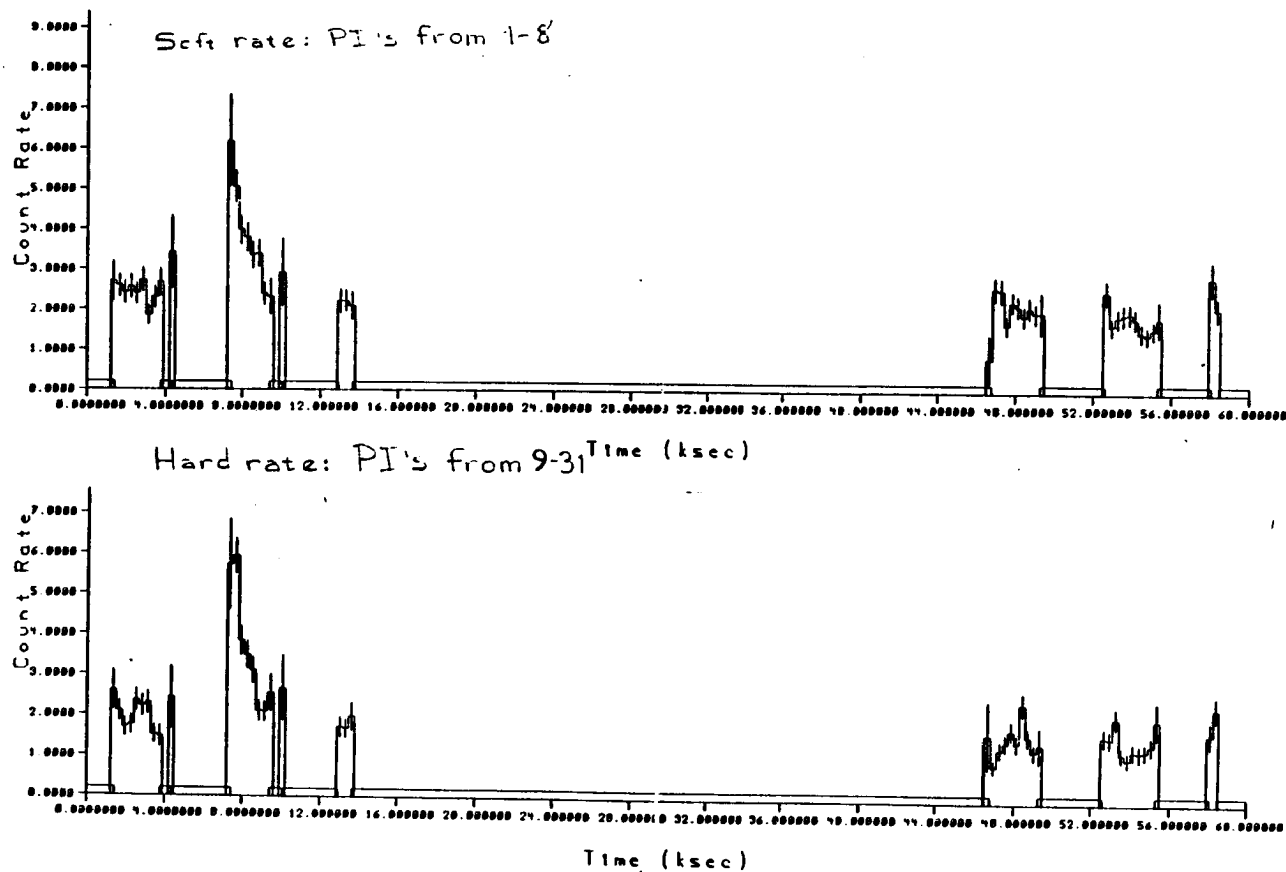
bolometric luminosity of between 3×10^{-4} and 5×10^{-4}, depending on how one partitions the X-ray emission between the two dM3e stars. This implies a high rotation rate, with a period of around 3-7 days (K. A. Jensen, J. H. Swank, private communication).

In Figure 5.5, we present a light curve from this observation. The break in the time axis represents a data gap of $\sim3.3\times10^{4}$ s. We note a small flare (on Mar 8, 1980 20:42:30 UT), with a peak flux about 3 times the quiesent rate, or with $L_x \sim 4\times10^{29}$ ergs-s^{-1}, and a total energy of $\sim3\times10^{31}$ ergs. Using the moderate spectral resolution of the IPC instrument, we found the spectrum to be consistent with the two temperature (0.2 keV, 1.5 keV) model used by Golub (1983). Studies using higher resolution X-ray data have implied the spectra are more realistically modelled by magnetic loops of plasma with the temperature varying continuously along its length (Swank and Johnson 1981; Schmitt and Stajno 1985; Schrijver 1985 and references therein). However if we interpret the temperature and emission measure as rough indicators of the amount of higher and lower temperature material, we found we could interpret the flare with an increase in the emission measure of the hotter (~1.5 keV) portion, consistent with other measurements of stellar coronae (Golub 1983; Schmitt and Stajno 1985).

The source was also observed by the European X-ray Observatory (EXOSAT) telescope on January 13, 1986, with the CMA (behind a thin lexan filter) at its focus The observation was originally intended to be coincident with an IUE observation of the dMe flare, but a high particle flux in the vicinity of EXOSAT forced the X-ray observation later, overlapping only about an hour of the IUE observation. From

Figure 5.6 The EXOSAT CMA (with thin lexan filter) light curve, in CMA cts-s^{-1} versus time in hours (of January 13 1986) presented with two different time binnings. In the top we used 30 minute bins; while in the bottom we used time bins of 5. minutes.

238
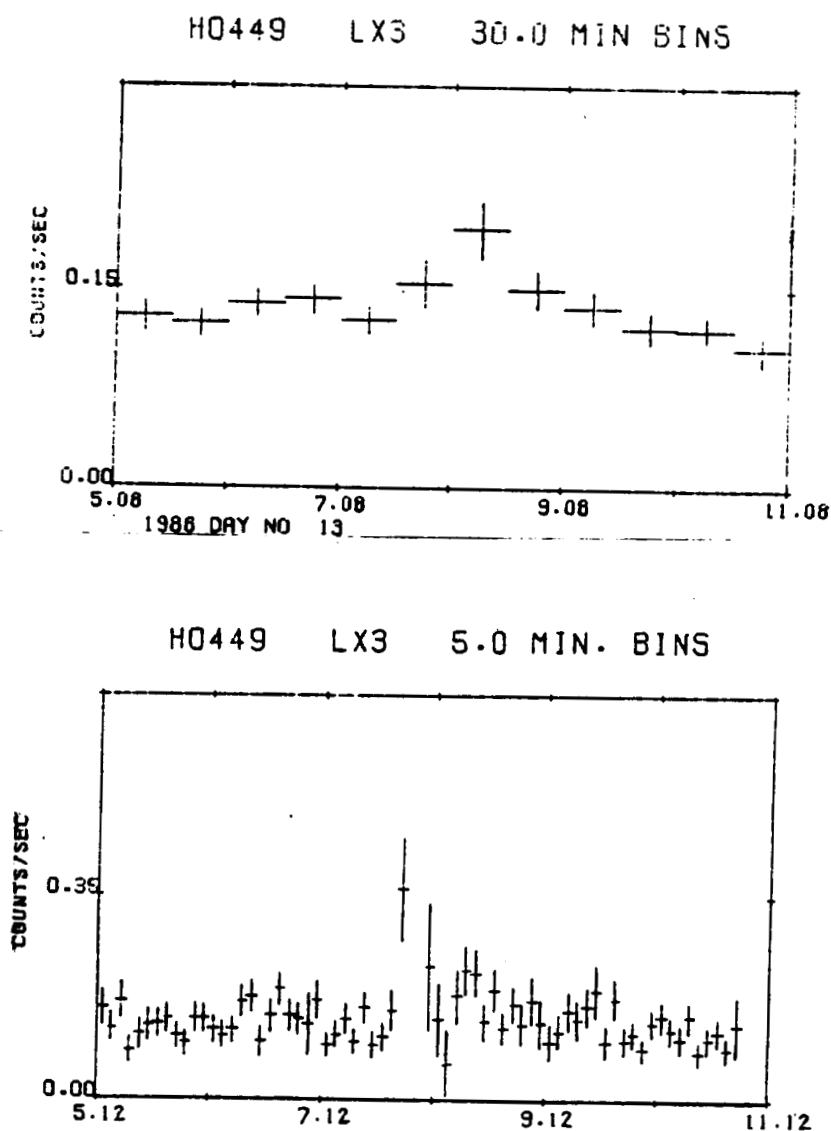
the 0.2-1.5 keV spectrum, we calculated that 0.4 IPC cts-s^{-1} were

equivalent to about 0.1 CMA cts-s^{-1}, in the 0.1-2.0 keV band of the

EXOSAT telescope for the CMA with a thin lexan filter. From Figure

5.6 one sees that this is approximately what was observed, but that

the source(s) again showed indications of variability, including a

faint gradual flare lasting for about an hour, with a peak luminosity

only about 30% higher than the quiescent flux, or ~ 4×10^{29} ergs-s^{-1}.

The two stars were easily resolved in the observation by the

International Ultraviolet Explorer, which preceded the EXOSAT

observation by several hours. The stars were aligned along the long

slit of the IUE spectrograph, but tilted at an angle of 41° to the

main axis, so that their spectra were not only dispersed by the 8.5"

seperation of the pair, but the positions of the wavelengths were

slightly offset from each other. We took three long wavelength

exposures, and three short wavelength exposures, each about 30 and 90.

minutes long, respectively. The line fluxes of LDS 131b (the fainter

star) appeared slightly brighter, on average, than those from

LDS 131b; for example, the average flux in the bright Mg II 2800 Å

blend was ~10^{-12} ergs-cm^{-2}-s^{-1} for LDS 131b, but

~4×10^{-13} ergs-cm^{-2}-s^{-1} for LDS 131a, with an uncertainty of nearly

25%. (The equivalent surface fluxes were calculated to be ~5×10^{5} and

2×10^{5}, respectively, following Linsky et al. 1982.) However we noted

that the emission from LDS 131a decreased by nearly an order of

magnitude during the ~6 hour duration of the US2 observation, as we

illustrate with Figure 5.7. The spectra were noisy, but certainly

consistent with those of other active cool dwarf stars, as compiled in

Linsky et al. (1982).

Figure 5.7 The 20 minute IUE long wavelength (LWP) spectra for LDS 131a (top) and LDS 131b (bottom), showing the varying intensity of the prominent Mg II blend at 2800 Å over the course of the 6 hour observation. The first and last exposures in each triplet have been offset in the Y-axis by -10^{-13} and $+10^{-13}$ ergs-cm^{-2}-s^{-1}, respectively, so that the exposures are time-ordered from the bottom.

240
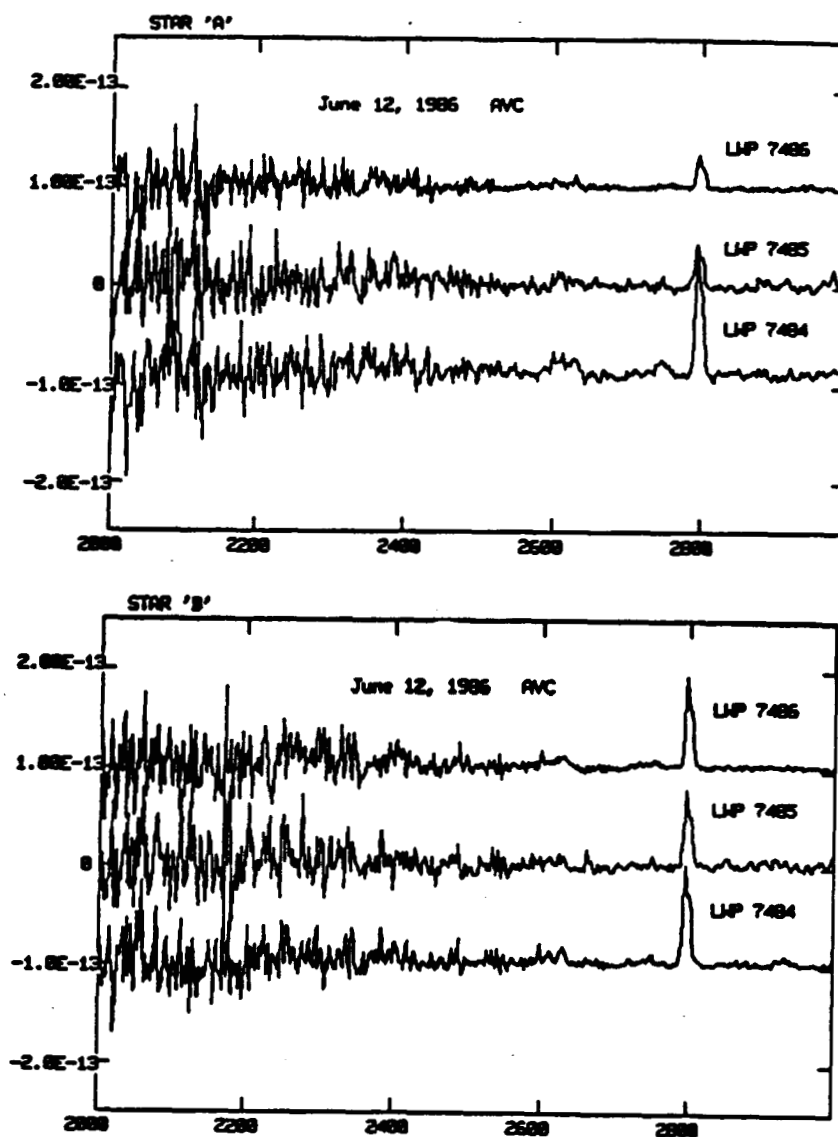
C. The Bright 6-Nov-77 Event Observed with OSO-8

On November 6, 1977, from 8:18:20 to 8:36:40 UT, the Goddard and Wisconsin experiments on board the OSO 8 satellite detected an intense X-ray event, from 1950.0 R.A. and Dec. $20^h 14^m 29^s$, $30° 53' 24"$ (Serlemitsos, Bunner, and Swank 1979). At peak, it was nearly twice as bright as the Crab, with a peak flux of $\sim 5 \times 10^{-8}$ ergs-cm^{-2}-s^{-1}, and a heavily absorbed spectrum. The source was seen this once, but never detected again in X-rays. We illustrate this in Figure 5.8 with three light curves, in cts-cm^{-2}-s^{-1} versus D.O.Y. 1975, from OSO-8 observations of the source region. The flux was consistent with zero everywhere save during the event itself.

The source region was also observed with the Einstein Observatory IPC. In Figure 5.9 we plot the positions of the three REV 1 IPC sources detected in its 1°x1° field of view during the observation. On the field, we have superposed 99% confidence limits on positions obtained from fitting the observed count rates, with all scans summed, to the response of the Goddard detector to a point source. The best-fit position had a reduced χ^2 of 0.9, for 49 degrees of freedom. The brightest IPC source, with a flux of ~ 0.04 IPC cts-s^{-1}, also fell closest to the error box, but a fit to the OSO 8 data assuming this position increased the reduced χ^2 to 2.0 (for 49 degrees of freedom). Also, the source was identified as a nearby K dwarf (Connors and Takalo 1985; Caillault et al. 1986), which is an unlikely source for such a heavily absorbed transient event. We estimated the probabilty of a dM-dK star within 30 pc falling that close to the position of the source to be about 8%, and concluded that

Figure 5.8 A long term light curve from OSO 8 data of the bright transient on November 6, 1977, in cts-cm^{-2}-s^{-1} versus days. An arrow marks the abrupt increase due to the transient.
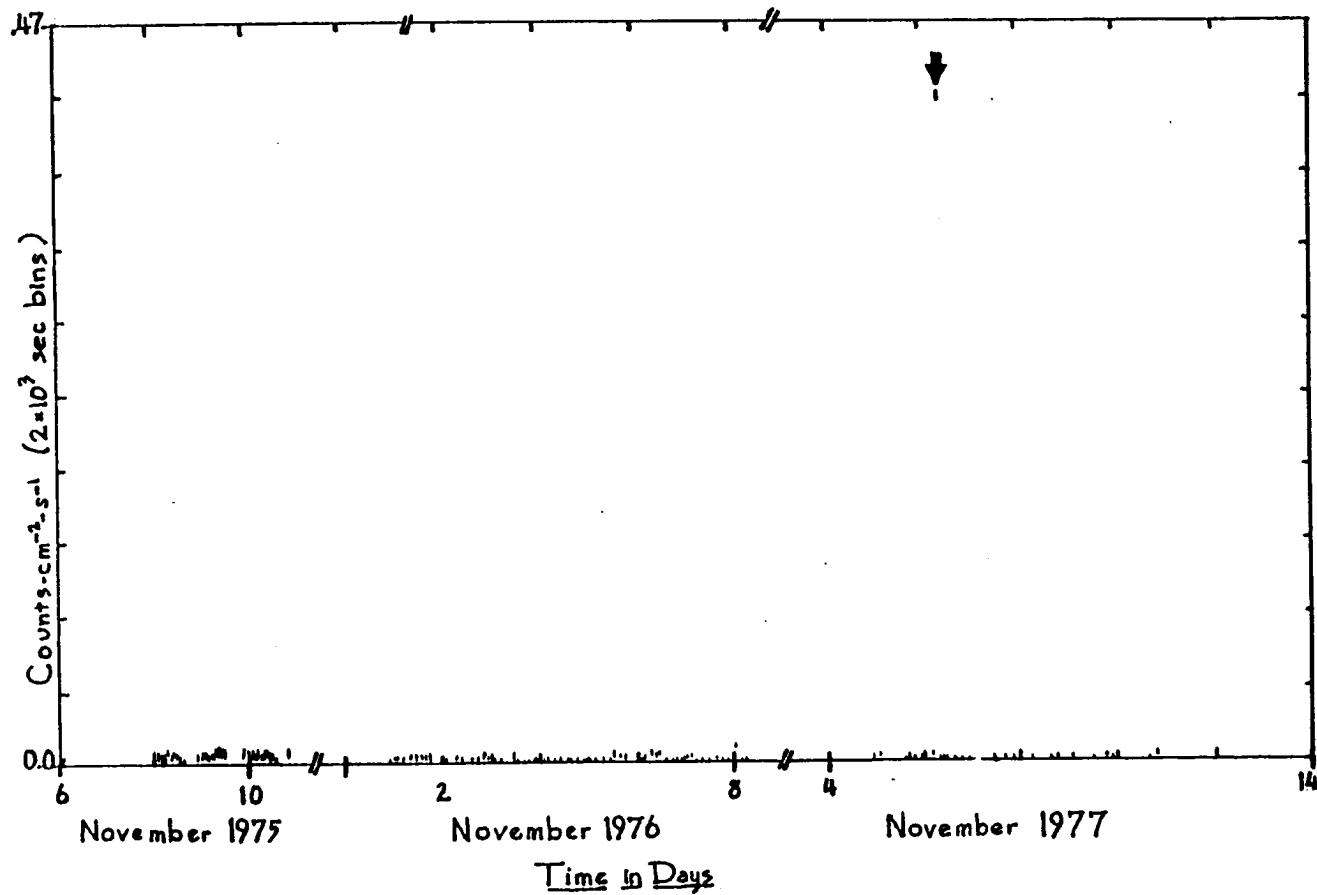
the association was serendipitous. We therefore obtained an upper limit on quiescent flux from the source to be $< 10^{-13}$ ergs-cm^{-2}-s^{-1}, in the 0.15-3 keV band of the Einstein IPC. Also, a search of the Harvard Plate Stacks uncovered no evidence of significant optical variability. Interestingly, there do seem to be two sources from the IRAS catalog within the transient error box (Hugh Johnson private communication).

Aside from the very high ratio of peak-to-quiescent flux ($>5 \times 10^5$), the event was also unusual in its temporal characteristics. In Figure 5.10 we showed the light curve of the event itself, which was highly variables, characterized by a ~2 minute 'precursor' and dramatic ~10 s 'spikes' in a roughly Gaussian envelope. However, this event was observed by a detector that spun with a period of about 10 s, so the 18 minute event was only viewed in 'snapshots' of ~2.8 s duration every ~10 s rotation. This limited the efficacy of timing analysis. Although to the eye the light curve looks suggestively like that of the intense flares from LMC X-4, during which 13.5 s pulsations were found (see especially the variable light curves at the end of Chapter 4), when we Fourier transformed the light curve, which was available in time bins as short as 160 ms, we found mainly aliases of the 10 s rotation period. A cross correlation analysis of the 160 ms data found no characteristic time, and in particular no evidence of <1 s variability.

No spectral information was available from the Goddard OSO-8 proportional counter experiment, but information from the University of Wisconsin experiment showed the average spectrum to be well fit by a thin thermal bremsstrahlung model with a temperature of ~12.3 keV.

Figure 5.9 A plot of the region of sky around the 6-Nov-77 OSO 8 transient, in 1950.0 R.A. and Dec. We show the 99% confidence position limits from OSO-8 data of the transient itself. The small stars mark positions of the IPC sources; the large stars indicate IRAS catalog sources.

244
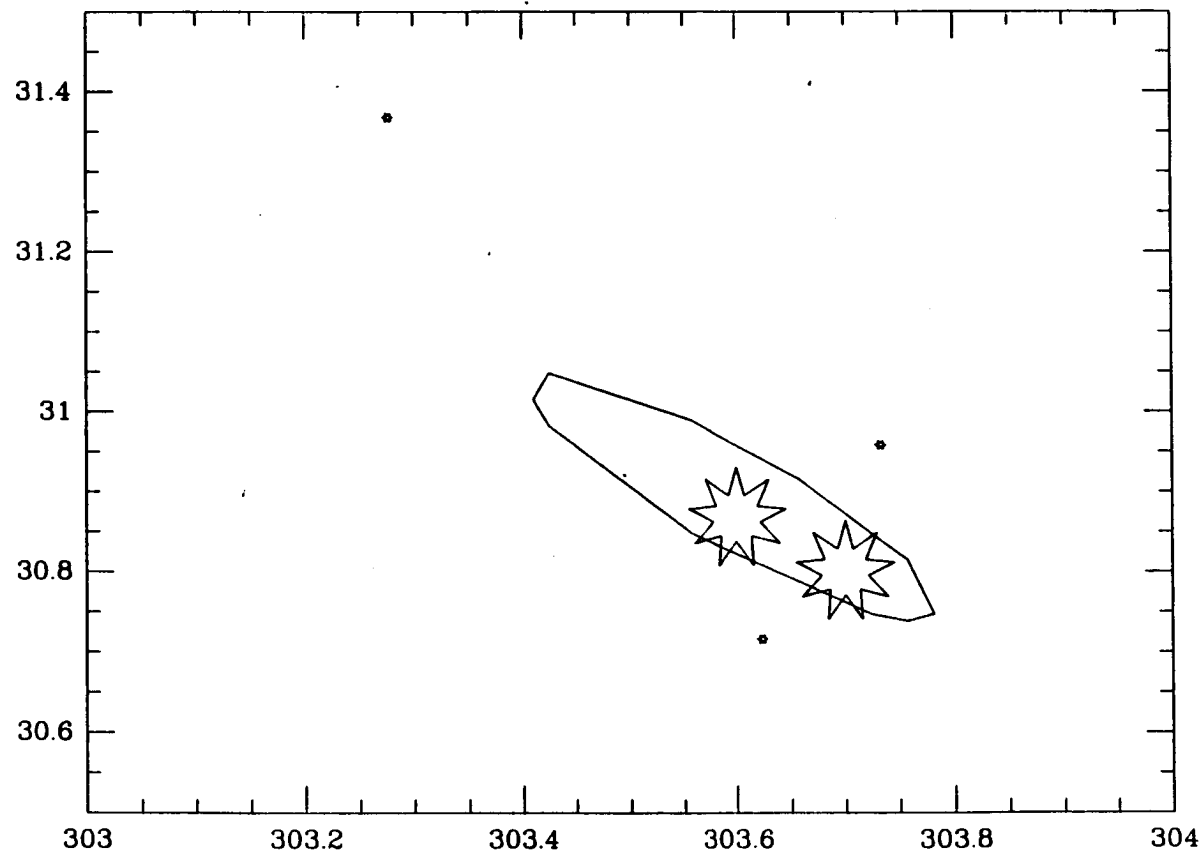
Figure 5.10 The light curve of the bright transient event, in OSO 8 cts-cm^{-2}-s^{-1} versus time in seconds. Each point is from ~2.88 s of data out of each 10 s scan.

OSO-8 6 NOV 77 FAST TRANSIENT: COUNTS VS TIME (SEC)

245
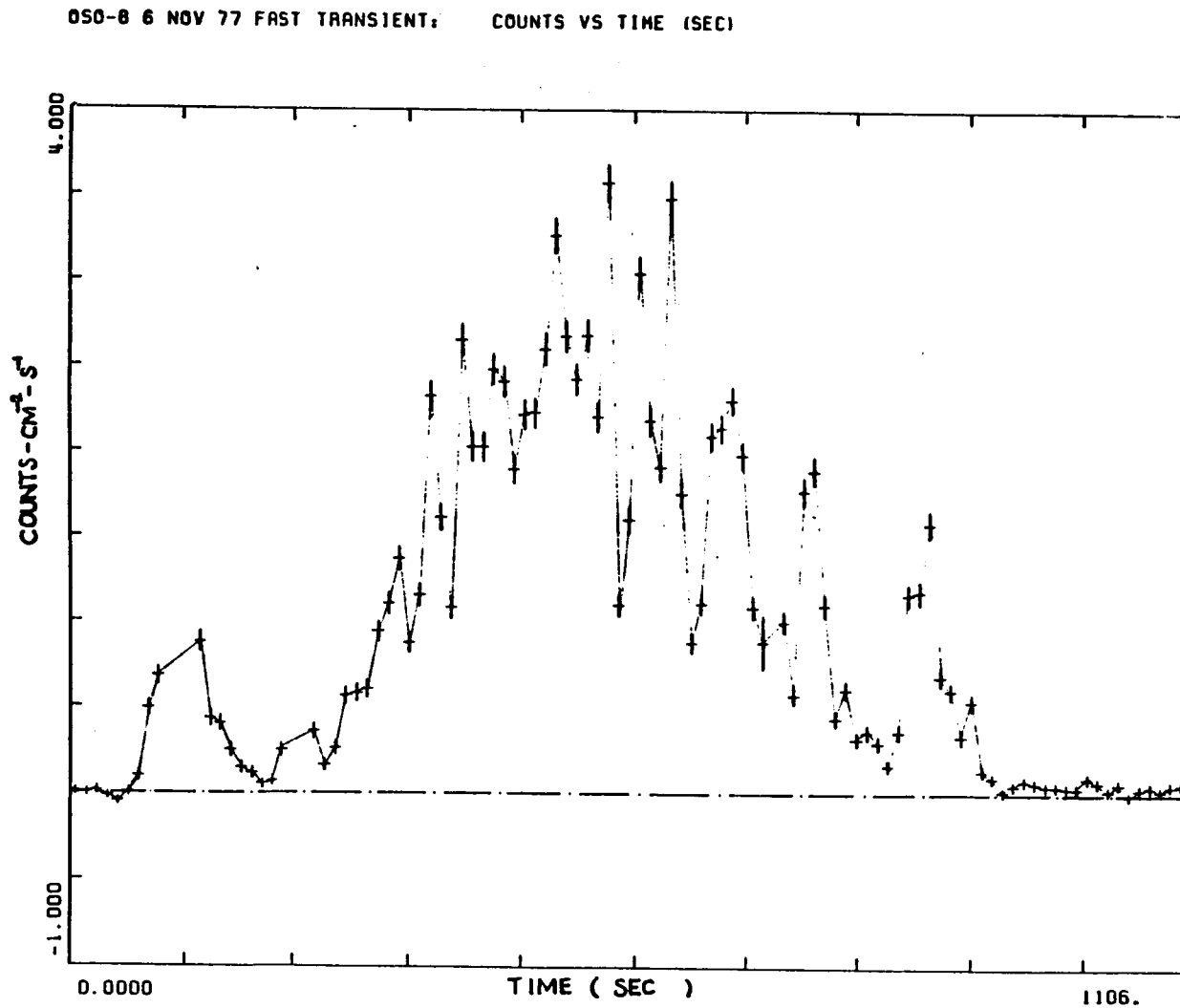
The spectrum is reproduced in Figure 5.11, from Serlemitsos, Bunner, and Swank 1979, and Bunner private communication. Bunner also noted the temperature fell from ~20 to 4 keV during the event, with heavy absorbtion (N_H ~ 2.3×10^{22} cm^{-2}) remaining constant throughout. However, he found "no particular difference between the spectra of intensity peaks and minima". The direction of the event happens to lie at the intersection of the Cygnus superbubble with a region of dense intersellar clouds called the Cygnus rift, where the average extinction is E(B-V) ~0.4 kpc^{-1}, but the material highly clumped into dense clouds (Lucke 1978). We therefore found it plausible to assume the absorption to have been interstellar in nature, implying a distance of between 2 to 7 kpc, a peak luminosity of $3 \times 10^{37-38}$ ergs-s^{-1}, and an upper limit on quiescent luminosity of $< 10^{32}$ ergs-s^{-1}.

The properties of this event do not match those of any other identified transient, although the apparent high luminosity suggests an origin on a compact object. The light curve was highly unusual. Although repeated sub-bursts in classic gamma-ray bursts tend to soften from event to event, they very rarely repeat for more than a few minutes, and the spectra are harder than is possible to fit with a thermal model in this energy range, particularly at the onset; they also show significant hard-to soft spectral variations within each peak (see Connors, Hueter, and Serlemitsos 1988). Soft gamma-ray repeaters (Atteia et al. 1987) are even less likely to exhibit repeated peaks this closely spaced in an event lasting tens of minutes; also, they exhibit very rapid variablity on time-scales as short as milliseconds. The dearth of quiescent X-ray flux appears to

Figure 5.11 The average spectrum of the event, from the Wisconsin experiment on OSO 8, taken from Serlemitsos, Bunner, and Swank (1979), and A. Bunner (private communication).
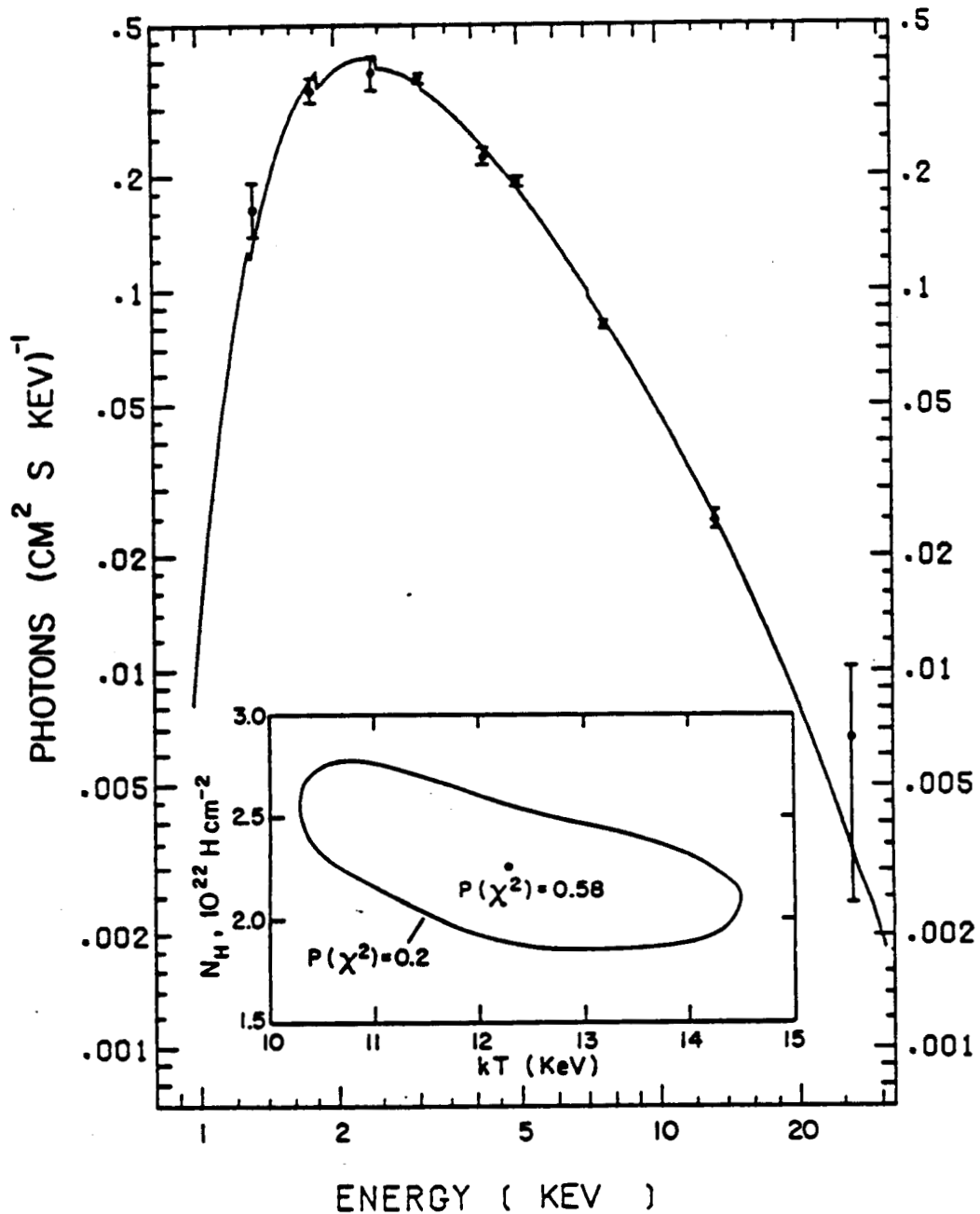
rule out an identification with a flare from a classic X-ray binary. Not only was the light curve very different from those observed from X-ray burst sources, but the spectrum was clearly not a black-body spectrum, or even a super-position of black-body spectra. The apparent high luminosity even suggests this event was dissimilar to the hard fast transients of Chapter 3, which we found constrained to be less than $\sim 10^{35}$ ergs-s^{-1}. The lack of quasi-periodic recurrence and stringent limits on quiescent flux also makes identification with a Be-neutron star binary questionable. We are left with the conclusion that there are rare types of transients that we do not yet understand, and until a similar event is detected from a region not heavily obscured by thick interstellar clouds, we are unlikely to be able to definitively identify the source population.

Chapter 6

Conclusions and Future Prospects

A. Summary

In the first chapter, we introduced the study of X-ray variability, and divided it into two kinds: an interuption of X-radiation from a source that was radiating continuously (as in X-ray eclipses); or a transient release of stored energy. Throughout this work, except in Chapter 4, we have dealt predominantly with the latter. We have concentrated on fast transient activity from sources that are, for the most part, X-ray dark (quiescent luminosities $< 10^{30}$ ergs-s^{-1}), with X-ray emission detectable mainly during outburst or flare activity. When that rare event occurs, one can briefly discern some of the underlying physical properties of the emitting region.

These transient events encompassed quite a range of physical phenomena, from electromagnetic energy release in plasmas confined by ~ 1000 gauss magnetic fields in the atmospheres of stars less dense than the sun, to the release of nuclear or gravitational potential energy on the surface of a neutron star, moderated by fields of $\sim 10^{12}$ gauss. Below we sketch out the scenario of X-ray fast transient activity over the whole sky, as it has been presented in this thesis. We move from the least luminous events to the most luminous, therefore proceeding from nearby sources (< 100 pc) to those visible (above 10^{-10} ergs-cm^{-2}-s^{-1}) from distances of ~ 0.5 Mpc.

As we wrote at the beginning, the patterns we discerned are often

at the limits of detectability. When considering possible identifications of barely detectable events, we implicitly assumed that they were similar to events that had been observed previously with greater clarity. New phenomena could therefore have been misidentified. Many of the identifications we summarize below were based on statistical or plausibility arguments. Therefore at the end one is left with few strong statements (such as a reasonable measurement of all-sky X-ray flaring activity among cool dwarf stars), but many directions for future inquiry.

In the HEAO 1 A-2 all-sky survey described in Chapter 3, out of ~ 104 days ($\sim 2 \times 10^6$ 5.12 s intervals during which at least one out of four detectors was 'on'), we found 15 good events. We inferred 8 of them to be flares from cool dwarf stars with active coronae. Stellar flares have a low peak luminosity ($< 10^{32}$ ergs-s^{-1} 2-20 keV), but dMe-dKe stars have a high space density ($\sim$ 1 per 25 pc^3). The flare frequency goes (very roughly) as the inverse of the total flare energy, with a maximum energy of 10^{35} ergs (2-20 keV), and with roughly 10% of the total event energy emitted in X-rays. The spectra were well fit by unabsorbed, cooling, thin thermal bremsstrahlung models, with peak temperatures of $\sim 10^{6-8}$ K. Overall we saw these events to be distributed isotropically, consistent with a local origin, with a rate over the whole sky of something like 10^4 per year over the whole sky above our minimum flux level of 10^{-10} ergs-cm^{-2}-s^{-1}. This is equivalent to a time averaged total power of $\sim 5 \times 10^{36}$ ergs-s^{-1} released in 2-20 keV X-rays throughout the Galaxy.

Our case for the identification of so many events with stellar

flares was based on statistical arguments, and on the properties of the small number of flares observed in X-rays. One of the most prominent of these was described in some detail in Chapter 5. From the narrow A-2 position error box and the X-ray brightness of LDS 131 when observed with the Einstein Observatory IPC and EXOSAT CMA, we strongly confirmed the original identification from A-3 and A-4 data by Griffiths et al. (1979). From the time-scales, intensity, and spectra of its variable X-ray activity (and UV and optical activity), we briefly traced the geometries of the emitting regions. We compared our observations to those of other active coronae stars. Giampapa and Liebert (1986) have demonstrated the shortcomings of the current decriptions of stellar coronae, which feature an atmosphere decreasing in density with increasing height, confined by magnetic field loops, attached via the assumption of common boundary conditions to the surface (photosphere) of an older, spherically symmetric, model of a cool main sequence star. This empirical description, when coupled with calculations of an internal stellar dynamo, leads to a prediction of a cessation of magnetic activity in very dim, low mass, stars, that seems counter the activity that has been observed.

We now direct our attention further outward. In the Galaxy, we found this faint isotropic flickering of X-ray flares from ubiquitous dMe-dKe stars appeared to be superposed on a disk distribution of harder, more luminous, fast transient events, which we tentatively identified as outbursts from neutron star-Be star systems. (These are normally X-ray faint, $L_x < 10^{34}$ ergs-s^{-1}, until optical activity and the approach of the neutron star at periastron apparently allow mass accretion, triggering a sudden increase in X-ray luminosity, with

$L_X \sim 10^{35-37}$ ergs-s^{-1}.) We suggested that 5 of the HEAO 1 A-2 all-sky fast transients (those with harder spectra and near the Galactic plane) to be members of this class of rarely visible neutron star systems. We suggested the short term variablilty observed in some events may turn out to be evidence of pulsations. From very preliminary work mapping out small slices of the Galactic disk, we suggest there may be $\sim 10^3$ of these systems, contributing an overall time-averaged 2-20 keV X-ray luminosity to the Galaxy of at most 10^{37} ergs-s^{-1}.

But is this tentative identification really correct ? X-ray surveys of the Galactic plane with imaging instruments have not proposed this class of very hard, ~ few hour, X-ray transients. Warwick et al (1985), using EXOSAT data, and Koyama, Ikeuchi, and Tomisaka (1986), using TENMA data, simply did not see them; while Hertz and Grindlay (1984), considering Einstein 0.15-4.5 keV data, proposed instead that they had detected foreground CVs (which are often less luminous above 2 keV), and suggested that the CV number densities inferred from optically selected samples may have been underestimates by an order of magnitude. It is possible that the hard Galactic plane transients that we propose have spectra which are too hard or highly absorbed, or that the number density (<0.2 per square degree) is too low, to be detected by the Einstein IPC or EXOSAT CMA. There may be preliminary evidence from a more extensive GINGA survey of the Galactic plane supporting the Be-system hypothesis (Koyama et al 1988). If these systems are like closer neutron star-Be star systems, at least 50% should show evidence (pulsations) of magnetic fields of ~ 10^{12} gauss, leading to the interesting question

of what fraction of the total power pumped into cosmic rays over the whole Galaxy comes from these hypothetical ~10^3 spinning compact objects.

Among the events picked up by the A-2 fast transient survey, there are a few rarer events. One of these is the bright gamma-ray burst observed through the sides of the A-2 detectors. Only one X-ray counterpart to a gamma-ray burst was observed through the front of the HEAO 1 A-2 detectors, and since that was during a pointed manuever, it was not in data meeting the fast transient search criteria (Connors, Hueter, and Serlemitsos 1988). The burst, with a >30 keV fluence of 7×10^{-7} ergs-cm^{-2}, lasted for over a minute below 30 keV, had a 2-20 keV X-rays fluence on the order of $1-3\times10^{-7}$ ergs-cm^{-2}, and was over two orders of magnitude above our search threshold. We noted that although the HEAO 1.A-2 fast transient search had a threshold over two orders of magnitude lower than that using the A-4 experiment (fluences of 10^{-9} ergs-cm^{-2} vs 10^{-7} ergs-cm^{-2}), which was co-aligned with A-2 but had a much larger field of view, the A-4 experiment detected roughly an order of magnitude more gamma-ray bursts through the front of its detectors during the lifetime of the HEAO 1 satellite (Hueter 1987). In other words, we are already seeing across the Galaxy at fluences of ~ 10^{-8} ergs-cm^{-2}, implying the energy released in a single gamma-ray burst is something like 10^{38} ergs, and the 90% upper limit on the total rate throughout the Galaxy is less than 1300 per year. With an assumption of an ~ 8 yr recurrence time (Schaefer and Cline 1985), this implies a total Galactic source population of something like 10^4.

In Figure 6.1, we plot estimates of event rate per year above a

253

certain fluence as a function of that fluence, on a log-log scale, for fast transient events (<u>not</u> quiescent emission) from cool dwarf stars, RS CVn-type systems, Cataclysmic variables, and both X- and gamma-ray bursts. (We chose fluence (ergs-cm^{-2}) rather than flux (ergs-cm^{-2}-s^{-1}) because the probability of detecting an event, in many types of X-ray instruments, is more nearly proportional to the former than the latter. In the HEAO 1 A-2 fast transient search, with a flux threshold of ~10^{-10} ergs-cm^{-2}-s^{-1}, the minimum fluence for detecting X-ray flares from dMe-dKe stars was effectively just over 10^{-8} ergs-cm^{-2} (2-20 keV), while for the longer flares from RS CVn-type systems it was closer to 10^{-6} ergs-cm^{-2}.) The plot does not reflect our uncertainty in normalization of the rates of each type of event.

The curve for flares from dMe-dKe stars is probably the best-determined. We used the normalization determined in Chapter 3 and Appendix B, with an uncertainty of only about a factor of three, and assumed a scale height of ~300 pc (Allen 1973) and a maximum energy of ~10^{35} ergs (2-20 keV). The lack of turnover at low fluences reflects the intrinsic rate versus size spectrum of flares from each star. We then assumed that the rate of flares from the active subgiants in RS CVn-type systems followed a similar functional form, but noted that the A-2 fast transient search had found fewer triggers from RS CVn-type systems by about a factor of 2-4. We suggest the curve plotted for these systems to be uncertain by roughly a factor of ten in the normalization.

Since we had excluded some regions containing X-ray bursters from the all-sky transient search, we could not use the results of this survey to estimate X-ray burst rates. Instead we used the estimates

of burst frequency in Bradt and McClintock (1983), and note that the distribution of X-ray burst sources and the intrinsic luminosities of X-ray bursts have been well determined (Ebisuzaki 1987). We estimate this curve to have an overall uncertainty in normalization of roughly an order of magnitude.

Our estimate of the gamma-ray burst log event rate versus log event fluence curve came from combining the A-2 survey upper limits with rates from the HEAO 1 A-4 gamma-ray burst survey (Hueter 1987) by assuming that the one burst observed through the fronts of both experiments was represenative except for being softer than average. We note, following Jennings (1987), that the normalization at high fluences is apt to be highly uncertain (because of the difficulty of correctly calculating burst fluences), but point to the evidence summarized above for a flattening, and a 90% upper limit on the gamma-ray burst rate of 1300 bursts per year over the whole sky, below $\sim 10^{-9}$ ergs-cm^{-2}.

Perhaps the most intriguing curves are for the types of events we did not plot in Figure 6.1: those that remain unidentified, whether from this search (D436.84) or from different experiments entirely (Serlemitsos, Bunner, and Swank 1979 - see Chapter 5; Ambruster and Wood 1986; Pye and McHardy 1983; Helfand and Vrtilek 1983). We estimated, based on a single detection each, that the rate curves for hard events such as the bright 6-Nov-77 transient and the hard and/or absorbed unidentified events from the HEAO A-1 and A-2 searches probably lie somewhere between that for gamma-ray bursts and our estimate of flares from RS CVn-type systems.

All these X-ray fast transient events are set against a backdrop

of the ~ 100 very luminous (~ 10^{37-38} ergs-s^{-1}) Galactic X-ray sources, the accreting high and low mass binaries that we touched on briefly in Chapter 3. These brightest X-ray sources are the ones we concentrated on in Chapter 4, which described the HEAO 1 A-2 fast transient survey of the Magellanic Clouds. Out of 37 events, we identified all but two with four out of five of the most X-ray luminous sources in the Large Magellanic Cloud. We identified the other two with flares from a nearby RS CVn-type system. We detected none from the Small Magellanic Cloud. We attributed the remaining thirty-five events to four of the five brightest X-ray binaries in the LMC. Interestingly, we found no events we could plausibly attribute to the high mass binary and black hole candidate LMC X-3. We identified eight events with the roughly periodic (~16.7 days) outbursts from the high mass binary A0538-66, the LMC Transient. We attributed two (one year apart) to the low mass binary LMC X-2, and five events to the luminous high mass X-ray binary LMC X-1. The events from both sources appeared similar to those from luminous high and low mass Galactic X-ray binaries touched on in Chapter 3.

We attributed the remaining twenty events to the high mass eclipsing binary pulsar LMC X-4, which also exhibits an overall intensity modulation on a ~30.5 day cycle (Li, Rappaport, and Epstein 1978; White 1978; Kelley et al 1983; Lang et al. 1981). We suggested that one event out of the twenty was a trigger on the change in X-ray flux during eclipse egress, although that event was abnormally bright. We identified the remaining nineteen events, with 20-60 minute long highly luminous flares ($\Delta L_x/L_{Edd}$ ~ 0.5-20), which all occured between phases 0.2 and 0.5 of the 30.5 day cycle.

We found no gamma-ray bursts (despite high coverage of the repeating gamma-ray burster associated with the SNR N49), and we found no events that may be typical Type I (or II) X-ray bursts. These conclusions were independent of our identifying all thirty-seven events with known luminous X-ray sources, and was based on the shape of the ~1 minute light curves and the lack of characteristic burst cooling seen during each event. We calculated a 90% upper limit on the average number of X-ray bursts per source per year from the LMC of < 1 per 0.43 days. This is consistent with the average rate of ~0.34 per source per year seen from the Milky Way; however, it is interesting to note that no observer has yet detected any 'moderate luminosity', moderate accretion rate Pop II X-ray binaries in the LMC, of the sort responsible for the majority of X-ray bursts in our Galaxy. In fact, this survey found no events from sources invisible to the Columbia Astrophysical Laboratory Einstien LMC survey, hidden either by high column density or long term variablity.

B. Thoughts for the Future

i. The Magellanic Clouds

As a consequence of both the satellite orbit and proximity of these sources to the South Ecliptic pole, HEAO 1 observations of the Magellanic Clouds provide continuing opportunities to track the long term behavior of these luminous X-ray binaries. Of particular interest are the spectral variations accompanying the variations in intensity indicated by in this search. There were suggestions in the events from the LMC Transient (A0538-66) of the shorter variations being harder than the overall outbursts, but it was not at all

conclusive. In the twenty events detected from LMC X-4, no underlying pattern of spectral variability seemed clear. In particular, since this effort apparently documented so many luminous flares from this system, it may be possible in the future to consider the statistical properties of these superluminal outbursts. Also, it was not clear how the phase portrait of the binary period changed with time; the brightness of one of our events seemed to indicate that the ~1.4 day light curve was not always similar to the earlier observations of White (1978).

The upper limit obtained by this HEAO 1 A-2 search on X-ray bursts from the Magellanic Clouds was intriguing but not conclusive. The launch of the Japanese satellite GINGA in early 1987 may make it possible to extend this limit. The smaller field of view of the GINGA Large Area Proportional Counters (~2.2°x4° FWFM) implies that the satellite will have a smaller expected number of possible bursters within its field of view each time it scans the Magellanic Clouds; however these tighter field of view will reduce source confusion problems, and the larger area counter (~4000 cm^2 for LAC versus ~800 cm^2 for each HEAO 1 A-2 detector) will help reduce the effective threshold for triggers on a burst. With the advent of Supernova 1987a near LMC X-1 in the Magellanic Clouds and the subsequent GINGA monitoring program, researchers may accumulate sufficient coverage of this region to substantially lower the HEAO 1 A-2 upper limit on X-ray bursts (Ebisuzaki private communication).

ii. The All-Sky Survey for Fast X-ray Transients

Unlike the Magellanic Clouds survey, the all-sky fast transient

survey dealt with stars that are primarily X-ray dark. We divided the events we found into two rough categories: softer and unabsorbed 'coronal' fast transients, originating from the active cornae of cool dwarf stars; and 'hard' fast transients, with harder or more highly absorbed power law specta, presumably from compact objects, found mostly along the Galactic plane.

The coronal sources, such as dMe-dKe stars and RS CVn-type systems, which could only be detected by the HEAO 1 A-2 MED and HED detectors during bright flares, are easily observed both in quiesence and during small flares at softer wavebands accesible to most X-ray telescopes. There is some speculation that the total energy budget of an active coronae comes from heating by numerous small flares, which become increasingly difficult to measure as the flare size decreases. Figure 6.1 illustrates that, since the frequency of flaring activity increases as flare size decreases, increasingly sensitive X-ray experiments (ROSAT, AXAF, with detection limits on the order of 10^{-11-12} ergs-cm^{-2}) should observe >5 times as many serendipitous stellar flares per year as did this fast transient survey, despite their smaller fileds of view.

Interesting follow up studies of coronal sources include mapping the cycles of activity over long periods of time. Is the X-ray flux modulated by rotation in the way one expects from observing optical and ultraviolet emission lines ? Does the rough correspondence between U-band and X-ray flare activity, delineated in Chapter 3 and Appendix B, hold when scrutinized in greater detail ? As a long time-scale database is accumulated, does one find evidence for decades-long cycles of stellar activity analogous to the 11 year sunspot cycle ?

Does this account for differences in activity of stars of otherwise similar spectral type ? One is interested, eventually, not only in detailed measurements of the physical mechanisms driving individual bright stellar flares, but in measuring varied flares from a broad sample of stars, for indications of stellar activity as a function of stellar mass, age, and rotation rate.

One of the most significant preliminary results coming out of this work is the suggestion of hard, ~few hour, fast transients (some showing < 1 minute variability) along the Galactic plane. If the 'hard' fast transients are like either some Be-neutron star systems, which can undergo quasi-periodic outbursts at times of optical activity ("Class II" of van den Heuvel and Rappaport 1986), or like gamma-ray burst sources, these objects will be virtually undetectable save during outbursts. That makes follow-up X-ray monitoring of the "hard" transients impractical in the extreme - the recurrence time for gamma-ray bursts is estimated to be on the order of years, while we suggest that for the Be-neutron star systems to be at best once a month. For these infrequently detectable X-ray sources, one must either take advantage of all data on an individual source, while it was on; or rely on surveys of the whole sky, for properties of the class as a whole. The HEAO 1 A-2 database, with its stable detector background, ~2-60 keV spectral range, observing each point on the sky every 0.5-2 hours (for ~100 s) for a week at a time, is ideal for investigating this hypothesized class of sources. However the current software tools are not set up for observing objects that vary on this time-scale (that is, ~hours): they are set up for either events that last seconds to minutes (software used in this search) or > 12 hours

(software used to make A-2 catalog). If this hypothetical class of sources does exist, it should be visible unmistakeably, in the A-2 data, and wants only the application of the proper software tools to deny or confirm (and illuminate) its existence. We suggest the clearest way to identify these sources is to map out the Galactic plane (and enough on either side to differentiate any isotropic populations) using integration times of several hours. (Some difficulty may be introduced by the expectation that ~50% will vary, if they are Be star pulsars, but not enough to warrant the additional computer time necessary for using tools such as the FINDP programs detailed in Appendix B, which are independent of such short time-scale variations.) After sources have been identified, the search for pulsations could prove interesting.

Since there were three other experiments besides A-2 on the HEAO 1 spacecraft (A-1, A-3, and A-4) it may be possible to get additional information on particularly interesting outbursts from these complementary databases. The A-4 experiment was coaligned with the A-2 detectors, had a much wider field of view, and covered a higher energy band (~30 kev-3 MeV). However, because of its small area, it was unlikely to have detected any of the A-2 fast transients. (Compare the threshold of the A-2 survey with that of the A-4 gamma-ray burst survey of Heuter 1987, for example.) The A-3 experiment, with the capapbility of constraining the positions of sources to within repeated error diamonds a few arcminutes on a side, also was a smaller area instrument, co-aligned with A-2 and A-4. Although the brightest fast transient event, that from LDS 131 on D405.85, was detected with over 20σ significance, the moderate

intensity flare attributed to AT Mic (on D298.62) appeared insiginificant, at most as a 'bare warming' in the A-3 detectors (R. Remillard private communication). The events with A-2 fluxes between that of these two events have not yet been thoroughly investigated in A-3 data, but may also prove too faint for significant detection. If the events from near the Galactic plane (D249.36, D343.12, D342.23, D345.62, and D494.15) were associated with low-level persistent emission lasting for hours or days, the A-3 experiment, which had less problems with source confusion, may have detected sufficient photons to set significant constraints on the source positions. The A-1 instrument incorporated detectors with larger areas than the A-2 instruments, covering an ~0.25-25 keV energy range. All but one of the seven A-1 modules pointed 180° away from the A-2 main detector axis; the seventh had a wide field of view in the direction of scan (7° FWHM) and often had a high background rate, making detection of faint transient events difficult. Ambruster and Wood (1986) surveyed the first six months of data from the six coaligned A-1 modules, in a fast transient survey similar to this one. As evident from Chapter 3, we referenced results from this complementary search to set constraints on source populations and occasionally event durations. However, the remainder of the A-1 database has yet to be comprehensively surveyed in this manner. Also, two of the A-1 modules had quite small fields of view, so it may be possible to more tightly constrain the positions of the sources of these events, if the event durations were greater than ~10^3 s. The eventual goal would be constraints on the optical counterparts of the sources of these fast X-ray transient events.

We have not yet addressed follow-up studies of the rare, hard, events, that we think are unlikely to be identified with Be-neutron star systems, such as that from the A-2 survey on D436.84, or that on 6-Nov-77 observed with the OSO-8 detectors. One method of identifying possible source populations is by more stringently constraining the rates of such events over the whole sky. Other interesting events -- such as the bright X-ray counterpart to a gamma-ray burst - were found by chance in HEAO 1 A-2 pointing data (which was not used in this survey). Since the incidence of fast transient events in HEAO 1 A-2 pointed data has not yet been completely investigated, accurate estimates of event rates for these interesting classes are difficult. Also, some bright events were observed in densely populated regions of the sky and may have been misidentified (see Chapter 3). With only slight modifications of the software tools used in the all-sky survey and the survey of the Magellanic Clouds, it would be possible to:

1. penetrate densely populated regions more carefully (the remaining 7-10% of the scanning database) after the manner of the LMC survey;

2. survey any unexamined pointed data, including blank-sky points (particularly along the Galactic plane), data from the offset (HED1) detector, and transients bright enough to be distinguished by position and/or variability from the target source. (Although A-2 data from some blank sky points were investigated by Tennant (1983) in his study of the X-ray variability of active Galaxies, a complete survey for fast transient activity - particularly using data near the Galactic plane and from the offset HED1 detector -

263

has not been performed.)

More complete, more sophisticated, fits of event rates over the whole sky (perhaps allowing for differences in Galactic latitude and longitude) would then be possible. Since gamma-ray bursts are so X-ray bright, lasting (in 2-20 keV X-rays) for ~100 s, constraining gamma-ray burst event rates with HEAO 1 data alone would be particularly exciting. However we point out, even using the current software tools, some regions containing bright and highly variable sources (such as Cyg X-1) trigger so often that thoroughly investigating them would be cumbersome and extremely time consuming.

What about the possibility of future X-ray missions observing and identifying these rare types of fast transient events ? We point out that in the compromise between wide field of view and high spatial resolution, after a decade of flying collimated proportional counters, the U.S. space science community has moved towards flying higher resolution instruments, with greatly increased sensitivities, but with an order of magnitude smaller fields of view. However useful it may be to resolve the X-ray sky when one is studying other types of X-ray sources (sources of diffuse emission, such as supernova remnants, or clusters of Galaxies, as well as AGNs and persistent Galactic X-ray sources), and however psychologically satisfying it seems to finally "see" the X-ray sky, a glance at Figure 6.1 shows that greatly increased sensitivity is unlikely to be enough to counterbalance the smaller fields of view for observing the "hard" fast transients. For example, during the ~1½ years HEAO 1 was aloft, in the combined A-2 fields of view of ~2x6°x3° (FWHM), we detected one X-ray counterpart to a gamma-ray burst. Since it appears that we are already seeing

across the Galaxy at fluences of 10^{-7-8} ergs-cm^{-2}, any increase in sensitivity leads to no greater number of detectable X-ray counterparts to gamma-ray bursts. Therefore even an instrument with a 2°x2° field of view (EXOSAT CMA, or ROSAT), if it had a comparable percentage of 'on' time as HEAO 1 A-2, would have to observe for ~seven years before detecting one event. Instruments with smaller fields of view (XMM, XTE, AXAF), one predicts, would have to observe for decades - clearly impractical (although if one is observed by any of the proposed high resolution instruments, it would be a spectacular find). Even attempting to observe classic gamma-ray bursts from the Magellanic Clouds would be prohibitive. Scaling down from the Galactic rate by the ratio of the masses of the Milky Way and the Magellanic Clouds, one expects <100 per year from the LMC as a whole, or (if they are distributed isotropically) ~2 bursts per year per square degree. Even with the advent of SN1987a (an exciting X-ray target in the LMC), a high resolution X-ray instrument is unlikely to stay pointed at the Magellanic Clouds for the better part of a year.

At the other extreme are instruments with wide fields of view, but much smaller effective area at ~10 keV (including a 5°x5° soft X-ray - extreme ultraviolet instrument on ROSAT, a ~2°x90° sky monitor on XTE; and the gamma-ray burst monitoring experiments). These share a drawback with many hard X-ray and gamma-ray detectors, in that they can only observe the srongest fluence events (typically $>10^{-5-7}$ ergs-cm^{-2}), and so would miss the rare hard transient events discussed here, which apparently have spectra, fluences, and source distributions falling between those of gamma-ray bursts and the more energetic coronal events from RS CVn-type systems. The exceptions may

prove to be instruments somewhat similar to HEAO 1 flown by other nations, including the Large Area Counters of the Japanese satellite GINGA, and the proposed Soviet Mission GRANAT (although the latter may have too high a threshold).

In other words, one of the most intriguing classes of events discussed in this survey, the rare hard fast transients, with characteristics intermediate between gamma-ray bursts and energetic coronal flares, may be undetectable by future U.S. X-ray missions. By historical accident, they were viewed for a decade, while moderate sensitivity, moderate field of view instruments, with broad (~1-60 keV) spectral coverage, were being flown. In the future (with apologies to Santayana op. cit. Robinson-Saba 1983 p. ii), these usually X-dark objects may flash signals of their nature, with no X-ray eyes scanning the sky to detect them.

Ground-based optical programs surveying wide fields for fast transient activity may prove less expensive than space-based programs. Two such experiments, the Explosive Transient Camera and the coordinated Rapidly Moving Telescope, designed to search for optical flashes from gamma-ray bursts, will probably also trigger on other types of fast transient activity, including stellar coronal flares. If any of the hard X-ray fast transients also flash in the optical, one may be able to measure event rates and identify the sources from the ground. However, if these sources are heavily absorbed even during outbursts, as the X-ray spectra may indicate, they may be undetectable by even these wide-field ground-based transient searches.

Figure 6.1 A rough plot of the observed rate of events per year, for four diferent kinds of X-ray fast transient events, as a function of instrument sensitivity, measured in fluence (ergs-cm^{-2} 2-20 keV).
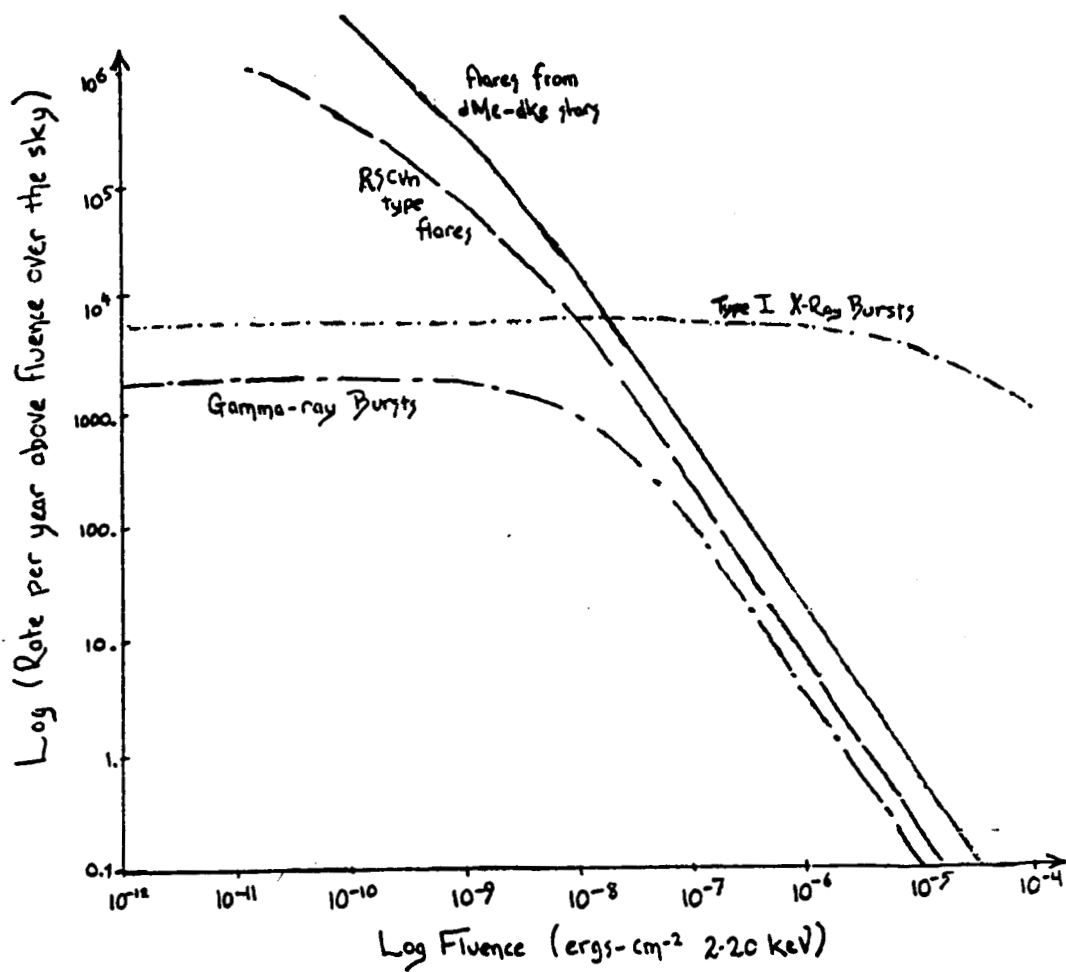
Appendix A

1. Calculation of Fast Transient Search Thresholds

We chose to err on the side of caution, and so required ~6σ confidence, which is equivalent to requiring the probability of a spurious trigger (in a single time bin) due to Poisson noise to be less than ~2×10^{-9}. In the first phase of the HEAO 1 A-2 fast transient survey, the "source free" search, we examined ~2×10^{6} 5.12 s bins (and four times that number of 1.28 s bins); and for the "all-sky" search we examined an additional 1.6×10^{6} 5.12 s time bins. We calculate an expected number of spurious triggers due to statistical fluctuations of ~0.02.

Whenever possible, we required coincidence among co-aligned detectors. If more than one of the co-aligned instruments were 'on', our requirement that the total probability be $\leq 2\times10^{-9}$ translated into the requirement that the product of the probabilities (of spurious triggers due to Poisson fluctuations) be less than this limit. Let $P_A(i)$, $P_B(i)$, and $P_C(i)$ represent the probabilities of finding by chance a count-rate above the trigger levels in time bin 'i' from detectors A, B, and C. In the simplest case, which is what we chose to work with for the HEAO 1 A-2 fast transient search, one requires, for two detectors 'on', $P_A(i) \leq (2\times10^{-9})^{\frac{1}{2}}$ and $P_B(i) \leq (2\times10^{-9})^{\frac{1}{2}}$; and for three detectors 'on', $P_A(i) \leq (2\times10^{-9})^{1/3}$, $P_B(i) \leq (2\times10^{-9})^{1/3}$, and $P_C(i) \leq (2\times10^{-9})^{1/3}$. Using the notation of Chapter 2, if the expected count-rate in the ith time bin is $C_0(i)$, and the current count rate is $C(i)$, and one defines the parameter $n = (C(i) - C_0(i))/(C_0(i))^{\frac{1}{2}}$, then, for a Poisson distribution, the upper limits on probability calculated

above will be satisfied if, for only one detector 'on', n≥6; for two co-aligned detectors 'on', n≥3.89; and for three n≥2.98. This is for the simplest case: triggering on a significant excess in count-rate in a single 5.12 s (or 1.28 s) time bin. These were the threshold levels used in the "source-free" search.

The results from the first phase of our survey, the "source-free" search, demonstrated that the majority of our events glowed with roughly constant intensity for the entire ~80 s it took for both the co-aligned and (trailing) offset detectors to sweep over a point source. We wished to take advantage of this long duration to lower our effective thresholds, by integrating over a longer time interval in a way which took into account the triangular response of the collimated detectors as they passed over a point source. Since HEAO 1 rotated at a rate of ~1° every 5.12 s, it took ~16 s for the ~1.5° FWHM fields of view to scan past a point source (twice that for the ~3° FWHM fields of view); and about 30 s for that point source to travel from the center of the co-aligned detectors' fields of view to that of the offset detector, HED1. We therefore consider the profile of a constant point source, as the detectors sweep past, on time-scales of three 5.12 s bins, and then eight 5.12 s bins. Let time bin 'i' contain the time of peak detector response, and let the time bins on either side be labeled by 'i-1' and 'i+1'. In general one does not know where the boundaries of the 5.12 s interval will fall, with respect to the time of the peak detector response, and so one does not find a general expression for the flux in bin i+1, given that in bin i (or for the flux in bin i, given that in bin i-1). However, we calculate the ratio of the excess flux in the ith time bin to the sum

of the excess flux in bins to either side,

$$(C(i-1)-C_0(i-1) + C(i+1)-C_0(i+1))/(C(i)-C_0(i)),$$

depends only weakly on the position of the time of peak detector response within the ith 5.12 s time interval.

Let η represent the displacement of the time of peak response from the center of time bin 'i', measured in degrees. We consider the effective area EFF_i, on a source stationed at scan angle $\phi=0$ and an off-scan angle $\theta=\theta_1$, of the combined ~3° and 1.5° fields of view (as was the case in the HEAO 1 A-2 fast transient survey for the two co-aligned detectors that were most frequently 'on'). Let ω designate the satellite spin rate of ~1° every 5.12 seconds, Δt the integration time of 5.12 s, θ_0 the collimator opening angle in the offscan direction (which is ~3° for all detector fields of view), and ϕ_0 the maximum collimator opening angle in the scan direction, which for this case is ~3°. (Note that $|\eta| \leq |\omega\Delta t|$.) We calculate

$$EFF_i = 1-\frac{3}{2}\left(\frac{\frac{\eta^2}{\omega\Delta t}+\frac{\omega\Delta t}{4}}{\phi_0}\right)\left(1-\frac{|\theta_1|}{\theta_0}\right), \text{ and}$$

$$EFF_{i-1}+EFF_{i+1} = 2\left(1-\frac{3\omega\Delta t}{2\phi_0}\right)\left(1-\frac{|\theta_1|}{\theta_0}\right).$$

If $C_0(i)$ represents the expected count rate in the combined fields of view of a detector during the time bin 'i', and $C(i)$ represents the current count-rate, which includes an excess contribution from a fast transient source, we calculate the expected value of the ratio

$$(C(i-1)-C_0(i-1) + C(i+1)-C_0(i+1))/(C(i)-C_0(i)),$$

to be 2/5/3, or ~1.2.

Therefore, when investigating a flux increase over three 5.12 s time bins, our requirement that the total probability of spurious triggers due to Poisson fluctuations be less than $2x10^{-9}$ becomes that the excess flux in the ith time bin, measured in units of $n=(C(i)-C_0(i))/(C_0(i))^{\frac{1}{2}}$, be greater than n15, and that the sum of the excess flux in the $i-1^{st}$ and $i+1^{st}$ (measured in the same manner) be greater than 1.2xn15; where, for one detector 'on', n15≈4.23; for two coaligned detectors 'on', n15=2.68; and for all three 'on', n15=1.96.

For the case of a fast transient event with an intensity that stays constant for the entire ~80 s that it is in the fields of view of the A-2 experiment, a detection in the offset detector (HED1, which trails the co-aligned ones by ~30 s) can in effect be considered as simultaneous with detections in the co-aligned instruments. If the offset detector and only one co-aligned detector were on, the threshold (for >60 s events) was set at n60=2.68; for the offset detector and two co-aligned detectors 'on', we set n60=1.96; if all four detectors were on, the threshold was set to its lowest level of n60=1.51. We have tabulated these values in the first table of Chapter 2.

2. Calculation of Detection Probabilities:
Deconvolving the Response of Collimated, Scanning Detectors

Here we assume that our small sample of fast transient events is representative of events over the whole sky, and infer from it event distribution rates. We have made two further assumptions to simplify

271

this particular calculation:

1. We have assumed the sky is more or less isotropic - we have not taken into account any variation of the sky with Galactic l^{II} and b^{II}, for example. Any anisotropy would only be reflected in a slope of the Log Number vs Log Intensity function that differed from -3/2.

2. For this work, we have only performed our event frequency calculations and fits for the "source-free" search, and so for now have side-stepped the questions of changing trigger levels with changing position on the sky inherent in our search of "source-full" areas. It may be that the complete calculation will be performed for Connors, Heuter, and Serlemitsos (1988).

With these caveats in mind, we proceed to calculate probabilities of detecting events in the "source-free" HEAO 1 A-2 fast transient search.

Consider the probability $P1(S,\tau)$ of detecting a transient of intensity S (measured in cts-s^{-1}), with duration τ, at scan co-latitude and longitude (θ,ϕ). As illustrated in Figure A.1, there is a limited region of sky, A_o, from which a collimated detector can start at time t_o in order to have this event in its field of view while the event (pictured as occurring at the origin) is on. The collimator opening angles are θ_o and ϕ_o; the experiment rotates at a rate ω_1 in the scan latitude direction, and at a rate $\omega_2 \ll \omega_1$ in the scan longitude direction. The probability that, at a random time, the look direction is in the infinitesimal area dxdy of the tangent plane at θ,ϕ is $dx/\pi\sin\theta \cdot dy/2\pi$. Then

$$P1(S,\tau) = \int\limits_{Ao} (dx/\pi\sin\theta)(dy/2\pi)\ P_D(x,y;\ S,S_0;\tau),$$

where $P_D(x,y;\ S,S_0;\tau)$ is the probability of detecting the event if, at its onset, the look direction is at (x,y), the intensity is S, and the threshold for detection S_0. P_D is the sum of probabilities of detecting the event in the successive time integration intervals Δt as the experiment scans across the sky. With $P_A(i)$ the Poisson probability that detector 'A' will register this event above search threshold in the ith integration interval, and requiring coincidence among coaligned detectors (denoted here as A, B, and C),

$$P_D = \sum_i P_A(i)\ P_B(i)\ P_C(i) \prod_{K=1}^{i-1}\{1 - P_A(k)P_B(k)P_C(k)\}.$$

We evaluated these expressions numerically. Figure A.2 illustrates the results for $\tau = 35$ minutes.

3. Fits to Frequency of Occurrence

We estimate the total number of events per year over the whole sky, given that we detected seven in the "source-free" survey of HEAO 1 A-2 scanning data. We denote the probability of detecting one event of duration τ and intensity S by $P1(\tau,S)$. If $R(S)$, the rate over the whole sky per year of events with intensity $\geq S$, has the form $R(S) = R_0 S^{-\Gamma}$, we calculate the number of transients $\Delta Y(S)$ detected in each interval ΔS to be

$$\Delta Y(S) = P1(\tau,S)\ \Delta R(S) = P1(\tau,S)\ (-\Gamma\ R_0\ S^{-\Gamma-1})\ \Delta S.$$

273

In Figure 3 we display the results from $\Delta Y(S)$ when all three detectors are coincident, with a search threshold $S_0 \approx 4$ millicrabs, assuming $\tau = 35$ min., $\Gamma = 1.5$. The analogous graph for when only two coaligned detectors are 'ON' and $S_0 \sim 6$ millicrabs looks nearly identical. The expected number of events ΔY per intensity interval ΔS peaks at $S \sim 1.5 \, S_0$ (for shorter τ, the peak approaches $\sim 1.1 \, S_0$), even for an event distribution $R(S)$ as skewed to faint events as $S^{-3/2}$. For bright events ($S/S_0 \rightarrow \infty$), ΔY falls off to a limiting value of $R(S)$ times the fraction of the sky covered by the detectors while the transient is on.

A maximum likelihood fit to the data shows any Γ between 0.3 and 1.7 to be acceptable within 1σ. We estimate the event frequency per year over the whole sky above search threshold S_0 to be, within 1σ,

$$10^4 \text{ events-yr}^{-1}\text{-sky}^{-1} \leq R(S_0) \leq 3 \times 10^5 \text{ events-yr}^{-1}\text{-sky}^{-1},$$

where $\tau = 2 \times 10^3$ s for the lower limit, and $\tau = 60$ s for the upper limit.

These calculations were performed for the "source-free" data. From the figures on sky coverage and threshold of Chapter 2, one finds that on average the trigger level was slightly higher in the "all-sky" survey than in the "source-free" survey, and that although there was ~60% more coverage in the "all-sky" survey, there was only slightly more coverage of the Galactic plane in the "source-full" sections of the search. Therefore it is reasonable that we found only a few more fast transient events on the Galactic plane, and ~60% more stellar flare candidates, in the "all-sky" survey; we do not expect that our estimate of the total event frequency to change if we do perform an event-size event-distribution fit over the whole "all-sky" search.

Figure A.1   Schematic diagram illustrating the calculation of the
probability that the field of view of an A-2 collimated proportional
counter (with opening angles ϕ_0 and θ_0 in the scan and off-scan
directions), scanning the sky at a rate ω_1, will intersect the world
line of a transient event of duration τ, for the case $\theta_0 < \omega_1\tau < 360°$.
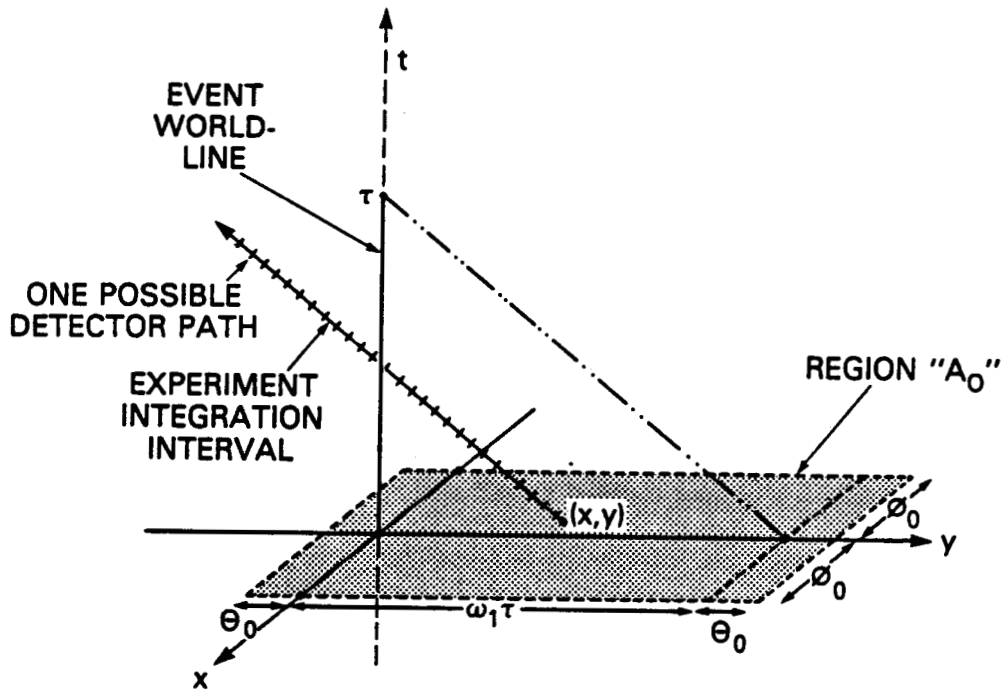
Figure A.2 The number of events expected, $\Delta Y(S, \Delta S)$ between $S - \Delta S/2$ and $S + \Delta S/2$ is plotted versus the intensity S. The intensity is measured in counts 'C' per experiment integration interval, divided by the threshold counts C_0 per interval. The bin size ΔS was chosen to be $0.1C_0$, the duration τ to be 35 minutes, α to be 1.5, and R_0 about 1 event per 3°x3° per 'ON' time. The graph assumes 3 detectors are 'ON', implying a threshold C_0 of about 4 millicrabs.

NUMBER OF EXPECTED EVENTS

3 DETECTORS 'ON'
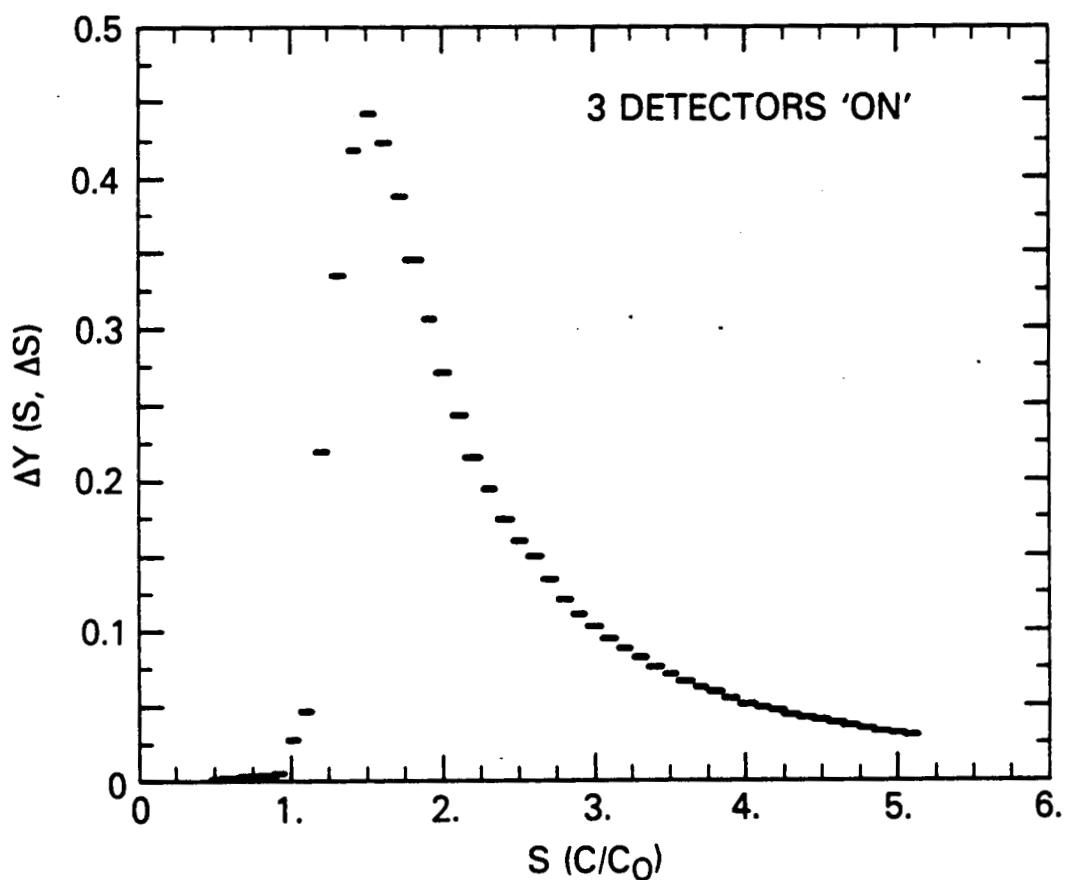
c-4

Appendix B

A Handbook on the New HEAO 1 A-2 Position Finding Programs

Here we describe the evolution of a series of programs to constrain the positions of variable sources (such as the A-2 short transients), and those observed in pointed data. These types of sources had not been addressed by earlier standard HEAO 1 A-2 position-finding programs. The position-fitting algorithms presented here were conceived and implemented by A. Tennant, J. H. Swank, and me. We present these algorithms in three stages.

1. Origins

In late 1983, interested in finding the position of a fast transient discovered by Allyn Tennant in a blank sky point, we considered a means of obtaining an intensity-independent parameter that described the position of a source. The original idea exploited the differing collimator sizes among the HEAO 1 A-2 detectors. The expected count rate in the ith time bin, $<C(IDET,IFOV,i)>$, of a particular detector IDET with a particular field of view (i.e. collimator width) IFOV, is a simple linear function of the intrinsic source intensity $I_S(i)$:

B.1 $<C(IDET,IFOV,i)>$

$$= <BACK(IDET,IFOV)> + I_S(i) \cdot EFFAREA(IDET,IFOV,\phi,\theta;\phi_1,\theta_1;\phi_0,\theta_0).$$

Here <BACK(IDET,IFOV)> is the expected background count rate (internal plus diffuse sky) for this detector and field of view; and the function EFFAREA represents the effective area of this detector on the source. For a square collimator, with detector axis pointing in the direction (θ_1,ϕ_1), and collimator opening angles θ_0 and ϕ_0,

B.2 $\mathrm{EFFAREA}(IDET,IFOV,\theta,\phi;\theta_1,\phi_1;\theta_0,\phi_0) \approx \left(1-\left|\frac{\phi-\phi_1}{\phi_0}\right|\right)\cdot\left(1-\left|\frac{\theta-\theta_1}{\theta_0}\right|\right)\cdot A_0$,

where A_0 is the total on axis area for that detector and field of view (typically about 400 cm^2 for each field of view). The parameters θ_0, ϕ_0, (collimator opening angles), are determined by the choice of IDET and IFOV; the parameters θ_1, ϕ_1 (detector look direction) depend also on the time bin, i. For each detector, $\theta_1(i)$, $\phi_1(i)$, and θ_0 are approximately the same, while ϕ_0, the collimator opening angle in the scan direction, differs between the two fields of view by about a factor of two ($3°$ and $6°$ for HED1 and HED2; $1.5°$ and $3°$ for HED3 and MED). See Shafer (1983), Robinson-Saba (1982), or Rothschild et. al. (1979) for more details.

Let A and B represent the smaller and larger fields of view on the detector IDET. We define the function

B.3 $R(IDET,i,\phi) \equiv \mathrm{EFFAREA}(IDET,A,i,\theta,\phi)/\mathrm{EFFAREA}(IDET,B,i,\theta,\phi)$

$$\approx \left(1-\left|\frac{\phi_1(IDET,i)-\phi}{\phi_0(IDET,A)}\right|\right)/\left(1-\left|\frac{\phi_1(IDET,i)-\phi}{\phi_0(IDET,B)}\right|\right)$$

If the background count rates, BACK(IDET,A) and BACK(IDET,B), are well determined, one can define the related random variable

B.4   r(IDET,i)

        ≡ (C(IDET,A,i)-BACK(IDET,A))/(C(IDET,B,i)-BACK(IDET,B)).

Notice that these are now measured quantities, rather than expected values, for the detector count rates and the associated background rates in the A and B fields of view. The function $R(IDET,i,\phi)$ is then the expected value of the numerator of r(IDET,i), divided by the expected value of its denominator. The early position-fitting program, FINDP, performed a standard least-squares fit (Bevington 1969) of the measured quantities r(IDET,i) to the function described by $R(IDET,i,\phi)$, for each time bin during which the source was in the field of view, in an effort to constrain the position of an X-ray source in a way that was independent of its intensity variations. Since the function $R(IDET,i,\phi)$ has no θ, or off-scan, dependence, but depends on $|\phi-\phi_1|$, this first algorithm produced a pair of parallel position error boxes whenever the detector axis was stationary. Figure B.1 displays 90% confidence contours for H2120+55, a fast transient in pointed data on D728.15; and for a flare from the dwarf star AT Mic, in scanning data.

There were several systematic problems with this approach. First, the background count rates have been shown to vary in time and position, even in regions well away from known sources (Shafer 1983 and references therein). Second, when neither detector field of view contained the source, the ratio became indeterminate (the uncertainties became so large that the ratio was a useless measure of position); however, especially for weak sources, the angles at which

279

a source appeared and disappeared from both fields of view provided strong constraints on its position.

The systematic errors in this approach were large enough to exclude the source AT Mic, at the 90% level, from the position error boxes in Figure B.1, when two other experiments on HEAO 1 had identified it as the source of this particular event.

2. Simultaneous Fitting of Several Fields of View

Instead, we decided to fit the counts in each time bin, in all fields of view. For a particular detector, for each of its two fields of view, we modeled the expected count rate in the ith time bin, $c(IDET,IFOV,i,\theta,\phi)$, by:

B.7 $c(IDET,IFOV,i,\theta,\phi) \equiv$
$BACK(IDET,IFOV) + I_S(i) \cdot EFFAREA(IDET,IFOV,i,\theta,\phi)$

The statistical uncertainty of the counts in each time bin can be described simply by the Poisson distribution. The source intensity in each time bin, $I_S(i)$, no longer cancels neatly out of the model equations, but has become a freely varying fit parameter, as has the background. The earlier algorithm also assumed the spin-axis (which defines the scan plane and therefore the scan and off-scan angles) to be fixed; in the one introduced here, we exploit the ~1° wobble in spin-axis position by introducing the off-scan angle, θ, as a fit parameter. The original program required fitting each detector independently. The new FINDP algorithm introduces three spectral parameters, called "detector ratios", that allow data from HED1, HED2,

280

MED, and HED3 to be fit simultaneously. We define three detector ratios, DR(IDET), to be the ratios of the on-axis efficiencies of each detector to that of HED3 (which was OFF the least). Since the detectors are misaligned by about $0.1°$, simultaneous fitting can place some constraints on θ. The complete expression for the expected count rate in the ith time bin is then:

B.8 $c(IDET,IFOV,i) \equiv$

$BACK(IDET,IFOV)+I_S(i) \cdot EFFAREA(IDET,IFOV,i,\theta,\phi) \cdot DR(IDET)$

Since we do not include any time dependence in DR(IDET), our model assumes any spectral changes are negligible over the duration of each event. This is not always the case, particularly with short events like gamma-ray bursts, but the dependence of the position solution on the spectrum is weak. The detector HED1 is a special case. Since the HED1 and HED3 detectors had the same response except for a geometry factor, for all our fits we fixed DR(HED1) at 0.921, which was the value determined from calibration runs using the Crab Nebula.

The program uses a standard Marquadt algorithm to find a minimum χ^2 fit of our model to the data (Bevington 1969). There are options for writing a light curve file containing the intensity parameters $I_S(i)$; for mapping out grids of χ^2 values versus scan (ϕ) and off-scan (θ) angles; and for drawing contours of constant χ^2 values.

This algorithm has the drawback of introducing a lot more fit parameters than were required by the first FINDP (about two dozen more, for a typical fast transient). Since it no longer uses ratios of count rates, it also needs to fit twice as many data points. The

program can therefore use over ten times more CPU time than the original FINDP. At first, the speed of the new FINDP was also limited by its size. Many calculations had to be performed over and over again, rather than calculated once and stored, because of size limits on the PDP 11/70 on which it was first implemented. The programs FINDBPT, FINDBPS, and FINDBPSO, which contained various options that would not fit in one task on the PDP 11/70, were therefore moved to the LHEAVX MicroVax, combined into one program named FASFINDP, and sped up by a factor of 2-3. FASFINDP was subsequently copied to NSSDCA, a Vax 8650, which was faster still by about an order of magnitude.

Figure B.2 illustrates how well FASFINDP worked with four different types of data. The three maps show the 90% and 99% confidence contours for the flare attributed to AT Mic, which used a single scan (100s) of data; for one day of scanning data (D.O.Y. 1977 260) on the Crab; and for $\sim 5 \times 10^4$s of pointed data (D.O.Y. 1977 547) on the AGN Abell 85. The flare star AT Mic is clearly within the 90% confidence contours (and AU Mic is not). The AGN Abell 85, which would have been excluded had only the scan (ϕ) limits at offscan angle = 0.0 (θ=0.0) been used, also now falls within the 90% confidence limits. For both the fits to the Crab and the Abell 85 contours, we assumed the source to be constant in intensity throughout the observation, a reasonable assumption which reduced the amount of CPU time required. To show how well the algorithm worked with rapidly varying pointed data, we have also plotted 90% and 99% confidence contours for three major frames ($\sim$123 s) of Cygnus X-1 pointed data. The program has no difficulty in finding the correct position of the

282

source.

3. The Propogation of Systematic Errors

Figures B.2 also illustrate the next problem we encountered with the position error boxes generated by the program FASFINDP. The 90% confidence contours generated by FASFINDP for the Crab exclude the actual source position. In fact, the systematic errors in determining the detector look-direction and spacecraft spin axis, the collimator opening angles in both directions, and the degree of slight misalignment among the detectors, are all about $0.02°$. This is larger than the width of the 90% confidence contours that exclude the Crab. The effects of these systematic errors become greatest near the edges of the rectangular collimators.

We approached this problem by adding the uncertainty due to these systematic errors, $\delta c(IDET,IFOV,i)$, to our calculation of the goodness of fit. To second order,

B.9 $\quad |\delta c(IDET,IFOV,i)|^2 = \{\sum_k (\frac{\partial c(IDET,IFOV,i)}{\partial V_k}) \cdot \sigma(V_k)\}^2.$

Here V_k, σ_k represent each detector parameter and the corresponding $\sim 1\sigma$ systematic uncertainties in determining them. The values for the $\sigma(V_k)$ came from in-flight detector calibrations performed by Kim Tolbert and Jean Swank.

For each detector and field of view, we considered the effects of uncertainties in the collimator opening angles in scan and off-scan direction; the detector rotation offsets with respect to the

experiment look-direction and spacecraft.spin axes; and the determination of the experiment look direction and space-craft spin axes.

Inspection of Equations B.2 and B.9 shows that the variance of our model due to systematic errors can be approximated by:

$$B.10 \quad |\delta c(IDET,IFOV,i)|^2 \approx [I_S(i) \cdot DR(IDET) \cdot A_0(IDET,IFOV)]^2 \times$$

$$\{|\frac{\sigma(\theta_1)}{\theta_0}|^2 + |\frac{\theta-\theta_1}{\theta_0}|^2 \cdot |\frac{\sigma(\theta_0)}{\theta_0}|^2 + |\frac{\sigma(\phi_1)}{\phi_0}|^2 + |\frac{\phi-\phi_1}{\phi_0}|^2 \cdot |\frac{\sigma(\phi_0)}{\phi_0}|^2\}.$$

In the version of our position finding program named FULFINDP, we added $|\delta c(IDET,IFOV,i)|$ in quadrature with the statistical uncertainty for each data point before calculating χ^2 for each fit. However, since the systematic errors in each time bin are not likely to be independent (and therefore not likely to be Gaussian), this method may underestimate the effects of systematic errors whenever one uses more than about 10 time bins. In Figure B.3, we display 90% and 99% confidence contours for At Mic, Abell 85, and the Crab, using the same data as the previous figure, but generated with FULFINDP instead of FASFINDP. Notice that this has indeed corrected the problem with the Crab, but not appreciably affected the other two position contours. This is what one expects, since these systematic errors are only important when they are about the same as those due to statistics.

Figure B.1 We show 90% confidence contours (in 1950.0 R.A. and Dec.) for the event on D728.15 (=H2120+55) and for the event on D298.62 attributed to the flare star AT Mic, illustrating problems with the first approach (FINDP).
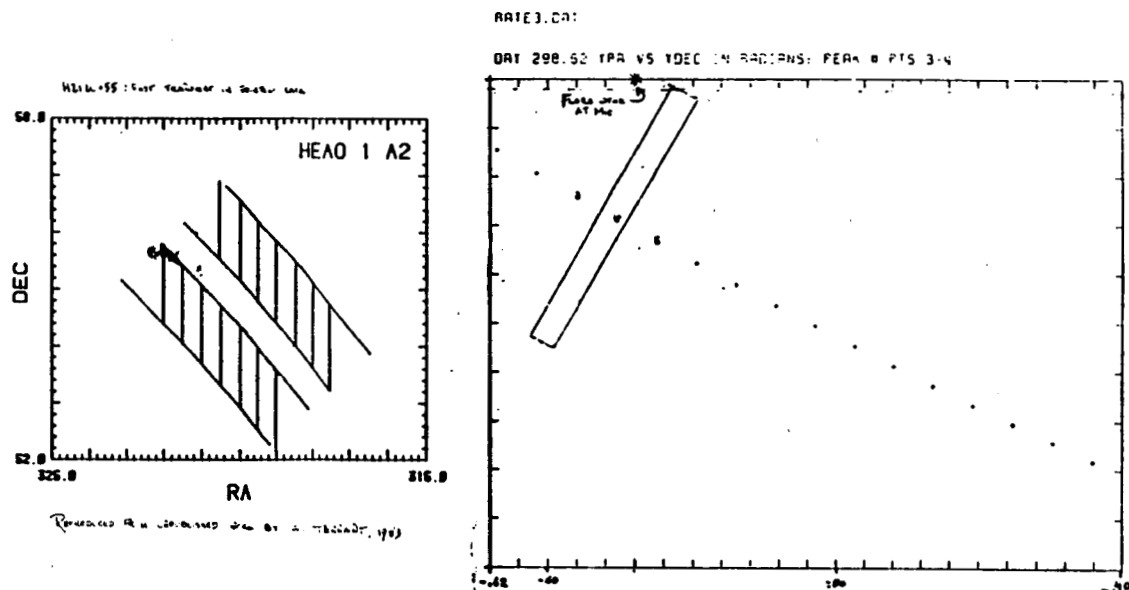
Figure B.2 We show maps (in 1950.0 R.A. and Dec.) of 90% and 99% confidence position limits for four different types of data, illustrating the successes and shortcomings of the second approach (FASFINDP). Starting clockwise from the top left: in the first we used 100 s of scanning data from the event on D298.62 from AT Mic, and allowed the intensity to vary in each time bin; for the second we used 5×10^4 s of pointed data (on D.O.Y. 1977 547) of the faint AGN Abell 85, but assumed the source was constant; for the third we used 123 s (three major frames) of pointed data of the highly variable source Cygnus X-1, allowing the intensity to vary freely; and in the last we used one day of scanning data (on D.O.Y. 1977 260) on the Crab Nebula plus pulsar, which was assumed to be constant.
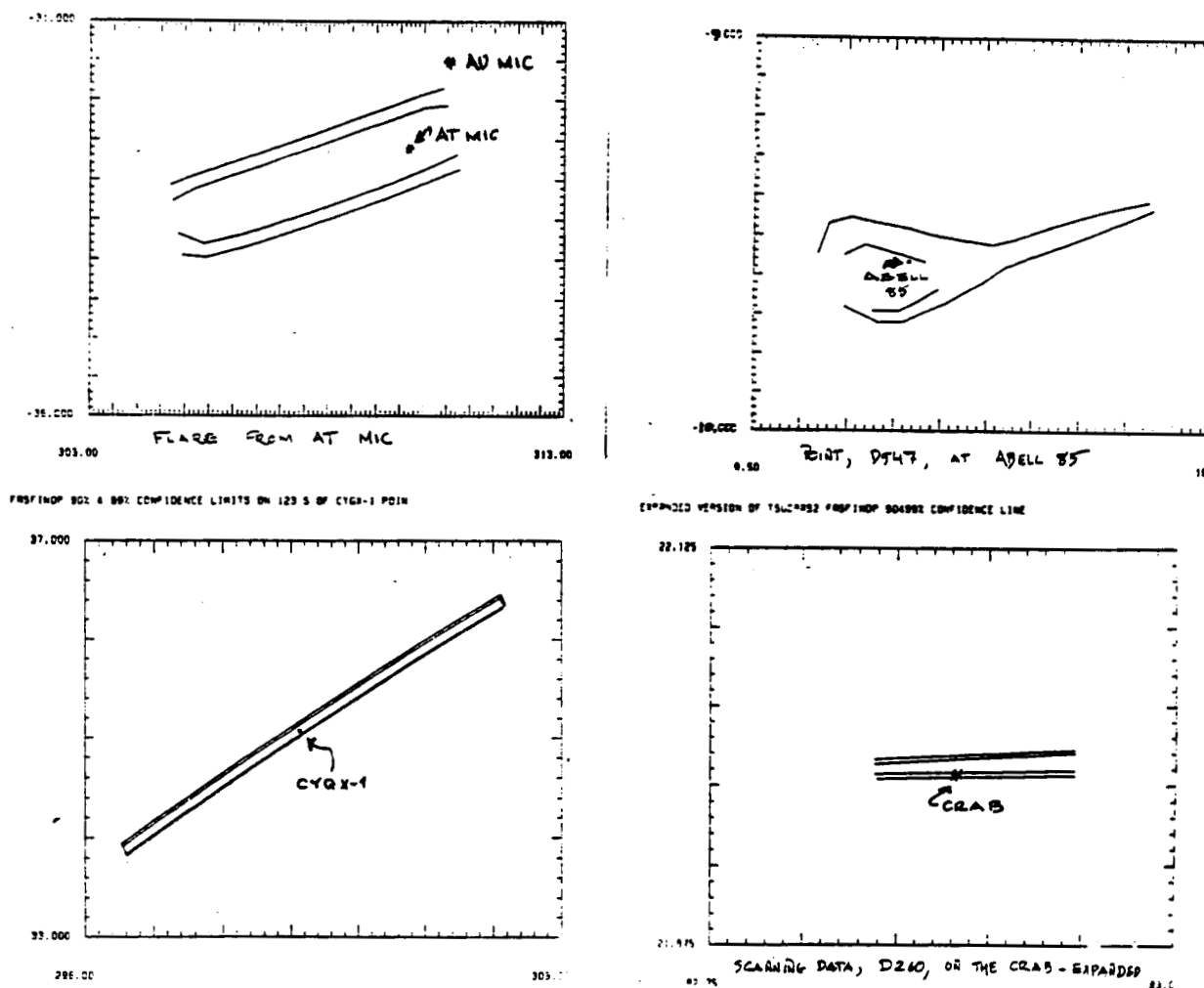
Figure B.3 We show maps of the 90% and 99% confidence position limits (in 1950.0 R.A. and Dec.), using the same data and same basic approach as in the last figure, but adding the effects of systematic errors (FULLFINDP).
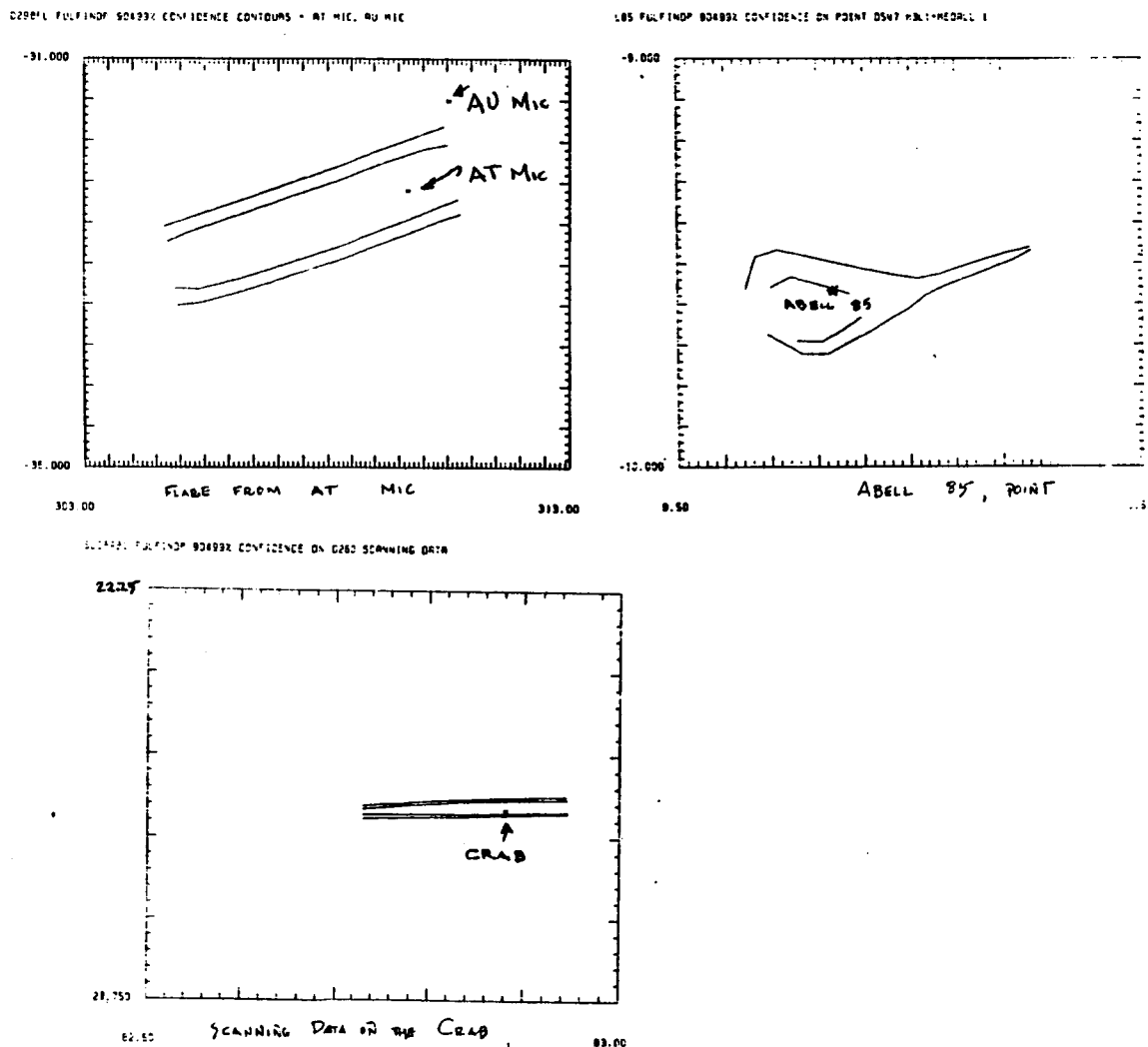
APPENDIX C

Statistics of Flaring Activity Extrapolated to X-Rays

The most complete statistical studies of flare frequencies have been carried out at optical wavelengths (Byrne 1983; Kunkel 1975a; Lacy, Moffett, and Evans 1976, hereafter LME). Extrapolating from U-band to X-ray flux introduces considerable uncertainty (Haisch 1983). However, as we describe below, reasonable estimates imply that we could expect X-ray flares from dMe-dKe stars at a rate consistent with the HEAO 1 A-2 observations.

LME demonstrate that $\nu(\geq E_U)$, the number of events per hour with total U-band energy $\geq E_U$, obeys their equation 18

$$C.1 \quad \log \nu(\geq E_U) = \alpha + \beta \log E_U,$$

for E_U in the range of the majority of their data. The flare rate declines to zero as E_U approaches a maximum energy E_{MAX}. The form

$$C.2 \quad \nu(\geq E_U) = 10^\alpha (E_U{}^\beta - E_{MAX}{}^\beta)$$

naturally includes this saturation effect.

LME observe that the parameters α, β, and perhaps E_{MAX} are functions of the quiescent U-band luminosity q_U. (The maximum energy may increase with increasing q_U, but this is not well determined - see Roizman and Shevchenko 1982.) For q_U between 3×10^{26} erg-s^{-1} and 2×10^{30} erg-s^{-1}, α falls from ~ 30 to ~ 13. If one instead

characterizes an event by its "equivalent duration" E_U/q_U, defining $\log \alpha_0 - \alpha = \beta \log q_U$ (Gershberg 1972; LME), then

$$C.3 \quad \nu(\geq E_U) = \alpha_0 [(\frac{E_U}{q_U})^\beta - (\frac{E_{MAX}}{q_U})^\beta] \ .$$

A least squares fit (using LME Tables 2 and 3) shows $\log \alpha_0 = 1.2\pm1$, independent of q_U.

Since the HEAO 1 A-2 search did not constrain event durations beyond requiring them to lie between 1 and 60 minutes, we find it convenient to rewrite equation (C.2) in terms of a peak luminosity L_U and an average flare decay time τ.

$$C.4 \quad \nu(\geq E_U) = \alpha_0 [(\frac{\tau L_U}{q_U})^\beta - (\frac{\tau L_{MAX}}{q_U})^\beta].$$

From Kunkel (1975a), one finds that if τ, measured in minutes, is the time it takes for an event to decay to half its peak, then, on average,

$$C.5 \quad \log \tau = (1.6 \pm 0.17) - 0.15 \, M_V \ .$$

Kunkel (1975a) notes that deviations from the mean of more than an order of magnitude are not uncommon. There is also some indication that X-ray decay times are longer than those in the U-band (Kahler et al. 1982; Haisch 1983).

To extrapolate C.4 to X-rays, we define $\lambda = L_U/L_X$. Some measurements suggest $\lambda \gtrsim 10$ (Haisch 1983). Then

C.6a $\quad \nu(\geq L_X) = \alpha_0 \ [(\frac{\tau\lambda L_X}{q_U})^\beta - (\frac{\tau\lambda L_{MAX}}{q_U})^\beta]$

For comparison it is also useful to use

C.6b $\quad \nu(\geq E_X) = \alpha_0 [(\frac{\lambda E_X}{q_U})^\beta - (\frac{\lambda E_{MAX}}{q_U})^\beta]$.

Before modeling the HEAO 1 A-2 data, we test our assumptions by comparing equation (C.5) to Einstein observations of known flare stars. In 1982, Haisch (1983) reported the detection of 9 flares from nearby stars (plus several from associations of young stars) in 1.1 x 10^5s of HEAO 2 flare star observations processed by mid 1981 (Seward and Williams 1981; Petterson 1976; Kunkel 1975a). For $p(M_V)$ the percentage of flare stars observed by HEAO 2 with absolute magnitudes between M_V and $M_V + dM_V$, and T the total star-hours observed, the expected number of events observed with X-ray luminosity $\geq L_X$ is

C.7a $\quad N_A(\geq L_X) = T\int dM_V p(M_V) \ \nu(\geq L_X),$

and the expected number of events with X-ray energy $\geq E_X$ is

C.7b $\quad N_B(\geq E_X) = T \int dM_V p(M_V) \ \nu(\geq E_X)$.

These functions have the form $N_A(\geq L_X) = \alpha_A L_{30}{}^\beta - \nu_A,$ and $N_B (\geq E_X) = \alpha_B(E_{32})^\beta - \nu_B,$ where L_{30} and E_{32} are the X-ray luminosity and energy in units of 10^{30} erg-s^{-1} and 10^{32} ergs respectively. The terms ν_A and ν_B go as $L_{MAX}{}^\beta$ and $E_{MAX}{}^\beta$. Though the maximum flare luminosity or energy may vary with quiescent luminosity (LME; Byrne

1983), our fits were not at all sensitive to it. We assumed
$L_{MAX} \sim 10^{32}$ erg-s^{-1} and $E_{MAX} \sim 10^{35}$ ergs (Kaluzienski et al. 1978a,b; Ambruster 1984; Roizman and Shevchenko 1982; Gurzadyan 1980). The normalization of the luminosity prediction, α_A, goes as $(\lambda\tau)^{\beta}$, while that for the energy form, α_B, depends only on λ^{β}.

We numerically integrated equation (A.7) with λ given by equation (C.4), $\lambda = 10$, and q_U, p(M_V) from Allen (1973), Petterson (1976), Joy and Abt (1974), and Gliese (1969) to predict $\alpha_A = 0.18$, $\nu_A = 0.02$ for $\beta = -1$ ($\alpha_A = 21$, $\nu_A = 4$ if $\beta = -0.4$), and $\alpha_B = 0.19$, $\nu_B = .002$ for $\beta = -1$ ($\alpha_B = 49$, $\nu_B = .05$ if $\beta = -0.4$). We performed three parameter, maximum likelihood fits to the detected Einstein Observatory flares as functions of luminosity and energy. In neither case could we distinguish between $\beta = -1$ and $\beta = -0.4$ at the one sigma level, and we could only constrain ν_A and ν_B to ν_A, $\nu_B < 1$. For the energy fit, $\alpha_B = 0.17\pm0.07$ for $\beta = -1$ ($\alpha_B = 1.5 \pm 0.6$ if $\beta = -0.4$), implying, an average, $\lambda = 10\pm4$ (or $\lambda \sim 10^5$ for $\beta = -0.4$, much larger than our expected uncertainty). For the luminosity fit, $\alpha_A = .033\pm.014$ for $\beta = -1$, indicating the average duration of an X-ray flare is ~ 5.5 times greater than that of a U-band flare. (The value is uncertain by a factor of ~ 2.5 in either direction.) This is similar to what was suggested by Kahler et al. (1982), and the decay times listed by Haisch (1983).

We now use C.6 to model the HEAO 1 A-2 data, assuming the mean X-ray duration, τ_x, is between 200s and 1.3×10^3s. Let ρ_0 be the density of dMe-dKe stars per cubic parsec, and p(M_V) the percentage with absolute magnitudes between M_V and M_V+dM_V. If S is the 2-20 keV flux (in ergs-cm^{-2}-s^{-1}) at earth, the expected number of flares per hour with

flux $\geq S$ is

C.8 $N(\geq S) = \rho_0 \int\int\int dM_v p(M_v) \, d\nu \, 4\pi r^2 dr,$

where r is integrated to the maximum distance at which flares with peak luminosities L_x to $L_x + dL_x$, which occur with frequency $d\nu$, can give a signal $\geq S$. So

C.9

$$N(\geq S) = \left(\frac{S}{S_0}\right)^{-3/2} \rho_0 \left[\frac{4}{3}\pi \left(\frac{L_{MAX}}{4\pi S_0}\right)^{3/2}\right] \left[\alpha_0 \frac{-\beta}{\beta+3/2} \left(\frac{\lambda\tau_0 L_{MAX}}{q_0}\right)^{\beta}\right] \int dM_v \left(\frac{\tau_5}{q_{29}}\right)^{\beta} p(M_v)$$

where S_0 is the search threshold of 4 millicrabs, $\tau_0 = 500s$, $q_0 = 10^{29}$ erg-s^{-1} and $\tau_5 \equiv \tau/\tau_0$, $q_{29} \equiv q_U/q_0$. We used the flare temperatures recorded in Haisch (1983) to estimate $\lambda = L_x/L_U$ for 2-20 keV, given $\lambda = 10\pm4$ for the Einstein IPC 0.1-4 keV energy band. A least-squares fit implied $\lambda(2\text{-}20 \text{ keV}) = 3\pm2$. The total rate has the form of an average density of ~ 0.04 stars-pc^{-3} times a total volume of ~ 2×10^6 pc^3, a rate of ~ 2×10^{-5} events-star^{-1}-hr^{-1} and a dimensionless integral of order unity. Stars of spectral type dM2e-dM3e make the largest contribution to the total rate. We assumed (conservatively) that $\beta = -1$, and L_{MAX} ~ 10^{32} erg-s^{-1} (Kaluzienski et al. 1978a,b). Calculating ρ_0, $r(M_v)$, and $q_U(M_v)$ from Joy and Abt (1974), Bahcall and Soneira (1980), Allen (1973), we numerically integrated equation (C.9) to find

C.10 $N(\geq S) = 1.1 \, (S/S_0)^{-3/2}$ events-sky^{-1}-hr^{-1}.

In the notation introduced in §V.a, for flare stars, equation (C.10) predicts $\Gamma = 1.5$ and $R(S_0) = 10^4$ event-yr^{-1}-sky^{-1}. The normalization is uncertain by about a factor of 3 in either direction, due chiefly to the uncertainty in the extrapolation to 2-20 keV, and in event duration.

BIBLIOGRAPHY

Alfven, H. 1986, <u>Physics Today, 39</u>, 22.

Allen, C. W. 1973, <u>Astrophysical Quantities</u> (London: Athlone Press).

Agrawal, P. C., Damle, S. V., Gokhale, G. S., Naranan, S., and
  Skeekantan, B. V. 1979, <u>X-Ray Astronomy (COSPAR)</u>, (New York:
  Pergamon Press), p. 515.

Ambruster, C. 1984, Ph. D. Thesis, University of Pennsylvania.

Ambruster, C., and Wood, K. 1984, <u>Proceedings of the Third Cambridge
  Conference on Cool Stars, Stellar Systems, and the Sun</u>, ed. S. L.
  Baliunas and L. Hartman, (New York: Springer-Verlag).

Ambruster, C., Sciartino, S., and Golub, L. 1987, <u>Ap. J.</u>, <u>319</u>, 1012.

Ambruster, C., Snyder, W. A., and Wood, K. S. 1984, <u>Ap. J.</u>, <u>284</u>, 270.

Ambruster, C. and Wood, K. S. 1986, <u>Ap. J.</u>, <u>311</u>, 258.

Ambruster, C. and Wood, K. S., Meekins, J. F., Yentis, D. J.,
  Smathers, H. W., Byran E. T., Chubb, T. A., and Friedman, H.,
  1983, <u>Ap. J.</u>, <u>269</u>, 779

Atteia, J.-L. <u>et al</u>. 1987, <u>Ap. J. Lett.</u>, <u>320</u>, L105.

Bahcall, J.N. and Soneira, R.M. 1980, <u>Ap.J. Suppl</u>, <u>44</u>, 73.

Batchellor, D. A. 1984, Ph. D. Thesis, Universisty of North Carolina

Batchellor, D. A., Cranell, C. J., Wiehl, H. J., and Magun, A. 1985,
  <u>Ap. J.</u>, <u>295</u>, 258.

Bethe, H. A. and Salpeter, E. E. 1977, <u>Quantum Mechanics of One- and
  Two- Electron Atoms</u>, (New York: Plenum Publishing Corp.).

Bradt, H. and McClintock, J. 1983, <u>Ann. Rev. Astr. Ap.</u>, <u>21</u>, 1.

Beurle, K., Bewick, A., Mills, J. S., and Quenby, J. J. 1981, <u>Astr.
  Space Sci. 77</u>, 201.

294

Bevington, P. R. 1969, Data Reduction and Error Analysis in the

  Physical Sciences, (New York: McGraw Hill)

Bewick, A., Coe, M. J., Mills, J. S., and Quenby, J. J. 1975, Nature,

  25, 686.

Boldt, E. A. 1987, Physics Reports, 146, 215.

Bopp, B. W., and Espenak, F. 1977, A. J., 82, 916.

Bookbinder, J. 1984, Ph.D., Harvard University.

Buckley, D. et al. 1988, in preparation.

Burstein, D. and Heiles, C. 1982, A.J. 87, 1165.

Byrne, P. B. 1983, in IAU Colloq. No. 71, Activity in Red Dwarf Stars,

  ed P. B. Byrne and M. Rodino (Dordrecht: Reidel) p. 157.

Caillault, J.-P., Helfand, D. J., Nousek, J. A., and Takalo, L. O.

  1986, Ap. J., 304, 318.

Caraveo, P. A. 1983, Space Sci. Rev., 36, 207.

Cline, T. L. 1984, High Energy Transients in Astrophysics, ed. S.

  Woosley, University of California at Santa Cruz (New York: AIP

  Conference Proceedings), p. 333.

Cline, T. L., Desai, U. D., Schmidt, W. K. H., and Teegarden, B. J.

  1977, Nature, 266, 694.

Connors, A., Serlemitsos, P. J., and Swank, J. H. 1986, Ap. J., 303,

  769.

Connors, A., Hueter, G. J., and Serlemitsos, P. J. 1988, in

  preparation.

Cowley, A. P., Hutchings, J. B., Crampton, D., and Hartwick, F. D. A.

  1987, Ap. J., 320, 296.

Cowley, A. P., Crampton, D., Hutchings, J. B., Helfand, D. J.,

  Hamilton, T. T., Thorstensen, J. R., and Charles, P. A. 1984, Ap.

J., <u>286</u>, 196.

De Santillana, G. and von Dechend, H. 1977, <u>Hamlet's Mill</u>, (Boston: David R. Godine).

Drake, Stillman 1978, <u>Galileo at Work: His Scientific Biography</u>, (Chicago: Chicago Press).

Ebisuzaki, T. 1987, <u>Publ. Astron. Soc. Japan</u>, <u>39</u>, 287.

Epstein, A., <u>et al</u>. 1978, <u>Ap. J.</u>, <u>216</u>, 103.

Evans, R. D. 1955, <u>The Atomic Nucleus</u>, (New York: McGraw Hill).

Fabian, A. C. and Rees, M. J. 1979, in <u>X-Ray Astronomy (COSPAR)</u>, ed. Baity, W. and Peterson, L. (New York, Pergamon Press), p. 381.

Fishman, G. J., Meegan, C. A., Watts, J. W. Jr., and Derickson, J. H. 1978, <u>Ap. J. (Letters)</u>, <u>240</u>, L13.

Garcia, M., Baliunas, S. L., Conroy, M., Johnston, M. D., Ralph, E., Roberts, W., Schwartz, P. A., and Tonry, J. 1980, <u>Ap. J. (Letters)</u>, <u>240</u>, L107.

Gershberg, R.E. 1972, <u>Ap. and Space Sci.</u>, <u>19</u>, 75.

Giacconi, R. 1974, in <u>X-Ray Astronomy</u>, ed. Giacconi, R. and Gursky, H. (Boston: D. Reidel Publishing Co.), p.155.

Giampapa, M. S. and Liebert, J. 1986, <u>Ap. J.</u>, <u>305</u>, 784.

Gliese, W. 1969, <u>Catalogue of Nearby Stars</u>, <u>Veroff. Astron. Rechen-Inst. Heidlberg</u>, No. 22.

Gliese, W., and Jahreiss, H. 1979, <u>Astr. Ap. Suppl.</u>, <u>38</u>, 423.

Golub, L. 1983, in IAU Colloq. No. 71, <u>Activity in Red Dwarf Stars</u>, ed. P. B. Byrne and M. Rodino (Dordrecht: Reidel), p. 83.

Griffiths, R. E., et al. 1979, <u>X-Ray Astronomy (COSPAR)</u>, ed. Baity, W. and Peterson, L. (New York: Pergamon Press), p. 93.

Gurzadyan, G. A. 1980, <u>Flare Stars</u> ed. Terzian, Y. (New York: Pergamon

Press).

Haisch, B. 1983, in IAU Colloq. No. 71, Activity in Red Dwarf Stars,
    ed P. B. Byrne and M. Rodino (Dordrecht: Reidel) p. 255.

Haisch, B. M., Linsky, J. L., Bornmann, P. L., Stencel, R. E.,
    Antiochos, S. K., and Golub, L. and Vaiana, G. S. 1983, Ap. J.,
    267, 280.

Hall, D. S. 1986, in Proceedings of the Fourth Cambridge Workshop on
    Cool Stars, Stellar Systems, and the Sun

Helfand, D. J. and Caillault, J.-P. 1982, Ap. J., 253, 760.

Helfand, D. J. and Vrtilek, S. D. 1983, Nature, 304, 41.

Henke, B. L., Lee, P., Tanaka, T. J., Shimabukuro, R. L., and
    Fujikawa, B. K. 1982, Atomic Data and Nuclear Data Tables, 27, 1.

Hertz, P. and Grindlay, J. E. 1984, Ap. J., 278, 137.

Herzo, D., Dayton, B., Zych, A. D., and White, R. E. 1976, Ap. J.
    (Letters), 203, L115.

Hueter, G. J. 1987, Ph. D. Thesis, University of California at San
    Diego.

Hutchings, J. B., Crampton, D., and Cowley, A. P. 1978, Ap. J., 225,
    548.

Jennings, M. C. 1982, Ap. J., 258, 110.

Jennings, M. C. 1984, High Energy Transients in Astrophysics, ed. S.
    Woosley, (New York: AIP Conference Proceedings), p. 412.

Jennings, M. 1987, B.A.A.S., 19, 693.

Johnston, M. D. et al. 1979, Ap. J., 230, L11.

Joy, A. H. and Abt, H. A. 1974, Ap. J. Suppl., 28, 1.

Kahler, S. et al. 1982, Ap. J., 252, 239.

Kahn, S. M., Linsky, J. L., Mason, K. O., Haisch, B. M., Bowyer, C.

S., White, N. E. and Pravdo, S. H. 1979, <u>Ap. J. (Letters)</u>, <u>234,</u>
L107.

Kaluzienski, L. J., Robinson-Saba, J. L., Boldt, E. A., Holt, S. S.,
Swank, J. H., Serlemitsos, P. J., and Rothschild, R. E. 1978a, in
<u>I. A. U. Circular 3714.</u>

Kaluzienski, L. J., Robinson-Saba, J. L., Boldt, E. A., Holt, S. S.,
Mushotzky, R. F., Rothschild, R. E., and Serlemitsos, P. J.,
1978b, <u>Bulletin of the AAS</u>, <u>10,</u> 516.

Katoh, H., Murakami, T., Nishimura, J., Yamagami, Y., Fuji, M., and
Itoh, M. 1984, <u>High Energy Transients in Astrophysics</u>, ed. S.
Woosley, (New York: AIP Conference Proceedings), p. 390.

Kelley R. L., Jernigan, J. G., Lerrine, A., Petro, L. D., and
Rappaport, S. 1983, <u>Ap. J.</u>, <u>264</u>, 568.

Koenigsberger, G., Swank, J.H., Szymkowiak, A.E., and White, N.E.
1983, <u>Ap. J.</u>, <u>268</u>, 782.

Koyama, K., Ikeuchi, S., and Tomasaka, S. 1987, <u>Publ. Astron. Soc.</u>
<u>Japan</u>, <u>38</u>, 503.

Koyama, K., Kondo, H., Makino, F., Nagase, F., Takano, S., Tawara, Y.,
Turner, M. J. L., and Warwick, R. S. 1988, to be submitted to the
<u>Pub. Astr. Soc. Japan.</u>

Kriss, G. A., Cominsky, L. R., Remillard, R., Williams, G. and
Thorstensen, J. R. 1983, <u>Ap. J.</u>, <u>266</u>, 806.

Kuhn, T. S. 1970, <u>The Structure of Scientific Revolutions</u>, (Chicago:
Chicago Press).

Kukarkin, B. V., <u>et al</u>. 1969, <u>General Catalog of Variable Stars</u>
(Moscow: Academy of Sciences of the USSR).

Kukarkin, B. V., <u>et al</u>. 1971, <u>First Supplement to the Third Edition of</u>

the General Catalog of Variable Stars (Moscow: Academy of Sciences of the USSR).

_____ 1974, Second Supplement to the Third Edition of the General Catalog of Variable Stars (Moscow: Academy of Sciences of the USSR).

Kukarkin, B. V., et al. 1976, Third Supplement to the Third Edition of the General Catalog of Variable Stars (Moscow: Academy of Sciences of the USSR).

Kunkel, W. E. 1975a, Ap. J. Suppl. 25, 1.

Kunkel, W.E. 1975b, IAU Symposium 67, Variable Stars and Stellar Evolution, ed. Sherwood, V.E. and Plaut, L. (Dordrecht: Reidel), p. 15.

Lacy, C. H., Moffet, T. J. and Evans, D. S. 1976 Ap. J. Suppl., 30, 85 (LME).

Lamb, D. Q. 1983, Eleventh Texas Symposium on Relativistic Astrophysics, ed. R.E. Lingenfelter, H.S. Hudson, and D.M. Worrall, (New York: Annals of the New York Academy of Sciences), p. 249.

Lampton, M., Margon, B., and Boyer, S. 1976, Ap. J., 208, 177.

Lang, F. L. et al. 1981, Ap. J. (Letters), 246, L21.

Laros, J. G., Evans, W. D., Fenimore, E. E., Klebesadel, R. W., Shulman, S. and Fritz, G. 1984, High Energy Transients in Astrophysics, ed. S. Woosley, (New York: AIP Conference Proceedings), p. 378.

Laros, J. G. et al. 1986, Nature, 322, 152.

Lewin, W. H. G. and Joss, P. C. 1981, Space Sci. Rev., 28, 3.

Li, F., Rappaport, S., Epstein, A. 1978, Nature, 271, 37.

Lin, C. C., Yuan, C., and Shu, F. H. 1969, _Ap. J._, _155_, 721.

Lin, C. C. and Lau, Y. Y. 1979, _Studies in Applied Mathematics_, _60_, 97.

Linsky, J. L. 1980, _Ann. Rev. Astr. Ap._, _18_, 439.

Linsky, J. L., Burnmann, P. L., Carpenter, K. G., Wing, R. F., Giampapa, M. S., Worden, S. P., and Hege, E. K. 1982, _Ap. J._, _260_, 670.

Long, K. S., Helfand. D. J., and Grebalsky D. A. 1981, _Ap. J._, _248_, 95.

Longair, M. S. 1981, _High Energy Astrophysics_, (Cambridge, England: Cambridge University Press).

Lucke, P.B. 1978, _Astr. Ap._, _64_, 367.

Luyten, W. J. 1963a, _Pub. Astr. Obs. Minn._, _3_, 12.

Luyten, W. J. 1963b, _Bruce Proper Motion Survey, The General Catalog_, _Vol. 1_, (Minneapolis: U. of Minn. Press)

Mason, K. 1985, _Space Science Reviews_, _40_, 99.

Matteson, J. L. 1978, AIAA Paper 78-35, available on microfiche from AIAA.

Mazets, E. P. _et al._ 1978, _Pis'ma Astr. Zh._, _4_, 349.

McIlwain, C.E. 1961, _J. Geophys. Res._, _66_, 3681.

Mead, J. M., and Hill, R. S 1983, _ADC Bull 217_, (July 1983).

Meegan, C. A., Fishman, G. J., Wilson, R. B. 1984, _High Energy Transients in Astrophysics_, ed. S. Woosley, (New York: AIP Conference Proceedings), p. 422.

Minkowski, H. 1908, "Space and "Time", translation of an address delivered at the 80th Assembly of German Natural Scientists and Physicians at Cologne, 21 Sept. 1908; in _The Principle of_

Relativity, ed. A. Sommerfeld, Dover Publications, 1952.

Morrison, Phillip and Morrison, Phyllis 1987, The Ring of Truth,

    (Random House: New York).

Nishimura, J. et al. 1977, 15th International Conference on Cosmic

    Rays, Conference Papers, 1, 179.

Norris, J. P. 1983, Ph. D. Thesis, University of Maryland.

Nugent et. al. 1983, Ap. Suppl., 51, 1.

Pallavicini, R., Golub, L., Rosner, R. Vaiana, G., Ayres, T. and

    Linsky, J. L. 1981, Ap. J., 248, 279.

Parmar, A. N. and White, N. E. 1985, Space Science Reviews, 40, 391.

Patterson, J. 1984, Ap. J., 54, 443.

Petterson, B. R. 1976, Catalog of Flare Star Data, No. 46, (Oslo:

    Inst. of Theor. Ast.).

Pounds, K. A. 1976, Comments Astr., 6, No. 5, 145.

Pye, J. P. and McHardy, I. M. 1983, Mon. Not. R. Astr. Soc., 205, 875.

Rappaport, S. J., and Heuvel, V.-d. 1983, in IAU Colloq. No. 98, Be

    Stars, ed M. Jaschek and M.-G. Groth, (Dordrecht: Reidel) p. 327.

Rappaport, S., Buff, J., Clark, G., Lewin, W. H. G., Matilsky, T., and

    McClintock, J. 1976, Ap. J., 206, L139.

Raymond, J. C. and Smith, B. W. 1977, Ap. J., 35, 419.

Ritter, H. 1986, Astr. Ast. Suppl, submitted.

Robinson-Saba, J. L. 1982, Ph.D. Dissertation, University of Maryland.

Roizman, G. Sh. and Shevchenko, V. S. 1982, Sov. Astr. Lett. 8, 85.

Rossi, B. 1952, High Energy Particles, (Englewood Cliffs, N.J.:

    Prentice-Hall).

Rothschild, R., et al. 1979 Space Sci. Instr., 4, 269.

Saar, S. H. and Linsky, J. L. 1985, Ap. J. (Letters), 299, L47.

Saar, S. H., Linsky, J. L., and Beckers, J. H. Ap. J., 302, 777.

Sandage, A. and Tammann, G. A. 1985, in Supernovae as Distance Indicators, ed. N. Bartel (New York: Springer-Verlag) p1.

Schaefer, B. E. and Cline, T. L. 1985, Ap. J., 289, 490.

Schaefer, B. E. 1988, in preparation.

Schnopper, H. W., Delvaille, J. P., Epstein, A., Helmken, H., and Murray, S. S., and Clark, G., Jernigan, G., and Doxsey, R. 1976, Ap. J., 210, L75.

Schrijver, C. J. 1985, Space Science Rev, 40, 3.

Schrijver, J., Brinkman, A. C., Heise, J., den Boggende, A. J. F., Gronnenschild, E. H. B. M., Mewe, R., Grindlay, J. E. and Parsignault, P. R. 1978, Astr. Ast., 69, L1.

Schwartz, D. A., Garcia, M., Ralph, E., Doxsey, R. E., Johnston, M. D., Lawrence, A., McHardy, I. M., and Pye, J. P. 1981, M.N.R.A.S., 196, 95.

Serlemitsos, P. J., Bunner, A., and Swank, J. H. 1979 Bulletin of the APS, 24, 584.

Seward, F. and Williams, D. 1981, Einstein Observations, Center for Astrophysics/High Energy Astrophysics Division Report, No. 81-022.

Shafer, R. A. 1983, Ph. D. Thesis, University of Maryland.

Shapiro, S. L. and Teukolsky, S. A. 1983, Black Holes, White Dwarfs, and Neutron Stars, (New York: Wiley and Sons).

Share, G. H., Wood, K., Meekins, J. and Yentis, D. J. 1982, Gamma Ray Transients and Related Astrophysical Phenomena, (New York: AIP Conference Proceedings), p. 35.

Skinner, K. et al. 1980, Ap. J., 240, 619.

Steiner, J. E. et al. 1981, Ap. J. (Letters), 249, L21.

Steiner, J. E. et al. 1984, Ap. J., 280, 688.

Stella, L., White, N. E., and Rosner, R. 1986, Ap. J., 308, 669.

Sturrock, P. A. 1986, in Rapid Fluctuations in Solar Flares, ed. B. R. Dennis, L. E. Orwig, and A. L. Kiplinger, (Washington, D. C.: NASA Conference Publications)

Swank, J. H., Becker, R. H., Boldt, E. A., Holt, S. S., Pravdo, S. H., and Serlemitsos, P. J. 1977, Ap. J. (Letters), 212, L73.

Swank, J. H., and Johnson, H. M. 1982, Ap. J., 259, L67.

Tananbaum. H., Peters, G., Forman, W., Giacconi, R., Jones, C. and Avni, V. 1978, Ap. J., 223, 74.

Tawara et al. 1988, in preparation

Tennant, A. F. 1983, Ph. D. Thesis, University of Maryland.

Tennant, A. F. and Swank, J. H. 1983, Bull. A.P.S., 28, 723.

Terrell, J., Belian, R. D., Conner, J. P., Evans, W. D., and Priedhorsky, W. C. 1982, B.A.A.S., 14, 619.

Tsikoudi, V. 1982, Ap. J., 262, 263.

Tsikoudi, V. 1983, Ap. J., 272, 381.

Tsuneta, S. 1984, Active Phenomena in the Outer Atmosphere of the Sun and Stars, ed. Pecker, J.-C. and Uchida, Y. (Paris), p. 243.

Upgren, A. R., Grossenbacher, R., Penhallow, W. S., MacConnell, D. J., and Frye, R. L. 1972, A.J., 77, 486.

Van den Heuvel, E. P. J., and Rappaport, S. 1986, in I.A.U. Colloquium 92, Be Stars, ed. A. Slettebak and T. D. Snow (Cambridge: Cambridge University Press).

Vilhua, O. and Heise, J. 1985, Space Science Reviews, 40, 55.

Wackerling, L. R. 1970, Mem. R. Astr. Soc., 73, 153.

Walter, F., Charles, P., and Bowyer, S. 1978, Nature, 274, 569.

Walter, F. M., Cash, W., Charles, P. A., and Bowyer, C. S. 1980, *Ap. J.*, *236*, 212.

Warwick, R. S., turner, M.J.L., Watson, M. G., and Willingale, R. 1985, *Nature*, *317*, 218.

Weast, R. C. *et al.* 1974, *Handbook of Chemistry and Physics*, (Cleveland: CRC Press).

Weisskopf. M. *et al.* 1984, *Ap. J.*, *278*, 711.

Wesdelink, A. J. 1985, in *Supernovae as Distance Indicators*, ed. N. Bartel (New York: Springer-Verlag) p166.

White, N. E. 1978, *Nature*, *271*, 78.

White, N. E. and Carpenter, G. F. 1978, *M.N.R.A.S.*, *183*, 11p.

White, N. E., Swank, J. H., Holt, S. S., and Parmar, A. N. 1982, *Ap. J.*, *263*, 277.

White, N. E., and Marshall, F. E. 1983, *Ap. J. 268*, L117.

White, N. E., Kaluzienski, L. J., and Swank, J. H. 1984, in *High Energy Transients in Astrophysics*, ed. S. E. Woosley (New York: A.I.P.), p31.

White, N. E. and Mason, K. 1985, *Space Science Reviews*, *40*, 167.

Worral, D. H., Marshall, F. G., Boldt, E. A., and Swank, J. H. 1982, *Ap J.*, *255*, 111.

Wood, K. S. *et al.* 1984, *Ap. J. Suppl.*, *56*, 507.

Woolley, R., Epps, E.A., Penston, M.J., and Pocock, S.B. 1970, *Roy. Obs. Ann.*, *5*.

CURRICULUM VITAE

Name: Alanna Connors

Permanent address: 706 Wayne Avenue, Silver Spring, MD 29010

Degree and date to be conferred: Ph. D., 1988

Date of birth: ███████████████

Place of birth: ██████████████

Secondary education:

　　Greenwich High Scool, Greenwich, CT Graduated June, 1974

College Institutions attended:　　　　　　Dates   Degree Date of Degree

　　Massachusetts Institute of Technology

　　Cambridge, MA　　　　　　　　　　　　1974-1978 S.B.   June 1978

Major: Physics

　　University of Maryland

　　College Park, MD　　　　　　　　　　1980-1984 M.S. December 1984

　　　　　　　　　　　　　　　　　　　　1984-1988 Ph.D. May 1988

Major: Physics

Professional publications:

　　1.　"Fast Transients: A Search in X-Rays for Short Flares, Bursts, and Related Phenomena" A. Connors, P. J. Serlemitsos, and J. H. Swank, 1986, Ap. J., 303, 769.

Presentations at professional meetings:

　　1.　"A Broad Band X-Ray Telescope", P. J. Serlemitsos, R. Petre, C. Glasser, and A. Connors, 1982, B.A.A.S., 14, 942.

　　2.　"Hard Transients From the HEAO 1 A-2 Short Transient Survey: Are They Flares from dMe Stars?" A. Connors, P. J. Serlemitsos, and J. H. Swank, 1984, B.A.A.S., 16, 472.

3. "The Bright 6-Nov-77 Fast Transient: Constraints on a Quiescent Counterpart" A. Connors and L. Takalo, 1985, <u>B.A.A.S.</u>, <u>17</u>, 598.

4. "A Progress Report on the Full HEAO 1 A-2 Fast Transient Search" A. Connors, P. J. Serlemitsos, and J. H. Swank, 1986, <u>B.A.A.S.</u>, <u>18</u>, 636.

5. "The HEAO 1 A-2 All-Sky Study of Fast X-Ray Transients: A Preliminary Report from the LMC" A. Connors and J. H. Swank, 1987, <u>Bull. A.P.S.</u>, <u>32</u>, 1112.

6. "An All Sky Study of Fast X-Ray Transients" A. Connors, 1987, <u>B.A.A.S.</u>, <u>19</u>, 720.

Professional Positions held:

1978 - 1980	Field Service Supervisor
	Kurzweil Computer Products, Cambridge, MA
1980 - 1982	Graduate Teaching Assistant
	University of Maryland, College Park, MD
1982-1988	Graduate Research Assistant
	Laboratory for High Energy Astrophysics
	Goddard Space Flight Center, Greenbelt, MD

BIBLIOGRAPHIC DATA SHEET

1. Report No. 88-014	2. Government Accession No.	3. Recipient's Catalog No.

4. Title and Subtitle An All Sky Study Of Fast X-Ray Transients	5. Report Date April 1988
	6. Performing Organization Code 666

7. Author(s) Alanna Connors (Univ. of Maryland)	8. Performing Organization Report No. 88-014

9. Performing Organization Name and Address Code 666 X-ray Astrophysics Branch Laboratory for High Energy Astrophysics NASA/Goddard Space Flight Center Greenbelt, Maryland 20771	10. Work Unit No.
	11. Contract or Grant No.
12. Sponsoring Agency Name and Address	13. Type of Report and Period Covered
	14. Sponsoring Agency Code

16. Abstract

In the HEAO 1 A-2 survey of fast X-ray transients, we searched 2-20 keV scanning data for brief increases in flux, >4 millicrabs, on timescales $\sim 1\text{-}10^4$ s above a 12 hour average. We divided the search into two regions an "all-sky" survey of the Galaxy, and a survey of the Magellanic Clouds. In the Magellanic Clouds survey, we found 37 events, and identified all with 4 of the 5 brightest sources in the LMC, plus 2 as flares from a foreground star. We found no X-ray bursts, no γ-ray bursts, and no events from the SMC. In the "all-sky" survey, after excluding well-known variable sources, out of the equivalent of ~ 104 days of data, we found 15 events, falling into two broad categories: flares from coronal sources, roughly isotropically distributed, with optically thin thermal spectra; and harder fast transients apparently distributed near the Galactic plane. We identified the first as flares from ubiquitous active cool dwarf stars. We hypothesized that the second may have been from distant Be-neutron star binaries. However, at least two of the harder, more luminous events remain unidentified. Intriguing questions for future research include the nature of these rare events, and how they may fit into a hierarchy of hard fast transients from γ-ray bursts to outbursts from pulsar systems.

17. Key Words (Selected by Author(s))	18. Distribution Statement

19. Security Classif. (of this report) U	20. Security Classif. (of this page) U	21. No. of Pages 324	22. Price*